55th Scientific Conference for Young Students of Physics and Natural Sciences

Open Readings 2012

March 28-31, 2012

Vilnius, LITHUANIA

Programme and Abstracts

LOCAL ORGANIZING COMMITTEE

Students' Scientific Association, Faculty of Physics, Vilnius University, LITHUANIA:

Vytautas Butkus
Jonas Berzinš
Ugnė Nevedomskaitė
Eglė Krištopavičiūtė
Birutė Dargytė
Lina Mažulė
Vytenis Pranculis
Vytautas Aukštikalnis
Giedrius Medzevičius

Faculty of Physics
Vilnius University
Saulėtekio Ave. 9-III, LT-10222 Vilnius
LITHUANIA

www.ff.vu.lt
www.openreadings.eu

ISSN 2029-4425

Conference programme

28 March
WEDNESDAY

TUTORIAL LECTURES ON SCIENTIFIC COMMUNICATION

10:00 Dr. Jean-luc Doumont, *Louvain School of Engineering, Belgium*
STRUCTURING YOUR RESEARCH PAPER

11:00 Dalia Vasiliauskienė, *Institute of Foreign Languages, Vilnius University, Lithuania*
GUIDELINES FOR PREPARING YOUR BEST SCIENTIFIC TALK

29 March
THURSDAY

9:00 OPENING CEREMONY

ORAL SESSION O1

9:10 **KILOHERTZ RATE PICOSECOND PULSES AMPLIFIER FOR OPCPA SYSTEM** *01-1* **14**
Kirilas Michailovas, Valerijus Smilgevičius, Andrejus Michailovas

9:30 **FABRICATION AND REPLICATION OF OPTOFLUIDIC MICROLENSES BY DIRECT LASER WRITING, UV LITHOGRAPHY AND SOFT LITHOGRAPHY** *01-2* **15**
Linas Jonušauskas, Kristupas Tikuišis, Albertas Žukauskas, Mangirdas Malinauskas

9:50 **DYNAMICS OF NG IN SINGLE-MODE SEMICONDUCTOR LASER UNDER EXTERNAL OPTICAL INJECTION** *01-3* **16**
Eugene Sokolov

10:10 **INVESTIGATION OF SMALL V AND HIGH Q SOI OPTICAL RESONATORS** *01-4* **17**
Darius Urbonas, Martynas Gabalis, Paul Seidler, Raimondas Petruskevicius, Thilo Stoeferle, Gediminas Raciukaitis

10:30 **GENERATION OF TERAHERTZ RADIATION IN ATMOSPHERIC AIR** *01-5* **18**
Dmitrij Chomčik, Ernestas Žeimys, Virgilijus Vaičaitis

10:50 **Q-SWITCHED MODE-LOCKED (QML) REGIME IN Nd:GdVO4 LASER WITH V3+ :YAG SATURABLE ABSORBER** *01-6* **19**
Liubou Krylova

ORAL SESSION O2

11:30 **STIMUTALED EMISSION AND CONCENTRATION QUENCHING OF PERYLENE DIIMIDE DERIVATIVES** *02-1* **22**
G. Armonaitė, K. Kazlauskas, A. Miasojedovas, S. Valiyaveettil, J.V. Gražulevičius, S. Juršėnas

11:50 **STUDY OF SPECTRUM RESOLVED PHOTOLUMINESCENCE AND PHOTOCONDUCTIVITY TRANSIENTS IN GaN AND Cu_2S/CdS STRUCTURES** *02-2* **23**
Tomas Babelis, Jevgenij Brytavskiy, Rokas Skaisgiris, Aurimas Uleckas, Eugenijus Gaubas

12:10 **THE FORMATION OF WATER-CONTAINING DONORS IN CRYSTALS IMPLANTED WITH PROTONS** *02-3* **24**
Julija Dyshlevich

12:30 **PYRENYL-FUNCTIONALIZED FLUORENE AND CARBAZOLE DERIVATIVES AS BLUE LIGHT EMITTERS** *02-4* **25**
Simonas Krotkus, Karolis Kazlauskas, Arūnas Miasojedovas, Alytis Gruodis, Saulius Juršėnas

12:50 **STIMULATED EMISSION AND PHOTOLUMINESCENCE EFFICIENCY DROOP IN EPITAXIAL GAN** *02-5* **26**
Jonas Jurkevičius

BREAK

ORAL SESSION O3

15:30 – 18:00 **POSTER SESSION P1**

18:00 Excursions

30 March
FRIDAY

ORAL SESSION O4

ORAL SESSION O5

BREAK

ORAL SESSION O6

15:30 – 17:00 **POSTER SESSION P2**

19:00 CONFERENCE PARTY

31 March
SATURDAY

Planetarium of Vilnius University
Institute of Theoretical Physics and Astrophysics
Konstitucijos pr. 12a, Vilnius

Dr. Stanislava Bartašiūtė**,** *Astronomical Observatory of the Vilnius University*

12:00 **EVERYTHING WE KNOW AND DO NOT KNOW ABOUT THE UNIVERSE: INSIGHTS OF MODERN COSMOLOGY**

CONFERENCE CLOSING

13:00 **VILNIUS UNIVERSITY PLANETARIUM SHOW**

List of poster presentations

29 March
THURSDAY

15:30 – 18:00 **POSTER SESSION P1**

30 March
FRIDAY

15:30 – 17:00 **POSTER SESSION P2**

ORAL SESSION
I

KILOHERTZ RATE PICOSECOND PULSES AMPLIFIER FOR OPCPA SYSTEM PUMPING

Kirilas Michailovas[1, 3], Valerijus Smilgevičius[2], Andrejus Michailovas[1, 3]

[1]Institute of Physics, Center for Physical Sciences and Technology, Lithuania
[2] Laser Research Center, Vilnius University, Lithuania
[3]UAB EKSPLA, Lithuania
k.michailovas@ar.fi.lt

One of the most promising ways to obtain laser radiation of petawatt level is using optical parametric chirped pulse amplification (OCPA) [1]. Infrared or second harmonic radiation of Nd or Yb doped high power lasers are used as a pump source for these parametrical amplifiers. Several laser systems based on OPCPA have been implemented, operating at repetition rates as high as 1 kHz or output energies beyond 100 mJ while maintaining the pulse duration of 9-10 fs. Typical configuration of these systems is as follows: fs master oscillator, pulse stretcher, regenerative amplifier using Nd doped laser material optically or electrically synchronized with master oscillator and producing pulses of 50 to 100ps duration, power amplifier for producing OPCPA pump pulses of 10 to 1000 mJ energy, OPCPA stage and compressor. Though this technique is well known it is still a challenge to produce a reliable pump laser

There is special interest in laser systems operating at higher than 100Hz repetition rates. In this work we concentrated on creating a ps pulses amplifier operating at 1kHz repetition rate based on laser diode (LD) pumped Nd:YAG modules. We have not paid special attention to synchronization of fs and ps systems as it is well established technology [2]. Despite good total efficiency of LD pumped laser systems thermal distortions in laser rod severely affect laser beam quality. In presented work we concentrated on depolarization compensation and beam profile modulation elimination. Nd:YVO crystal based mode-locked laser running at 1kHz repetition rate producing 48ps and 1mJ pulses was chosen as seed source for amplifier.

A 2-pass scheme, with image relaying from active medium to a returning mirror and back, was chosen experimentally (Fig.1). A Faraday rotator is used to rotate the polarization. Having passed through the Faraday polarization rotator twice tangential and radial polarization components exchange places, therefore, during the second pass through an active medium the effect experienced by different polarization components is equalized. This also helps compensate the difference in thermal lens optical power for different polarization components. Unlike a quarter-wave plate Faraday rotator's effect is independent of the incident radiation's polarization direction, thus making it more suitable for depolarization compensation. To weaken the non-linear interaction a quarter-wave plate is used before a laser module. This turns linearly polarized light into circularly polarized light before passing through the laser module. Non-linear interaction is 1.5 times weaker for circularly polarized light than for linearly polarized light. To prevent air breakdown due to high intensity a vacuum cell is placed in the image relaying telescope, which is used to preserve spatial constituents of the beam.

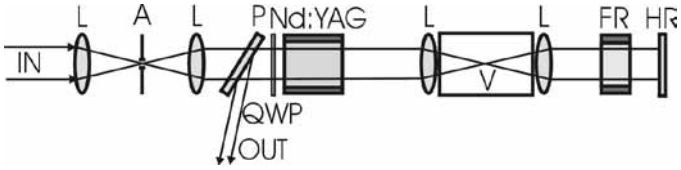

Fig. 1. Single amplifier cascade. L – lens, A- aperture, P – polarizer, FR – Faraday polarization rotator, HR – high reflectivity mirror, QWP – quarter-wave plate, V – vacuum cell.

The final amplifier system can be composed of several of described amplifier cascades. Image relaying is performed between separate amplifier cascades to preserve the needed intensity distribution. Image relaying telescope with aperture is also used to perform spatial filtering of the beam. This improves the quality of the beam and removes small-scale spatial irregularities caused by non-linear interaction, which could otherwise cause self-focusing of the beam. The telescope could be used to increase the diameter of the beam where needed. An isolator, consisting of a Faraday rotator and half-wave plate, is also placed between separate amplifier cascades, protecting the system from unwanted reflection and depolarized light amplification in preceding amplifier cascades.

A system composed of 3 aforementioned amplifier cascades using laser chambers with rod active media of 3, 5 and 6.3mm in diameter was realised. Pulse energies of about 70 mJ were reached with up to 52% conversion efficiency to second harmonic. The M^2 parameter of the beam was 3.4 for both the vertical and horizontal axis. The intensity distribution was quite homogeneous. Experiments using chamber with a 7mm rod are planned.

[1] A.Dubietis, G.Jonušauskas, A.Piskarskas, Powerful femtosecond pulse generation by chirped and stretched pulse parametric amplification in BBO crystal, Opt. Commun. **88**, 437-440 (1992).
[2] S. Witte et al., "A source of 2 terawatt, 2.7 cycle laser pulses based on noncollinear optical parametric chirped pulse amplification", Opt.Express, **14**, 8168-8177 (2006)

FABRICATION AND REPLICATION OF OPTOFLUIDIC MICROLENSES BY DIRECT LASER WRITING, UV LITHOGRAPHY AND SOFT LITHOGRAPHY

Linas Jonušauskas, Kristupas Tikuišis, Albertas Žukauskas, Mangirdas Malinauskas

Department of quantum electronics, Vilnius university, Saulėtekis ave., 9, LT-10222, Vilnius, Lithuania
linas.jon@gmail.com

In recent years there has been a surge of developments in micro and nanoresearch, including such fields as microoptics and microfluidics. Most of these developments showed possibilities to use light and liquids in ways it was never used before as well as raised several new device conceptions such as "lab on chip" [1].

These developments could be realized because of huge advances in micro and nanostructuring technologies, such as direct laser writing technique using multi-photon polymerization. This particular technology allows fabrication of free geometrical architecture 3D objects [2] with sub-diffraction features as small as tens of nanometers [3]. Combined with fast replication technologies such as soft lithography [4] or UV lithography, it becomes possible to fabricate micro and nanostructures with high spatial resolution and precision in short periods of time.

In this work we present a study of microlens arrays fabricated in SZ2080 photopolymer using direct laser writing technique. These microlenses are specially designed for use in microfluidic devices such as optofluidic sensors capable to detect changes in liquids' optical refractive index or light absorption in all or some part of spectrum. These sensors could be applied in various fields ranging from medical applications to unique industrial devices. Finally, possible optimization and simplification of fabrication process using soft and UV lithography are investigated.

Fig. 1. Microoptical prism fabricated using direct laser writing technique.

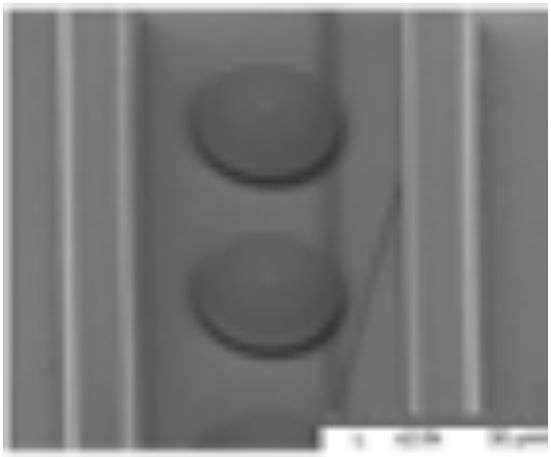

Fig. 2. An example of optofluidic microlens array integrated directly in to microfluidic channel.

[1] P. Abgrall and A-M. Gu´e., Lab-on-chip technologies: making a microfluidic network and coupling it into a complete microsystem—a review, J. Micromech. Microeng. **17**, 15–49 (2007).

[2] S. Juodkazis, V. Mizeikis, H. Misawa., Three-dimensional structuring of resists and resins by direct laser writing and holographic recording, Adv. Polym. Sci. **213**, 157-206 (2008).

[3] M. F. Qi, Y. Li, D. Tan, H. Yang, Q. Gong., Polymerized nanotips via two-photon photopolymerization, Opt. Express **15 (3)**, 971-976 (2007).

[4] Y. Xia and G. M. Whitesides., Soft lithography, Annu. Rev. Mater. Sci. **28**, 153–184 (1998).

Investigation of Small V and High Q SOI Optical Resonators

Darius Urbonas[2], Martynas Gabalis[2], Paul Seidler[1], Raimondas Petruskevicius[2], Thilo Stoeferle[1], Gediminas Raciukaitis[2]

[1]IBM Research – Zurich, Säumerstrasse 4, 8803 Rüschlikon, Switzerland
[2]Center for Physical Sciences and Technology, Savanoriu ave. 231, Vilnius LT-02300, Lithuania
darius.urbonas@ff.stud.ff.vu.lt

Recently, various wavelength-sized 1D, 2D or 3D cavities with theoretical Q of 10^5 and ultra small modal volume V of 0.04 $(\lambda/2n)^3$ have been reported, however in most of these cavities air is used as low dielectric material (λ is the wavelength, and n is the refractive index). Here we implement three-dimensional finite-difference time-domain simulations to investigate physical phenomena in more detail and demonstrate that it is possible to achieve a high Q over V ratio by employing 1D periodicity and various types of materials as low dielectric material.

There are two different methods to store photons for longer than one nanosecond in a wavelength-sized volume. One way is to rely on total internal reflection (ring or disc resonators), and the second is to employ strong light confinement of a photonic band gap in a well-designed structure [1, 2]. A combination of, these effects may also be employed, e.g. use of a photonic band gap in one dimension and total internal reflection in the other two dimensions. Total internal reflection only holds for a certain restricted range of wave vectors, and thus it becomes ineffective when the cavity size becomes small because localization in real space leads to delocalization in k-space, which eventually breaks the total internal reflection condition. Photonic band gap confinement works regardless of the wave vector range, and thus it is essentially better for confining light in a small volume than total internal reflection.

A modification of the original bowtie structure [3] is suggested in Fig. 1. Here we use different low dielectric material and buried channel [4] instead of a slit that goes all the way through the structure in the z direction. To excite our cavity we use an $\mathbf{E}_y$ field. However, because of the scattering element in the center of the structure (in this case a channel), other **E** field components appear ($\mathbf{E}_x$ and $\mathbf{E}_z$). These two additional **E** field elements are not confined in the structure and are radiated away. Therefore, $\mathbf{E}_x$ and $\mathbf{E}_z$ components in the center of a cavity are very small compared to the $\mathbf{E}_y$ field.

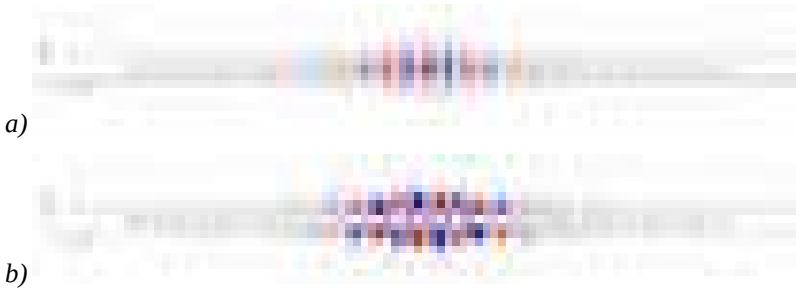

a)

b)

Figure 1. Bowtie structure with implemented channel or slit in the center. The field strength is shown in blue and red shades, where the saturation is normalized to the respective E-field maximum (a - $\boldsymbol{E_y}$ field, b - $\boldsymbol{E_x}$ field.).

In conclusion high Q and low V structures were simulated. Different designs of photonic crystal micro cavities were investigated and it was shown in more details that it is possible to get low modal volume by introducing a channel or a slit in the center of the micro cavity which however in turn causes delocalization in k-vector space and a low quality factor. It was demonstrated that a channel is better than a slit because of guiding by total internal reflection in the z direction. In addition to this, it was shown that cavities which have silicon dioxide as the low dielectric material are worse compared to cavities with air because of reduced total internal reflection. This drawback, however, has to be taken into account when considering devices with cladding instead of air bridges, because the latter are not useful for integrated devices.

[1] M. Notomi, E. Kuramochi, H. Taniyama, Ultrahigh-Q Nanocavity with 1D Photonic Gap, OPTICS EXPRESS, Vol. 16, No. 15, 11095-11102 (2008).
[2] Eiichi Kuramochi, Hideaki Taniyama, Takasumi Tanabe, Kohei Kawasaki,Young-Geun Roh, and Masaya Notomi, Ultrahigh-Q one-dimensional photonic crystal nanocavities with modulated mode-gap barriers on SiO2 claddings and on air claddings, OPTICS EXPRESS, Vol. 18, No. 15, 15859-15869 (2010).
[3] Ping Yu, Biao Qi, Xiaoqing Jiang, Minghua Wang, and Jianyi Yang, Ultrasmall-V high-Q photonic crystal nanobeam microcavities based on slot and hollow-core waveguides, OPTICS LETTERS, Vol. 36, No. 8, 1314 – 1316 (2011).
[4] A. Gondarenko, M. Lipson, Low modal volume dipole-like dielectric slab resonator, OPTICS EXPRESS, Vol. 16, No. 22, 17689-17694 (2008).

GENERATION OF TERAHERTZ RADIATION IN ATMOSPHERIC AIR

Dmitrij Chomčik[1], Ernestas Žeimys[1], Virgilijus Vaičaitis[2]

[1] Faculty of Physics, Vilnius University, Saulėtekio Ave. 9-III, LT-10222 Vilnius, Lithuania
[2] Laser Research Center, Department of Quantum Electronics, Vilnius University, Saulėtekio Ave. 10, LT-10223 Vilnius, Lithuania
dmitrij.chomcik@ff.stud.vu.lt

Generation and detection of terahertz (THz) electromagnetic radiation (with frequencies from 0.1 to 10 THz, and wavelengths from 0.03 to 3 mm) have not been investigated actively for a long time, though it's application in many different fields (medical imaging, spectroscopy, security screening, etc.) may be very fruitful. The reason for such a situation was the impossibility of applying radioelectronic devices or optical methods to examine THz radiation signals directly: terahertz frequency is too high for radioelectronic devices and too low for optical methods. Situation changed essentially when ultrafast lasers, which could generate femtosecond pulses, had been invented and became widely commercially available. Applications of these lasers have made new ultrafast optoelectronic methods of generation and detection of THz signals possible. One of these methods is the generation of THz radiation in the atmospheric air during the four-wave rectification process. The main advantage of this method is that it allows to use laser pulses of practically unlimited power and as a result extremely powerful broadband terahertz pulses can be produced by this method [1].

In our experiment plasma volume was created in atmospheric air by focused femtosecond laser pulses, and THz radiation was generated efficiently. As a pump source the Ti:Sapphire laser (pulse energy about 1 mJ, pulse duration about 120 fs, wavelength – 804 nm, pulse repetition frequency – 1 kHz) was used. The efficiency of terahertz radiation generation rises tens or even hundreds times when bichromatic pump pulses are used, therefore not only light pulses of 804 nm wavelength were used for air excitation but also second harmonic of the above-mentioned laser generated in nonlinear 100 μm-thick BBO crystal was used for the four-wave rectification in air.

Properties of generated THz pulses were investigated using the phenomenon of light polarization rotation in nonlinear crystals, exposed to the electric field of low-frequency electromagnetic radiation (electro-optical terahertz radiation detection method): a beam of femtosecond laser pulses, synchronized with the excitation, was probing electro-optic 0.5 mm-thick ZnTe crystal, which was exposed to the THz radiation electric field, and then this beam was split into two parts by a polarizing prism. Small changes of power of the obtained two beams are proportional to the electric field strength of THz pulses, so THz pulses can be fully characterized by means of changing the delay time between the probe and THz pulses. All measurements were controlled by the PC.

A few sets of dependencies of THz field strength on the distance d between the plasma volume and nonlinear BBO crystal as well as on the pump polarization have been registered. It was found that THz field strongly depends on d and pump polarization angle. The dependencies usually were periodic on d and showed some distinct maxima at pump polarization angle around 10, 120, 220 and 320 degrees. After optimization of experimental parameters the maximum THz energy conversion efficiency exceeded 10^{-6}, allowing to perform preliminary spectroscopic measurements.

Experimentally obtained results were compared to those obtained from the four-wave rectification model. The result of the comparison was encouraging – the four-wave rectification model suited experimental results well, though small mismatches arising from imperfections of this model still took place.

Typical form of the electric field of THz pulse registered under such conditions is shown in Fig. 1. One can see that the duration of generated THz pulse is several picoseconds and its electric field has both positive and negative components. Fourier analysis of such temporal electric field shape shows that pulse spectrum spans from 0.5 to 4 THz.

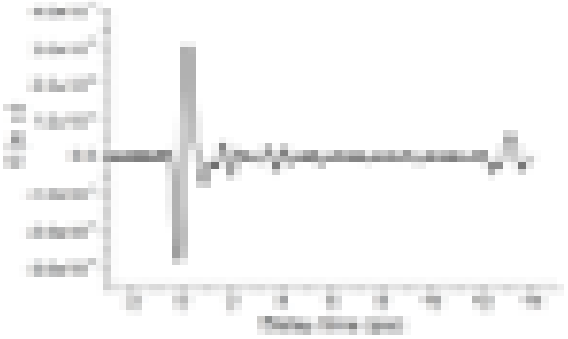

Fig. 1. Temporal electric field strength dependence of generated THz pulse (in arbitrary units).

Preliminary measurements of the absorption spectra of some materials (polyethylene, paper and nonlinear optical crystals) in 0.5-4 THz spectral range were also performed using this experimental setup.

Acknowledgements. Dmitrij Chomčik acknowledges Student Research Fellowship Award from the Lithuanian Science Council.

[1] D. J. Cook, R. M. Hochstrasser, Opt. Lett. **25**, 1211 (2000).

Q-SWITCHED MODE-LOCKED (QML) REGIME IN Nd:GdVO4 LASER WITH V3+ :YAG SATURABLE ABSORBER

Liubou Krylova[1]

[1]Department of Physics, Belarusian State University, Belarus
krylova lubou@mail.ru

The pulses at 1.3 μm have a great number of applications in various technical, technological and scientific applications. In present, many different laser materials are used, including Nd:KGW, Nd:YAG, Ng:$GdVO_4$. Several saturable absorbers such as semiconductor saturable absorber mirrors (SESAM), Co^{2+}-doped crystals, V^{3+}-doped crystals are employed as passive Q-switches. Crystals of V^{3+}:YAG have attracted great interest due to their excellent physical and optical performance at 1.34 μm, namely high ground state absorption cross-section, low density of saturation energy, high damage threshold. It makes them very attractive not only for effective passive Q-switched regime, but also for Q-switched mode locked (QML) regime applications. At that moment theoretical modeling for QML is done with the use of time-dependent spatially-concentrated model. Following model makes impossible to study pulse evolution dynamics and eliminates possibility of parametric optimization.

In previous paper [1] a time-space distributed model was introduced for laser which operated in continuous-wave regime. A range of microchip laser medium parameters that allows achieving optimal output parameters was considered in [2]. In this work a similar model is used to simulate QML regime in Nd:GdVO4 laser with V^{3+} :YAG saturable absorber. Two goals are pointed out. The first one is to obtain the dynamics of the laser pulse formation. The second one is to determine influence of the resonator geometry and influence of additional reflection (at the end of medium rod) on lasing. The system solved is as follows:

$$\frac{1}{c}\frac{\partial I^{\pm}_{gen}}{\partial t} \pm \frac{\partial I^{\pm}_{gen}}{\partial x} = (\gamma_1 n_1 + \gamma_3) I^{\pm}_{gen} + \delta \frac{1}{\tau} n_2 N_0 \hbar \nu_{gen} L_{med} + \gamma_3 \Delta_1 (1-y) \Delta_2 y I^{\pm}_{gen}; \tag{1}$$

$$\frac{dy}{dt} = \theta_3 (1-y) - \left(I^{+}_{gen} + I^{-}_{gen}\right) y \theta_1; \quad \frac{dn}{dt} = (1-n_2) I_0 \alpha_1 - \alpha_2 \left(I^{+}_{gen} + I^{-}_{gen}\right) n_2 - n_2 \alpha_3. \tag{2}$$

Where $I^{\pm}_{gen}$ stands for lasing intensity, I_0 for pump intensity, y for density of the ground states of saturable absorber related to saturable absorber concentration, n_2 for density of the exited neodim ions related to overall concentration. This system is solved numerically by the means of finite-difference scheme [3]. The simulation result is on fig. 1

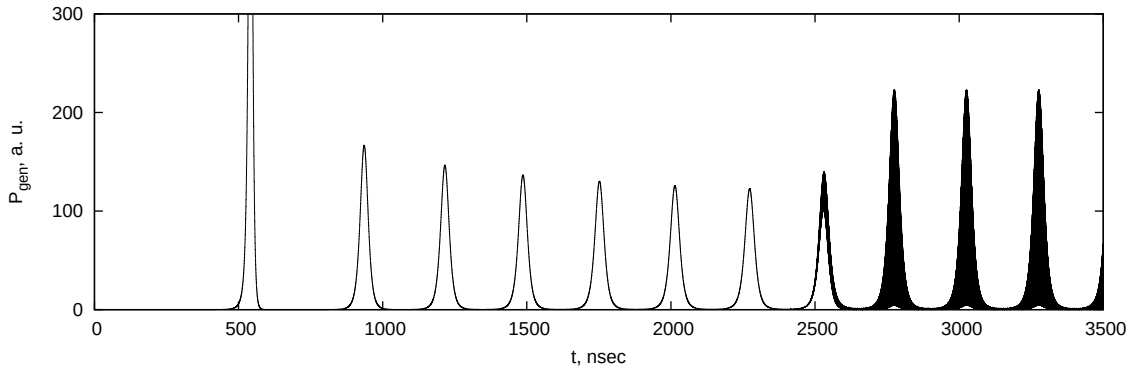

Fig. 1. Output power time dependency

This figure illustrates the process of the pulse train formation dynamics in the case, when there are no gaps between input mirror, medium, saturable absorber and output mirror. One can see, that the first pulse is the most powerful, consequent pulses gradually transform to a broad pulse with high-frequency modulated structure.

Finally, the process of the pulse train forming was considered at different parameters, namely resonator length and the position of saturable absorber. Obtained results open a possibility of parametric optimization of dynamical characteristics.

[1] L. G. Krylova et. al., *Influence of Spatial Nonhomogenity of Pump Energy Distribution on Output Characteristics of Yb:Er Laser with Longitudinal Pump*, Nonlinear Phenomena in Complex Systems, **13**, 368-380 (2010)
[2] L. I. Burov, L. G. Krylova, *Er-Yb laser microchip optimization*. JAS (accepted to publication) (2012)
[3] V. A. Iljina, P. K. Silaev. *Numerical methods for physisits-theoreticians (in russian)*, part 2. (Moscow, 2004).

ORAL SESSION II

STIMUTALED EMISSION AND CONCENTRATION QUENCHING OF PERYLENE DIIMIDE DERIVATIVES

G. Armonaitė[1], K. Kazlauskas[1], A. Miasojedovas[1], S. Valiyaveettil[2], J.V. Gražulevičius[3], S. Juršėnas[1]

[1] Institute of Applied Research, Vilnius University, Saulėtekio 9-III, LT-10222 Vilnius, Lithuania
[2] S5-01-01, Materials Research Laboratory, Department of Chemistry, National University of Singapore, 3 Science drive 3, Singapore 117 543
[3] Department of Organic Technology, Kaunas University of Technology, Radvilėnu pl. 19, LT-50254, Kaunas, Lithuania
armonaite.gintare@gmail.com

Perylene diimide (PDI) derivatives are one of the most stabile organic compounds found in literature. Moreover, they demonstrate well expressed π-conjugation and high fluorescence (FL) quantum yield. These properties enable optoelectronic applications such as organic light emitting devices or organic lasers. However, a few problems need to be solved yet. First, PDI-based emissive layer should demonstrate spectral tunability and, second, fluorescence concentration quenching should be minimized. Structural modification of the PDI by substituents at the bay position of the PDI core seems to be promising. Substituents are shown to cause PDI core twisting and steric hindrance effects, which prevents close molecule packing resulting in the suppression of excitation migration, and thus, FL concentration quenching [1].

Here we report amplified spontaneous emission (ASE) as well as FL concentration quenching results of three PDI derivatives with different substituents at the bay position. For comparison, unsubstituted PDI derivative was also explored. By examining the concentration dependence of the fluorescence, absorption and transient absorption spectra as well as FL quantum yield, ASE and fluorescence transients structure-property relationship of the PDI derivatives was determined.

Fluorescence and absorption spectra indicated that electron withdrawing substituents have pronounced impact on exitonic interaction. The unsubstituted PDI compound at high concentrations showed absorption spectrum broadening and red shift of the fluorescence spectrum, which suggested the formation of J-type aggregates [2]. Fluorescence and absorption spectra of the PDI compound with bromine substituent demonstrated smaller broadening at high concentrations than unsubstituted PDI. This can be attributed to the twisting of the perylene diimide core induced by the bromine substituent at the bay position. Moreover, 2,4-di(trifluoromethyl)phenyl-substituted PDI showed the smallest shift of the emission maximum as a function of concentration. Quantum chemical calculation indicated that 2,4-di(trifluoromethyl)phenyl-substituted PDI, in addition to the core twisting, exhibits substituent out-of-plane twisting [3]. Similar twisting was also present in the 4-pyridyl-substituted PDI. For these two compounds absorption spectra showed minimal broadening. The results clearly demonstrate that the bay-substitution of PDI prevents molecule close packing and suppress aggregate formation in the solid state. This reduces excitation migration and thus minimizes fluorescence concentration quenching. Fluorescence quantum yield dependence on the PDI doping level was also examined. The bay substitution allowed 3-4 times higher doping levels (as compared to the doping with unsubstituted PDI) at which half of the initial FL quantum yield was still preserved. High fluorescence quantum yield at high doping levels is essential for high efficiency emissive layers. Transient absorption measurements indicated presence of the stimulated emission in all the PDI compounds studied. Thus, ASE in the PDI derivatives was investigated in detail and ASE threshold dependence on the PDI concentration was determined. It was found that electron withdrawing substituents have high impact on the ASE spectral behavior and ASE threshold value. For all the PDI derivatives at low concentrations ASE threshold decreased, while at higher doping levels it increased. The increase in ASE threshold at high PDI concentration is due to the formation of molecular aggregates acting as quenchers of molecular emission. Minimal ASE threshold was as low as 70 kW/cm^2 for bromo-substituted PDI, 170 kW/cm^2 for 2,4-di(trifluoromethyl)phenyl-substituted PDI and 820 kW/cm^2 for 4-pyridyl-substituted PDI at an optimal concentration of 0.25-0.5 wt %. Although obtained ASE thresholds were significantly higher as compared to that of the unsubstituted PDI (20 kW/cm^2), the bay-substitution benefited in allowing observation of ASE at one order of magnitude higher concentrations and for a wider concentration range (0.06 – 4 wt %). Additionally, photostability for all the PDI was measured. The results indicate that the bay-substituted PDI derivatives show about an order of magnitude higher photostability as compared to other various organic compounds including other bay-substituted PDIs.

In conclusion, amplified stimulated emission and FL quantum yield studies suggest that PDI derivatives substituted at the bay position of the PDI core are suitable for active media in laser applications. Bay substituents allow achieving significantly lower ASE thresholds, higher FL quantum yield and photostability at high PDI concentrations as compared to the unsubstituted PDI.

[1] A. Miasojedovas, K. Kazlauskas, G. Armonaitė, S. Valiyaveettil, V. Gražulevičius, S. Juršėnas, Dyes and Pigments, 2012, 92, 1285.
[2] V. Sivamurugan, K. Kazlauskas, S. Juršėnas, A. Gruodis, J. Simokaitienė, J. V. Gražulevičius, S. Valiyaveettil, J. Phys. Chem. B; 2010, 114, 1782.
[3] T. E. Keiser, V. Stepanenko, F. Würthner, J Am Chem Soc; 2009, 131, 6719.

STUDY OF SPECTRUM RESOLVED PHOTOLUMINESCENCE AND PHOTOCONDUCTIVITY TRANSIENTS IN GaN AND Cu_2S/CdS STRUCTURES

[1)]Tomas Babelis, [2)]Jevgenij Brytavskiy, [1)]Rokas Skaisgiris, [1)]Aurimas Uleckas, [1)]Eugenijus Gaubas

[1)]Institute of Applied Research, Vilnius University, Sauletekio Ave. 9-III, LT-10222 Vilnius
[2)]Odessa Mechnikov National University, Dvoryanskaya 2, Odessa, Ukraine
tomas.babelis@ff.stud.vu.lt

GaN-based materials that are widely used in fabrication of efficient short-wavelength light emitters [1-3] have also a high potential in radiation-hard particle detectors [4] and GaN/In tandem solar cells [2]. The Cu_2S/CdS heterojunction structures are also promising in fabrication of solar cells [5]. The key issue of these materials quality is high dislocation density (10^8–10^{10} cm^{-2}) and of different species of point defects. The role of these defects in radiative and nonradiative recombination depends on dislocation core structure, dislocation orientation and type and density of point defects. Recently, deep-trap saturation effects under high excitation and non-linear carrier trapping transient phenomena have been demonstrated in GaN. In this study, the correlation between the photoconductivity (PCT) transients and time resolved photoluminescence (PL) spectra in GaN epilayers as-grown by metalorganic chemical vapor deposition (MOCVD) and polycrystalline structures have been examined.

A set of samples under investigation consisted of 2-12 μm thick films of semi-insulating epitaxial GaN layers as-grown by MOCVD on sapphire substrate with unintentionally doped n-GaN buffer. The sapphire substrates were polished and transparent, so PL signals were recorded from GaN face-surface as well as from substrate side. The Cu_2S/CdS heterojunction structures of 25/1 μm thick films were deposited on glass substrates.

Room temperature PL and PCT measurements were carried out under excitation by pulsed 400 ps yttrium-aluminium-garnet (YAG:Nd^{3+}) laser at 356 nm wavelength. The PL signal was dispersed by a double monochromator or by using band filters and detected using a UV-enhanced photomultiplier. Measurements of the carrier decays were performed using non-invasive microwave (MW) probed photoconductivity technique. The needle-tip MW antenna was exploited to probe UV excited area (1 mm^2) of the sample. Thereby, the PCT and PL transients were registered simultaneously.

The excess-carrier density decays in GaN were obtained to be observable in a wide time scale ranging from 1 ns to 400 ms. The two-componential character of these decays has been revealed. Initial, fast PCT component, with relaxation shape close to exponential decay, with durations of the order 1 ns correlates well with that of PL transients. However, the second long time relaxation component can be only approximated by using stretched-exponent approach [6,7]. The similar behaviour and correlation of PCT and PL transients have been revealed in Cu_2S/CdS heterojunction structures.

The parameters of decay rate have been extracted based on analysis of the PL and PCT transients. The initial decay component has been attributed to excitonic and trap-assisted radiative recombination inside micro-crystalline volumes within disordered structures. The stretched-exponent decay PCT component is ascribed to non-radiative recombination assisted by random–walk carrier transport within defect-rich material surrounding the micro-crystalline columns or inclusions within the polycrystalline structures.

[1] S.Nakamura and G.Fasol, *The Blue Laser Diode: GaN Based Light Emitters and Lasers*. Springer, Berlin, 1997.
[2] M.A.Reshchikov and H.Morkoc, Luminescence properties of defects in GaN, J. APPL. PHYS. **97** (2005) 061301.
[3] A.Žukauskas, M.S.Shur, R. Gaska, *Introduction to Solid-State Lighting*. Wiley, New York, 2002.
[4] E.Gaubas, S.Juršenas, S.Miasojedovas, J.Vaitkus, A.Žukauskas, Carrier and defect dynamics in photoexcited semi-insulating epitaxial GaN layers. J. APPL. PHYS. **96** (2004) 4326.
[5] J.Oualid, D.Sarti, J.Gervais, S.Martinuzzi. Characterisation of electron traps in Cu_2S-CdS polycrystalline cells by capacitance transient measurements. J.Phys.C: Solid State Physics, **12** (1979) 2313.
[6] G.Pfister and H.Sher, Advances in Physics, **27** (1978) 747.
[7] L.Pavesi, J. Appl. Phys. **80** (1996) 216.

PYRENYL-FUNCTIONALIZED FLUORENE AND CARBAZOLE DERIVATIVES AS BLUE LIGHT EMITTERS

Simonas Krotkus[1], Karolis Kazlauskas[1], Arūnas Miasojėdovas[1], Alytis Gruodis[2], Saulius Juršėnas[1]

[1] Institute of Applied Research, Vilnius University, Saulėtekio 9-III, LT-10222, Vilnius, Lithuania
[2] Department of General Physics and Spectroscopy, Vilnius University, Saulėtekio 9-III, LT-10222, Vilnius, Lithuania
simonas.krotkus@ff.stud.vu.lt

Synthesis and characterization of the novel molecular systems stimulates ongoing growth of the field of organic optoelectronics. Among rich variety of organic compounds the class of small molecules is beneficial especially for the field of organic light emitting devices due to their exceptionally high purity, well-defined structure and possibility of the film formation from either solution or sublimation in vacuum. Whereas, since common purification techniques of column chromatography, recrystallization and vacuum sublimation are not applicable to solution processed polymer films, they suffer from difficult control of molecular weight, polydispersity and high density of impurities which results in strong fluorescence quenching and trapping of the injected charges. Therefore, research interest in solution processed small molecule light emitting devices which combine both advantages of easy synthesis and low cost production process was growing rapidly in recent years. However, thermal and morphological stability of solution-processed films in addition to optimization of device fabrication procedure still needs to be improved in order to reach the level of performance demonstrated of their vacuum-deposited counterparts. Consequently, search of new organic compounds with superior optical and electrical properties in addition to high glass transition temperature and low tendency to crystallize is in demand. Current attention is being focused on multifunctional compounds consisting of several bridged polycyclic aromatic moieties which are considered to be promising raw material for the state-of-the-art solution-processable light-emitting device.

In this work, series of pyrene-functionalized soluble 9-alkyl-carbazole and 9-alkyl-fluorene compounds have been designed, synthesized and investigated as blue emitting materials.. Most of the synthesized compounds were capable to form glasses with glass transition temperatures up to 105 °C. The mono- and di-substituted compounds exhibited efficient emission in a diluted form with the peak wavelengths of 416 nm and 422 nm, and quantum yields of 0.72 and 0.82, respectively. Photophysical properties of the compounds in dilute solutions and solid state were investigated experimentally and rationalized by density functional theory calculations. The calculations revealed low energy barrier for intramolecular twisting in the ground and excited states. The electronic spectra of the compounds were dominated by an allowed “pyrene-like” S0 → S2 transition prevailing in nearly perpendicularly-twisted molecular structures and competitive S0 → S1 transition becoming increasingly allowed for more planar conformers. The di-substituted compounds demonstrated 3-fold enhanced oscillator strength of S0 → S1 transition giving rise to the enhanced fluorescence quantum yield, significant shortening of the fluorescence lifetimes (from 2.5 ns down to 1.0 ns) and 3-fold reduced amplified spontaneous emission threshold as compared to those of the mono-substituted compounds. Introduction of the bulky dihexyl group into the pyrenyl di-substituted fluorene enabled remarkable suppression of emission concentration quenching in a solid state and ensured high emission quantum yield (0.63) in the wet-casted neat films. Pyrenyl di-substitution of fluorene and sterically hindered aliphatic group enabled observation of a low amplified spontaneous emission threshold (20 kW/cm^2) for the compound dispersed in the inert polystyrene host at a rather large (5 wt %) chromophore concentration.

STIMULATED EMISSION AND PHOTOLUMINESCENCE EFFICIENCY DROOP IN EPITAXIAL GaN

Jonas Jurkevičius

Department of Semiconductor Physics, Vilnius University, Saulėtekio Ave. 9-III, LT-10222 Vilnius, Lithuania
getjonas@gmail.com

III-nitride compounds are an important wide band-gap semiconductor group for development of light emitting diodes (LED) and laser diodes with emission ranging from green to UV. One of the key challenges encountered in many LED applications is the efficiency droop effect, i.e., decrease of luminescence efficiency with increasing driving current density or photoexcitation power density. The origin or origins of the droop are still not clear, though several mechanisms have been proposed to interpret the droop. To minimize the possible origins of the droop, we studied GaN epilayers, instead of LED heterostructures, which are more thoroughly but still not productively studied.

In this report, we present the study of photoluminescence (PL) efficiency in epitaxial GaN layers with different carrier lifetimes ranging from 40 to 3600 ps. PL spectra were measured under quasi-steady-state excitation conditions in front face and edge emission configurations to study spontaneous and stimulated emission spectra, respectively. Frequency quadrupled Nd:YAG laser radiation was used as a pulsed photoexcitation source (pulse duration 10 nm). Measurements were carried out under various excitation densities (0.01 – 1 MW /cm^2) at room temperature.

PL efficiency dependences on excitation power densities were obtained in two measurement configurations. PL efficiency growth with increasing excitation power density might be explained by saturation of nonradiative recombination centers and increasing contribution of bimolecular recombination. Growth of PL efficiency is faster in samples with higher carrier lifetimes. At high excitation power density, PL efficiency droop is evident in all samples under study. In samples with lower carrier lifetime, droop onset is observed at higher excitation power densities. Stimulated emission threshold dependences on carrier lifetime obtained both in front face and edge configurations show that stimulated emission threshold decreases with increasing carrier lifetime. At excitation power densities exceeding the threshold, a larger increase in PL efficiency growth rate is observed for samples with higher carrier lifetimes. Additionally, we show that stimulated emission thresholds in edge configuration coincide with the onset of the decrease of PL efficiency at front face configuration. These results show that PL efficiency droop in GaN epitaxial layers might be related to the onset of stimulated emission.

ORAL SESSION III

QUANTUM TRANSPORT IN DISORDERED LATTICES

Vytautas Abramavičius[1], Darius Abramavičius[2]

[1] Department of Theoretical Physics, Faculty of Physics, Vilnius University, Saulėtekio 9, LT-10222 Vilnius, Lithuania
vytautas.ab@gmail.com

Good understanding of charge and energy transport phenomena in molecular materials is crucial for practical applications, e.g., in solar cells. At a molecular level these are quantum systems which interact strongly with the environment. This interaction leads to irreversible charge and energy excitation dynamics. Transport processes are usually described using methods based on the calculation of reduced density matrix of the system under consideration (Redfield [1], Lindblad [2] equations). All these methods require great amount of computational power.

In this work we describe the system using a stochastic Hamiltonian with fluctuating elements which reflect the influence of the environment on relevant parameters of the system. We apply this fluctuating Hamiltonian for the charge transfer in cubic lattice and describe how real and complex fluctuations affect system's population dynamics and the charge mobility.

We investigate charge transfer processes in a cubic lattice with N sites. One site represents a charged (or uncharged) state characterized by an energy value. We consider a disordered system, thus site energies E_{site} are random values with uniform distribution. Moreover, a constant external electric field can be applied across the lattice. In this case site energies E_{s} are equal to

$$E_{\text{s}} = E_{\text{site}} + \left(\mathbf{F}\cdot\mathbf{r}\right), \tag{1}$$

where **F** is external electric field vector and **r** is site radius-vector.

If there is only one charge in the lattice it can be described by a general Hamiltonian which includes our system, its surrounding environment (bath) and system-bath coupling and acts in Hilbert space of system and bath:

$$\hat{H}_{\text{s+b}} = \hat{H}_{\text{s}} + \hat{H}_{\text{b}} + \hat{H}_{\text{coup}} = \sum_i E_i^{(\text{s})} \left|i\right\rangle\!\left\langle i\right| + \sum_i \sum_j J_{ij} \left|i\right\rangle\!\left\langle j\right| + \sum_\alpha E_\alpha^{(\text{b})} \left|\alpha\right\rangle\!\left\langle\beta\right| + \sum_u \hat{K}_u \hat{\Phi}_u \tag{2}$$

Here $\left|i\right\rangle$ is the site basis in system's Hilbert space, $\left|\alpha\right\rangle$ is harmonic oscillator eigenbasis in bath's Hilbert space, $\hat{K}_u$ is the system part of coupling, $\hat{\Phi}_u$ is the bath part of coupling.

The bath consists of infinite number of quantum harmonic oscillators coupled to each state of our system. This influence is accounted by introducing quasiclassically a fluctuating external field represented by time-dependent random-valued functions $W(t)$ into the system Hamiltonian part thus making it equal to

$$\hat{H}(t) = \hat{H}_{\text{s}} + \hat{H}_{\text{t}}(t) = \sum_i E_i^{(\text{s})} \left|i\right\rangle\!\left\langle i\right| + \sum_i \sum_j \left(J_{ij} + W_{ij}(t)\right) \left|i\right\rangle\!\left\langle j\right|. \tag{3}$$

Functions $W(t)$ have a correlation function equal to that of fluctuating bath operators: $C(t) = \left\langle \hat{\Phi}(0)\hat{\Phi}(t)\right\rangle$. Depending on $C(t)$ functions $W(t)$ can be either real-valued or complex-valued, thus system Hamiltonian can therefore be either Hermitian or non-Hermitian.

The state of the system is described by a state vector $\left|\psi(t)\right\rangle$. Its evolution is given by the propagator $\hat{U}(t,t_0)$. When the time difference $\Delta t = t - t_0$ is sufficiently small the propagator can be written in the following way:

$$\hat{U}(t,t_0) = \exp\left(-\frac{i}{\hbar}\hat{H}_0\Delta t\right)\exp\left(-\frac{i}{\hbar}\hat{H}_t(t_0)\Delta t\right)\left|\psi(t_0)\right\rangle \tag{4}$$

Having state vector dependency on time we can calculate the distribution of system's populations with respect to state energies. Due to the fact that system's Hamiltonian is stochastic we must average over many realizations of the state vector to get accurate results.

We can observe that complex fluctuations correctly depict system's population dynamics while real fluctuations correspond to infinite temperature regime. We also note that charge mobility depends on external electric field strength when using complex fluctuations and does not depend on it with real fluctuations.

[1] V. May, O Kühn, *Charge and Energy Transfer Dynamics in Molecular Systems – 2nd ed.,* (Wiley-VCH, Weinheim, 2004).

[2] H. P. Breuer, F. Petruccione, *The Theory of Open Quantum Systems,* (Oxford University Press, New York, 2007).

ASYMPTOTIC TRANSMISSION COEFFICIENT FORMULA FOR ONE-DIMENSIONAL NON-STATIONARY QUANTUM TRANSPORT

Maxim Belov[1], George Krylov[2]

[1],[2]Department of Physics, Belarusian State University, Republic of Belarus
mpui@tut.by

Nanoscale device predictive simulations are undoubtedly vital for development of several branches of science and technology. Among approaches to the nanoscale device simulation, coherent quantum transport calculations can be pointed out. These calculations provide electric properties of given samples, namely resistance or conductance dependencies. Landauer-Büttiker formalism expresses system conductivity (specific conductance) through it is transmission coefficients [1]. Transmission coefficients are determined from solutions of Schrödinger equation, that describes system. Plane wave approximation [2] is usually used; it is based on time-independent Schrödinger equation:

$$\hat{H}\psi_E(x) = -\frac{\hbar^2}{2m}\frac{\partial^2}{\partial x^2}\psi_E(x) + U(x)\psi_E(x,t) = E\psi_E(x). \tag{1}$$

Potential $U(x)$ is chosen constant at $x < x_{\sigma'}$ and $x > x_\sigma$ and has the following form

$$U(x) = \theta(x_{\sigma'} - x)U_l + \theta(x - x_{\sigma'})\theta(x_\sigma - x)U_m(x) + \theta(x - x_\sigma)U_r, \tag{2}$$

where $\theta(x)$ stands for Heaviside theta function. As the potential can be chosen regardless to a constant term, so the case of $U_l = 0$ is chosen. Thus eigenfunctions $\psi_E(x)$ of equation (1) are as follows:

$$\psi_E(x) = \theta(x_{\sigma'} - x)(1 + r(E))\exp(\mathrm{i}\frac{\sqrt{2mE}}{\hbar}x) + \theta(x - x_{\sigma'})\theta(x_\sigma - x)f(x) + \theta(x - x_\sigma)t(E)\exp(\mathrm{i}\frac{\sqrt{2m(E - U_r)}}{\hbar}x), \tag{3}$$

where $r(E)$ and $t(E)$ stand for reflection and transmission amplitude for a particle with fixed energy E. Appropriate transmission coefficient is determined with respect to particle flux:

$$T(E) = \sqrt{\frac{E}{E - U_r}}\,|t(E)|^2. \tag{4}$$

However, this approach renders no possibility to represent particle states with wave packages. In order to do that, one has to solve time-dependent Schrödinger equation with the same potential as in (2) and initial conditions representing a wave package on the left to the system:

$$\mathrm{i}\hbar\frac{\partial}{\partial t}\psi(x,t) = \hat{H}\psi(x,t) = -\frac{\hbar^2}{2m}\frac{\partial^2}{\partial x^2}\psi(x,t) + U(x)\psi(x,t), \tag{5}$$

$$\psi(x,0) = \theta(x_{\sigma'} - x)\psi_0(x), \tag{6}$$

and calculate the transmission coefficient as probability of a wave package to pass through the system

$$T = \lim_{t\to\infty}\int_{x_\sigma}^{\infty} |\psi(x,t)|^2\,dx. \tag{7}$$

However, solution of (5) is much more complicated than solution of (1). A novel approach is presented to link the non-stationary (7) and the stationary (4) transmission coefficients. Plane wave decomposition is done for initial wave package (6):

$$\psi_0(p,0) = \frac{1}{\sqrt{2\pi}}\int_{-\infty}^{\infty}\psi(x,0)\exp(-\mathrm{i}px)dx. \tag{8}$$

Final formula expresses non-stationary T with stationary T(E):

$$T = \int_0^{\infty} T(E)\,|\psi_0(E,0)|^2\,dE = \int_{-\infty}^{\infty} T(E(p))\,|\psi_0(p,0)|^2\,\frac{p}{m}dp, \tag{9}$$

where momentum is chosen as the integration variable in the right part, replacing $E(p) = \frac{p^2}{2m}$, and, appropriately, $dE = \frac{pdp}{m}$. This formula is validated for cases of free motion and step potential and rectangular barrier potential, some other consistency checks are done.

Finally a formula was obtained that helps one to avoid solution of (5) when he only wants to determine transmission coefficients. However it still requires strict mathematical prove.

---

[1] M. Büttiker, Y. Imry, R. Landauer and S. Pinhas., Phys. Rev. **B 31**, 6207(1985)
[2] L. D. Landau, E. M. Lifshitz. *Quantum Mechanics: Non-Relativistic Theory.* **Vol. 3** (3rd ed.) (Pergamon Press. 1977)

Anderson localization in random quantum walks with shift operation disorder

Vladimir Chorošajev[1], Andre Ahlbrecht[2], Albert H. Werner[2], Volkher B. Scholz[2], Reinhard F. Werner[2]

[1]Department of Theoretical Physics, Faculty of Physics, Vilnius University, Saulėtekio Ave. 9-III, LT-10222, Vilnius, Lithuania

[2]Institut für Theoretische Physik, Leibniz Universität Hannover, Appelstr. 2, 30167 Hannover, Germany

vladimir.chorosajev@gmail.com

Classical random walks have numerous applications in search and connectivity algorithms. Their quantum variant, named *quantum walks*, and its applications was extensively studied over the last decade, the main reason for that being the fact that quantum walks based search algorithms can exhibit polynomial and even exponential speedup compared to the classical case. Quantum walks have also been shown to form a convenient base for a number of simulations, ranging from energy transfer in biological systems to quantum cellular automata. Recently multiple experimental realizations of quantum random walks have been demonstrated, such as neutral atoms in an optical lattice etc. The crucial distinction between classical and quantum random walks is that the classical random walk is essentially a diffusive process, while its quantum counterpart can spread ballistically due to quantum coherences. The faster spreading rate thus provides the speedup in algorithms based on quantum walks. On the other hand, they have proven to be very sensitive to perturbations, which can alter the dynamics of the system considerably.

In its simplest form a quantum random walk is given by a spin-$\frac{1}{2}$ particle on a one-dimensional lattice with discrete-time evolution. The Hilbert space of the system is hence $\mathscr{H} = \ell_2(\mathbb{Z}) \otimes \mathbb{C}^2$, with $\ell_2(\mathbb{Z})$ being the space of square-summable sequences over $\mathbb{Z}$. The general state of the walker is then written as $|\Psi(t)\rangle = \sum_{x,i} a_{x,i}(t)|x,\phi\rangle$,with the normalization condition $\sum_{x,i} |a_{x,i}(t)|^2 = 1$, and $|x,\phi\rangle = |x\rangle \otimes |\phi\rangle : x \in \mathbb{Z}, \phi \in \mathbb{C}^2$. We denote by $|+\rangle, |-\rangle$ the orthonormal standard basis of $\mathbb{C}^2$.

Each step in the time evolution of the system is described by a unitary *walk operator* W, which is assumed to be constant in time. It is defined as a product of two types of unitary operators, the first being the *coin* C, acting locally on the internal particle degrees of freedom (traditionally called the "coin" subspace, with reference to "flipping the coin"), and the second being the *shift* S, acting on the lattice position degree of freedom. As the local coin operation we take the commonly used Hadamard operator, applying it at each lattice point:

$$C = \bigoplus_{i \in \mathbb{N}} H, \text{ where } H = \frac{1}{\sqrt{2}} \begin{pmatrix} 1 & 1 \\ 1 & -1 \end{pmatrix} \tag{1}$$

The shift operation is defined locally as:

$$S|x,+\rangle = \sqrt{p_x}|x+1,+\rangle - \sqrt{1-p_x}|x,-\rangle \tag{2}$$

$$S|x,-\rangle = \sqrt{p_{x-1}}|x-1,-\rangle + \sqrt{1-p_{x-1}}|x,+\rangle \tag{3}$$

It has been shown, that in case the system is translation invariant, i.e. p_x is the same at each lattice point, the quantum walker spreads ballistically on the lattice. Breaking the translation invariance by means of individually independently drawing each local coin operation from the $SU(2)$ group has been studied in detail in [1]. In this work we perform the analysis of the system dynamics in case the local shift parameter p_x is independently identically distributed corresponding to any non-degenerate distribution. In this case, just like in the case with coin operation disorder, the behaviour of the particle exhibits dynamical localization. It means that a particle stays in a finite region in the position subspace up to exponential tails. Strictly speaking, there exists such a function $L(n)$ that goes to zero faster than any polynomial in n,such that:

$$\mathbb{E}\left(\sup_{t \in \mathbb{N}} |\langle x,\phi|W^t|y,\psi\rangle|\right) \leq L(|x-y|) \tag{4}$$

This phenomenon is similar to disorder in crystals, described by Anderson in [2], although instead of random space-dependent potential the characteristic behaviour of the system is governed by randomness in the unitary evolution. The main result is presented in the following theorem:

Theorem. *Let μ be any non-degenerate distribution, and let W_ω be a random quantum walk with shift disorder characterized by a shift parameter distribution μ. Then W_ω exhibits dynamical localization with respect to a subset O of the unit circle $\mathbb{T}$ for all but up to four points in the spectrum of W_ω.*

In the presentation a condensed version of the proof of the stated theorem will be given, with some numerical results illustrating the phenomena and giving a comparison between the undisturbed walk and the dynamics in presence of the shift disorder.

---

[1] A. Ahlbrecht, V. B. Scholz, and A. H. Werner, Disordered quantum walks in one lattice dimension, J. Math. Phys. **52**,102201 (2011).

[2] P.W.Anderson, Absence of Diffusion in Certain Random Lattices, Phys. Rev.**109**, 1492-1505 (1952).

INSIGHTS ON THE MODELS OF PHOTOSYSTEM II REACTION CENTER FROM TWO DIMENSIONAL OPTICAL SPECTROSCOPY

Andrius Gelžinis[1], Darius Abramavičius[1,2], Leonas Valkūnas[1,3]

[1] Department of Theoretical Physics, Faculty of Physics of Vilnius University,
Sauletekio Avenue 9, build. 3, 10222 Vilnius, Lithuania
[2] State Key Laboratory of Supramolecular Complexes, Jilin University,
2699 Qianjin Street, Changchun 130012, PR China
[3] Center for Physical Sciences and Technology, Savanoriu Avenue 231, 02300 Vilnius, Lithuania

andrius.gelzinis@ff.stud.vu.lt

Photosystem 2 is a unique biological system because it is capable of oxidizing water to molecular oxygen [1]. Its reaction center (RC) is responsible for primary charge separation process [1]. The exact mechanisms ant timescales of charge transfer in this system are still not clear, thus the PS II RC system is currently under active investigation.

Much of the information about PS II RC is due to spectroscopic measurements [1]. Theoretical models are necessary in order to correctly interpret the experiments. Two rather different models of PS II RC, which employ completely different bath spectral density, were developed by Novoderezhkin [2] and Renger [3]. Both of them can be used to successfuly explain the linear spectra (absorption, fluorescence, etc.) of the system at various temperatures. More elaborate experiments are needed in order to distinguish between these models.

Two dimensional (2D) optical spectroscopy is a novel tool that greatly contributed to our understanding of photosynthetic systems [4]. Recently, 2D spectra of PS II RC were measured [5]. In this work we simulate the 2D spectra of PS II RC using both models. We show that while absorption spectra calculated from these models are very similar, there are significant differences in 2D spectra (see Fig. 1.). We conclude that Renger's model better agrees with the experiment.

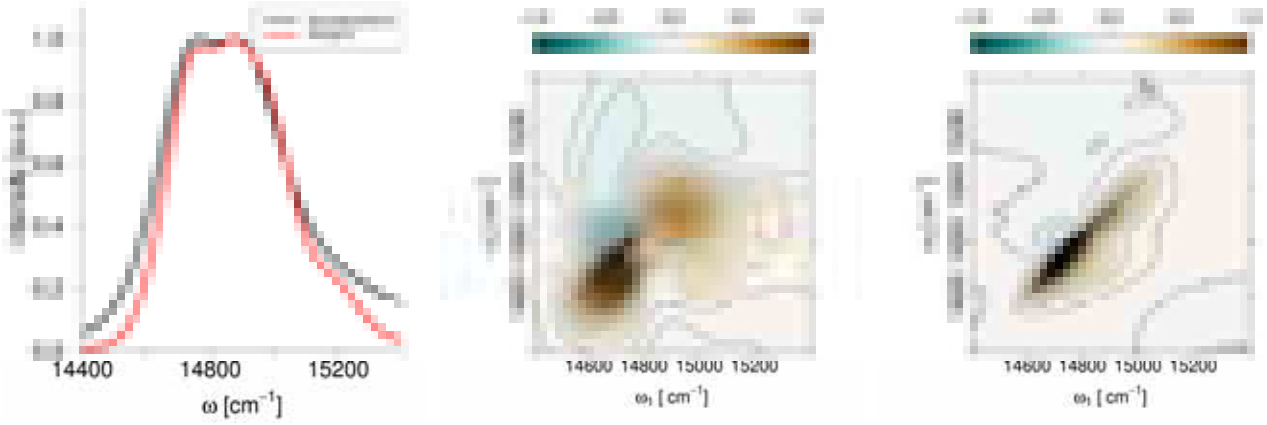

a) b) c)

Fig.1. Absorbtion spectra of PS II RC calculated using Novoderezhkin's and Renger's models a); sample 2D spectra of PS II RC calculated using b) Novoderezhkin's and c) Renger's models.

[1] R. E. Blankenship, *Molecular Mechanisms of Photosynthesis* (Blackwell Science Ltd, Oxford, 2002).

[2] V. I. Novoderezhkin, E. G. Andrizhiyevskaya, J. P. Dekker, R. van Grondelle, Pathways and timescales of primary charge separation in the photosystem ii reaction center as revealed by a simultaneous fit of time-resolved fluorescence and transient absorption, Biophys. J. **89**, 1464 – 1481 (2005).

[3] G. Raszweski, W. Saenger, T. Renger, Theory of optical spectra of photosystem II reaction centers: Location of the triplet state and the identity of the primary electron donor, Biophys. J. **88**, 986–998 (2005).

[4] T. Brixner, J. Stenger, H. M. Vaswani, M. Cho, R. E. Blankenship, G. R. Fleming, Two-dimensional spectroscopy of electronic couplings in photosynthesis, Nature **434**, 625–628 (2005).

[5] J. A. Myers, K. L. M. Lewis, F. D. Fuller, P. F. Tekavec, C. F. Yocum, J. P. Ogilvie, Two-dimensional electronic spectroscopy of the d1-d2-cyt b559 photosystem ii reaction center complex, J. Phys. Chem. Lett. **1**, 2774–2780 (2010).

STATISTICAL ERRORS IN OVERCOMPLETE QUANTUM TOMOGRAPHY

Aleksander M. Kubica[1]

[1] Institute for Quantum Information, California Institute of Technology,
1200 E California Blvd, MC 305-16, Pasadena, CA 91125, USA
akubica@caltech.edu

Probably everyone has heard about quantum computers [1]. Using a quantum computer we can do things which are unimaginable or at least very counter-intuitive to perform in classical world. The very famous examples are: Shor's algorithm and quantum teleportation [1]. Shor's algorithm solves a problem of finding prime factors of an integer N in time polynomial in log(N), whereas classical counterparts work in sub-exponential time. This task is not only of interest to mathematicians but is vital in modern cryptography (e.g. RSA algorithm used for public-key cryptography is based on the difficulty of factoring large numbers). In case of quantum teleportation, quantum entanglement is harnessed to transfer qubits (basic units of quantum information) from one location to another. This issue seems to be very difficult to resolve because a qubit, unlike a classical bit, is not either 0 or 1 but rather a superposition of 0 and 1. Surprisingly, it turns out that sending only a few classical bits one can transfer a qubit.

To build a quantum computer one must be able to prepare appropriate input states and measure obtained output states. Quantum tomography [1,2] helps to tackle a problem of measuring and reconstructing quantum states. Here, reconstruction of a quantum state with density matrix ρ means a process of measuring the state in different bases and proposing a density matrix ρ_{rec}, which describes ρ best. To use quantum tomography, one needs to optimize the methods of reconstruction, because in a real experiment there is only a finite number of copies of system to be measured and time for carrying out the experiment is limited, too.

In my bachelor's thesis research I considered different methods of reconstructing density matrices of 2-qubits states: the Pauli Matrices method (PM) [3], the Maximum-Likelihood method without constraints (ML) and the Maximum-Likelihood method with constraints (ML+) [4]. I compared the quality of reconstructions obtained by these three methods for arbitrarily chosen density matrices. The quality of reconstruction was defined as a distance dist(ρ,ρ_{rec}) between two matrices – the one I wanted to reconstruct ρ and the obtained result ρ_{rec}, where the distance was a Hilbert-Schmidt norm of $\rho - \rho_{rec}$. Then I checked if observed differences had any statistical significance to be able to conclude which method gave better results (typical results are shown in (Fig. 1)). Furthermore, I also verified how the quality of reconstruction depended on von Neumann entropy [1] of the reconstructed state (Fig. 2), where von Neumann entropy for ρ is defined as Tr[$-\rho\ln(\rho)$].

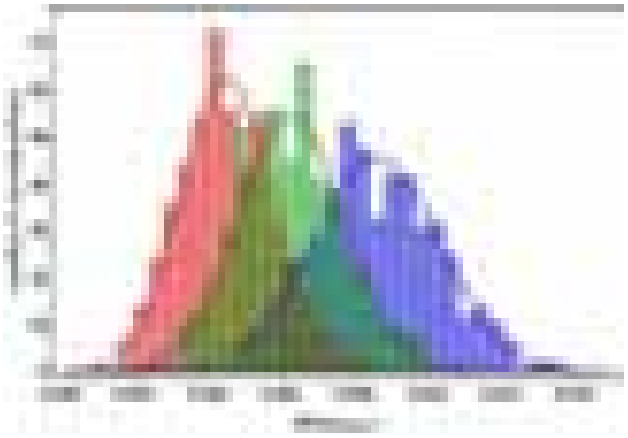

Fig.1. Typical results of reconstruction of an arbitrary density matrix for methods: MP – blue, ML – green, ML+ – red. Each method was repeated 500 times.

Fig.2. Mean distance of reconstruction as a function of von Neumann entropy of reconstructed state. Results for methods: MP – blue, ML – green, ML+ – red.

[1] M. A. Nielsen, I. L. Chuang, *Quantum computation and quantum information*, Cambridge University Press, 2000
[2]G. M. D'Ariano, M. G. A. Paris, M. F. Sacchi, *Quantum tomography*, Advances in Imaging and Electron Physics **128**, 205-308 (2003)
[3] D.F.V. James, P.G. Kwiat, W. J. Munro, A.G. White, *Measurement of qubits*, Phys. Rev. A **64**, 052312 (2001)
[4] Banaszek, G. M. D'Ariano, M. G. A. Paris, M. F. Sacchi, *Maximum-likelihood estimation of the density matrix*, Phys. Rev. A **61**, 010304(R) (1999)

ORAL SESSION IV

SPATIAL STRUCTURE OF Au-BSA NANOCLUSTERS DETERMINED WITH ATOMIC FORCE MICROSCOPY AND QUASIELASTIC LIGHT SCATTERING

Marija Matulionytė[1,2], Ričardas Rotomskis[1,2]

[1] Laboratory of Biomedical Physics, Vilnius University Institute of Oncology, Lithuania
[2] Department of Quantum Electronics, Faculty of Physics, Vilnius University, Lithuania
maria.matte@gmail.com

Application of nanotechnologies in medicine has been one of the most active research fields during the past decade. Various nanoparticles were investigated as promising contrast agents for MRI and X-ray spectroscopy, targeted drug delivery or as photothermal or photodynamic therapy agents. Photoluminescent gold nanoclusters are one of the latest and very promising findings in nanomedicine field because of their remarkable optical properties for a wide range of applications such as sensing, biolabeling and imaging [1]. However, only few studies have been reported on the growth of gold nanoclusters capped with bovine serum albumin (BSA). In this work spatial structure of gold nanoclusters capped with BSA (Au BSA) was investigated using atomic force microscopy (AFM) and quasielastic light scattering techniques.

Au-BSA nanoclusters were synthesized following synthesis conditions published by Xie, et al. [1]. Several different Au to BSA molar ratios were chosen in order to find synthesis conditions for Au-BSA nanoclusters showing the best photoluminescence properties. Further experiments for estimation of spatial structure were performed on Au-BSA nanoclusters synthesized under optimal Au to BSA ratio.

Hydrodynamic diameter of Au-BSA nanoclusters was measured with "ZetaPlus" - particle size measurement equipment based on quasielastic light scattering using approximation of nanoparticles as spheres. Results showed that in aqueous solution Au-BSA nanoclusters were around 9 nm in diameter (Fig.1, b). This is approximately the diameter of the BSA molecule reported in literature [2].

Atomic force microscopy measurements were performed in tapping mode. Samples were prepared on freshly cleaved mica's surface using spin coating technique. Round ~1.3 nm in height and ~30 nm in width structures were observed on the surface (Fig.1, a).

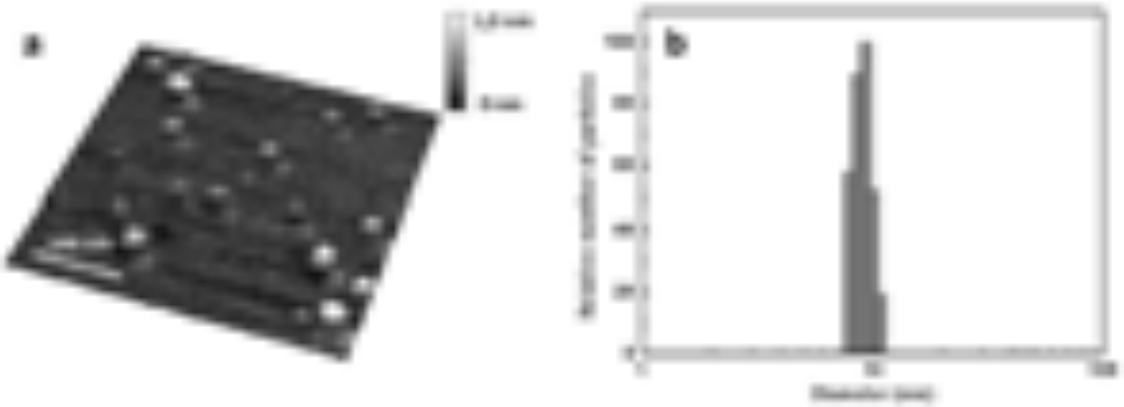

Fig. 1. Topography of Au-BSA nanoclusters spread on mica's surface measured with AFM (a), hydrodynamic size distribution of Au-BSA nanoclusters in solution (b).

The estimated spatial structure differences could be due to the different environment of Au-BSA nanocluster when different measurement techniques were used. In order to explain these differences the modeling calculations were performed. The spherical shape of the Au-BSA nanoclusters could be suggested in aqueous solution in case of quasielastic light scattering method used. On the surface of mica the spherical structure should be flattened. The change of the spherical shape structure was simulated theoretically by the flattening it till the height of the round structures measured with AFM. The diameter of the flattened ellipsoid was two times smaller than the diameter of round structure estimated from AFM measurements. It seems that change of Au-BSA nanoclusters shape is not only due to environment phase changes but also because of the interaction of BSA with hydrophilic mica's surface which is reported to have strong electrostatic interaction with BSA molecules.

However despite the drastic changes of spatial structure of BSA, gold atoms inside remained bound together and clusters on mica's surface showed typical absorbance and photoluminescence spectra.

[1] J. Xie, Y. Zheng, J.Y. Ying, J. Am. Chem. Soc. 131, 888–889 (2009)
[2] M.L. Ferrer, R. Duchowich, B. Carrasco, J.G. Torre, A.U. Acuna, Biophysical J. 80, 2422–2430 (2001)

APPLICATION OF RAMAN SPECTROSCOPY FOR STRUCTURAL STUDIES OF URATIC KIDNEY STONES

Paulius Naujalis and Valdas Šablinskas.
Departament of General Physics and Spectroscopy, Faculty of Physics, Vilnius University, Saulėtekio Ave. 9-III, LT-10222 Vilnius, Lithuania
P.Naujalis@GMail.com

Formation of kidney stones is very painful urinary pathology. Approximately 8-15% of people in Europe suffer from urinary stones disease. 65 different organic and inorganic chemical compounds can be found in urinary stones [1]. Oxalatic and uratic stones are most common types of kidney stones. Every piece of information about composition and formation of kidney stones is important in searching ways for treatment. Raman spectroscopy is very informative method for structural studies of molecular substances. Unfortunately, application of this method is very limited in case of "real" non-purified substances due to strong fluorescence background appearing in Raman spectra of such compounds. In this work an attempt was made to apply Raman spectroscopy for uratic kidney stones, which are problematic for Raman spectroscopy samples due to strong fluorescence background.

10 uratic stones, removed surgically or by ultrasound technique from urological patients of "Santariškių klinikos" were taken for structural studies by means of Raman spectroscopy. The samples for Raman experiments were prepared in 3 ways: (I) untreated stones (II) cross sectioned stones and (III) powdered stones. Three different lasers (514.5, 671 and 1064 nm) were used for excitation of Raman spectra of the stones, but only in third case (FT-Raman with NIR excitation) the Raman spectrum was not masked by fluorescence background (see fig. 1). FT-Raman spectra were obtained for all 10 uratic stones, which differ in shape, colour, porosity, etc. (see fig. 2). It was found that 8 of them consist from pure uric acid while 2 – from calcium oxalate and uric acid. After close up examination of the stones, which included calcium oxalate it was found that white stripes between calcium oxalate and uratic part of stone is pure calcium oxalate.

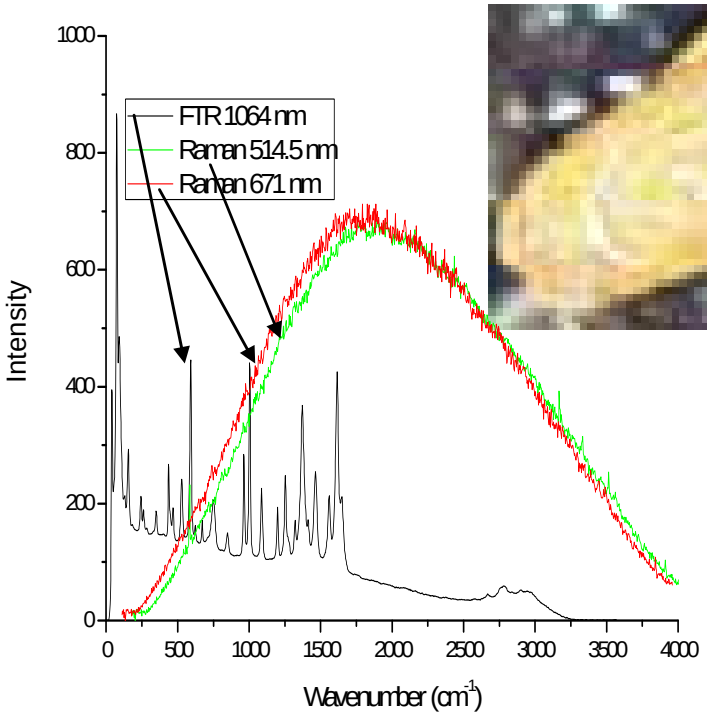

Fig. 1. Raman spectra of uratic kidney stone obtained using different lasers for excitation

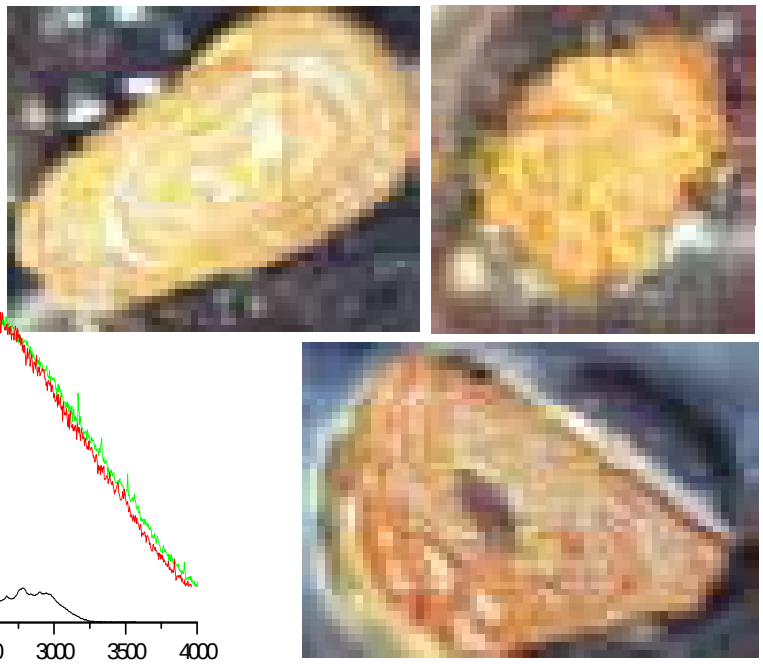

Fig. 2. Various uratic stones, which differ in size, colour, porousity, etc.

Notable, that main method used for determination of kidney stone type in hospitals is optical examination of shape and colour of the stone. These physical properties not always represent chemical composition. To sum up FT-Raman spectroscopy gives more information about structure of kidney stones than traditional optical methods and can be used in medical practice.

[1] P. G. Sofia, I. Ionescu, G. Rodica, P. Anisoara, The use of Infrared spectroscopy in the investigation of Urolithiasis (2010).

BSA-ENCAPSULATED GOLD NANOCLUSTERS: CURRENT RESULTS AND FUTURE PERSPECTIVES

Deividas Sabonis[1,2,3], Vilius Poderys[2], Ričardas Rotomskis[1, 2, 3]

[1] Biophotonics group of Laser Research Center, Vilnius University, Saulėtekio 9, c.3, LT-10222, Vilnius
[2]Laboratory of Biomedical Physics, The Institute of Oncology Vilnius University, Baublio 3B, LT-08406, Vilnius
[3] Faculty of Physics, Vilnius University, Sauletekio. 9, LT-10222, Vilnius
Sabonis.Deividas@gmail.com

Nanomedicine is currently an active field. This is because new properties emerge when the size of a matter is reduced from bulk to the nanometre scale. These new properties, including optical, magnetic, electronic, and structural, make nanosized particles (generally 1-100 nm in diameter) very promising for a wide range of biomedical applications such as cellular imaging, molecular diagnostics and targeted therapy depending on the structure, composite and shape of the nanomaterials.

Fig.1. Gold nanoparticles color is dependent on particles size.

Gold nanoparticles have been brought to the forefront of cancer research in recent years because of their easy synthesis and surface modification, strongly enhanced and tunable optical properties (**Fig. 1**), as well as excellent biocompatibility feasible for clinic settings. Gold nanoclusters are assemblies of small number (2 - 30) of gold atoms, typically having the size no bigger than 1 nm. These nanoclusters demonstrate molecule-like properties distinct from bulk metals or atoms. Stabilization of these nanoclusters in aqueous solutions protects them from aggregation. Reduced gold atoms aggregate within the bovine serum albumin (BSA) to form small and large nanoparticles. This protein-directed synthesis of highly fluorescent gold nanoclusters was firstly investigated by [1] . Here based on [1] we investigate optical properties of bovine serum albumin coated gold nanoclusters.

Fig.2. Three-axial motion platform for nanopositioning in nanofothothermolysis.

At the moment the process of BSA–gold nanoclusters interactions, photoluminescence and absorbance spectra, temperatures kinetics interpretation or two photon excitation cross sections is very poorly or absolutely unknown. In this report results on spectra, fluorescence kinetics interpretation, two photon cross sections of BSA coated gold nanoclusters will be presented. At the moment there are only few articles investigating the tumor NIR fluorescence imaging *in vivo* with the ultrasmall gold nanoclusters which exhibits brightly NIR fluorescence, high photostability and contains no toxic elements [1] .The uptake by the RES system *in vivo* is also much less than other nanomaterial due to the ultrasmall hydrodinamic size.

Looking forward gold nanoparticles are shown to be good to carry out non invasive cell optoporation (nanofothothermolysis). Using femtosecond laser system PHAROS (Light Conversion Ltd.) operating at λ = 1030 nm and delivering pulses of 270 fs at 200 kHz repetition rate and sample mounted on a three-axial motion platform (**Fig. 2**), controlled with the SCA software (Altechna Ltd.) precise cell optoporation will be caried out. So scientists believe that the biocompatible, ultrasmall, NIR gold nanoclusters are promising fluorescent candidates for optical imaging *in vivo* and related biomedical applications.

[1] Xie, J., Yuangang Zheng and Jackie Y.Ying (2009

DEGRADATION OF ARCHAEOLOGICAL WOOD FROM THE SWEDISH WARSHIP "VASA" STUDIED BY INFRARED MICROSCOPY

Milda Pučetaitė[1], Valdas Šablinskas[1], Per Uvdal[2]

[1] Department of General Physics and Spectroscopy, Faculty of Physics, Vilnius University, Lithuania
[2] Department of Chemical Physics, Chemical Center, Lund University, Sweden
milda.pucetaite@gmail.com

The Swedish warship "Vasa" is one of the largest marine archaeological artefacts in the world. After the salvage in 1961, after more than 300 years in the sea, it has been preserved by spraying polyethylene glycol – one of the first reliable and relatively simple methods for preservation [1, 2]. During its time at the sea bottom as well as in a museum hall, the wood of the "Vasa" experienced a lot of changes. These changes cause degradation of the wood which may not be visible at first sight. It is important to determine the main causes to the deterioration of the wood condition in order to ensure its proper preservation in the future; thus many studies have been carried out on the "Vasa", however the degradation processes are still uncertain [2]. Fourier transform infrared (FTIR) absorption spectroscopy is applied for investigation of the "Vasa" in this work. The infrared spectra are like 'fingerprints' of the molecular compounds. Thus, by analysing the spectra one can determine chemical composition or, as in this case, chemical changes occurring compared to the reference sample.

Infrared spectra were recorded using a Hyperion 3000 IR microscope combined with an IR spectrometer IFS66V/S from Bruker (Max-Lab laboratory, Lund, Sweden) with globar IR light source and a single point MCT (mercury cadmium telluride) detector. The samples were prepared using the KBr (potassium bromide) pellet technique.

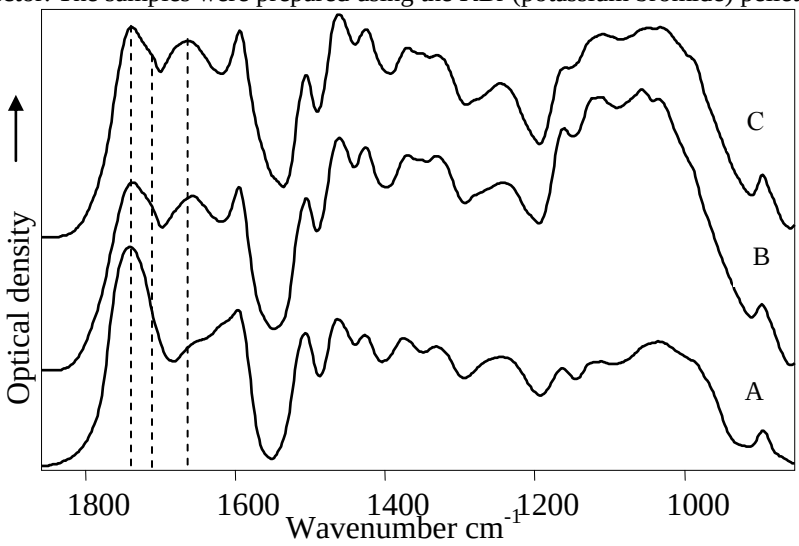

Fig. 1. Infrared spectra of oak wood Qercus Robur (A) and of preserved with PEG Vasa hull wood: B – inner, C – surface,; spectra were shifted from each other in vertical direction for clarity

Differences between the spectra of the "Vasa" wood and fresh oak wood (used as a reference) indicate degradation of the timber due to oxidation as well as alterations in functional groups of the wood polymers (cellulose, hemicelluloses, lignin). For example, new spectral band appearing at 1666 cm^{-1} (Fig. 1) is probably caused by conjugated C=O stretching vibration. Conjugated C=O bond could be formed in lignin in the course of oxidation reactions caused by the presence of iron ions (Fenton's reactions) [2].

In conclusion, with the aid of FTIR microspectroscopy, degradation of polysaccharides and lignin could be monitored. Spectral changes indicate oxidation of organic molecules in the wood occurring in the presence of iron ions. Differences in chemistry between surface and inner samples, for example, the amount of polyethylene glycol (PEG) – the preservation material - in the wood can be observed as well.

Acknowledgement: This work was carried out at infrared beamline at Max-Lab laboratory in Lund, Sweden. The help of dr. Gunnar Almkvist and dr. Anders Engdahl is greatly acknowledged.

[1] Donny L. Hamilton, Methods of Conserving Underwater Archaeological Material Culture, Conservation Files: ANTH 605, Conservation of Cultural Resources I. Nautical Archaeology Program, Texas A&M University (1998).
[2] Gunnar Almkvist, The Chemistry of the Vasa, Doctoral Thesis No. 2008:57. Swedish University of Agricultural Sciences (2008).

SURFACE-ENHANCED RAMAN SPECTROSCOPY OF BACTERIA

Evelin Witkowska[1,3], Anna Kelm[2,3], Agnieszka Michota-Kaminska[3], Robert Holyst[3]

[1]Faculty of Chemisty, University of Warsaw
[2]College of Inter-Faculty Individual Studies in Mathematics and Natural Sciences, University of Warsaw
[3]Department of Soft Condensed Matter, Institute of Physical Chemistry, Polish Academy of Sciences
ewitkowska@ichf.edu.pl, akelm@ichf.edu.pl

Surface-enhanced Raman scattering (SERS) is a spectroscopic technique dating back to 1970s [1] that utilizes metal (Ag, Au, Cu) nanoparticles and roughened metal surfaces to enhance Raman signal from adsorbed molecules. Primary effect responsible for SERS enhancement by 5 to 6 orders of magnitude comes from local surface plasmons excited by incident laser radiation [2]. Secondary effect (providing ~10^2 enhancement) involves resonant charge-transfer (CT) transitions between adsorbate and metal [3]. Currently, applications of SERS range from surface chemistry [4] to biological chemistry [5] and biomedical analysis [6]. Investigations on employing SERS in bacteria characterization and analysis made a huge progress during last 10 years. Thanks to this method, microorganism detection and identification in food, clinical, and environmental samples could be much easier than other time-consuming, complicated, traditional procedures like PCR-based methods (reporter labeling, cell lysis, DNA extraction) [7] or new immunoassay methods [8]. The microfluidic chip with a roughened metal surface for on-chip SERS detection of bacteria has already been demonstrated to be a good method to distinguish gram positive and gram negative Prokaryota [9]. Further development of this technique would enable determination of bacteria species.

[1] M. Fleischmann, P.J. Hendra, A.J. McQuillan, *Raman spectra of pyridine adsorbed at a silver electrode*, Chemical Physics Letters, 26(2):163 – 166, 1974.

[2] Harald Kneipp, Katrin Kneipp, Martin Moskovits, editor, S*urface-Enhanced Raman Scattering. Physics and Applications*, chapter: S*urface-Enhanced Raman Spectroscopy: a Brief Perspective,* Springer-Verlag, Berlin Heidelberg, 2006.

[3] R. Aroca, *Surface enhanced vibrational spectroscopy*, chapter 4. *Chemical Effects and the SERS Spectrum,* Wiley, 2006.

[4] W. B. Caldwell, K. Chen, B. R. Herr, C. A. Mirkin, J. C. Hulteen, R. P. Van Duyne, *Self-assembled Monolayers of Ferrocenylazobenzenes on Au(111)/mica Films: Surface-Enhanced Raman Scattering (SERS) Response vs. Surface Morphology*, Langmuir 1994, 10, 4109-4115.

J. Weaver, *Electrochemical Interfaces: Some Structural Perspectives*, Journal of Physical Chemistry 1996, 100, 13079-13089.

[5] N. Weissenbacher, B. Lendl, J. Frank, H. D. Wanzenböck, B. Mizaikoff, R. Kellner, *Continuous surface enhanced Raman spectroscopy for the detection of trace organic pollutants in aqueous systems*, Journal of Molecular Structure 1997, 410-411, 539-542.

X. Zhang, M. A. Young, O. Lyandres, R. P. Van Duyne, *Rapid Detection of an Anthrax Biomarker by Surface-Enhanced Raman Spectroscopy*, Journal of the American Chemical Society 2005, 127, 4484-4489.

[6] T. Vo-Dinh, D. L. Stokes, G. D. Griffin, M. Volkan, U. J. Kim, M. I. Simon, *Surface-enhanced Raman Scattering (SERS) method and instrumentation for genomics and biomedical analysis*, Journal of Raman Spectroscopy 1999, 30, 785-793.

[7] C.C. Chen, L.J. Teng, S.K. Tsao, T.C. Chang, *Identification of Clinically Relevant Viridans Streptococci by an Oligonucleotide Array*, Journal of Clinical Microbiology, 43(4): 1515- 1521, 2005.

[8] A. Gupta, D. Akin, R. Bashir, Detection of bacterial cells and antibodies using surface micromachined thin silicon cantilever resonators, Journal of Vacuum Science and Technology B, 22: 2785- 2792, 2004.

[9] I.F. Cheng, C.C. Lin, D.Y. Lin, H.C. Chang, A dielectrophoretic chip with a roughened metal surface for on-chip surface-enhanced Raman scattering analysis of bacteria, Biomicrofluidics, 4(3): 034104, DOI: 10.1063/1.3474638, 2010.

PULSE-WIDTH MODULATED LED RESPONSE CHARACTERISTICS AND PSYCHOPHYSICAL COLOR MATCHING

Renārs Trukša[1], Sergejs Fomins[2], Māris Ozoliņš[1,2]

[1] University of Latvia, Optometry and Vision Science Department, Kengaraga 8, Rīga, LV-1063
[2] Institute of Solid State Physics, Kengaraga 8, Rīga, LV-1063

In previous research [1] we developed LED based anomaloscope [2]. Pulse width modulation technique was used to control LEDs brightness with computer controlled microcontroller. It is possible to control up to 6 LEDs at same time with different PMW (pulse □width modulation) frequencies simultaneously. We were able to correctly classify [3] persons with color vision deficiencies. Developed device prototype identified color matching range for trichromatic vision is 103 to 171 units on red-green scale. Normal color vision patients make consistent matches in specified region. Additional accessories like interference filters could improve the spectral characteristics of device, but will increase the expenses.

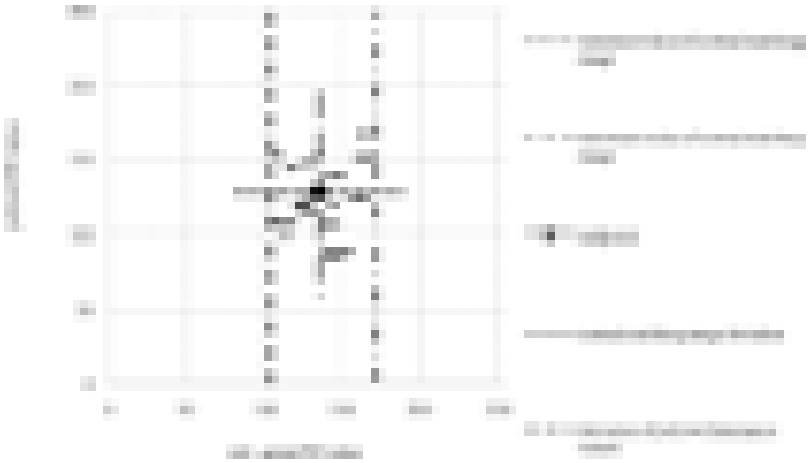

Fig. 1 Matching ranges were 9 ±1 units with deviation 4 units. Industrially produced anomaloscopes red green scale are from 0 to 73 and matching range from 42 to 44 units on red □green scale. If we compare scales proportionally that 89 % of our patients matching ranges fit in normal matching range [1].

Experimenting with LEDs we find that increasing PWN frequency linearly increases brightness [1] also LEDs spectrum shifts toward to right side of CIE color diagram. We measured red, green, blue and yellow LEDs spectrum at 17 different PWM frequencies from 15 to 255 and calculated color we would perceive. As expected, specific cone response significantly decreased increasing pulse frequency, except yellow LED. This is due to red and green cones are almost equally aroused by yellow LED. However increasing PWM frequency to red LED, long wavelength cone response maintain constant, while blue and green cone responses decreased. In all cases LEDs emitted light shifted towards to right up to 35 nm ; yellow -15 nm, green 5 -10 nm, blue - 15 nm, red - 35 nm. Increase of PWM frequency results in more intense saturation of LEDs color. .

In further research our aim is to determine whether brightness distribution (wave form) change in time have impact on psychophysical response. There is plausible information that sensitivity on OFF - sawtooth stimuli are greater than ON- sawtooth stimuli[4]. Theoretical assumptions enable chance that there is brightness distribution to what our visual system is more sensitive than other wave forms. Our hypothesis is that such wave forms would help to increase the specificity of anomaloscope match and link color vision phenotype with existing genetic model.

1. Trukša, R., Fomins, S., Ozoliņš, M. Rayleigh Equation Anomaloscope from Commercially Available LEDs.
2. Woods, R. L, Rashed, A. L, Benavides, J. M, Webb, R. H. A Low-power, LED-based, High-brightness Anomaloscope *Vision Research,* 46 2005: pp. 3775 □3781.
3. Birch, J. Diagnosis of Defective Colour Vision. Oxford University Press, 1993: pp. 58 □59.
4. P.J., Demarco, V.C., Smith, J., Pokorny. (1993). Effects of sawtooth polarity on chromatic and luminance detection. *Visual Neuroscience.* Vol. 11. pp: 491-499.

ORAL SESSION V

MONTE CARLO CALCULATION OF VVER-440 REACTOR COMPONENT ACTIVATION AND FUEL EVOLUTION USING MCNP

Benjaminas Marcinkevičius, Artūras Plukis
Center for Physical Sciences and Technology, Savanoriu ave. 231, Vilnius LT-02300, Lithuania
benjaminas.marcinkevicius@ff.stud.vu.lt

During exploitation of nuclear reactors or after shutdown component activation analysis is required to ensure safety during activated components and used fuel transportation, decommissioning and storage. There are two ways determining activity and isotopic composition: physical measurement and computer modeling. Computer modeling can be deterministic (TRITON code from SCALE program package) or stochastic (MCNPX code [1]). Usually validation of computation can be done by comparing results with measurements or calculations using different computer codes. In this work calculations will be done using stochastic method with MCNP5 and MCNPX. This gives advantage to model complex structures, calculate mass fraction of isotopes and activities without need to work with radioactive samples or specific equipment, ability to calculate possible dose to human.

VVER reactor is Russian construction pressurized water reactor using water as moderator and coolant. VVER 440 unit maximum electrical power is 440 MW. Fuel assembly geometry is hexagonal with 126 fuel rods in assembly and up to 349 fuel assemblies inside core. For fuel cladding and assembly wall ZrNb alloy is used, most of the other reactor components are made of steel. Different enrichment UO_2 fuel is used, possible enrichment: 1.6 %, 2.4%, 3.4%.

For accurate and fast calculations important parameters have to be determined [2]: fuel composition and burnup, which reactor components can be omitted from model or simplified, selection of important nuclides for activation calculation.

Reactor core fuel burnup and isotopic composition was calculated in order to load reactor model with different burnup fuel. Neutron flux differences in low energies can be visible (Fig. 1) and could play important role calculating activation of core surrounding components. For calculation one burnup step was selected 100 days and total burning time was 800 days, average burnup of fuel in VVER reactor is ~ 20 GWd/MTU, which is reached after 600 days of burning. One of the components which activity calculation will be conducted is dummy assembly. Dummy assembly is construction part used in the reactor core to replace fuel assembly for different core fuel loading patterns (Fig. 2). During long term reactor operation fuel burnup and loading varies, in calculations it was compared how flux and activation changes loading core with different burnup fuel.

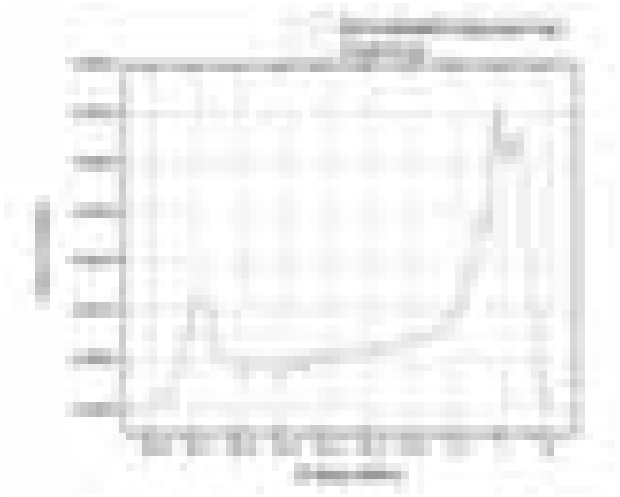

Figure 1. Neutron flux comparison in fresh and burned fuel.

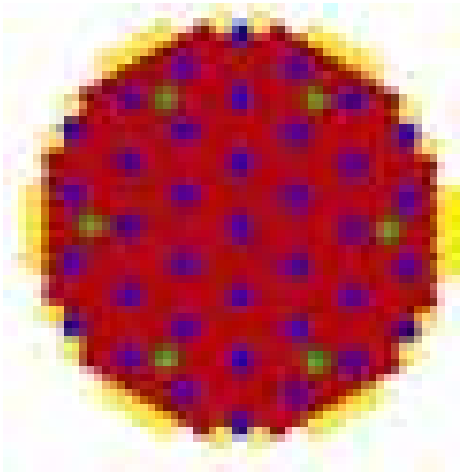

Figure 2. Fuel, control rods and dummy assembly loading pattern inside reactor core. Yellow dummy assembly. Blue control rods, Red 3.6 % enriched fuel , Green 1.6% enriched fuel.

[1] D. B. Pelowitz, *MCNPX User's Manual. Version 2.6.0*, LA-CP-07-1473, Los Alamos National Laboratory (LANL) (2008).

[2] S. Czifrus, Activation calculation methodologies, IAEA Workshop on the Determination of Neutron Induced Activity for Decommissioning Purposes Budapest, (1-4 June 2010).

THE CHAOTIC DYNAMICS OF HYPERION

Mariusz Tarnopolski

Jagiellonian University, Cracow, Poland
mariusz.tarnopolski@uj.edu.pl

Chaotic behaviour has been firstly observed, yet not comprehended, by Poincare [1]. Well established research about a system of diferential equations describing the convective motion of the atmosphere was held by Lorenz in 1963. Further investigation showed the existence of many discrete (logistic, Chirikov standard map) and continuous (Henon-Heiles, Duffing oscillator) systems. In fact, the amount of nonlinear systems behaving chaotically is much greater than the 'properly' behaving linear ones. It turns out, that even drops dripping from the tap are acting chaotically [1].

A classical mechanics example for a system that could be chaotic for some specified parameters is a rotation of a non-spherical rigid body. Fixing the spin axis orthogonally to the orbit's plane one can achieve the equation of motion [2] in the form (1). Although, the non-sphericity must be sufficiently big, that is there should *not* be (B-A)/C<<1, where A, B, C are the principal moments of inertia. For Hyperion we have $\omega_0^2 = 3(B-A)/C = 0.87$, so it is expected to find a large chaotic zone in the phase space. That is actually true, as shown in figure 1.

$$\ddot{\theta} + \frac{3(B-A)}{C}\sin\theta\cos\theta = 0 \tag{1}$$

The Lyapunov theory of stability shows that the model of Hyperion actually acts chaotically and the Chirikov criterion states that the critical value of ω_0 is given by

$$\omega_0^{RO} = \frac{1}{2+\sqrt{14e}}, \tag{2}$$

which for e=0.1, the mean eccentrity of Hyperion is equal to $\omega_0^{RO} = 0.31$.

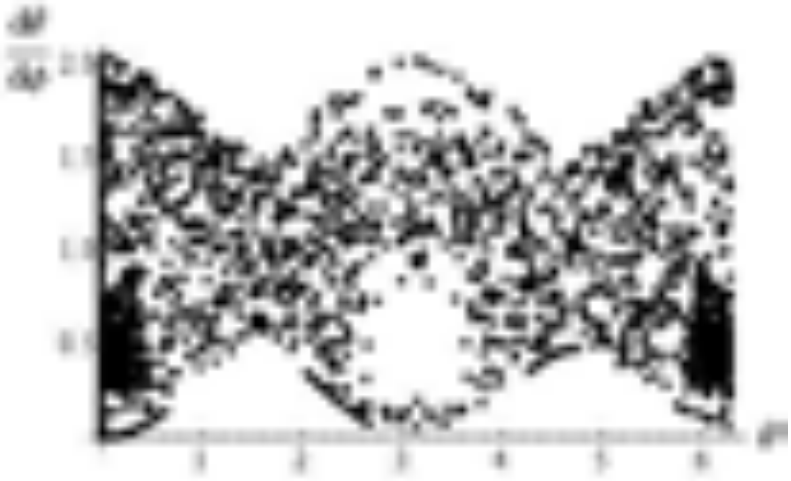

Fig. 1. Section of surface for Hyperion: $d\theta/d\phi$ versus θ at successive periapse passages.

[1] I. Stewart, Does god plat dice? The new mathematics of chaos, Blackwell Publishing, 1989.
[2] J. M A. Danby, Fundamentals of Celestial Mechanics, McMillan, 1962.
[3] J. Wisdom, S. J. Peale, F. Mignard., The Chaotic Rotation of Hyperion, Icarus **58**, 137-152 (1984).
[4] M. Shahzad, Control of Chaos in Rotational Motion of a Satellite in an Elliptic Orbit, Higher Education of Nature Science, Vol. 1, No. 1, 2011, pp. 10-13.
[5] P. T. Boyd, G. B. Mindlin, R. Gilmore, H. G. Solari, Topological Analysis of Chaotic Orbits: Revisiting Hyperion.

ANALYSIS OF ELECTRICAL AND OPTICAL FLUCTUATIONS OF LIGHT-EMMITING DIODES USED IN LCD MONITORS

Vytautas Martinaitis, Arvydas Vencius

Radiophysics Dep., Vilnius University, Lithuania
Vytautas.Martinaitis@ff.stud.vu.lt
Arvydas.Vencius@ff.stud.vu.lt

Nitride compound semiconductors are widely used in light-emitting diodes (LEDs) for ultraviolet and visible spectra. However the nitride-based LED fabrication encounters some problems such as a large number of threading dislocations in the active layer. This leads to non-radiative recombination processes that lower the light-emitting device efficiency and accelerate device ageing [1].

Investigation of noise is known to yield valuable information on dominant physical processes in semiconductor materials and structures [2].

In this experiment output light power, current-voltage and noise characteristics of blue LEDs have been measured at room temperature in current range from 0,049 mA to 21 mA. We used Cooley-Tukey fast Fourier transformation for measurements of noise spectra in the frequency range from 10 Hz to 20 kHz. A special attention was pointed to the measurement and interpretation of simultaneous cross-correlation factor between electrical and optical fluctuations. In order to evaluate the correlation factor, the electrical and optical fluctuations measurements were performed simultaneously. Processing of noise signals was produced with two identical channels comprised from custom made low noise amplifiers, filter systems, analog digital converter (National Instrument PCI-6115 card). The cross-correlation was measured over full frequency range and in every one-octave frequency range.

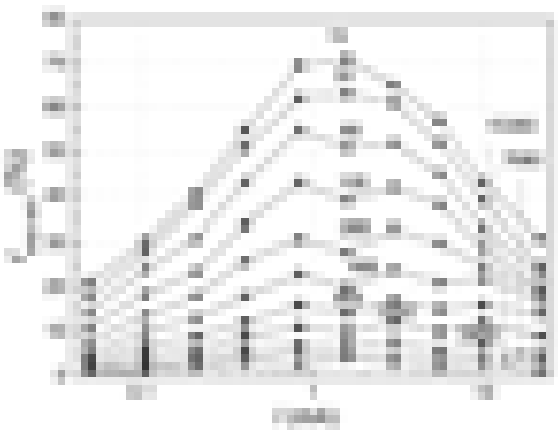

Fig.1. The cross-correlation factor between electrical and optical fluctuations in one-octave frequency band dependency on d.c. current at different central frequencies f_c of octave filters.

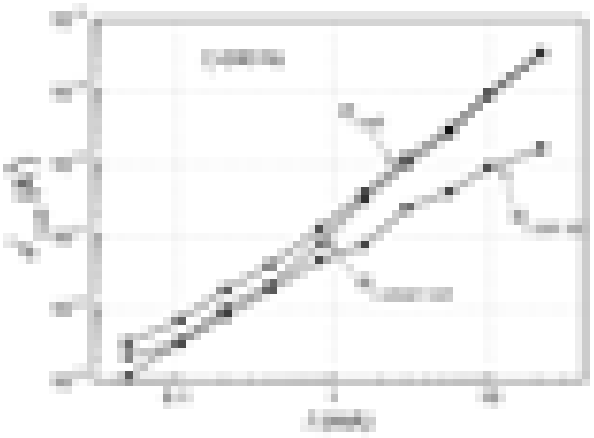

Fig.2. Comparison of current fluctuations variances at f_c=240 Hz.

The simultaneous cross-correlation factor in the frequency band from 10 Hz to 20 kHz was measured on the ground of this expression:

$$r_{\exp} = \frac{< u_{el\ total}(t) \cdot u_{ph\ total}(t) >}{\sqrt{\sigma^2_{el\,\Sigma} \cdot \sigma^2_{opt\,\Sigma}}} \qquad (1)$$

Where brackets <□ > mean averaging both on time and on number or realizations.

It is seen from Fig 2 that at low currents optical fluctuations are caused by defects near quantum wells, because the correlated part of the fluctuation is almost equal to the total level of fluctuations. At high currents the correlated part is about an order lower than the total level of fluctuations. It shows that the main part of recombination centers is in the passive layers of the LED.

[1] K.-M. Chang, J.-Y. Chu, and C.-C. Cheng, Highly reliable GaN-based light emitting diodes formed by p.In0:1Ga0:9N.ITO structure, IEEE Photon. Technol. Lett. 16, 1807.1809 (2004).
[2] V. Palenskis, Flicker noise problem, Lithuanian J. Phys. **30**, 107.152 (1990).

LANGMUIR-BLODGETT THIN FILMS SPECTROSCOPY: LOW DIMENSIONAL EFFECTS

Angelina Shiryaeva
Physics faculty, Belarusian State University
linashiryaeva@gmail.com

In this work spectra of excitation and spectra of fluorescence of thin films with different number of monolayers were obtained. Quartz was used as a substrate. The purpose of this work is to reveal low dimensional effects that rise in Langmuir-Blodgett films (LB-films) using spectroscopic methods. Iron-doped LB-films of ditienilepyrrole were used.

To obtain spectra of excitation and spectra of fluorescence, the spectorfluorometer Solar 1211A was used. 150 watt high pressure xenon arc lamp was used as the light source. It gives almost continuous spectrum except several narrow lines near 470 nm, 660 nm and 800-1000 nm. [1]

The technique of experiment included the preliminary calibration of the device. The calibration consists in obtaining of fluorescence and excitation spectra of the quartz substrate without LB-films. These spectra were needed to subtract them from final ones. Then the spectra of excitation of samples with LB-films were measured with registration at wavelengths of 400 nm and 460 nm. Consequently the samples are excited on the wavelength corresponding to the maximum of the spectra of excitation. Then the maximum of the fluorescence spectrum was determined, and the excitation spectrum of samples was measured again. This procedure should be repeatedly done until the wavelength of registration would be in a correspondence with the wavelength of the maximum of the fluorescence spectrum, and, oppositely, the wavelength of excitation would be in a correspondence with the wavelength of the maximum of the excitation spectrum.

The obtained spectra of fluorescence are shown at Fig.1. The wavelength of excitation is 219 nm. On the graph one can observe the maximums of fluorescence spectra at the wavelength of 296 nm for the 3-layered film, 302 nm for the 5-layered film, 303 nm for the 7-layered film. For the 9-layered film the maximum at this wavelength is not observed.

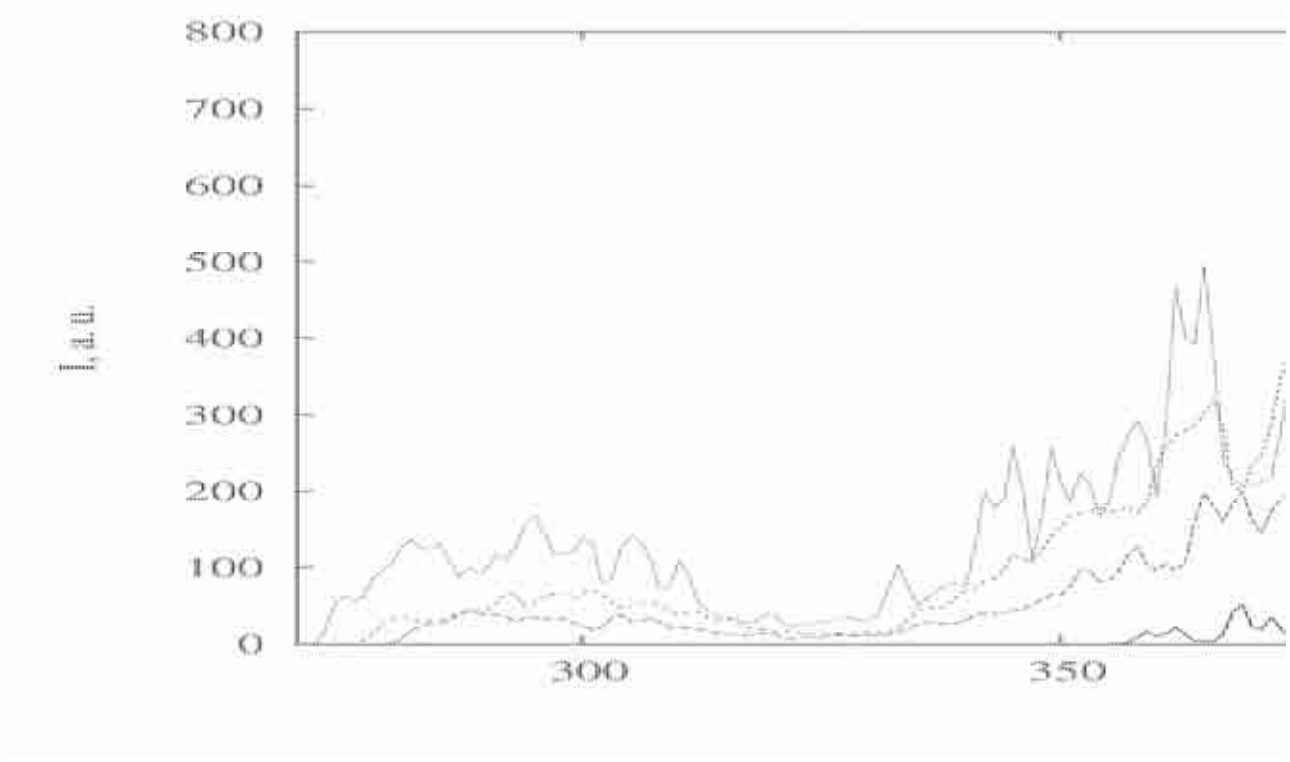

Fig1. Spectra of fluorescence of 3,5,7,9-layered films

This phenomenon can be explained as follows. In the films which consist of 9 and more monolayers medium can not be treated as a low-dimensional sample, and conventional zone theory is to be applied. This is due to the fact that interactions between layers become considerable. So the thin films lose their special properties, including appropriate scattering phenomena that were observed for samples with 3, 5 and 7 layers.

[1]. Xenon short-arc lamps http://www.ushio.co.jp/en/products/list/lamp/lamp_06.html

ORAL SESSION VI

AB INITIO UNHARMONIC CALCULATIONS AND LOW TEMPERATURE MATRIX FTIR SPECTRA OF ETHANOL MONOMER ROTOMERS

E.Kozlovskaya[1], I.Yu.Doroshenko[2], V.Ye.Pogorelov[2], V.Sablinskas[3], G.Pitsevich[1]

[1]Belarusian State University, Minsk, Belarus
[2]Kyiv National Taras Shevchenko University, Kyiv, Ukraine
[3]Vilnius University,Vilnius, Lithuania
kozlovskayaen@gmail.com

Low-temperature FTIR spectra of the ethanol in an argon matrix obtained for a series of temperatures in the range 20-50 K and the ratio of 1:1000, 1:2000 for the number of the molecules to the number of atoms in the matrix. Preliminary interpretation of the spectrum is made on the basis of temperature changes in the spectra and literature data. Structure calculations of conformers of ethanol, rotational constants, barriers to internal rotation of the methyl and hydroxyl groups are made in the approximation of B3LYP/cc-pVTZ. In the same approximation calculations of harmonic and anharmonic IR spectra of cis and trans conformers were done. For a common set of dependent coordinates are calculated and compared the force fields of the two conformers, the potentional energy distribution (PED) for the normal vibrations, the anharmonicity constants. The possibility of taking into account the anharmonicity effects by introducing the spectroscopic masses for hydrogen atoms in the performance calculations of normal vibrations in the harmonic approximation. In comparison with methanol the number of publications devoted to the spectral-structure characteristics of ethanol is not so large [1, 2]. The dynamics of the C-O stretch vibration in ethanol in CCl_4 was investigated in [3], the calculations of the structure of some ethanol clusters in the approximations B3LYP/6-311G(d,p) and MP2/6-311+G(2df,2pd) are presented in [4, 5], IR spectra of ethanol and some heterodimers with the investigated molecule were obtained in [6,7]. Besides the typical as well for methanol possibility of the inner rotation around C-O bond in ethanol molecule there is the additional possibility of the inner rotation around C-C bond. Moreover, the investigated molecule can form some energetically non-equivalent conformers [4, 5, 7]. These factors essentially complicate the vibrational spectrum of ethanol.

---

[1] V.Pogorelov, A.Yevglevsky, I.Doroshenko, L.Berezovchuk. Superlat, and Microstruct., 2008, **44**, 571.
[2] Ph.Zielke, M.A.Suhm. Phys. Chem.Chem.Phys., 2006, **8**, 2826.
[3] M. Broek, H.K.Nienhuys, H.J.Bakker. J.Chem.Phys., 2001, **114**, 3182.
[4] P.Borowski, J.Jaroniec, T.Janowski, K.Wolinski. Mol.Phys., 2003, **101**, 1414.
[5] R.L.Rowley, C.M.Tracy. J.Chem.Phys., 2006, **125**, 154302.
[6] S.Coussan, M.E.Alikhani, J.P.Perchard, W.Q.Zheng. J.Phys.Chem. A, 2000, **104**, 5475.
[7] S.Coussan, P.Roubin, J.P.Perchard. J.Phys.Chem. A, 2004, **108**, 7331.
[8] http://www.msg.ameslab.gov/GAMESS/GAMESS.html

INTENSITY STABILITY MEASUREMENTS OF HIGH-FREQUENCY ELECTRODELESS DISCHARGE LAMPS

Anda Svagere[1], Janis Skudra[1]

[1] Institute of Atomic Physics and Spectroscopy, University of Latvia, Skunu str. 4, LV-1050, Riga
anda.svagere@gmail.com

High-frequency electrodeless lamps (HFEDLs) are widely used as high intensity sources of narrow spectral lines, covering the spectrum from the vacuum ultraviolet to the infrared. Such lamps have been used in various scientific devices such as emission and absorption spectrometers, spectrometers for refractive index measurements and frequency standards. Because of the high intensity of HFEDLs, they have been used as emission sources in double-resonance experiments, sensitized fluorescence experiments and the measurement of the shifts and broadening of spectral lines. Such lamps are very convenient for plasma-surface interaction studies due to lack of electrodes, which can cause impurities in plasma [1].

Depending on the application, the requirements for the light source are different. For example, the main requirements for light sources for use in AAS are: (1) high intensity of spectral lines; (2) emission stability; (3) narrow and not self-absorbed line profiles; and (4) long-operating life. It is necessary to investigate and optimize the light sources for each particular use.

The HFEDL contains a bulb and a short side arm containing the working element. The lamp bulb is located in a HF generator coil to induce an inductively coupled electrodeless discharge. The excitation frequency of the applied high-frequency field is 100 MHz. Initially the discharge occurs in buffer gas (usually, argon), then due to the increase in temperature, the vapour pressure increases and the emission of the working element can be observed.

In this work are presented the intensity stability measurements of HFEDLs containing As, Se, Tl, Sn and Pb, developed in our laboratory for different analytical devices, particularly, atomic absorption spectrometers. The lamps were operated at different excitation generator voltage values (20-30V), and the emission spectra changes in time (for about 20 minutes) were analyzed. For several lamps the intensity stability measurements were performed for about 8 hours (Fig.1.) at one particular excitation generator voltage value.

The emitted light spectra were registered using AVANTES AVS-PC2000 plug-in spectrometer with a 2048-element linear CCD-array detector. The spectra were recorded in the wavelength range from 190 till 850 nm.

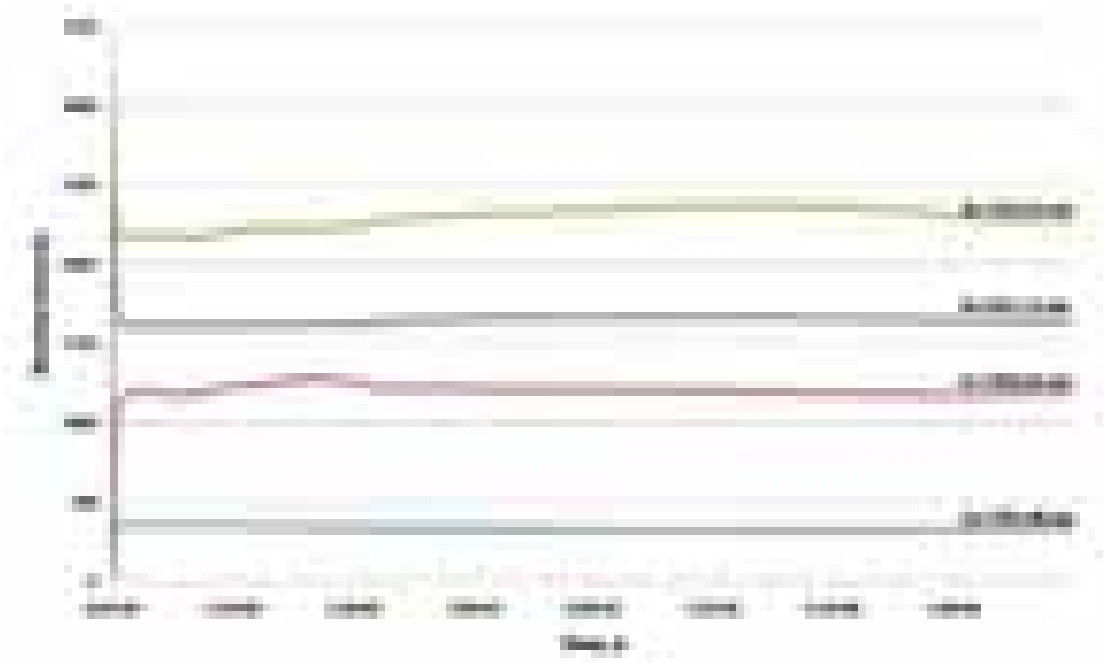

Fig. 1. Example of intensity stability measurements for Se+Ar lamp at 25 V during 8 hours.

Such measurements indicate the time needed for the lamp to stabilize (mostly about few minutes), and the intensity behaviour at different voltages shows which of the regimes could be most appropriate for the particular lamp.

Acknowledgments: The work was partly supported by European Social Fund project Nr. 2009/0210/1DP/1.1.1.2.0/09/APIA/VIAA/100.

[1] A. Skudra, Z. Gavare, N. Zorina, M. Zinge, E. Gavars, R. Poplausks, A. Svagere, Plasma Temperature and Surface Studies of Argon-Hydrogen Containing Low-Temperature Dumbbell form Light Sources, Journal of Materials Science and Engineering B **1**, 439-444(2011)

HYDROGEN ADSORPTION STUDIES OF NATURAL ZEOLITE

Peteris Lesnicenoks[1], Liga Grinberga[2], Janis Kleperis[2]

[1] Faculty of Materials Science and Applied Chemistry, Riga Technical University;
[2] Institute of Solid State Physics, University of Latvia
peteris.lesnicenoks@rtu.lv

There are a lot of controversial reports about applicability of zeolite as appropriate material for hydrogen storage. On the one conclusion researchers shares - namely, that the zeolite adsorbs significant quantities of hydrogen at low temperatures (77 K, for example). We have shown that the zeolite can adsorb hydrogen up to 4 % by weight of zeolite at room temperature. For hydrogen adsorption measurements the thermogravimetric equipment SHIMATZU DTG - 60/60H was adapted, by adding two gases - argon and hydrogen – to gas flow system. Samples were analyzed in the following way: 1) heating to 200 (300) ° C in an argon atmosphere at the speed 10 deg/min, 2) cooling down in automatic mode to room temperature in the hydrogen atmosphere. In some experiments secondary heating in argon atmosphere and cooling down in hydrogen atmosphere were done without removing the sample from apparatus.

The applicability of the method was tested using palladium powder as reference sample. It is known that palladium metal absorbs hydrogen at given temperature in exothermic reaction and palladium hydride $PH_{0.7\text{-}0.8}$ forms. Zeolite samples were prepared from natural clinoptilolite (Ukraine), supplied as a coarse, medium and fine powder material. Activation of the samples was carried out in ion-exchange process soaking zeolite powder in the solution, and in pyrolysis process, coating palladium nanoparticles on zeolite powder particles

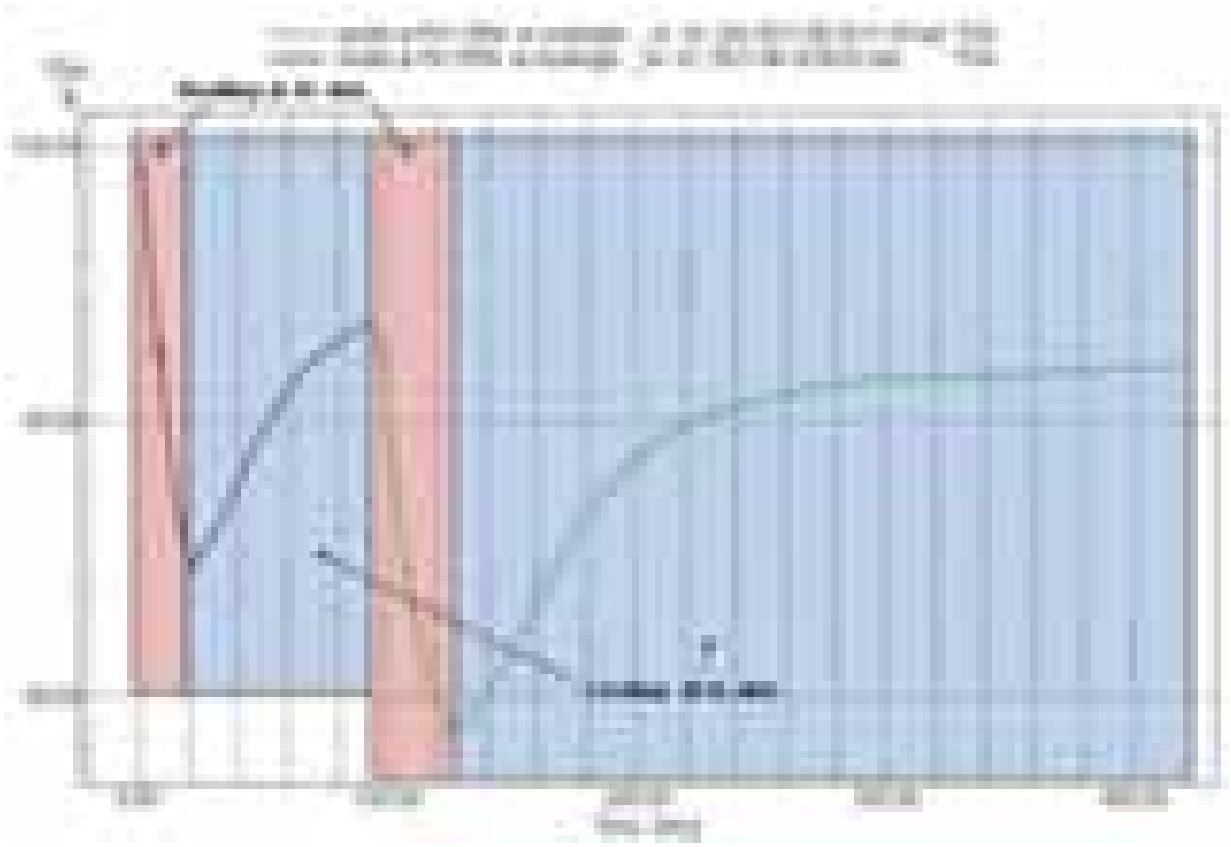

Fig. 1. Experimental results of natural Zeolite: cleaning from gases (heating at argon atmosphere from RT to 200 (300) ° C) and adsorbtion of hydrogen (cooling from 200 (300) ° C to RT).

SMART SOLID-STATE LIGHTING FOR THE ART SCENES

Andrius Petrulis[1], Arūnas Tuzikas[1]

[1] Institute of Applied Research, Vilnius University, Lithuania
andrius.petrulis@gmail.com

Here we present a novel solid-state lighting method for paintings and other visual art scenes. Recently we have shown that solid-state lighting with controlled colour quality can be used to increase the visual attractiveness of fresh fruits and vegetables [1], therefore such a technique can be optimized for the art.

Paintings usually do have an unstable colour appearance in long term time scale due to the permanent exposure of the light. Therefore the proper selection of lighting conditions is of crucial importance. The main recommendation for the art are reviewed in the literature [2]: spectral components of the wavelength shorter than 400 nm and longer than 700 nm have to be eliminated; it is not recommended to use more than 200 lx illuminance for ordinary paintings and more than 50 lx for very sensitive works; the light source has to be characterized with high colour rendition parameters; it is recommended to use a lower correlated colour temperature (CCT) sources meaning the lowering of the blue and red light component ratio; it is noted that radiant exposure instead of luminous exposure is responsible for the long term harm for the paintings, therefore it is recommended to use lighting with a maximized luminous efficacy; paintings accumulate the lighting damage, therefore movement sensors during the exposition time can reduce long term damage. Furthermore the trade-of between visual representation and lighting damage has to be considered since the illuminance below 50 lx reduces colour discrimination.

Art illumination recommendations can be realized and most of the problems solved with smart solid-state lighting. Such a technology is the most advanced for current time since the optimized colour quality white light sources can be designed and easily adopted for certain illumination requirements. For example the fading colours can be compensated by colour-saturating LED cluster containing red, pc amber, green and blue (RAGB) LEDs; aging varnish can be corrected with a higher CCT; an ultraviolet and infrared radiation is easily eliminated by selecting the proper solid-state lamp spectral power distribution; a luminous efficacy can be increased by otimising the primary colour sources; suitable and attractive lighting can be controlled considering art experts, exposition visitors, authors remarks and opinions.

Here we present our recent work with the painting of well-known Lithuanian artist Mikalojus Konstantinas Čiurlionis. His paintings were performed by using lower quality materials and the effects of aging varnish and colour fading can be observed. The research was started by collecting the trismulus values and chromaticity coordinates of the paintings by using the imaging photometer-colourimeter. Whole painting colour gamut can be drawn and lighting effects applied (fig. 1).

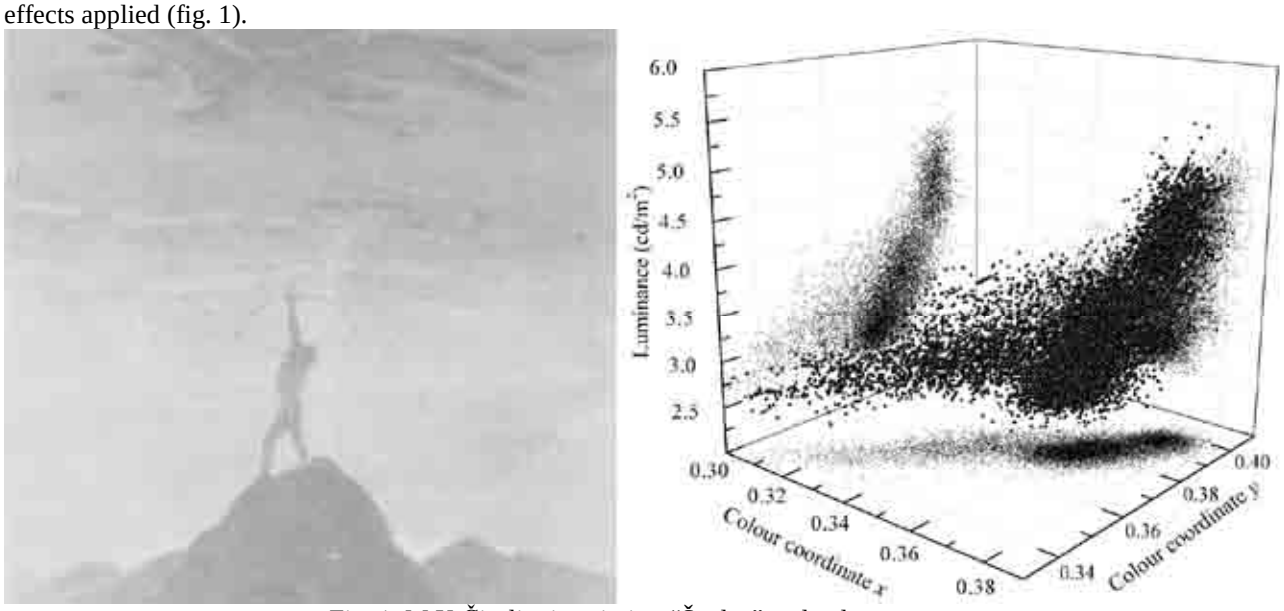

Fig. 1. M.K.Čiurlionis painting “Šaulys” and colour gamut.

[1] A. Žukauskas et. al., Color rendition engine, Optics Express Vol. 20, Issue 5, pp. 5356-5367 (2012).

[2] *Museum and art gallery lighting: A recommended practice*, New York: Illuminating Engineering Society of North America, IESNA (1996).

POSTER SESSION I

TWO BEAM PUMPED PARAMETRIC AMPLIFIER OF CHIRPED PULSES

Giedrė Marija Archipovaitė

Department of Quantum Electronics, Faculty of Physics, Vilnius University, Saulėtekio Ave. 9-III, LT-10222 Vilnius, Lithuania
giedre.archipovaite@ff.stud.vu.lt

Discovery of self-mode-locked Ti:sapphire lasers revolutionized the development of ultra-short laser systems. Typical pulse energy of these lasers varies from nanojoules generated in laser-oscillator to several milijoules in regenerative amplifiers and is sufficient for nonlinear optics or ultra-fast spectroscopy experiments, but laser-matter interaction experiments demands higher pulse energy, which is impossible to attain by unamplified pulse [1].

There are two ways to amplify chirped pulses: chirped pulse amplification in laser material (CPA) and optical parametric chirped pulse amplification (OPCPA). Both methods are based on pulse stretching, amplification and pulse compression. When short pulse is stretched in time its peak power is reduced and capability to damage amplifying crystal or laser material is lowered. An important parametric amplification feature is the possibility to use several pump beams. Each of pump beams must satisfy the phase-matching condition and generated idler pulse eliminates phase difference between pump and signal pulses [2].

The goal of this research was to design and investigate a two beam pumped parametric chirped pulse amplifier. Ti:sapphire oscillator was used to generate femtosecond pulses which were stretched in a bulk SF57 glass up to 10 ps. Pump pulses were generated in two parallel Nd:YAG regenerative amplifiers. The duration of pump pulses was ~50 ps and pulse energy of each channel was ~2,3 mJ. Stretched broadband seed pulses were amplified parametrically in a noncollinear configuration in two subsequent BBO crystals.

In order to examine properties of designed parametric amplifier we measured energy and spectrum of amplified pulses. After two amplification stages all broadband spectrum of Ti:sapphire laser was amplified. Pulse is amplified $5 \cdot 10^5$ times and the efficiency of amplification is 7 %. Spectra are shown in Fig. 1. The amplified signal spectrum in two-beam pumped configuration was shown to be as broad as in a single-beam pumping configuration and different pumping geometry is considered for increase of parametric conversion efficiency.

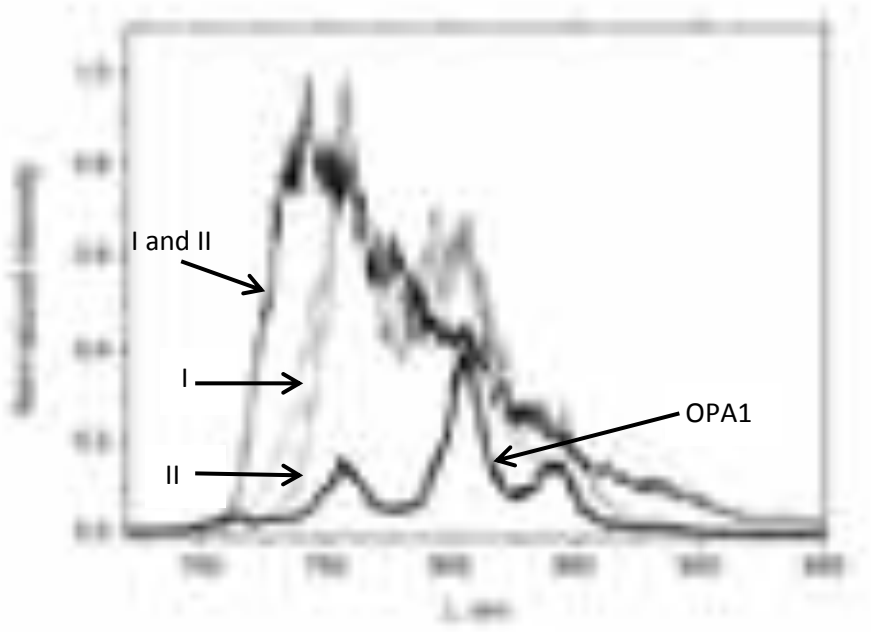

Fig. 1. In the first OPA stage amplified signal spectrum (OPA1) and spectra of signals amplified by separate pump beams and two beams together (I and II).

[1] A. Dubietis, R. Butkus and A.P. Piskarskas, Trends in chirped pulse optical parametric amplification, IEEE J. Sel. Top. Quantum Electron. 12(2), 163-172 (2006).

[2] A. Dubietis, R. Danielius, G. Tamošauskas and A. Piskarskas, „Combining effect in a multiple-beam-pumped optical parametric amplifier“, J. Opt. Soc. Am. B **15**(3), 1135-1139 (1998).

FABRICATION OF THREE—DIMENSIONAL POLYMER PHOTONIC CRYSTALS AND THEIR CHARACTERIZATION

Martynas Bertašius, Marius Rutkauskas, Lina Maigytė, and Mangirdas Malinauskas

Department of Quantum Electronics, Faculty of Physics, Vilnius University, Saulėtekio Ave. 9-III, LT-10222 Vilnius, Lithuania
martynas.bertasius@ff.stud.vu.lt

In recent years interest in photonic crystals has significantly increased. A photonic crystal is a microstructure, analogous to a crystal lattice, of which refractive index is periodically modulated. This quality of the crystal enables formation of structures possessing band gaps – energy ranges which restrict propagation of light waves of certain frequency and direction. Of these structures, three-dimensional photonic crystals are the most promising [1, 2].

Three-dimensional crystals of woodpile geometry can be fabricated by laser polymerization technique. Due to multiphoton light absorption, process of polymerization occurs and enables formation of three-dimensional structures, which exhibit spatial resolution that exceeds the diffraction limit [3].

Photonic crystals exhibit strong spatial dispersion properties which make spatial light-beam filtering possible [4]. This provides us with new possibilities of optical beams propagation control and self-collimation. Experimental investigation of propagation effects is mostly conducted on planar photonic crystals, which are easier to fabricate, yet full propagation control can only be achieved by using three-dimensional crystals [1].

We have fabricated variously structured photonic crystals of woodpile geometry using laser polymerization technique which possess visible and near-infrared range periods suitable for spatial light-beam filtering. We introduce the qualities of photonic crystals, properties of laser beams, and basic principles of multiphoton polymerization. Photosensitive materials, the equipment used in the experiment, fabrication steps and parameters are also presented. Moreover, samples of fabricated photonic crystals are introduced, their height, filling and spatial resolution are evaluated, and collimation effect of the crystals is investigated.

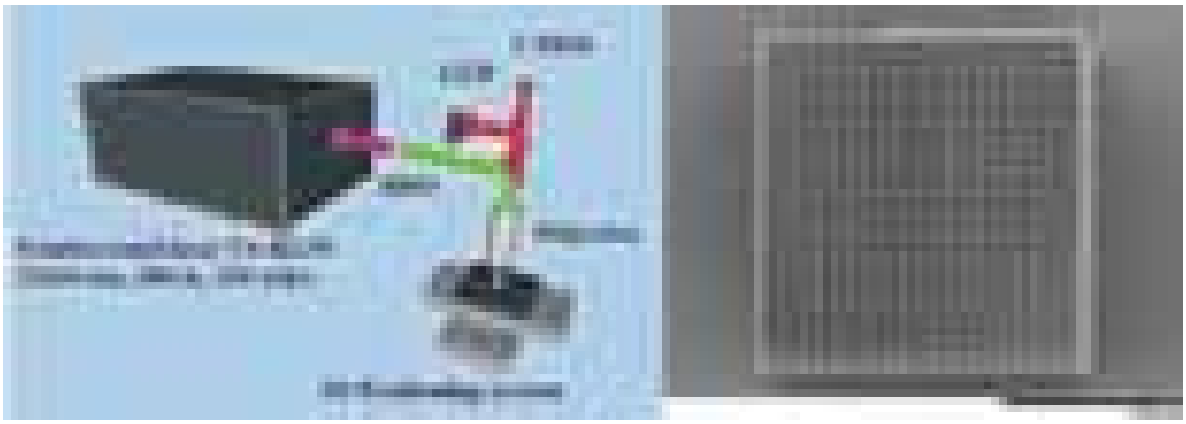

Fig. 1. Laser polymerization system scheme and fabricated photonic crystal.

[1] R. Iliew, C. Etrich, and F. Lederer, Self-collimation of light in three-dimensional photonic crystals, Opt. Express **13**, 7076-7085 (2005)

[2] J. D. Joannopoulos, S. G. Johnson, J. N. Winn, and R.D. Meade, Photonic crystals molding the flow of light, 2nd. ed. (Princeton University Press, Pinctonas and Oxford, 2008).

[3] J. Trull, L. Maigyte, V. Mizeikis, M. Malinauskas, S. Juodkazis, C. Cojocaru, M. Rutkauskas, M. Peckus, V. Sirutkaitis, and K. Staliunas, Formation of collimated beams behind the woodpile photonic crystal, Phys. Rev. A **84**, 033812 (2011)

[4] R. Zengerl, Light propagation in singly and doubly periodic planar waveguides, J. Mod. Opt. **34**, 1589-1617 (1987)

CHARACTERIZATION OF A GRISM STRETCHER BY WHITE-LIGHT SPECTRAL INTERFEROMETRY

Rimantas Budriūnas, Saulius Frankinas, Roman Antipenkov, Arūnas Varanavičius

Department of Quantum Electronics, Faculty of Physics, Vilnius University, Lithuania
rimantas.budriunas@ff.stud.vu.lt

Chirped pulse amplification and its extension, optical parametric chirped pulse amplification are some of the most widely used methods for producing high-energy ultra-short light pulses. In these techniques, laser pulses are stretched to avoid damage to certain optical components, amplified and then compressed again. Various stretching/compression methods have been proposed, including grisms [1]. The negative dispersion grism stretcher consists of a pair of prisms placed between two diffraction gratings. This setup is advantageous to several other systems due to compactness, high stretching ratio and tunability [2]. In this paper we present results of computer modeling and experimental characterization of a grism stretcher.

As the stretcher must be matched to the compression stages in the laser system, precise characterization of spectral phase introduced by the stretcher is required. Spectral phase can be expanded in Taylor series in the neighbourhood of a selected central frequency as

$$\Phi(\omega) = \Phi_0 + \Phi\prime(\omega-\omega_0) + \frac{1}{2}\Phi\prime\prime(\omega-\omega_0)^2 + \frac{1}{3!}\Phi\prime\prime\prime(\omega-\omega_0)^3 + \ldots$$

where the derivatives are evaluated at $\omega = \omega_0$. $\Phi\prime$ is called group delay and corresponds to the difference of arrival times of different spectral components at a point of observation. Once group delay values for different frequencies are known, relative spectral phase can be retrieved by integration. We performed an experiment of spectral interferometry [3] which allows direct measurement of group delay. The setup of our experiment is depicted schematically in Fig. 1.

The measurement system is based on the Michelson interferometer. As the mirror mounted on the delay line is moved, optical path lengths are equalized between the two arms of the interferometer for different wavelengths and interference fringes can be located in the spectra recorded by the spectrometer, thus allowing to determine group delay as a function of wavelength.

Having chosen the angle of incidence (AOI) of beam upon the face of the first prism, θ, as the variable parameter, we obtained several datasets corresponding to different AOIs. Group delay curves retrieved from experimental data are shown in Fig. 2 along with modeling results produced by our geometrical ray-tracing simulation.

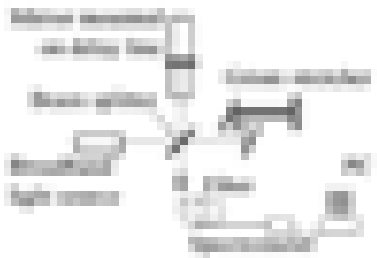

Fig. 1. Experimental setup. Standa STA-01 microchip laser pulses spectrally broadened by self-phase modulation in a photonic crystal fiber were used as the light source. In our experiment the footprint of the grism stretcher was smaller than 50mm x 60mm.

Fig. 2. Measured group delay curves and theoretical calculations for various incidence angles. Group delay has been set to zero at selected central wavelengths for convenient comparison.

In conclusion, experimental results generally confirm modeling predictions. Measurements at different angles had to be taken at different wavelength intervals because the operational spectral range of the stretcher is strongly dependent on AOI (in general, spectral range shifts to longer wavelengths with decreasing incidence angles). Reasonably accurate modeling allows implementation of the stretcher in an operational high-power laser system.

[1] J. Squier, S. Kane. Grism-pair stretcher-compressor system for simultaneous second- and third-order dispersion compensation in chirped-pulse amplification. JOSA B **14**, 661–665 (1997).

[2] H. Zacharias, J. Zheng. Design considerations for a compact grism stretcher for non-collinear optical parametric chirped-pulse amplication. Appl. Phys. B **96**, 445-452 (2009).

[3] C. Sainz, P. Jourdain, R. Escalona, and J. Calatroni. Real time interferometric measurements of dispersion curves. Opt. Commun. **110**, 381-390 (1994).

INVESTIGATION OF THE ELECTRICAL CHARACTERISTICS OF THE POWER-SUPPLY DRIVERS FOR SOLID-STATE LIGHTING

Laurynas Dabašinskas[1]

[1] Institute of Applied Research, Vilnius University, Lithuania
laurynas.dabasinskas@tmi.vu.lt

Solid-state lighting systems based on light emitting diodes (LED) become an important technology of general and niche lighting. One of the most attractive issues of this technology is a relatively high efficiency of light generation in LEDs in comparison to incandescent and fluorescent lamps. Nevertheless the major energy loss due to light conversion in a diode, the efficiency of power supplies are of high importance and has to be optimised [1].

The goal of current research was to investigate the electronic circuits of the high-power LED driving supplies with the main focus into the efficiency, the dimming ability and the electromagnetic interference. Four different integrated circuits realized according to manufacturer recommendations were tested and their ability of handling the excess voltage was investigated in the range of 15 V to 21 V at 3 diodes load. The results showed that switch-mode power supplies coped with excess voltage easily end exhibited efficiency of at least 95%. Meanwhile linear current stabilizer was not so advanced and demonstrated energy efficiency value in the range of 40% to 60% depending on excess voltage. Furthermore the efficiency and the average output current were investigated as functions of the dimming factor realized by a pulse-width modulation (PWM) in the range of 1 % to 99 % of duty cycle. The results showed that using certain switch-mode power supplies acceptable efficiency and linear current characteristics can be obtained. Nevertheless during the investigation of internal and output signals the switch-mode power supplies exhibited undesirable high-frequency oscillations which should be considered seriously in order to fulfil the standards of the electromagnetic interference and emission.

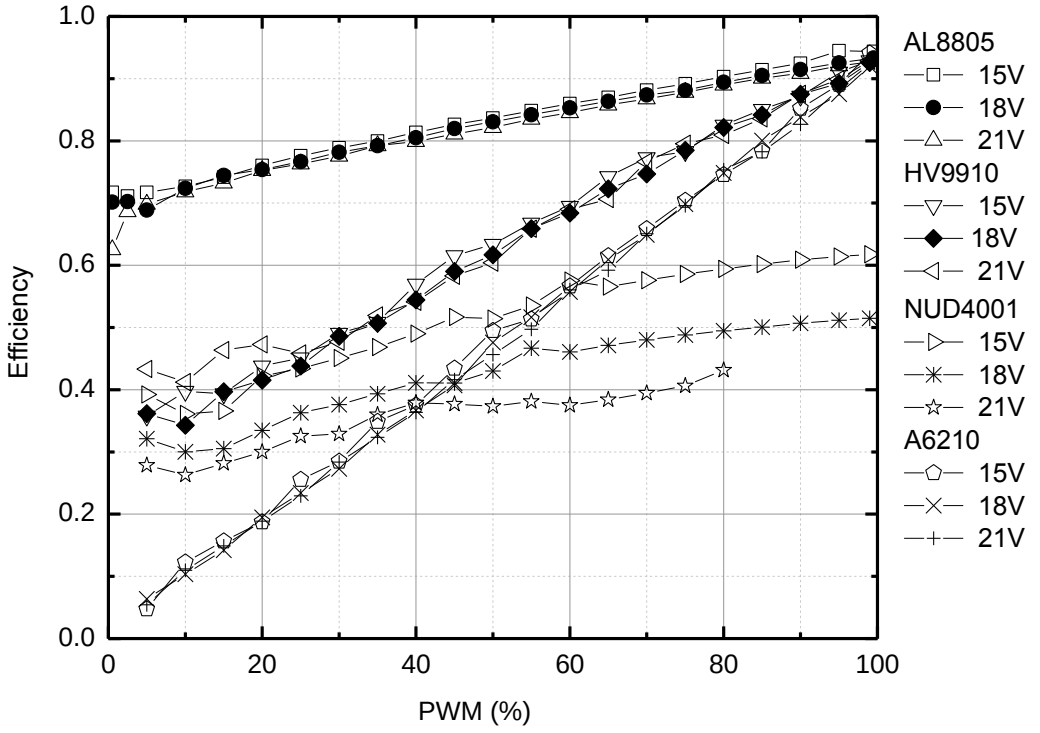

Fig. 1. Efficiency coefficient versus PWM duty cycle and supply voltage.

[1] S. Yoo, K. Um, H. Kim, „Highly Efficient LED Light Driver With Dimming Control Using Delta Sigma Modulation", *Telecommunications Energy Conference INTELEC 2009. 31st International*, 2009, pp. 1-4.

Comparison of radial, azimuthal, linear and circular polarization in laser micromachining under normal focusing conditions

Tomas Jankauskas[1], Titas Gertus[1], Martynas Beresna[2], Mindaugas Gecevičius[2]

[1]Vilniaus universitetas, Fizikos fakultetas, Saulėtekio al. 9, LT-10222 Vilnius
[2]Optoelectronics Research Centre, University of Southampton, SO17 1BJ, United Kingdom
tomas.jankauskas@ff.stud.vu.lt

Radial and azimuthal polarization beams which belong to axially symmetric beam class gained a lot of interest in recent years due to extraordinary features they exhibit. According to recent studies, beams with radial polarization can be focused to a tighter spot ($0{,}16(1)\lambda^2$) compared to linear polarization ($0{,}26\lambda^2$) under sharp focusing conditions [1]. Here sharp focusing conditions mean that the beam has to be focused using high numerical aperture (NA) objectives (>0.85) in order to obtain this feature. In this work focusing of beams with different polarizations under normal conditions is compared, i.e. using low NA lenses. Radial and azimuthal polarizations are obtained using polarization converter made by prof. G. Kazansky group of University of Southampton. This converter is based on inducing birefringent volume gratings with femtosecond pulses in fused silica [2].

In the experiments we used laser PHAROS which emits 1030 nm, 300 fs pulses. We have compared focusing of linear and radial polarization beams using plano-convex lens with focal length of 125 mm. Beam diameter was measured with CCD camera at different distance from the lens.

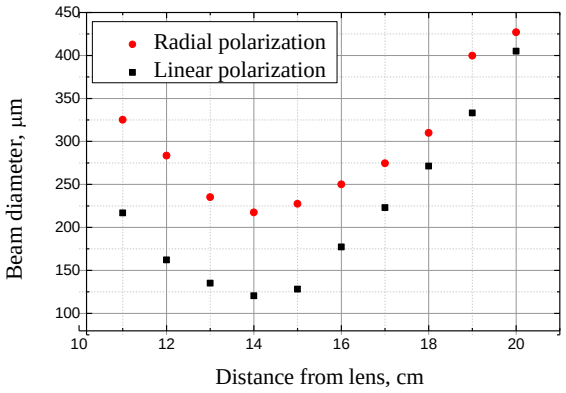

Fig. 1. Beam diameter vs. distance from lens

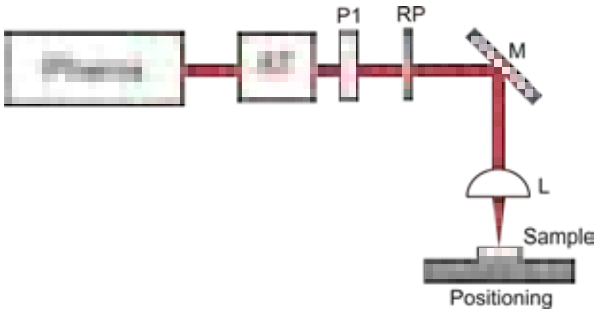

Fig. 2. Experimental scheme. AT – attenuator for control of beam power, P1 – half- or quarter-waveplate, M – system of high reflectivity mirrors for beam delivery, L – focusing lens.

In the other experiment a glass substrate with thin chromium layer was chosen and irradiated with different polarizations. Same conditions were chosen for each polarization: pulse repetition rate was fixed at 200 kHz, max. power of the beam before focusing aspheric lens with 0.4 NA lens was 74 mW. Beam diameters before lens at $1/e^2$ were 4.2 for radial/azimuthal and 3.9 for linear/circular polarizations respectively. Experimental scheme is shown in Fig. 2.

Samples were investigated using Olympus BX51 optical microscope. We have measured spot sizes of ablated chromium layer under different irradiation conditions and fixed power level. Number of pulses per spot or pulses per millimeter was varied during this part of the experiment. Results are shown in Table 1, smallest spot sizes marked in bold.

Table 1. Comparison of removed chromium layer spot sizes under different conditions.

Conditions	Single pulse	625 pulses	5000 pulses/mm	10000 pulses/mm
Radial	4,686	3,386	3,128	4,062
Azimuthal	4,626	2,937	2,936	4,348
Linear	**3,89**	2,234	2,106	**3,044**
Circular	4,156	**1,979**	**1,979**	3,318

After analyzing the results we have discovered that both radial and azimuthal polarizations are inferior in terms of spot size at the focal distance under normal focusing conditions. In addition, beams with radial and azimuthal polarization maintain non-homogeneous doughnut shape at the focal distance which can be advantageous in some laser micromachining applications.

[1] R. Dorn, S. Quabis, and G. Leuchs, Sharper Focus for a Radially Polarized Light Beam, Phys. Rev. Letters **91** (23), 233901-1 - 233901-4 (2003)
[2] M. Beresna, M. Gecevičius, and P. G. Kazansky, Polarization sensitive elements fabricated by femtosecond laser nanostructuring of glass, Opt. Mat. Expr. Vol. 1, No. 4, 783-795 (2011)

THE INFLUENCE OF THE IDLER WAVE LINEAR ABSORPTION ON THE PARAMETRIC AMPLIFICATION BANDWIDTH

Karolis Kalantojus[1], Gintaras Valiulis[1]

[1]Department of Quantum Electronics,Vilnius University,
Saulėtekio 9, Bldg. 3, LT-10222 Vilnius, Lithuania
karolis.kalantojus@gmail.com

The amplification bandwidth of the optical parametric amplifier (OPA) defines the duration of the signal and idler pulse. Usually the OPA bandwidth is defined by material dispersion and interaction geometry. [1]. However, even in the case of large linear absorption of the idler wave it is still possible to get effective amplification [2]. In current work we investigate the influence of the idler wave linear losses to the OPA bandwidth and efficiency. The equations governing parametric amplification were solved analytically within the plane wave approximation and dispersion approximation till 3-rd order. Pump wave were monochromatic and undepleted. Usually, if OPA delivers near infrared signal and middle infrared idler waves, just absorption of idler wave becomes significant and should be accounted for. In such case $\alpha_2 > 0, \alpha_1 \approx 0$, and OPA possess some new features. The solution of the equations describing OPA for the signal wave in spectral domain reads as:

$$S_1(\omega, z) \approx \frac{1}{2} S_{10}(\omega) \exp(-\mathrm{i} D_0(\omega) z) \exp\left\{ z\left[\sqrt{\Gamma_0^2 - \left[K_0(\omega) + \frac{\mathrm{i}}{2}\alpha_2(\omega) \right]^2} - \frac{1}{2}\alpha_2(\omega) \right] \right\}. \quad (1)$$

Here $S_{10}(\omega)$ is the signal pulse spectrum ant the input of the OPA, $D_0(\omega)$ is the parameter describing signal pulse dispersion, Γ_0 is the stationary gain coefficient, $K_0(\omega)$ is the parameter describing the parametric gain dependence on frequency i.e. the bandwidth of the OPA, when the linear absorption is negligible $\alpha_2(\omega) = 0$. The following conclusions could be done from the solution (1):

1) if idler wave absorption is dominant over material dispersion $K_0(\omega) << \alpha_2(\omega)$, thus instead of Eq.(1) we have $S_1(\omega, z) \propto \exp\left\{ z\left[\sqrt{\Gamma_0^2 + \frac{1}{4}\alpha_2(\omega)^2} - \frac{1}{2}\alpha_2(\omega) \right] \right\}$. Apparently the gain coefficient is always positive ($\sqrt{\Gamma_0^2 + \frac{1}{4}\alpha_2(\omega)^2} - \frac{1}{2}\alpha_2(\omega) > 0$). Even in the case of large absorption ($\Gamma_0 << \alpha_2(\omega)$) OPA still performs exponential amplification $S_1(\omega, z) \propto \exp\left\{ \frac{\Gamma_0^2 z}{\alpha_2(\omega)} \right\}$.However, at very high losses the gain coefficient drops from maximum possible in OPA value $\Gamma_0 z$ by factor $\frac{\Gamma_0}{\alpha_2(\omega)}$. Thus, the same amplification as in lossless medium could be also achieved in absorbing material, but in longer propagation distance.
2) In the case, when idler wave absorption is large and nearly independent on frequency ($K_0(\omega) << \alpha_2(\omega) = \alpha_2 = const.$), the gain during parametric amplification becomes also independent on frequency ω i.e. the gain bandwidth becomes broader (or even unlimited).
3) So, in the case of large idler wave absorption parametric amplifier sustains exponential gain with broaden amplification bandwidth. This imply, that despite large losses pulse spectral components could be amplified till the same level as in lossless medium, but within broader spectral range, and consequently, should have larger energy. In such way the idler wave absorption can increase OPA conversion efficiency.
4) The dispersion of the absorption coefficient should affect also amplification bandwidth and material dispersion. As can be seen from Eq.(1), the dependence of absorption coefficient on frequency also causes the gain dependence on frequency. The inhomogeneous amplification of different spectral components leads to formation of the pulse with the non-symmetric spectra.

Acknowledgement

Karolis Kalantojus acknowledges Student Research Fellowship Award from the Lithuanian Science Council

[1] G. Valiulis, A. Dubietis, and A. Piskarskas, PHYSICAL REVIEW A **77**, 043824 _2008
[2] G. Rustad, G. Arisholm ,Ø. Farsund, OPTICS EXPRESS, **19**, 2815 (2011)

INVESTIGATION OF FEATURE SIZE DEPENDENCE ON MULTIPATH SCANNING IN DIRECT LASER WRITING OF PHOTOPOLYMERS

Eglė Kaziulionytė, Sima Rekštytė, Domas Paipulas, Mangirdas Malinauskas

Vilnius University, Physics Faculty, Department of Quantum Electronics, Laser Research Center, Saulėtekio al. 10, LT-10223 Vilnius
Egle.Kaziulionyte@ff.vu.lt

Concerning high-resolution three-dimensional laser micro fabrication, the two-photon polymerization (2PP) technique using femtosecond laser pulses for processing photosensitive materials is the state-of-the-art method up to date [1-3]. 2PP is based on quadratic dependence of two photon absorption rate on light intensity in a photosensitive material. This confines polymerization area to be spatially highly localized at the focal point of a laser beam [1, 4]. By precisely moving the sample or beam focus position one can point-by-point solidify the photopolymer. After exposure the rest of the unexposed material is washed out by the solvent during developing process and only the desired structure remains on the substrate. [5,6]

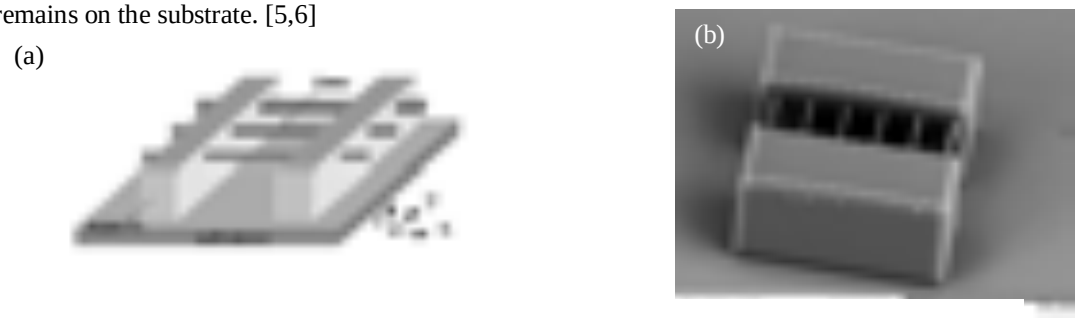

Fig. 1. (a) Scheme for the fabrication of lines. Lines thicken as the number of scans increases from 1 to 3 corresponding from bottom to top; (b) the microstructure out of Zr containing hybrid organic-inorganic biocompatible polymer SZ2080. [7]

To be able to form precise structures it is required to investigate how modification of the different fabrication influences the resolution of the fabricated structure. In this report, we present micro structures fabricated out of photopolymer SZ2080.The dependence of fabrication parameters on laser irradiation power, number of scans and sample translation velocity was investigated. The resolution dependence was analyzed by measuring the width and the height of all lines of the structures. Therefore, it was obtained that as the number of scans over the same area is increasing, the width and the height of lines are also increasing. Other conclusions were derived from the investigations of line width and height dependences on sample translation velocity and irradiation power.

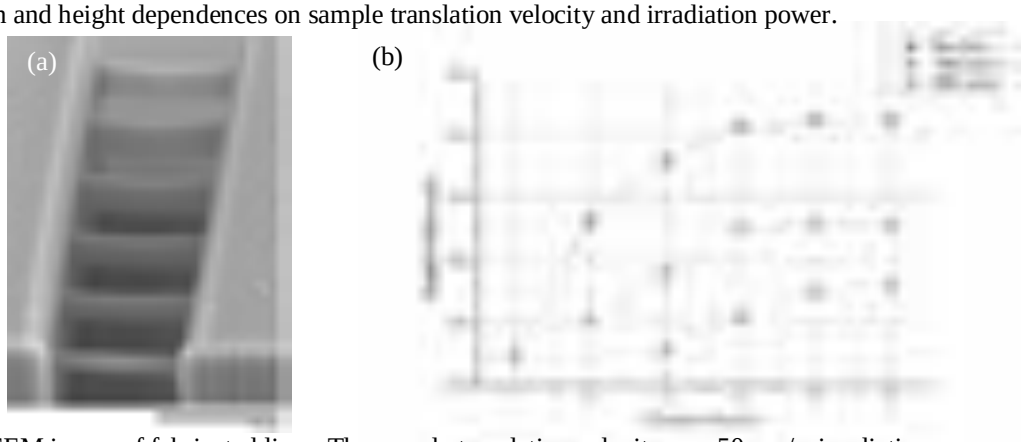

Fig. 2. (a) SEM image of fabricated lines. The sample translation velocity was 50 μm/s, irradiation power - 14 mW and the number of scans increased from 1 to 6 corresponding from bottom to top. The height of lines varies from 2,23 to 4,12 μm; (b) the graph shows the height of line dependence on number of scans with different sample translation velocities.

[1] S. Kawata, H.-B. Sun, T. Tanaka, K. Takada: Nature 412, (2001) 697-698.
[2] J. Serbin, A. Egbert, A. Ostendorf, B. N. Chichkov, R. Houbertz, G. Domann, J. Schulz, C. Cronauer, L. Fröhlich, M. Popall: Opt. Lett, 28(5), (2003) 301-303.
[3] R. Houbertz: Appl. Surf. Sci. 247, (2005) 505.
[4] S. Juodkazis, V. Mizeikis, K.K. Seet, M. Mima, H. Misawa, Two-photon lithography of nanorodsin SU-8 photoresist, Nanotechnology **16**, 846 849 (2005).
[5] H. -B. Sun and S. Kawata, Two-Photon photopolymerization and 3D lithographic microfabrication, Adv. Polym. Sci. **170**, 169-273 (2004).
[6] M. Malinauskas, H. Gilbergs et al., Femtosecond laser-induced two-photon photopolymerization for structuring of micro-optical and photonic devices, Proc. of SPIE **7366**, 736622 (2009).
[7] A. Ovsianikov, J. Viertl, B. Chichkov, M. Oubaha, B. MacCraith, I. Sakellari, A. Giakoumaki, D. Gray, M. Vamvakaki, M. Farsari and C. Fotakis, Ultra-Low Shrinkage Hybrid Photosensitive Material for Two-Photon Polymerization Microfabrication, ACS Nano **2**(11), 2257-2262, 2008.

DEVELOPMENT OF LASER TECHNOLOGIES FOR GLASS PROCESSING USING THIN WATER FILM

Edgaras Markauskas, Paulius Gečys

Center for Physical Sciences and Technology, Savanoriu ave. 231, LT-02300, Vilnius, Lithuania
Edgaras.Markauskas@ff.stud.vu.lt

The main obstacle in applying laser processing technology in specific applications such as glass cutting are the debris [1] and micro-crack formation [2]. Cracking, chipping and laser induced thermal effects could lead to the degradation of the mechanical and bending strength of the glass.

Some studies have shown increased ablation quality and efficiency in underwater or water-assisted laser machining [3]. The effect of water in laser processing mostly consists of conversion of part of the light energy to mechanical impulse, which transports debris, nano-particles away from the working area, cools the workpiece more effectively than gases. Usage of water may cause useful chemical reactions with material surface and reduce atmospheric pollution by waste gases and aerosols [4].

Solid-state Nd:YVO_4 laser with picosecond pulse duration (100 kHz rate and 1064 nm wavelength) together with airbrush spraying water mist on sample surface were used in the experiments. Soda-lime-silica glass plates of thickness of 1.3 mm where used as the samples.

In the experiments trenches on glass surface were scribed by changing laser scanning speed, laser power and angle of airbrush which sprayed water mist forming thin water film on glass surface. Scribes were done in two regimes: laser processing in ambient air and using airbrush.

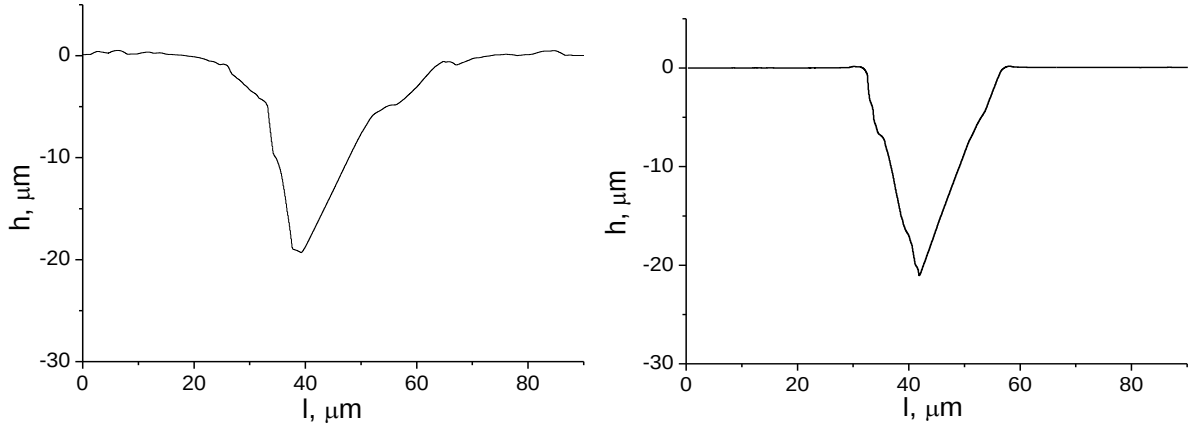

Fig. 1. Cross-sectional profiles of scribed trenches a) in ambient air b) underwater.

Optimization of water spray system was performed. Optimal parameters such as aerograph inclination angle and nozzle distance from the surface were defined. Further, the ablation thresholds of glass were measured for water assisted ablation and in ambient air. Line scribing experiments were also realized. For the scribing speeds lower than 32 mm/s water assisted processing enabled to increase the *h* depth and reduce the *l* width of the trenches compared to processed in ambient air (Fig. 1).

Water assistance in glass cutting applications is a perspective technology and able to increase the ablation rate and optimize the cutting process.

[1] T. A. Mai, *Toward debris-free laser micromachining.* Industrial Laser Solutions, 2008. **23**(1).
[2] C.-H. Tsai, C.-C. Li, *Investigation of underwater laser drilling for brittle substrates.* Journal of Materials Processing Technology, 2009. **209**(6): p. 2838-2846.
[3] A. Dupont, et al., *Enhancement of material ablation using 248, 308, 532, 1064 nm laser pulse with a water film on the treated surface.* Journal of Applied Physics, 1995. **78**(3): p. 2022-2028.
[4] K. Arvi, *Underwater and water-assisted laser processing: Part 1 general features, steam cleaning and shock processing.* Optics and Lasers in Engineering, 2004. **41**(2): p. 307-327.

A SYSTEM FOR MEASURING SURFACE ROUGHNESS BY TOTAL INTEGRATED SCATTERING

Lina Mažulė[1*], Simona Liukaitytė[1], Valdas Sirutkaitis[1]

[1] Laser Research Centre, Vilnius University, Sauletekio 10, 10223 Vilnius, Lithuania
Lina.mazule@ff.stud.vu.lt

Surface roughness, contaminations, micro scratches, fractures, various defects and fluctuations of the density in the bulk of optical component reduce quality of the components and increase scattering of the incident light [1]. There are several techniques for testing surface topography. The Nomarski microscope, atomic-force microscope, electron microscope, scanning tunneling microscope and other microscopes are used for direct investigation.

Light scattering measurements are indirect methods for testing the topography of a surface. These measurements allow the rapid evaluation of larger surface areas [2, 1]. The theory of light scattering enables us to calculate the surface roughness from light scattering, and the measurements can have resolution appropriate for the evaluation of super-polished surfaces (the roughness of surfaces in the range of few Å).

A system for measurement of surface roughness based on total integrated scattering (TIS) at 1064nm, 532 nm and 355 nm is built and demonstrated (Fig. 1). Surfaces up to 25 mm×25 mm are scanned in 6 minutes with a spatial resolution of 0.4 mm. Careful attention to reducing stray light and purging the measurement chamber with filtered air allow scattering resolution better than 10^{-5} (Table 1). Surface roughness measurements better than 1 nm RMS are demonstrated and confirmed by comparison measurements with an atomic-force microscope [3].

Fig. 1 Total integrated scattering measurement setup (1 - laser with harmonic generators, 2 – the other laser (wavelengths: 1030, 515 and 343 nm), 3 – attenuator, 4, 5, 9 and 11 mirrors, 6, 7 and 8 – filters, 10 - 1 m focal lens, 12 – aperture, 13 – Ulbricht sphere, 14 - translation stage, 15 - detector, 16 – beam dumps, 17- the chamber of measurements, 18 - clean air flow, 19 - return air flow, 20 – computer).

Table 1 The scattering measurement resolution for different wavelengths

Wavelength, nm:	1064	532	355
The scattering signal without the sample, ppm:	4.2±0.1	4.5±0.5	9.6±0.9

Fig. 2 The surface roughness of high reflectance mirror at 1064 nm AOI=0 deg.

[1] Amra C, Torricini D and Roche P 1993 Multiwavelength (0.45-10.6 μm) angle-resolved scatterometer or how to extend the optical window *Appl. Opt.* **32** 5462-74

[2] Bennett J M and Mattsson L 1999 *Introduction to surface roughness and scattering* (Washington, D.C.: Optical Society of America)

[3] L Mazule S L, R C Eckardt, A Melninkaitis, O Balachninaite, V Sirutkaitis 2011 A system for measuring surface roughness by total integrated scattering *Journal of Physics D: Applied Physics* **44** 9

MEASUREMENTS OF CARRIER RELAXATION TIME IN SINGLE LAYER NB_2O_5 COATINGS

Simona Paurazaitė, Kipras Redeckas

Laser Research Center, Department of Quantum Electronics, Vilnius University, Saulėtekio Ave. 10, LT – 10223 Vilnius, Lithuania
simona.paurazaite@ff.stud.vu.lt

Thin film coatings are widely used in many high-tech applications in order to improve or modify optical properties of surfaces. Niobium pentoxide (Nb_2O_5) is very important material for optical coating technology in the visible spectral region. It is used considerably when making high refractive index thin film layers. The experimental samples of single layer coatings were deposited by using a modified ion – beam sputtering (IBS) technique on 1 mm thick fused – silica (UV grade KU 1 glass) substrates. High – energy IBS deposition is known to fulfill demanding requirements and result in high optical quality [1]. However, when dealing with high intensity lasers the optical resistance of laser components becomes an important factor limiting the lifetime of optics. In femtosecond regime laser-induced damage is driven by optical energy coupling in electron subsystem. Therefore by employing pump-probe technique here we study the electronic relaxation processes in niobia coatings induced by femtosecond laser irradiation.

Table 1. Properties of experimental niobia samples.

Material	l_{ph}, nm	n_{1064}	n_{1030}	E_{gC}, eV	E_{gT}, eV	E_{gU}, eV
Fused silica substrate	1 mm	1,46	1,46	-	-	≈ 9
Nb_2O_5 layer	717	2,23	2,23	3,43	3,46	3,92

E_g - optical band gap obtained by different methods; l_{ph} – physical thickness; n – refractive index;

The pump-probe technique is based on measurements of transient laser-induced absorption. The main idea: sample is firstly exposed with an ultra-short UV pulse (pump); afterwards a broadband white light supercontinuum pulse (probe) travels through the irradiated zone and is partially absorbed by the sample. In this way, by changing the delay time between pump and the probe pulses, we can record temporal dynamics of the absorption spectrum. The initial source of both pump and probe laser pulses is a commercial femtosecond laser system, which consists of a titanium sapphire oscillator operating in a Kerr lens synchronization mode and is further amplified by (Millenia/Tsunami/Evoliution-X-/Spitfire, Spectra Physics) laser system. Most of the beam coming from the laser (95%) is directed into an optical parametric amplifier (TOPAS, Light Conversion) and the rest of the beam (5%) – to probe delay line.

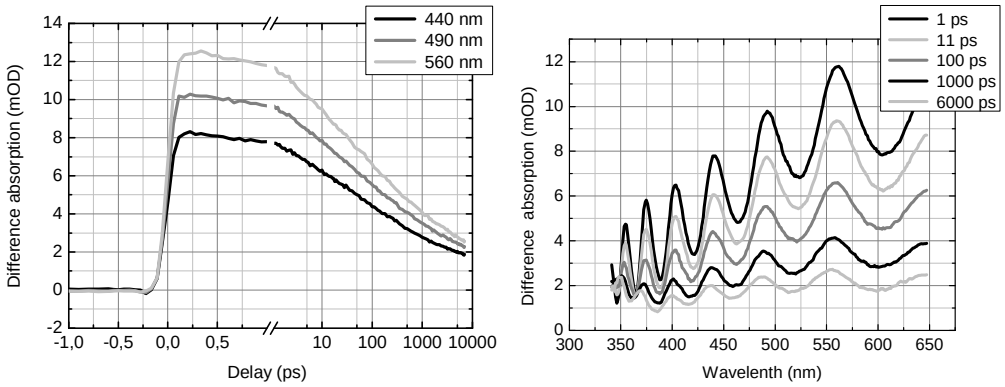

(a) (b)

Fig.1. Experimental results of the pump-probe measurements of Nb_2O_5 sample (λ = 330 nm, E = 600 nJ, τ = 150 fs). (a) the kinetic traces at selected wavelengths and (b) time – gated spectra at different delay times.

The sum of three exponential curves provides a good approximation of experimental data. The fit indicates three electronic transitions that correspond to 6ps, 200 ps, and 13 ns characteristic lifetimes. Sample absorption spectrum is blue shifted compared to unexcited state.

Acknowledgements

This work was partly supported by the Lithuanian Science Council Research Fellowship Award (S.P.).

[1] A. Melninkaitis, T. Tolenis,L. Mažulė, J. Mirauskas, V. Sirutkaitis, B. Mangote, X. Fu, M.Zerrad,L. Gallais, M. Commandré, S. Kičas, R. Drazdys, Characterization of zirconia– and niobia silica mixture coatings produced by ion-beam sputtering, APPLIED OPTICS, Vol. 50(9), 2011

Subwavelength Lüneberg lens on silicon-on-insulator for spot-size converter

Mindaugas Pranaitis[1], Darius Urbonas[2], Raimondas Petruškevicius[2]

[1] Faculty of Physics, University of Vilnius, Lithuania
[2] Department of Laser Technologies, Institute of Physics, Center for Physical Sciences and Technology, Lithuania
Mindaugas.Pranaitis.2@ff.stud.vu.lt

Currently there is a huge interest in Silicon-on-Insulator (SOI) nanophotonics and its application for signal processing and transmitting [1]. One of the main problems in SOI nanophotonics is efficient coupling of light into the optical circuits. Efficiency of end-fire and butt coupling methods very much depends on reflections from interfaces and spatial alignment of waveguides and their fields. An alternative method to couple light is using of diffraction gratings, made out of periodic sub-wavelength structures. Efficiency of such couplers may exceed 50% or even 70%, if multilayer reflectors are used.

The aim of this work was to create a device composed of sub-wavelength structures that would work as a lens spot-size converter for wavelength of 1.55 μm (optical communication wavelength). Such device would allow to significantly decrease length of tapers, that connect SOI waveguides and diffraction gratings couplers.

Here we propose a subwavelength SOI structure with effective gradient index similar to Lüneburg lens, mentioned in [2]:

$$n(r) = n_0\sqrt{2 - k(r/R)^2}$$

Where R is the radius of the lens region, k is the ratio of lens area and ideal Lüneburg lens area, n_0 is the ambient index outside the lens region and r is the radial polar coordinate with the lens region as origin. Unlike the ideal Lüneburg lens, which focuses a plane wave on the spot of its surface, this lens has a greater focal length, which depends on k.

The effective refractive index of the SOI media was calculated using methods described in [2] and [3]. For simulation of electromagnetic wave propagation in such structures we used "MEEP" software package [4] based on a Finite Difference Time Domain (FDTD) method.

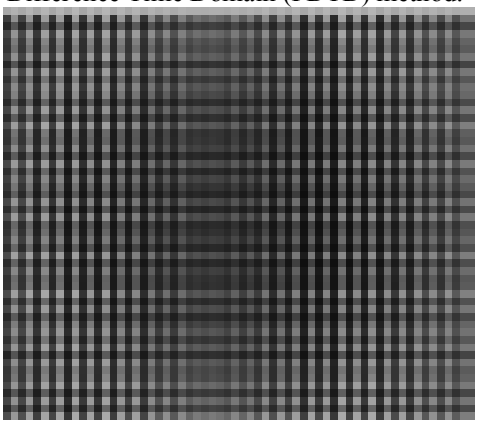

Fig. 1. Example of lens structure.

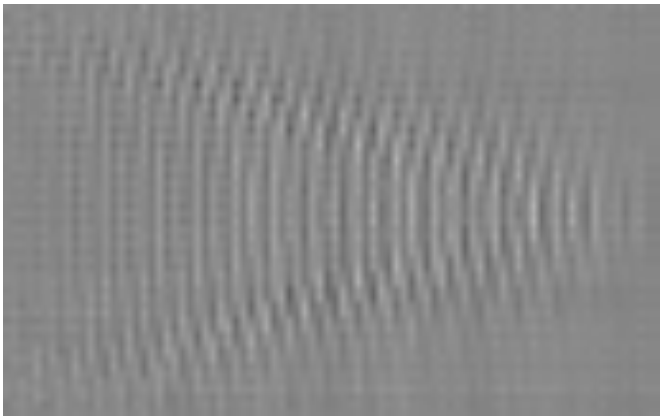

Fig. 2. Simulation of electromagnetic wave propagation through the lens.

An example of simulation results is presented in Fig. 1 and Fig. 2. Fig. 1 shows a design of gradient index lens structure. White color represents material of low permittivity, while black color represents material of high permittivity. Fig. 2 shows how this lens focuses a plane wave.

In conclusion, it was shown, that modulating the size of holes in subwavelength SOI structure, the effective gradient index Lüneburg lens can be created to convert spot-size of coupled waves to SOI waveguides.

[1] P.Dumon, G.Priem, L.R.Nunes, W.Bogaerts, D. van Thourhout, P.Bienstman, T.k.Liang, M.Tsuchiya, P.Jaenen, S.Beckx, J.Wouters, R.Baets *Linear and nonlinear nanophotonics devices on Silicon-on-Insulator wire waveguides* (Japanesse Journal of Applied Physics, Vol. 45, No.8B, 6589, 2006)

[2] H. Gao, B. Zhang, S. G. Johnson, G. Barbastathis *Design of thin–film photonic metamaterial L¨uneburg lens usinganalytical approach* (OPTICS EXPRESS, Vol. 20, No. 2, 1617, 2012)

[3] R. Brauer, O. Bryngdahl *Design of antireflection gratings with approximate and rigorous methods* (APPLIED OPTICS, Vol. 33, No. 34, 7875 1994)

[4] A.F. Oskoor, D.Roundy, M.Ibanescu, P.Bermel, J.D.Joannopoulos, S.G.Johnson *Meep: A flexible free-software package for electromagnetic simulations by FDTD method* (Computer Physics Communications, Vol. 181, 687, 2010)

AN INVESTIGATION OF ULTRAFAST NONLINEAR DYNAMICS IN THIN GAN FILMS BY TIME RESOLVED DIGITAL HOLOGRAPHY

Nerijus Šiaulys, Aivaras Urniežius, Tomas Stanislauskas, Viačeslav Kudriašov, Andrius Melninkaitis

Laser Research Center, Vilnius University, Saulėtekio 10, 10223 Vilnius, Lithuania
Nerijus.Siaulys@ff.stud.vu.lt

Nonlinear propagation of ultrashort pulses in transparent materials is an active field of research with many remarkable phenomena and applications [1]. Also, there is an increasing interest in nonlinear interactions in artificial materials suitable for all-optical applications [2,3]. Among various media GaN is considered to be one of the most prospective materials for future photonic devices [4]. However, to efficiently exploit it's properties, a better understanding of the interplay between linear and nonlinear effects is needed, requiring more sophisticated methods to detect the processes occurring on ultrafast temporal scales.

In this work, for the first time nonlinear propagation and filamentation of femtosecond pulses in thin GaN crystalline films were studied by means of time resolved digital holography [5] with 25 fs temporal and better than 2 μm spatial resolution (both amplitude and phase). 13,5 μm thickness GaN films used in our experiments were grown on sapphire substrate using metal-organic chemical vapor deposition method. For the studies of ultrafast nonlinear dynamics in these films we used femtosecond Yb:KGW laser („Pharos", Light Conversion) that generates λ=1,03 μm wavelength and τ=300 fs duration pulses. Ultrafast response in GaN films was excited with fundamental Yb:KGW pulses focused to the diameter of 13,4 μm (1/e) on the edge of GaN. To probe ultrafast dynamics a digital holographic microscope with Mach-Zehnder configuration was used. λ=522 nm wavelength probe pulses were generated by the non-collinear parametric amplifier. This system allowed us to study light-matter interaction in transmittance mode by changing the energy and polarization of the pump pulse and its delay relative to the probe. Amplitude- and phase-contrast images reconstructed from the experimentally registered holograms are shown in Fig.1. These images clearly indicate nonlinear propagation features of the 300 fs pump pulse (1030 nm) in GaN. Direct observations show a wide range of interesting nonlinear effects occurring in GaN film at high intensity: Kerr effect, formation of free electron plasma and pulse defocusing are few to mention. Phase contrast images also allowed us to directly evaluate the nonlinear refractive index change induced by 1030 nm pulses from the phase change at 522 nm probe pulse. Using time delay between the pump and probe pulses an observation of the pump pulse propagation at different time is possible. It allows direct calculation of the refractive index in GAN at 1030 nm wavelength. In overall, we demonstrated that femtosecond digital holography is a novel tool well suited for the investigation of a whole range of nonlinear phenomena taking place in transparent semiconductors and dielectrics.

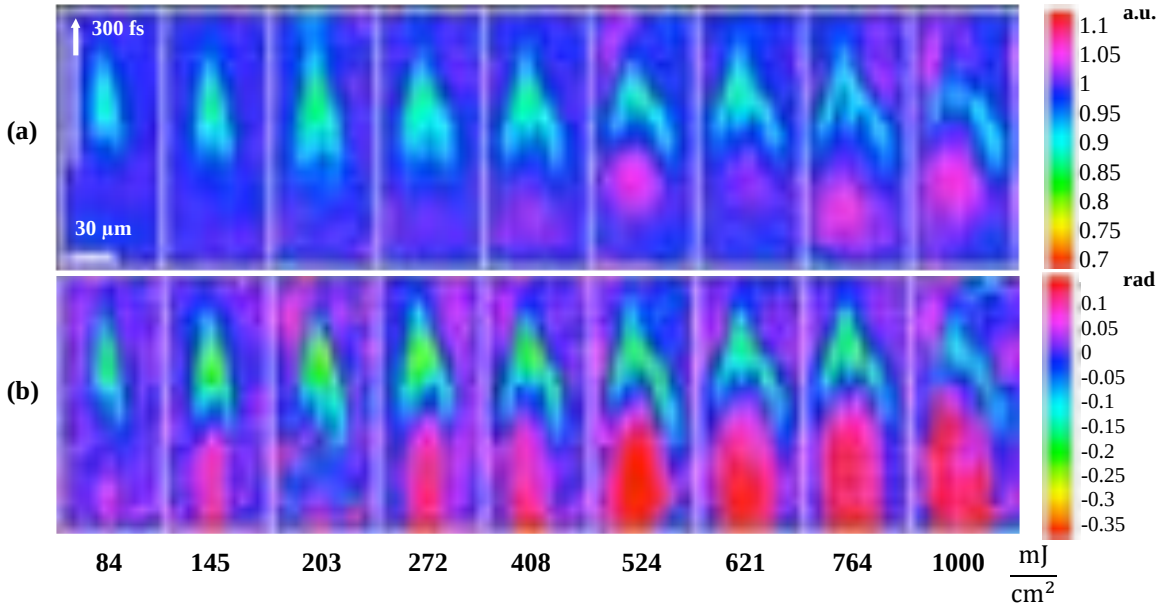

Fig.1. Amplitude (a) and phase (b) contrast images reconstructed from the probe pulse digital holograms in GaN film at different pump pulse energy densities.

[1] A. Couairon and A. Mysyrowicz, Phys. Rep. **441**, 47 (2007).
[2] R. Dekker, N. Usechak, M. Forst, and A. Driessen, J. Phys. D: Appl. Phys. **40**, R249 (2007).
[3] H. Ishikawa, ed., Ultrafast All-Optical Signal Processing Devices, Wiley, 2008, 258 p.
[4] B. Gil, ed., Group III Nitride Semiconductor Compounds, Oxford University Press, 1998, 470 p.
[5] T. Balciunas, A. Melninkaitis, G. Tamosauskas, and V. Sirutkaitis, Opt. Lett. **33**, 58 (2008).

CHARACTERIZATION OF DEGRADATION PROCESS IN HIGH POWER WHITE LIGHT NITRIDE-BASED LEDs BY LOW-FREQUENCY NOISE

Augustinas Trinkūnas, Jonas Matukas, Bronius Šaulys, Sandra Pralgauskaitė, Vilius Palenskis

Faculty of Physics, Vilnius University, Lithuania
augustinas.trinkunas@ff.stud.vu.lt

Nowadays light-emitting diodes (LEDs) span all visible light spectrum and beyond. Nitride-based materials are used for green-blue radiation, to cover ultraviolet region, also for white LEDs.

However, nitride layers in heterostructure lead to additional defects due to lattice mismatch with substrate [1]. Also phosphor layer used in the white LEDs can be additional source of device degradation. The defects worsen LED optical and electrical characteristics, increase leakage current that lowers LED efficiency and accelerates degradation processes [2]. The questions: in which part of the structure defects appear, how they influence device operation characteristics and how they behave during device aging, are always actual for any semiconductor structure. At this point, noise investigation gives valuable information and is useful for evaluating semiconductor device quality and predicting lifetime [3].

The aim of the work was to investigate white light emitting diode low frequency noise characteristics, to clear up physical processes that take part in different parts of the LEDs and influence their lifetime. High power nitride-based white light emitting diode has been investigated. Noise characteristics (electrical noise and optical noise spectra, cross-correlation factor) have been measured in low frequency (20 Hz – 20 kHz) region for initial samples and after accelerated aging. LED output light power and optical noise signal is measured by 3 photodiodes array. These photodiodes (PDs) are sensitive to different part of visible spectrum: the first PD sensitivity maximum coincides with blue light peak (around 460 nm), the third – with broad phosphorous radiation peak ((540-700) nm). Therefore, we are able to separate and investigate different parts of the white LED optical spectrum: "blue" optical signal from the active region and "phosphorous" - from the phosphor layer. Such division of radiation spectrum enables us to separate physical processes that take part in different parts of the structure and find out, which of them influence device degradation foremost. There is positive (40-50) % cross-correlation between electrical fluctuations and "blue" optical noise signal; similar cross-correlation is observed between electrical and "phosphorous" optical noises. Such cross-correlation values are observed at low frequencies, where 1/f $^{\alpha}$-type fluctuations dominate both in optical and electrical noises. Cross-correlation factor is low (close to zero) at frequencies above 100 Hz, where optical shot noise (caused by random photon emission process) is intensive. The results show that there are defects in the investigated LED structure that lead to the 1/f $^{\alpha}$-type electrical fluctuations and these fluctuations partly modulate current flow through the active region. Cross-correlation between two optical ("blue" and "phosphorous") signals is high ((80-90) %) and positive over all investigated current region. Therefore, phosphor layer and further light transmission path from the active region to open space do not have any influence to the propagating light.

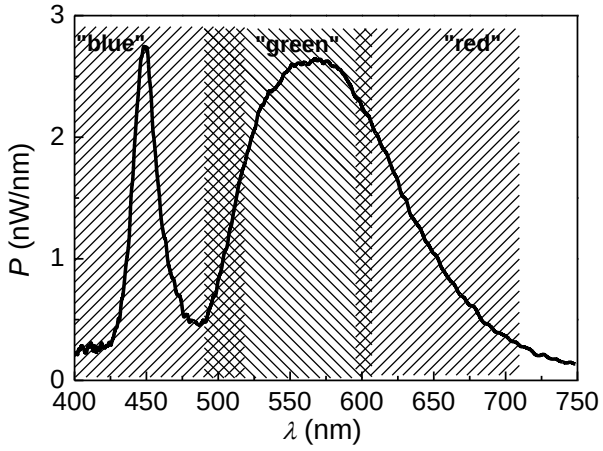

Fig. 1. Radiation spectrum of investigated white LED at 300 mA forward current. Lined areas show spectrum part that is covered by each of the photodetectors

[1] [1] Y.-J. Lee, H.-C. Kuo, T.-C. Lu, S.-C. Wang, K. W. Ng, K. M. Lau, Z.-P. Yang, A. S.-P. Chang,.S.-Y. Lin, J. Light. Technol. 26, 1455 (2008).

[2] [2] Z. Li, P. T. Lai, and H. W. Choi, IEEE Photon. Technol. Lett. 21, 1429 (2009).

[3] [3] D. Ursutiu and B. K. Jones, Semicond. Sci. Technol. 11, 1133 (1996).

TERAHERTZ IMAGING IN THE REFLECTION GEOMETRY

Laurynas Tumonis[1,2], Rimvydas Venckevičius[2]

[1] Vilnius University faculty of physics, Saulėtekio al. 9, bldg. III, LT-10222 Vilnius, Lithuania
[2] Semiconductor Physics Institute of Center for Physical Sciences and Technology,
A. Goštauto str. 11, LT-01108, Vilnius, Lithuania
tumonis.laurynas@gmail.com

Terahertz (THz) radiation is in the frequency gap between the microwave and far infrared regions of the electromagnetic radiation spectrum. Terahertz sensing and imaging technology has been investigated in various fields, including security, medicine, biochemical applications. THz radiation offers a non-destructive and non-ionizing way of imaging and spectroscopy measurements. Recent work [1] has shown that THz waves can be used for material inspection and spectroscopy imaging.

In this work THz imaging set up and solid solar cell image in reflection geometry is presented. The THz imaging setup of the experiment is shown in (Fig. 1a). The main laser beam is divided by the beam splitter BS in two parts, where one travels to a parabolic mirror M1 and is focused on the reference detector D1. This signal is used to monitor the changes of radiation power of the THz laser. Other part of the beam is used to measure reflectivity of the sample. Off-axis parabolic mirrors M2 and M3 were used to focus the beam on the sample and collect reflected radiation. For low-noise signal detection beam was modulated with optical chopper. Detector signals were measured with synchronous amplifiers (lock-in).

We scanned the solar cell with defected contact to test our reflection system. THz image of the monocrystalline Si solar cell was recorded by moving the objected in XY plane. Scanning takes place while object is moved in direction X with the fast linear stage with a constant speed of 10 mm/s. Using this method image recording time depends on imaging area, sample translation velocity, speed of detection system and desired image resolution. The reflection image of solar cell taken with THz radiation of frequency 2.54 THz is shown in (Fig. 1c) while its visible light photo is in (Fig. 1b). Color scale of signal value shown on the right side of picture normalized in logarithmic scale. Total scanning time of area 90×99 mm^2 with pixel size 0.3×0.5 mm^2 was about 30 minutes.

a) b) c)

Fig. 1. The THz imaging setup (a) of the experiment where M1, M5 – spherical mirrors; M2, M3- off-axis parabolic mirrors; M4- flat mirror; monocrystalline Si solar cell with defected top contact (b); image of the solar cell taken with THz radiation in reflection geometry (c);

To summarize, in this work the THz imaging setup in reflection geometry was created and solar cell image with defected top contact at 2.54 THz was presented. We have shown that areas where the contact is bulged or otherwise damaged can be easily excluded from the image.

This work was partly supported by the Lithuanian Science Council Student Research Fellowship Award (L. T.).

[1] I. Kašalynas, R. Venckevičius, D. Seliuta, I. Grigelionis, G. Valušis, InGaAs-based bow-tie diode for spectroscopic terahertz imaging, Journal of applied physics 110, 114505 (2011)

Studies of ultrafast laser ablation by the means of time-resolved digital holography and plasma emission imaging

Aivaras Urniežius, Nerijus Šiaulys, Viačeslav Kudriašov, Andrius Melninkaitis

Laser Research Center, Vilnius University, Saulėtekio al. 10, Vilnius LT-10223, Lithuania
aivaras@fidi.lt

Femtosecond lasers opened up completely new possibilities in material processing, where events of excitation and subsequent relaxation are well separated in time [1]. This led to the use of femtosecond lasers in micro-machining, medicine and other important areas where high intensity and short pulse durations are required. With femtosecond light pulses a thin layer of material is removed with minimum damage by heat to surrounding area and therefore resulting in highest precision available. On the other hand it allowed development of the new diagnostic techniques for monitoring such ultra-fast events [2]. Regime of material ablation (surface removal) is of particular importance here, both from practical and fundamental viewpoint. The ablation process includes rich physics where different disciplines intersect. Better understanding of how high intensity short laser pulses interact with matter is essential not only to make manufacturing more efficient, but also to understand the fundamental laws of physics. In order to characterize a non-uniform density distribution close to the targets surface shadowgraphic methods can be applied. However, when the charge density of plasma is low plasma becomes transparent and therefore invisible for probing pulses. In this case light travels trough plasma with a phase velocity higher than the speed of light in vacuum and as a result a strong negative change in refractive index is induced. Interferometric methods using coherent illumination are more sensitive to such phase distributions and therefore can be used for the reliable mapping of induced changes in optical density. Herewith the advantages of a new time-resolved microscopic technique [3] are demostrated as a combination of time resolved of–axis digital holography (TRDH) and time integrated plasma emission imaging (TIPEI). Such approach allows obtaining images of the ablated plume simultaneously from both time resolved transmission (amplitude and phase) and time integrated emission in a single shot mode. The transmittance data provides information about the processes occurring inside a shock wave, while the plasma emission data gives information about spatial energy distribution. For investigation of early fs ablation dynamics a tempered carbon steel sample was chosen, because this material is widely used in industry. To achieve the desired effect often more than one laser pulse is used in the manufacturing process therefore the effect of multi–pulse ablation behavior is also investigated in this study. Spatio–temporal effects are investigated by using various pump–probe time delays while exposing the material above the ablation threshold (max. 6.45 J/cm^2).

The typical results from holographic ablation experiments are shown in Fig. 1. Temporal evolution of the shock wave (Fig. 1a), emission of the ablation plume, and absorption in transmission images simultaneously (Fig. 1b), after single–pulse irradiation. Furthermore to study fatigue effect multi–pulse irradiation was used (Fig. 1b).

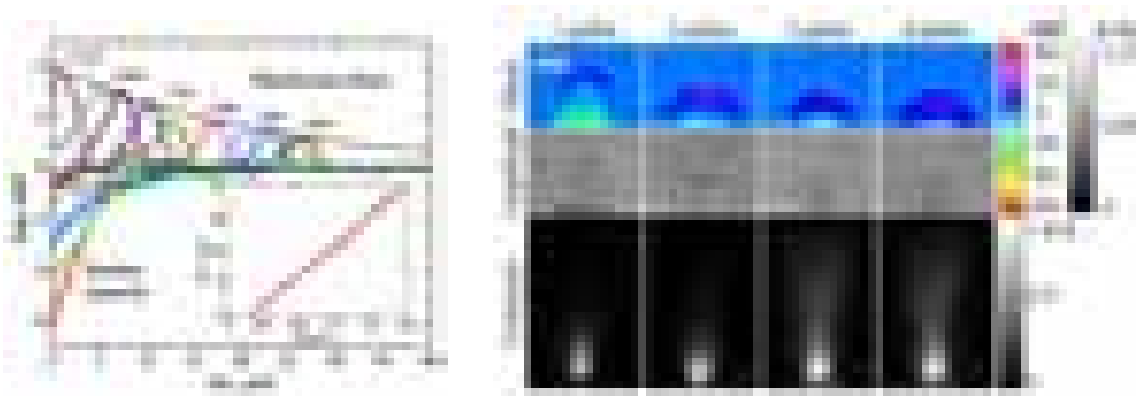

(a) (b)

Fig. 1. Fig. 2. (a) Vertical cross sections of the phasecontrast images. Denoted peaks correspond to the shock wave front positions. Dependence of the shock wave front position on time delay is shown in the inset. (b) Early dynamics of laser ablation plume at time delay 1.8 ns. Reconstructed phase– and amplitude–contrast images of 4 consecutive laser pulses together with plasma emission images of identical magnification.

[1] B. N. Chichkov, C. Momma, S. Nolte, F. von Alvensleben, and A. Tnnermann, Femtosecond, picosecond and nanosecond laser ablation of solids, Applied Physics A: Materials Science and Processing **63**, 109115 (1996).

[2] M. Hauer, D.J. Funk, T. Lippert, A. Wokaun, Time resolved study of the laser ablation induced shockwave, Th. Sol. Film. (453–454), 584–588 (2004).

[3] T. Balciunas, A. Melninkaitis, G. Tamosauskas, and V. Sirutkaitis, Time-resolved off-axis digital holography for characterization of ultrafast phenomena in water, Opt. Lett. **33**, 5860 (2008).

DEVELOPMENT OF SILICON WAFER CUTTING PROCESSES USING HIGH-POWER NANOSECOND FIBER LASER

Simonas Varapnickas[1,2], Artūras Greičius[2]

[1]Faculty of Physics, Vilnius University, Lithuania
[2]ELAS, Ltd, Vilnius, Lithuania
simonas.v@e-lasers.com

Despite the significant advances achieved in DPSS lasers with thin disks and crystal rods lasing medium architecture during last decade, the considerable problems are encountered in practical employment of such lasers in industrial micromachining processes. Harsh conditions, which are often met in industrial environments, strongly affect reliability and durability of DPSS lasers. Also, in order to achieve relatively high pulse energy, lasing medium cooling issues arise to be dealt with [1]. Advantages of DPSS lasers such as availability of higher harmonics generation are difficult to apply due to costly harmonics generators and thus expensive optical components required. Usually higher throughputs are more important for the industrial processes than the best possible fabrication quality gained. Obviously, as new solutions for rapid industrial micromachining are necessary, diode - pumped fiber lasers could be a possible choice to overcome the problems mentioned above [2, 3].

Silicon being one of the most significant elements used in nowadays industry, was chosen to be as a sample material for micromachining using high brightness Yb doped fiber laser based on MOPA architecture (E_{max} = 1 mJ, λ = 1070 nm, τ_{pulse} = 120 ns). The main objective of our experiments was to define the set of micromachining parameters for high - speed silicon wafers cutting. Both crystalline and poly – crystalline silicon wafers were used for cutting process development. X–Y positioning system with accuracy of 1 μm and v_{max} = 500 mm/s was employed for sample scanning.

Silicon ablation rate dependence on laser beam scanning speed was evaluated. In Fig. 1 the profiles (measured using stylus profiler Dektak 150) of kerfs formed in silicon wafers using different laser beam scanning speeds are presented. The optimal scanning speed was estimated to be 110 mm/s which correspond to 85 % laser pulse overlap. Average cutting speeds of 2.5 mm/s (for crystalline silicon) and 3.3 mm/s (for poly – crystalline silicon) were achieved (wafers' thickness 450 μm). The quality of cutting edges can be seen in Fig. 2. Heat affected zones and micro cracks penetration was observed in the width less than 20 μm for crystalline and less than 30 μm for poly-crystalline silicon wafers.

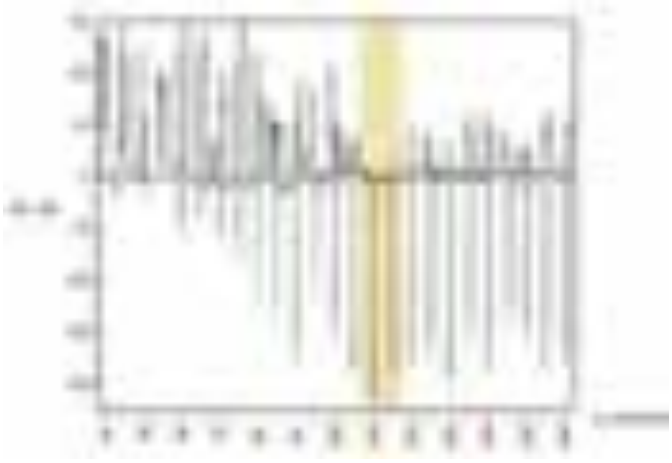

Fig. 1. Profiles of kerfs formed on silicon wafer using different laser beam scanning speeds.

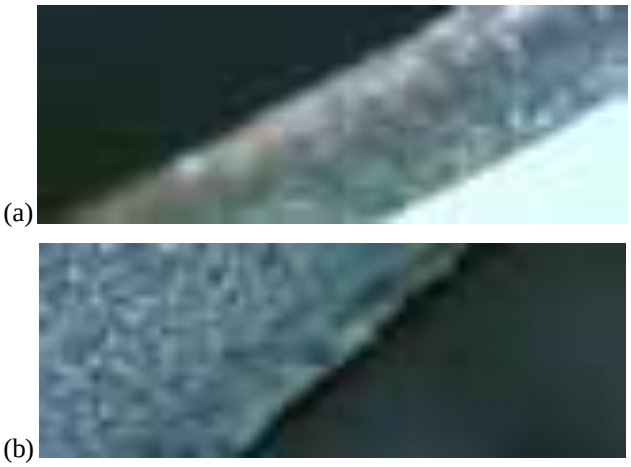

Fig. 2. Optical images of a) crystalline and b) poly-crystalline silicon wafers' edges after laser processing.

Our experiments revealed that silicon wafers laser cutting process using high power nanosecond fiber laser could be considered as a key technology for semiconductors electronics and solar energy industries and should be developed further. Optimal set of parameters for both crystalline and poly-crystalline silicon wafers micro-cutting was defined. The throughput of the process is high enough while keeping required quality of structures micro machined. Relatively low price of MOPA architecture based laser systems leads to cost effective process for R&D activities as well as mass production.

[1] J. Gabzdyl, M. Brodsky, Micro-cutting with nanosecond pulsed fiber lasers, Proceedings of *International Congress on Applications of Lasers & Electro- Optics, ICALEO 2010*, M901 (LIA Pub, 2010).
[2] W. O'Neill, K. Li, High-Quality Micromachining of Silicon at 1064 nm Using a High-Brightness MOPA-Based 20-W Yb Fiber Laser, IEEE J. Sel. Top. Quant., **15**(2), (2009).
[3] J. Meijer, Laser beam machining (LBM), state of the art and new opportunities, J. Mater. Process. Technol., **149,** 2–17 (2004).

SIZE CHARACTERIZATION OF LASER GENERATED COLLOIDAL NANOPARTICLES USING THEIR ABSORPTION SPECTRA

Antanas Vinčiūnas[1], Gediminas Račiukaitis[2]

[1] Vilnius University, Faculty of Physics, Lithuania
[2] Center for Physical Sciences and Technology, Institute of Physics, Lithuania
antanas.vinciunas@ff.stud.vu.lt

Nanotechnology is a field of great interest because nanoparticles exhibit unique properties and can be used in a lot of different areas such as biomedicine, electronics, chemical catalysis, material science etc. Pulsed laser ablation of solids in liquids is an attractive method to synthesize nanoparticles due to simplicity of the procedure, high chemical purity of nanoparticles and possibility to generate nanoparticles of various materials (metals, alloys, semiconductors) [1].

Electromagnetic field, incident upon nanoparticles of noble metals, excites localized surface plasmons (LSP), i.e. collective oscillations of conduction electrons in nanoparticles [2]. Resonant LSP frequency lies in UV-Vis spectral region and depends on the size and shape of nanoparticles so it is possible to determine the mean size of nanoparticles from their absorption spectra [3, 4].

The aim of our work was to generate gold nanoparticles in distilled water using fundamental (1064 nm) and second (532 nm) harmonics of nanosecond diode-pumped Nd:YVO_4 laser and to evaluate their sizes. The goal was to find the optimal experimental conditions for the highest productivity of nanoparticles.

Absorption spectra of colloids, obtained using different scanning speeds (different interpulse distance on the target) are shown in Fig. 1. Fundamental harmonic (average power 5.5 W, pulse repetition rate 10 kHz) was used and ablation time was 15 minutes.

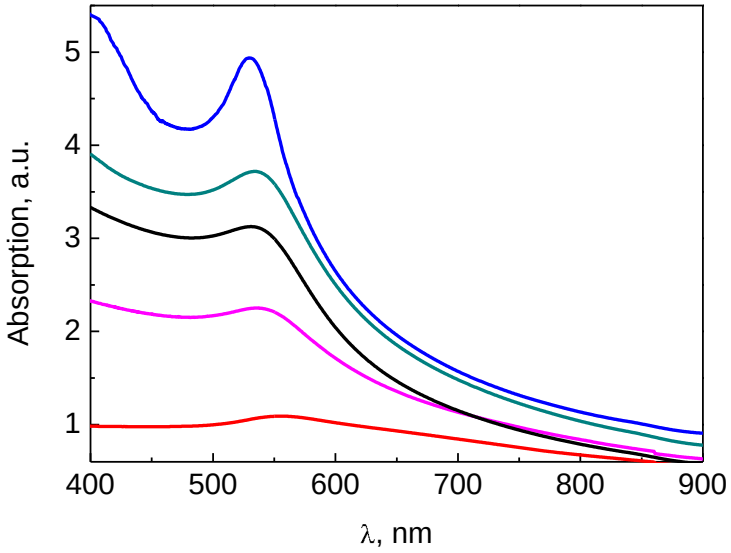

Fig. 1. Absorption spectra of colloids, obtained using different scanning speeds. From the top to the bottom: 10, 50, 100, 500, 1000 mm/s.

The mean sizes of nanoparticles obtained in different experiments varied from 30 to 90 nm. However, repeatability of our experiments was quite low, therefore further investigations are needed for better understanding of the nanoparticle generation processes.

Research was done at Department of Laser Technologies of the Center for Physical Sciences and Technology.

[1] T.E. Itina, On Nanoparticle Formation by Laser Ablation in Liquids, The Journal of Physical Chemistry C **115** (12), 5044-5048 (2010).

[2] C.F. Bohren and D.R. Huffman, *Absorption and Scattering of Light by Small Particles* (Wiley, New York, 1983).

[3] W. Haiss, N.T.K. Thanh, J. Aveyard, and D.G. Fernig, Determination of Size and Concentration of Gold Nanoparticles from UV-Vis Spectra, Analytical Chemistry **79** (11), 4215-4221 (2007).

[4] S. Link and M.A. El-Sayed, Size and Temperature Dependence of the Plasmon Absorption of Colloidal Gold Nanoparticles, The Journal of Physical Chemistry B **103** (21), 4212-4217 (1999).

Laser patterning – an alternative method to prepare sapphire substrate for GaN growth

Marius Alsys[1], Edgaras Jelmakas[1], Roland Tomašiūnas[1], Paulius Gečys[2]

[1]Vilnius University, Institute of Applied Research, Saulėtekio Ave. 10, LT-10222 Vilnius, Lithuania
[2]Center for Physical Sciences and Technology, Savanoriu Ave. 231, LT-02300 Vilnius, Lithuania
malsys@gmail.com

Laser micromachining is a well established technique for fabrication of microstructures [1]. In our work we present use of surface patterning by picosecond laser technique for growth of high quality gallium nitride. Laser ablation is much cheaper and less time consuming technique as photolithography. Quality improvements by use of epitaxial lateral overgrowth (ELO) technique were investigated.

c-plane sapphire surface ablation was accomplished using picosecound Nd:Yag (wavelength 1064 nm) laser, repetition rate – 100 KHz, used wavelength 266 nm (forth harmonic), pulse duration – 10 ps, sapphire surface ablation power 60-670 mW. Laser ablations made across, in parallel, in 30 degrees and in 120 degrees turn in point to a sapphire plane.

After laser ablation sapphire wafers were cleaned using aqua regia (HNO_3+HCL, in proportion 1:3 respectively) and etched using sulphuric and phosphoric acids solution (H_2SO_4 and H_3PO_4, in proportion 3:1 respectively). SEM images after wet chemical etching shows less surface roughness (Fig. 1) and it could open sapphire crystalline planes.

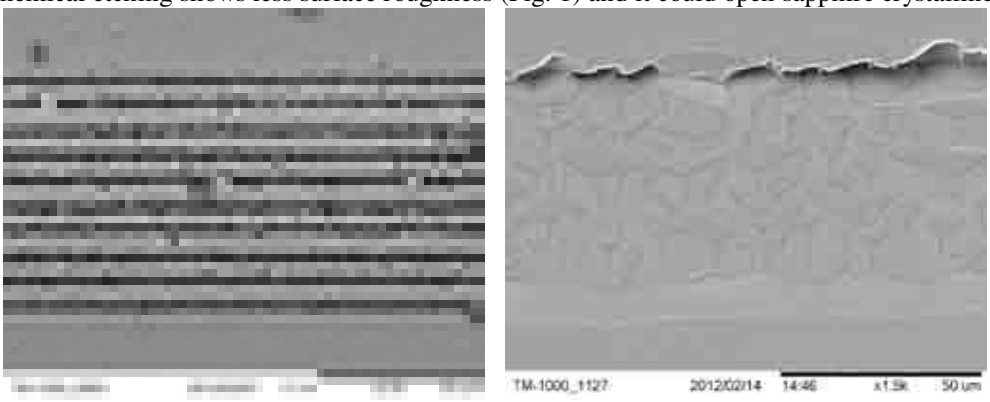

Fig. 1. 300 mW laser power ablated sapphire wafer surface before and after chemical etching (SEM images)

Undopped gallium nitride samples were grown by metal-organic chemical vapour deposition (MOCVD). GaN growth conditions: III/IV ratio – 1500, reactor pressure 150 mBar, growth rate ~2,1 μm/h temparature – 1065^0C. Coalescense layer thickness 1,7 μm, buffer layer thickness 20 nm.

SEM and AFM results shows reduction of dislocation density in gallium nitride layer growth using ELO method on laser patterned (300 mW power) sapphire substrates.

[1] W. Kautek at all. Femtosecond pulse laser ablation of anodic oxide coatings on aluminium alloys with on-line acoustic observation Applied Surface Science vol. 186, pages 374-380, 2002.

INVESTIGATION OF THICKNESS DEPENDENT DEFECT DENSITY IN EPITAXIALLY GROWN GaN LAYERS

Aurina Arnatkevičiūtė

Department of Advanced Technology, Institute of Applied Research, Vilnius University, Lithuania
aurina.arnatk@gmail.com

Gallium nitride (GaN) is leading material in bright light-emitting diodes since the 1990s. Its wide band gap of 3.4 eV affords special properties for applications in optoelectronic, high-power and high-frequency devices. Control over defects in the material growth is the main task to ensure quality of future products. One of the most serious problem in development of III-N based devices is lack of suitable substrate material on which lattice-matched layers can be grown. The collection of extended structural discontinuities in the lattice, such as interfaces, dislocations and stacking faults, is referred to as the microstructure of the material. The microstructure is sensitive to steps involved in crystal growth, such as the substance used for epitaxy, the growth method itself, and variations in chemical composition during growth. By far the most useful substrate to date is sapphire. This is surprising given the large differences in thermal expansion and in lattice parameter between sapphire and the nitrides. However, epitaxy of nitrides on sapphire has produced the best device performances [1]. Notwithstanding, the nitride materials, grown on sapphire contain a large density of threading dislocations. It is well established that threading dislocations are degrading the performance and the operating lifetime of optoelectronic devices [2].

Institute of Applied Research, Vilnius University, works on GaN growth using metal organic chemical vapor deposition (MOCVD) and characterization of grown layers. Our interest in growth of GaN concerns evolution of defects, when higher thickness of layer is reached (up to ~25.2 μm). Structural quality of a set of samples with sequential increase in thickness was inspected first using optical and electron microscopy means. Using Hall measurement technique the mobility and equilibrium carrier concentration in the samples were defined. Due to these results, a decrease of dislocation density with increasing thickness of samples was observed. There was not enough to have these results to ensure correct characterization of GaN layers because of some indeterminacy. To investigate carrier dynamic light-induced transient grating (LITG) technique was applied (Fig. 1). Results from this method have supplemented previous hypothesis, however, raised some new questions which we intend to resolve using alternative techniques: XRD (measurements to determine lattice plane imperfections in direct way), electron microscopy (SEM, TEM).

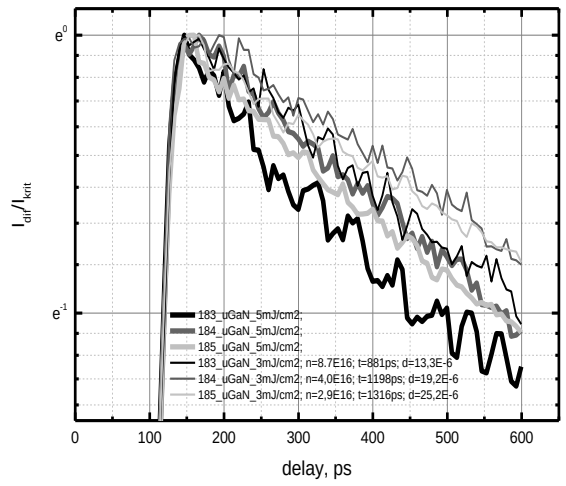

Fig. 1. LITG kinetics measured in thick GaN samples at different fluence (13.3 μm, 19.2 μm, 25.2 μm).

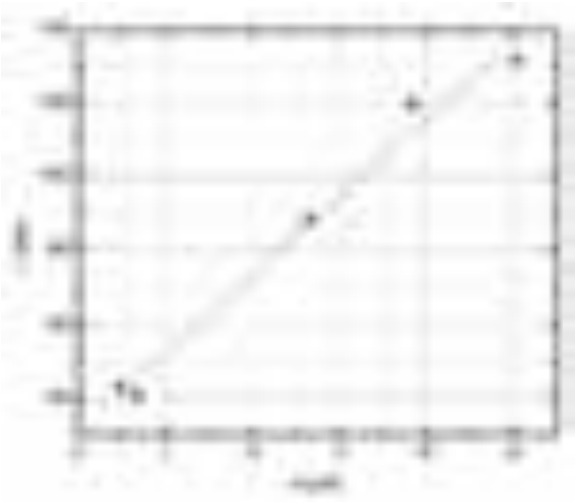

Fig. 2. Carriers lifetime dependence on layer thickness.

The obtained dependence between thickness of the layer and carrier lifetime could be explained by the existence of less frequent dislocations due to improved base structure (grown in several stages) (Fig. 2). According to our measurements (around 30 samples), it is possible to determine optimal growth conditions (temperature, steam of NH3, duration regimes, etching time and temperature).

[1] B.Gil. Group III Nitride Semiconductor Compounds. Physics and Applications. Oxford Science Publications 123, 125 (1998).
[2] T. Malinauskas. Investigation of Carrier Dynamics in Wide Bandgap Semiconductors by Light-induced Transient Grating Technique. PhD thesis 49 (2009)

ANNEAL DEPENDENT VARIATIONS OF THE DLTS AND BELIV CHARACTERISTICS IN Si THYRISTOR STRUCTURES

Darius Bajarūnas, Tomas Čeponis, Aurimas Uleckas, Eugenijus Gaubas

Institute of Applied Research. Vilnius University, Saulėtekio av. 9-III, LT-10222 Vilnius, Lithuania
darius.bajarunas@gmail.com

Power thyristors operate at very high voltages with flowing large currents. Such devices are attractive for power distribution networks to reduce the total number of devices required in a high-voltage DC (HVDC) station and for other applications [1]. Materials in fabrication of these devices should be very pure to avoid breakdown of junctions and to reduce leakage currents. However, imperfections of materials due to technologically introduced impurities and other defects are inevitable.

In this work, investigations of deep traps were performed to identify the defects in thyristor structures and to find out the optimal parameters for annealing of these technological defects. These investigations were implemented by combining the deep level transient spectroscopy (DLTS), the small test signal capacitance - voltage (C-V) [2] as well as the pulsed barrier evaluation by linearly increasing voltage [3] techniques.

A set of investigated thyristor samples contained the industrially fabricated, at enterprise "Vilniaus Ventos Puslaidininkiai", pnp Si structures taken from a technological route and the terminated devices Spectra of defect levels in thyristor structure samples have been examined by using a commercial DLS-82E spectrometer. Measurements of C-V characteristics have been performed by employing high precision QuadTech 7600 LRC meter. BELIV transients were measured by VU assembled instrument. The samples were annealed isothermally at the ~400 °C.

It has been revealed that both the DLTS spectra and the C-V characteristics are significantly modified by deep traps located within base region of the thyristor structures. The asymmetric C-V characteristics have been obtained in the as-fabricated samples, indicating the presence of high density traps. A time scale of the electrical activity of these traps was clearly resolved by analyzing variations of the BELIV transients. It has been determined that density of rather shallow traps can be reduced by isothermal anneals within moderate temperature (~400 °C) range.

[1] B. J. Baliga, Fundamentals of Power Semiconductor Devices. (Springer Science Business Media, LLC, New York, 2008).

[2] P.Blood and J.W. Orton, The Electrical Characterization of Semiconductors: Majority Carriers and Electron States (Academic Press Inc., San Diego, 1992).

[3] E.Gaubas, T.Čeponis, V.Kalendra, J.Kusakovskij, and A.Uleckas. „Barrier evaluation by linearly increasing voltage technique applied to Si solar cells and irradiated pin diodes". ISRN Materials Science, vol. 2012, article ID543790, 17 pages doi:10.5402/2011/543790

CONDUCTIVITY STUDIES FOR for $BaCe_{0.9}Y_{0.1}O_{3-\delta}$ CERAMIC PROTON CONDUCTORS PREPARED WITH DIFFERENT PRESSURES

Juste Banyte[1,2], Qianli Chen[2], Artur Braun[2], Thomas Graule[2,3], Antanas Feliksas Orliukas[1]

[1] Department of Radiophysics, Faculty of Physics, Vilnius University, Saulėtekio Ave. 9-III, LT-10222 Vilnius,
[2] Laboratory for High Performance Ceramics, Empa. Swiss Federal Laboratories for Materials Science and Technology, CH-8600 Dübendorf, Switzerland
[3] Institute of Ceramic, Glass-and Construction Material, TU Bergakademie Freiberg, D-09596 Freiberg, Germany
juste_banyte@yahoo.com

The Protons conducting solid electrolytes have a wide range of technological applications in batteries, fuel cells, sensors, dehydration/ hydration of hydrocarbons, electrolysers and etc. The proton conductor Yttrium doped Barium cerate for example $BaCe_{0.9}Y_{0.1}O_{3-\delta}$ (BCY10) shows the highest conductivity among all proton conductors [1].

In the previous studies it was found that pressing increases the proton conducting activation energy [2]. This is an indication that activation energy decreases linearly with the lattice parameter. Here only the lattice volume was considered, but the pressure also affects other structural properties of the materials, for instance the size of grains, and the crystal orientations, and thus influence the proton conductivity [3]. In this work, we apply different pressures (100-600 MPa) during the preparation of the pellets.

The X-ray diffraction was measured and the peak height ratio was calculated for neighboring diffraction peaks. It was observed, that the ratio of the peak intensity varies upon pressure. It means that pressure changes the preferred orientation of the crystals The Highest Peak Height Ratio is at the pellet prepared using 500 MPa pressure. The height ratio of (2 0 2): (0 4 0) peaks is the highest, therefore we assume that more crystallites are orientated in (2 0 2) direction instead of (0 4 0). The size of crystallites was calculated. The largest crystallites were obtained at the 500MPa pellet, the smallest at 600 MPa and the others in between.

The impedance spectrum was measured in the frequency range of 0.1 Hz – 10MHz at the 448 K – 873 K in two different atmospheres using O_2 gases. Figure 1 shows the grain boundary conductivity dependence according to the temperature for the pellets pressed using different pressures. The conductivity increases with a size of crystallite. Here it was noticed that highest conductivity was reached at the pellet pressed with 500 MPa pressure, which indicates an anisotropy in conductivity (protons prefer to move in (2 0 2) direction).

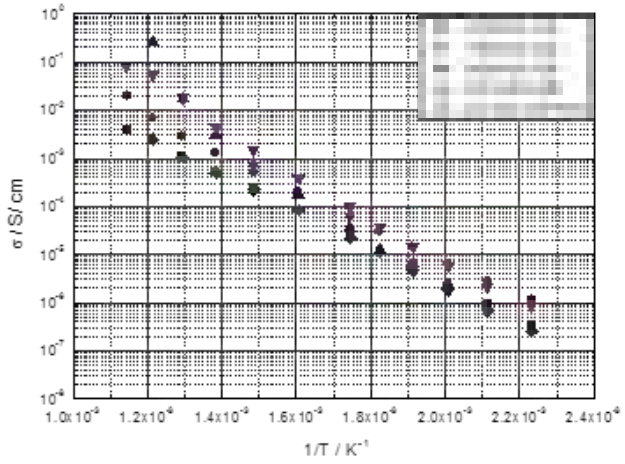

Fig. 1. Grain boundary conductivity dependence according to the temperature applying different pressure in wet atmosphere.

[1] H. Iwahara, Solid State Ionics 52 (1992) 99.
[2] Q. Chen, A. Braun, S. Yoon, et al., J. Eur. Ceram. Soc. 31 (2011) 2657.
[3] S. Duval, Dissertation, Empa/TU München, 2008

DEEP LEVEL SPECTRA IN Ge DOPED Si DIODES MEASURED BY TECHNIQUE OF CAPACITANCE TRANSIENTS

Dominyka Blaževič, Mantvydas Mikulis, Eugenijus Gaubas, Romualdas Pūras, Aurimas Uleckas

Institute of Applied Research, Vilnius University, Saulėtekio av. 9-III, LT-10222 Vilnius, Lithuania
Dominyka.Blazevic@ff.stud.vu.lt

Defect engineering by intentionally introduced different dopant atoms in Si lattice is one of the trends in improving and modifying specific parameters of Si devices. It is known that Ge doping of Si during the Czochralski (Cz) growth process has a beneficial effect on strength of Si wafers and thus on reduction of processing induced dislocation nucleation [1]. Also, introduction of Ge into Si has additional advantages because it is an isovalent impurity and does not introduce electrically active deep centres. Therefore, it is also a promising dopant for the tuning of the internal gettering capacity [1]. Ge doping above 10^{20} cm^{-3} leads to the formation of germanium clusters acting as gettering centres for the intrinsic point defects. The effect of germanium doping has also important consequences for radiation-induced defect formation and population dynamics [1,2].

Results of a comparative study of deep level transient spectroscopy implemented on diodes processed on n-type Cz grown Si without and with Ge doping concentration of about 10^{19} cm^{-3} and 10^{20} cm^{-3} are presented. Diodes were irradiated with 2 MeV electrons with fluences in the range between 10^{14} and 10^{17} e/cm^2 to clarify an impact of Ge doping on irradiation induced defect formation. Deep level transient spectroscopy (C-DLTS) has been performed to identify generation centres and there concentration after electron irradiation. Also photoconductivity decay transient probed by 22 GHz microwaves have been additionally examined to reveal recombination lifetime variation dependent on electron beam irradiation fluence and on Ge doping density.

[1] J. Vanhellemont, J. Chen, W. Xu, D. Yang, J. M. Rafi, H. Ohyama, and E. Simoen, J. Cryst. Growth (2010), doi:10.1016/j.jcrysgro.2010.11.024.

[2] J.M. Rafi, J. Vanhellemont, E. Simoen, J. Chen, M. Zabala, F. Campabadal, Physica **B 404** (2009) 4723.

VARIATIONS OF CAPACITANCE CHARACTERISTICS IN THYRISTOR STRUCTURES AFTER ISOCHRONAL ANNEALS

Paulius Cicėnas, Tomas Čeponis, Eugenijus Gaubas

Institute of Applied Research, Vilnius University, Saulėtekio Ave. 9-III, LT-10222 Vilnius, Lithuania
paulius.ccs@gmail.com

Power device structures are formed by employing high temperature diffusion procedures to introduce dopant atoms of certain concentrations and at proper depths. However, undesirable impurities can be introduced together with dopants as well. These impurities act as generation/recombination and trapping centers, and affect the operational parameters of power devices [1]. Furthermore, these centers may unpredictably transform under operational heating and change the parameters of power devices [2]. So, it is very important to analyze the behaviour of introduced centres after thermal treatments.

In this work, small test harmonic signal induced and pulsed [3] capacitance-voltage as well as capacitance - frequency characteristics have been examined within layered thyristor structures to evaluate an impact of deep traps on operational characteristics of devices. The pulsed technique is based on measurements and analysis of barrier capacitance current transients by applying the linearly increasing voltage pulse. Combining current transient measurements with additional illumination allows evaluating of the parameters of carrier traps and generation centres. The dopant profiles can be also evaluated by employing the modified pulsed technique [4]. The latter technique is implemented by step-positioning of the needle-tip probe, located on the cross-sectional boundary of a parallel-plate layered structure. The spreading current pulsed measurements are performed by scanning the boundary of the structure using a needle-tip electrode. The other contact is connected to the parallel plate electrode at planar sample surface.

It has been revealed that even small deviations of density of impurities induced by technological high temperature double-diffusion processes lead to a crucial degradation of the device functioning. Anneal of the structures at moderate temperatures <500 ^{o}C allow suppressing of the impact of deep traps. It has been demonstrated that pulsed barrier evaluation by linearly increasing voltage (BELIV) technique was more sensitive tool for inspection of the barrier capacitance characteristics influenced by harmful impurities induced by heating based technological procedures. It is shown that junctions formed by diffusion procedures lead to an asymmetry of junction location within pnp structures. This can be a reason for a reduction of the blocking voltage in power device.

[1] B. J. Baliga, Power Semiconductor Devices (PWS Publishing Company, Boston, 1996).

[2] D.K.Schroder, Semiconductor material and device characterization 3rd Ed. (John Wiley and Sons, New Jersey 2006).

[3] E. Gaubas, T. Čeponis, J. Kusakovskij, and A. Uleckas. Barrier evaluation by linearly increasing voltage technique applied to Si solar cells and irradiated pin diodes. ISRN Materials Science **2012**, Article ID 543790 (2012).

[4] E. Gaubas, T. Čeponis, and J. Kusakovskij. Profiling of barrier capacitance and spreading resistance by transient linearly increasing voltage technique. Review of scientific instruments **82**, 083304 (2011).

INVESTIGATION OF STIMULATED EMISSION IN ZnO EPITAXIAL LAYERS

Vilius Čeledinas, Tomas Kristijonas Uždavinys, Mindaugas Karaliūnas

Institute of Applied Recearch and Department of Semiconductor Physics, Vilnius University, Saulėtekio Ave. 9-III, LT-10222 Vilnius, Lithuania

cipis@fidi.lt uzdavinys@fidi.lt

In the past few decades zinc oxide (ZnO) has attracted much attention due to its unique properties, which are very desirable for applications in optoelectronic. ZnO is a direct band gap semiconductor with 3.4 eV band gap energy at room temperature and extremely high exiton binding energy (60 meV). Large exciton binding energy opens the possibility to make an excitonic stimulated emission (SE) based semiconductor laser (SL) with several advantages over regular SL. However, for applications in optoelectronic a stable, high, and reproducible p-doping is obligatory. Though progress has been made in this crucial field, this aspect still represents a major problem [1].

In this work, four ZnO epitaxial layer samples was investigated. SE effect was studied for different samples in order to characterize optical properties. Samples A and B were grown using metaloorganic chemical vapor deposition technique (MOCVD) on a (0001) plane sapphire substrate in Institute of Photonics and Optoelectronics of National Taiwan University. Samples C and D were grown using molecular beam epitaxy (MBE) technique on a $(11\bar{2}0)$ plane sapphire substrate in Virginia Commonwealth University [2]. The epitaxial layers were optically excited using frequency tripled (λ_{exc} = 355 nm) and quadrupled (λ_{exc} = 266 nm) pulsed YAG:Nd^{3+} laser beam. The pulse duration was 4 ns and repetition rate was 10 Hz. The variable stripe length technique was employed for optical gain measurements [3]. The excitation beam was focused on the sample surface using cylindrical lens to create a narrow excitation stripe of 30 μm and 25 μm in width for frequency quadrupled and tripled excitations, respectively. Edge photoluminescence (PL) dependency on excited stripe length l was measured by partially screening the sample with a metal plate. PL signal was collected to a double monochromator of 0.6 m focal length and registered using a photomultiplier tube. The PL was measured utilizing boxcar integrator in quasistationary excitation regime.

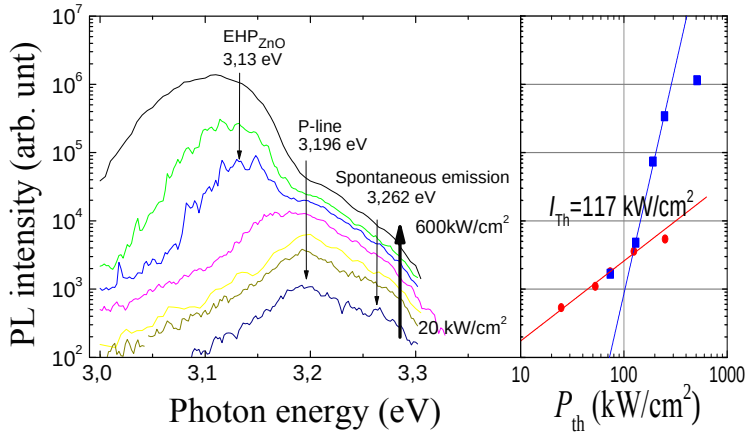

Fig. 1. Sample C FL intensity dependence of excitation power density

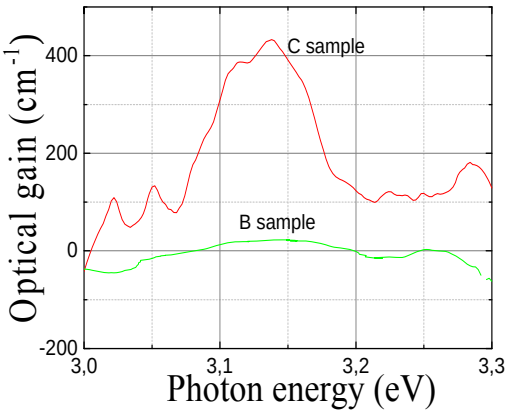

Fig. 2. Optical gain coefficient spectra

In Fig. 1, the PL spectra dependence on excitation power density P_{exc} is shown. Three spectral lines can be identified namely, spontaneous emission line at 3.262 eV, exciton-exciton radiative interaction PL line (P-line) at 3.196 eV, and electron-hole plasma (EHP) induced SE line at 3.130 eV, which appears at elevated P_{exc}. The SE threshold was indicated from integrated PL intensity dependence on P_{exc} in double-logarithmic scale (Fig. 1. inset). The lowest SE threshold P_{th} = 105 kW/cm^2 was measured for sample D and the highest P_{th} = 522 kW/cm^2 was measured for sample B.

The optical gain coefficient (OGC) spectra were obtained by analyzing the measured edge PL spectra. The optical gain spectra dependence on l and P_{exc} was investigated. The saturation process occurs at high l or/and P_{exc} values and reduces the actual OGC of the medium. Therefore the optimal experimental conditions has to be ensure for OGC measurements. The maximum OGC measured in the experiment was 400 cm^{-1} for sample C (Fig. 2). In contrast, very low OGC of around 5 cm^{-1} was measured for sample B. This indicates the much better optical and crystal qualities of MOCVD grown ZnO epitaxial layers.

[1] Claus F. Klingshirn. ZnO: Material, Physics and Applications. ChemPhysChem, 8, 782 (2007).
[2] Hadis Morkoc, and Ü mit Ö zgür Zinc Oxide ISBN: (2009) 978-3-527-40813-9
[3] K.L.Shaklee, R.E. Nahory, R.F. Leheny, Optical gain in semiconductors 284 (1973)

PHOTO-IONIZATION SPECTROSCOPY OF DEEP LEVELS IN Si RADIATION DETECTORS

Aušra Čerkauskaitė[1], Vidmantas Kalendra[1,2], Eugenijus Gaubas[2]

[1] Faculty of Physics, Vilnius University, Saulėtekio 9-III, LT-10222 Vilnius, Lithuania
[2] Institute of Applied Research, Vilnius University, Saulėtekio 9-III, Vilnius, Lithuania
ausra0618@yahoo.com

Silicon is the most widely used material for fabrication of particle detectors [1]. The main problem arises due to low radiation tolerance of the Si detectors under irradiation fluences of hadrons above 10^{15} particle/cm^2. Thus, an expensive procedure of the detectors replacement is inevitable. The main objective of this work is to analyse the deep level spectra in the as-fabricated in Si detectors as well as irradiated with high fluencies of hadrons and to study variations of the deep centres densities.

The photo-ionization spectroscopy instruments based on recording of the microwave probed pulsed photoconductivity and of the steady–state current within diode structures have been installed and approved. The diode structure sample is placed into vacuumed cryostat and cooled by liquid nitrogen, to record photo-ionisation spectra with reduced electrical noises. Photo-ionisation is implemented by a halogen lamp biased by dc voltage. The DMR-4 monochromator is exploited to disperse the excitation light. This monchromator is placed in between the cryostat and the halogen lamp. Changing of excitation wavelength is handled by a step-motor which is connected through Line Print Terminal (LPT) to a parallel port interface of a personal computer. A platinum thermo-resisting sensor is used for the temperature measurements on the sample. This sensor signal is measured by the Agilent 34401A multi-meter. Current measurements are performed by employing Keithley 6487 pico-amper-meter with internal DC source. The data sampling and processing is performed by personal computer using Labview System Design Software.

The spectral scans were performed by increasing excitation photon energy to avoid undesirable emptying of the shallower levels before photo-ionisation during record of spectrum.

The photo-ionization spectra were analyzed by employing the Lucovsky model [2]. According to this model the photocurrent (I) is given by:

$$I \sim n_M \Delta E_M^{0.5} (h\nu - \Delta E_M)^{1.5} / (h\nu)^3 ,$$

where ΔE_M is the optical activation energy of the deep centre, $h\nu$ is the photon energy, n_M is the initial trap filling.

The optical activation energy values obtained from the photo-ionization spectra can be related with the excitation of electrons from the filled deep centres or generation of free holes by excitation of electrons from the valence band into the empty deep levels.

[1] www.cern.ch
[2] G. Lucovsky, *Solid State Comm*, 3 (.1965) 299.

OPTICAL AND MECHANICAL PROPERTIES OF SiO_X DOPED DLC COATINGS

Agnė Čiučiulkaitė[1], Nerijus Armakavičius[1], Asta Tamulevičienė[2], Sigitas Tamulevičius[2]

[1]Department of Physics, Kaunas University of Technology, Studentų 50, LT- 51368, Kaunas, Lithuania
[2]Institute of Materials Science of Kaunas University of Technology, Savanorių pr. 271, LT-50131 Kaunas, Lithuania
agne.ciuciulkaite@gmail.com

Diamond-like carbon (DLC) films possess many excellent properties, e.g. high hardness; high wear resistance, low friction coefficients, atomic-level smoothness and high transparency. Thus these films are often used to improve mechanical and tribological properties of soft materials [1]. The incorporation of additional elements (Si, SiO, Ag, Au, etc.) in the films gives further improvement of film properties and wider application possibilities [2]. Introduction of certain amount of silicon and oxygen into DLC enables to change optical properties of the film and to produce films with the reduced residual stress level and coefficient of friction [3].

In the present research the optical and mechanical properties of SiO_x doped DLC (DLC:SiO_x) films were analysed. DLC:SiO_x films (with thickness of 200 nm) were formed from hexamethyldisiloxane with acetylene carrier gas employing closed drift ion beam source changing ion beam energy from 300 eV to 800 eV. As substrates p-type silicon (100) and fused silica were used. Determination of mechanical properties was done using homemade scratch tester with Berkovich type indenter and maximal force of 250 mN. The experiment was carried out gradually increasing normal force F_N and registering tangential force F_T. The principal experiment scheme is shown in Fig. 1. For every sample at least three scratches were done and force value as a function of scratch dimensions was registered. The scratch mark left after the applied load was investigated employing optical microscope. Employing this technique one can evaluate the adhesion of coatings on the substrate. Analysing scratch track, one can determine the critical force (peel off). The friction coefficient was determined from following equation:

$$\mu = \frac{F_t}{F_n} \quad (1)$$

Optical properties (optical bandgap) of the films were evaluated by measuring transmittance and reflectance (spectrometer "Avantes", 200-1000 nm) of the films formed on fused silica. The absorption coefficient was calculated from following equation:

$$\alpha = \frac{1}{t}\left(\frac{1-R}{T}\right) \quad (2)$$

Here t is film thickness in cm, R, T - reflectance and transmittance coefficients respectively.

The optical band gap E_g of the films was determined employing Tauc formula $\sqrt{\alpha E} = \beta(E - E_g)$, where E is the photon energy and β is the Tauc slope (approximating linear part of a graph, see Fig. 2). The energy E_{04} (energy when $\alpha=10^4 cm^{-1}$) was also determined and values compared with Tauc gaps. The optical bandgap dependence on ion beam energy was determined.

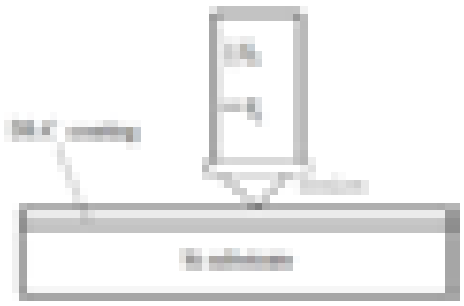

Fig. 1. Scheme of scratch test

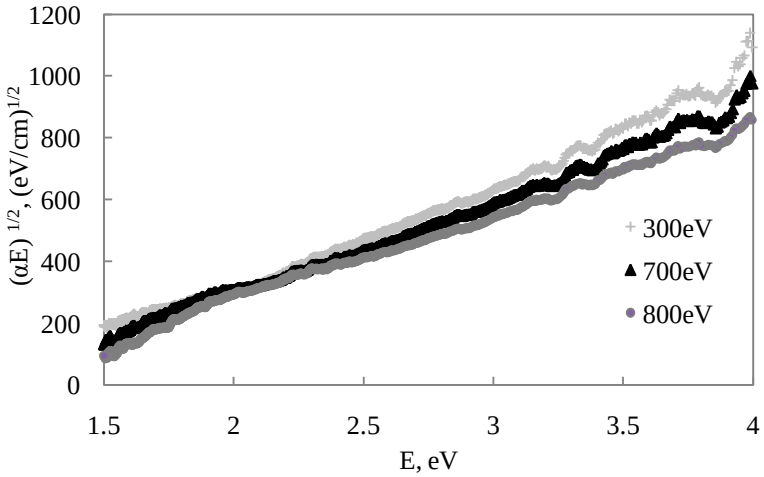

Fig. 2 Optical absorption spectra of the films

Acknowledgment. AČ and NA acknowledge Student Research Fellowship Award from the Lithuanian Science Council.

[1] N. Yamauchi et al., Friction and wear of DLC films on magnesium alloy, Surface & Coatings Technology **193** 277– 282 (2005).
[2] M. Ikeyama et al., Effects of Si content in DLC films on their friction and wear properties, Surface & Coatings Technology **191** 38– 42 (2005).
[3] L.K. Randeniya et al., Molecular structure of SiO_x-incorporated diamond-like carbon films; evidence for phase segregation, Diamond & Related Materials **18** 1167-1173 (2009).

MOCVD GROWTH OF In-RICH InGaN FILMS USING TRANSITIONAL LAYER WITH GRADED INDIUM CONCENTRATION

Mantas Dmukauskas, Tomas Grinys

Institute of Applied Research, Vilnius University, Saulėtekio Ave. 9-III, LT-10222 Vilnius, Lithuania
mantasdmuk@gmail.com

Indium gallium nitride (InGaN) has been the subject of extensive research, because of their wide application in optoelectronics, e.g. for solar cells, because of good spectral match to the sun light. InGaN can cover up light to the near-infrared range, depending on In and Ga concentration ratio. The growth of good In-rich InGaN layers on sapphire substrates is a great challenge, because of lattice mismatch and the different melting temperatures.

This work is devoted to In-rich InGaN films grown by metal-organic chemical vapor deposition (MOCVD) on sapphire. The task was to increase the crystalline quality of In-rich InGaN layers.

$In_xGa_{x-1}N$/GaN structures (100 nm InGaN / 3 µm GaN) were grown on sapphire C-plane substrates in a vertical flow close-coupled flip-top showerhead reactor using trimethyl gallium, trymethil indium and ammonia as precursors, hydrogen for GaN or nitrogen for InGaN as the carrier gases. The growth was monitored using in situ laser interferometer, determining process steps, alloy quality and its thickness. In concentration was determined using X-Ray diffraction measurement.

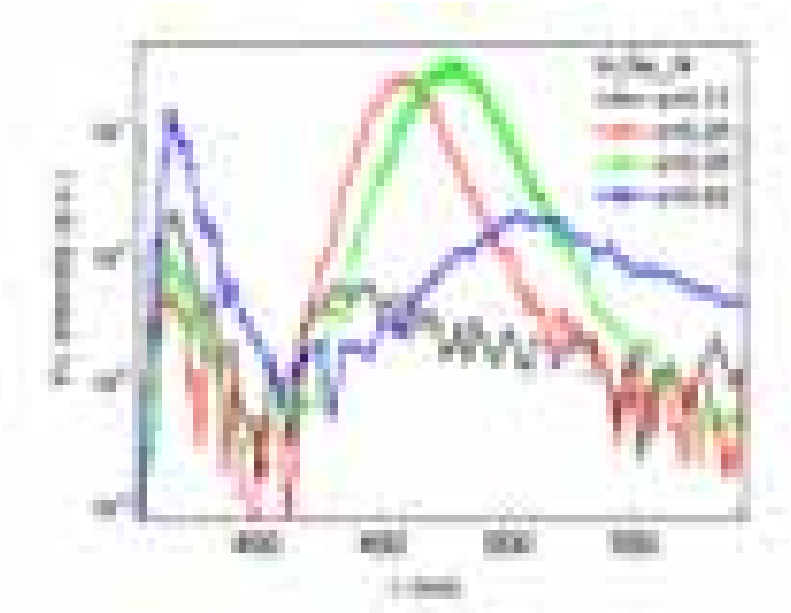

Fig.1. PL spectra measured in $In_xGa_{x-1}N$ layers with different In content. For comparison PL data of layer grown without interlayer is given (x=0.17).

In-rich InGaN layers have been successfully grown with 25%, 35% and 42% In content using transitional InGaN thin interlayer with graded In distribution on GaN template. This additional layer is distributing a tension resulting from the difference between grating periods of GaN and InGaN crystals in a larger volume. It results in a growth of InGaN layer with lower concentration of defects. The improvement of crystalline quality can be observed from photoluminescence (PL) measurements (Fig. 1, x=0.25, x=0.35 and x=0.42). PL efficiency increases several orders of magnitude in the layer with 25% of In compared to the layer grown directly on GaN template (see black empty squares, x=0.17) The growth conditions of interlayer used to enhance crystal quality of In-rich InGaN layers will be discussed.

FLUENCE DEPENDENT CAPACITANCE-VOLTAGE AND CURRENT-VOLTAGE CHARACTERISTICS IN Si PARTICLE DETECTORS IRRADIATED BY REACTOR NEUTRONS

Remigijus Dvaranauskas, Tomas Čeponis, Eugenijus Gaubas

Institute of Applied Research, Vilnius University, Sauletekio Ave. 9-III, LT-10222 Vilnius
Remigijus.Dvaranauskas@ff.stud.vu.lt

Future high energy physics experiments such as experiments at CERN, will use silicon detectors for fast and high precision tracking of particles. Heavily irradiation by high energy particles causes the formation of extended defects inside the metallurgic junction area. The radiation defect attributed energy levels are introduced into the bandgap thus changing the electrical properties such as leakage current, full depletion voltage U_{FD} and charge collection efficiency (CCE). Enhanced leakage current is observed after irradiation, and this leads to the enhanced electronics noise and to decrease of the spatial resolution of particle detectors. U_{FD} might either increase after irradiation, when radiation donors are introduced, or a full depletion state can be reached without external voltage, when carrier capture centres cause complete reduction of the efficient doping, those eventually lead to the unstable operation regimes of the particle detectors.

In this study, the combined analysis of the capacitance-voltage (C-V), current-voltage (I-V) characteristics and BELIV (barrier evaluation by linearly increasing voltage) characteristics has been performed on Si detectors irradiated by reactor neutrons.

The rectification properties of pin diodes are clearly observed for detectors irradiated with rather small fluencies, while symmetry of I-V characteristics, at forward and reverse biasing, occurs in heavily neutron irradiated diodes. These observations correlate rather well with C-V characteristics measured on the same detectors, when crucial deviations between conductance and impedance C-V characteristics give rise with enhancement of neutron irradiation fluence. The unveiled effects are explained by the increased role of the carrier capture/generation processes within depleted diode base regions. The technique for barrier evaluation by linearly increasing voltage (BELIV) [1-4] based on measurements of current transients at reverse and forward biasing has been additionally applied to comprehensively unveil the reasons of junction degradation under heavy irradiations. The BELIV pulsed technique enables one to clarify a few significant aspects: to identify the charge extraction regime and to estimate a barrier capacitance value, to clarify competition between barrier capacitance charging and generation currents, and to clarify a full depletion state for heavily irradiated diodes. BELIV technique showed a decrease of full depletion voltage with enhancement of irradiation fluence. This observation can be explained by a crucial reduction of the carrier density, when concentration of deep traps significantly exceeds dopants density within defect-rich material surrounding the micro-crystalline columns or inclusions within the polycrystalline structures.

[1] E. Gaubas, T. Ceponis, and J. Kusakovskij, REVIEW OF SCIENTIFIC INSTRUMENTS **82** (2011) 083304
[2] E.Gaubas, T.Čeponis, S.Sakalauskas**,** A.Uleckas, and A. Velička, **LJP** (Lithuanian Journal Physics), **51** (2011) 227–233.
[3] E.Gaubas, T.Čeponis, V.Kalendra, J.Kusakovskij, and A.Uleckas, ISRN Materials Science, vol. 2012, article ID543790 doi:10.5402/2011/543790
[4] E. Gaubas, T. Ceponis, and J. Vaitkus, JOURNAL OF APPLIED PHYSICS 110 (2011) 033719.

ELECTRON MOBILITY ENHANCEMENT IN GAN SUPERLATTICES

Edgaras Dvinelis[1,3], Algirdas Mekys[1,3], Paulius Malinovskis[1,3],
Vytautas Rumbauskas[1,3], Arūnas Kadys[2], Jurgis Storasta[1,3]

[1] University of Vilnius, Faculty of Physics, Institute of Applied Research, Saulėtekio av. 9, LT-10222, Vilnius
[2] University of Vilnius, Institute of Applied Research, Saulėtekio av. 10, LT- 10223, Vilnius
[3]University of Vilnius, Faculty of Physics, Semiconductor Physics department, Saulėtekio av. 9, LT- 10222, Vilnius
edgaras.dvinelis@tmi.vu.lt

Gallium nitride (GaN) is widely used for optoelectronics, high-power and high-frequency applications due to wide band gap of 3,4 eV. The main task of this work was to investigate the samples of quantum n-GaN/AlN structures. The technique of Hall effect has been used in these samples to measure electron Hall mobility temperature dependencies (100 K – 400 K).

Samples were grown on sapphire by MOVPE in Institute of Applied Research at University of Vilnius. The AlN monolayers (0,3 nm) periodically were formed inside GaN crystal. Thicknesses of GaN layers are 3-5 nm (sample 178) and 15 nm (sample 177) also carrier concentrations are 10^{19} cm^{-3} and $2 \cdot 10^{19}$ cm^{-3} respectively. AlN monolayers confine the phonon modes in GaN crystal, but are transparent to electrons [1]. This quantum structure can be interpreted as a two-dimensional system of quantum wells for optical phonons [1]. Since at temperatures $T > 80$ K electron – optical phonon interaction plays a dominant role determining various electronic properties including mobility, decreased electron-phonon scattering rate due to phonon confinement results in enhancement of electron mobility [1]. Also confined optical phonon vibration vanishes very close to heterojunction interface like in GaAs/AlAs [1].

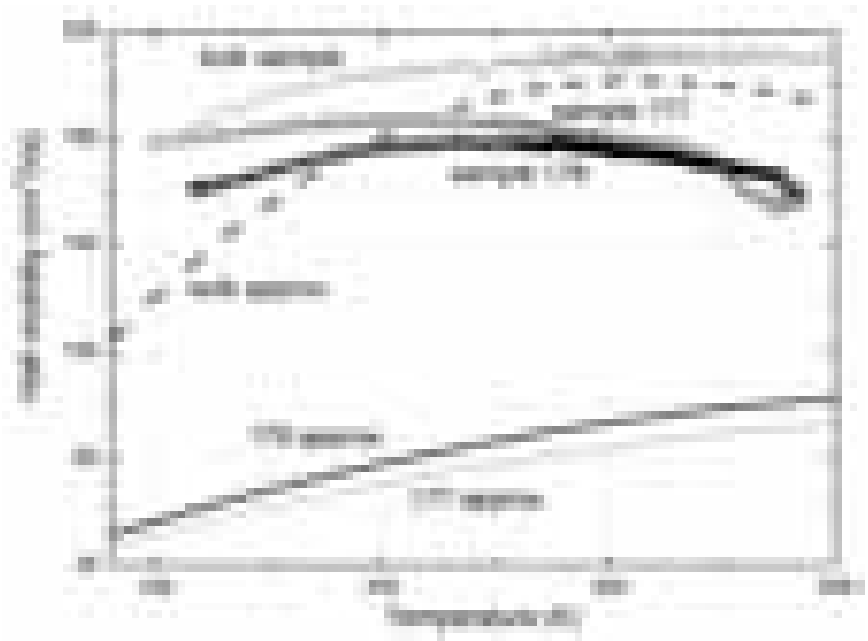

Fig. 1. Measured Hall mobility temperature dependencies (○, □, Δ symbols) and approximations (straight and dash lines).

As can be seen in figure 1, measured data have been compared with an approximation of charge carrier mobility temperature dependencies in bulk GaN material [2]. The establishment of this approximation function was based on experimental data reported in scientific literature [2]. Additionally bulk GaN sample (charge carrier concentration is $2 \cdot 10^{18}$ cm^{-3}) was investigated in order to verify this approximation, which provides rather well agreement with experimental data at temperature of 300 K as it can be seen in figure 1 (bulk sample). Electron mobility in the samples of quantum n-GaN/AlN structures greatly increased from 70 cm^2/Vs as it should be in bulk GaN crystal according to approximation, to 180 cm^2/Vs (300 K). Also this electron mobility enhancement can be confirmed by comparing data with experimental data reported in [2]: the values of electron mobility from 30 cm^2/Vs to 100 cm^2/Vs were measured in bulk GaN samples of the same doping level as 177 and 178 samples.

[1] J. Požela, V. Jucienė, and K. Požela, Enhancement of Electron Mobility in 2D MODFET Structures. Physics and Computer Modeling of Devices Based on Low-Dimensional Structures, 1995, 90 – 93 pp.

[2] Tigran T. Mnatsakanov, Michael E. Levinshtein, Lubov I. Pomortseva, Sergey N. Yurkov, Grigory S. Simin, M. Asif Khan. Carrier mobility model for GaN. Solid-State Electronics 47 (2003) 111–115 pp.

NOISE INVESTIGATION OF InGaAs QUANTUM STRUCTURES FOR TERAHERTZ DETECTION

Paulius Eidikas[1], Valdas Eimontas[1], Jonas Matukas[1]

[1] Radiophysics Dep,. Faculty of Physics, Vilnius University
Paulius.Eidikas@ff.stud.vu.lt

Rapid innovations in terahertz (THz) technology increased the demand for room temperature operating, stable and compact THz detectors. Special attention is given to increase the response time, providing versatility for imaging, medical diagnostic, and security aims [1]. Semiconductor electric and noise investigations can provide valuable information about the sample and its quality [2]. I-V characteristic can define samples macroscopic properties, but to understand how defects influence samples performance, voltage fluctuation analysis can be used [3]. Furthermore, noise investigation can determine how the amount of imperfections differs in separate samples made by same technology, specifying the quality of the sample and the manufacturing.

Bow-tie InGaAs-based diode with broken symmetry, used for terahertz detection at room temperature has been investigated. It consists of two leafs. One is metalized while the other is the active part, made of semiconductor. The device operation principle is based on non-uniform electron heating in its active part that contains two-dimensional electron gas while the metalized part couples the incident radiation to it. Samples electric and low-frequency noise characteristics are shown in Fig1,2 respectively.

Current-voltage analysis depicts that samples differential resistance depends on currents polarity. The asymmetrical shape of the diode influences different electric field distribution in the active region for positive and negative voltages, resulting in asymmetrical I-V characteristic.

The voltage fluctuations has been measured sustaining load resistance many times larger than the differential resistance of the sample. Fluctuations spectral density in low-frequency region can be characterized as $1/f$ function. This shows, that low-frequency noise is caused by recombination and capture processes in defects of the sample.

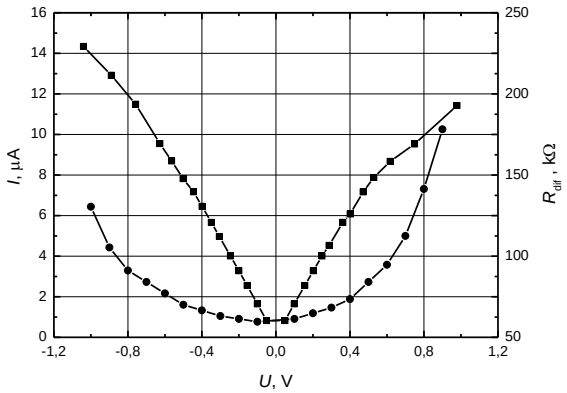

Fig. 1. Samples I-V characteristic and its differential resistance.

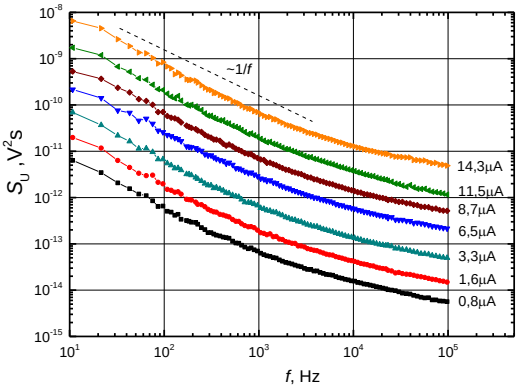

Fig. 2. Voltage fluctuation spectral density dependency on frequency at different backward currents.

[1] I. Kašalynas, D. Seliuta, R.Simniškis, V. Tamošiūnas, V. Vaičikauskas, I. Grigelionis, R. Nedžinskas, K. Köhler and G. Valušis, *The response rate of room temperature terahertz InGaAs-based bow-tie detector with broken symmetry*, 33rd International Conference on Infrared, Millimeter and Terahertz Waves, (Pasadena, California, September 15-19, 2008).

[2] S.An, M.J. Deen, *Effect of mesa overgrowth on low-frequency noise in planar seperate absorption, grading, change, and multiplication avalanche photodiodes*, IEEE Journal of Quantum Electronics **35** (8), 1196-1202 (1999).

[3] B. Šaulys, J. Matukas, V. Palenskis, S. Pralgauskaitė, *Red light-emitting diode degradation and low-frequency noise characteristics*, 18th International Conference on Microwave Radar and Wireless Communications, (Vilnius, Lithuania, June 14-16, 2010).

DIELECTRIC PROPERTIES OF $0.98Pb(Mg_{1/3}Nb_{2/3})O_3 - 0.02La(Mg_{2/3}Nb_{1/3})O_3$ CRYSTAL

Džiugas Jablonskas[1], Robertas Grigalaitis[1], Zuo-Guang Ye[2], Alexei A. Bokov[2]

[1] Vilniaus universitetas, Fizikos fakultetas, Saulėtekio al. 9, LT-10222 Vilnius
[2] Departament of Chemistry, Simon Fraser University, Burnaby, British Columbia, Canada VSA 1S6
dziugas.jablonskas@ff.stud.vu.lt

$Pb(Mg_{1/3}Nb_{2/3})O_3$ (PMN) is one of the most known, classical ferroelectric relaxors (FR). At room temperature PMN has cubic ABO_3 perovskite structure, where Pb^{2+} occupies A-sites while Mg^{2+} and Nb^{5+} share B-sites. The chemically ordered regions (CORs) as well as the polar nanoregions (PNRs) – small nanometer-sized uniformly polarized regions, which persist at temperatures well above the temperature of the dielectric constant maximum T_m are often believed to be the origin of the characteristic relaxor ferroelectric behavior. Such behavior was observed only in those compounds where the nanometre-scale CORs are present. Accordingly, it was suggested that CORs act as sites to localize the dynamic PNRs responsible for the relaxor behavior. In pure PMN, the size of the CORs was found to be smaller than 5 nm. A-site La^{3+}-doping has been found to be an effective way to enhance B-site cation order in PMN [1]. In $0.98Pb(Mg_{1/3}Nb_{2/3})O_3 - 0.02La(Mg_{2/3}Nb_{1/3})O_3$ (PLMN) crystal there are marked decreases in the value of the maximum of relative permittivity, the temperature of peak permittivity and the freezing temperature [1]. However, it is not clear how the CORs affect the dynamics of PNRs. Thus the investigation of broadband dielectric properties of (PLMN) crystal promotes the deeper understanding of the mechanisms of relaxor behavior and PNRs dynamics.

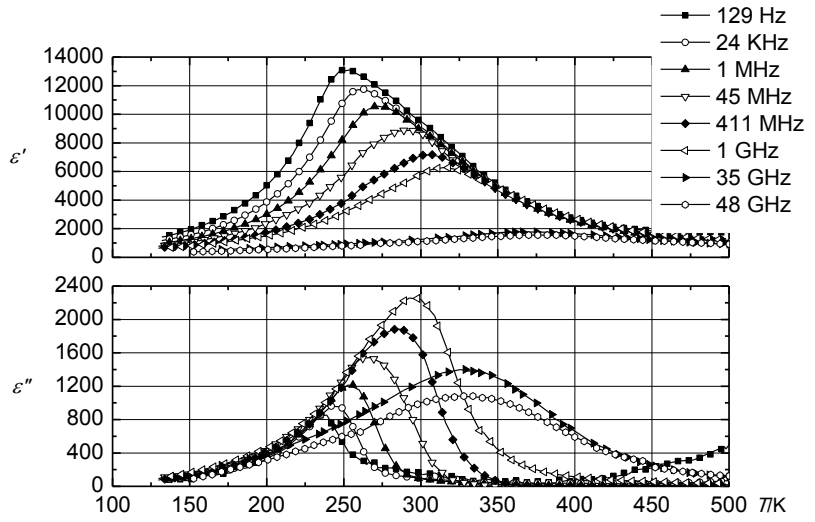

Fig. 1. Temperature dependency of complex dielectric permittivity of PLMN single crystal

The dielectric properties of PLMN crystal were observed in frequency range of 100 Hz – 48 GHz and in temperature range of 110 K – 500 K. The sample was heated to 500 K temperature in order to eliminate "memory effects" – dissarange "frozen" PNRs. The measurements of dielectric permittivity took part in freezing cycle with 1 K/min temperature drop rate. Fig. 1 shows the temperature dependency of complex dielectric permittivity. The peak of $\varepsilon'(T)$ goes towards higher temperatures with increase of frequency. This is common behavior of FR and is caused by the broad distribution of PNR relaxation times. The dispersion of complex dielectric permittivity $\varepsilon^*(f)$ was fitted with Cole – Cole (1) formula, which describes the conventional relaxation process rather well. Although, another dispersion was found in frequencies $f < 1$ kHz, which requires further investigations.

$$\varepsilon^*(\omega) - \varepsilon_\infty = \frac{\Delta\varepsilon}{1 + (i\omega\tau)^{1-\alpha}} \tag{1}$$

The temperature dependency of mean relaxation time τ, which was obtained from Cole – Cole fits, increases with decrease of temperature. The increase is non-linear even in logarithmic scale and it can be described with Vogel – Fulcher formula (2). Such behavior shows that the dynamics of the system slow down with decrease of temperature and slow down critically at temperature $T_f = 191$ K.

$$\tau(T) = \tau_0 \exp\left(\frac{E}{k(T - T_f)}\right) \tag{2}$$

[1] X. Long, A. A. Bokov, Z-G. Ye, W. Qu, X. Tan, Enhanced ordered structure and relaxor behavior of $0.98Pb(Mg_{1/3}Nb_{2/3})O_3 - 0.02La(Mg_{2/3}Nb_{1/3})O_3$ single crystals, J. Phys.: Condens. Matter **20** 015210 (2008)

CELIV experiment automation and optimization

Vytautas Janonis, Vaidotas Kažukauskas

Institute of Aplied Research, Vilnius University, Saulėtekio Ave. 9-III, LT-10222, Vilnius, Lithuania
Vytautas.Janonis@ff.stud.vu.lt

Photo induced Carrier Extraction by Linearly Increasing Voltage (CELIV) is a relatively new method of simultaneous determination of charge carrier mobility and lifetime in organic semiconductors, where active layers are few hundred nanometers thick [1]. Other method of carrier mobility investigation in such semiconductors is Time Of Flight (TOF) method, but it has several limitations, which CELIV has not. For example, TOF method sometimes requires up to ten times thicker samples, than that assuring optimal performance of bulk heterojunction solar cells. Moreover, the number of charge carriers in TOF experiments is limited to 10% of the capacitive charge. Also with CELIV samples of high conductivity can be examined, where TOF cannot be used.

The photo-CELIV experimental setup that was used consists of the high power (up to 3 W) light emitting diode, which is controlled by the programmable Agilent 33220A function generator, through the self-made amplifier and fed by the digital TTI QL355P power supply unit. Linearly increasing voltage over the sample is generated by the programmable HAMEG HMF 2550 function generator. The kinetics of the current flowing through the sample was measured by the Tektronix TDS 2022 digital oscilloscope. Sample was placed in the Janis VPF-475 cryostat, and temperature was regulated by the Cryo-Con 32B temperature controller.

The work consisted of two parts. The first one was the optimization of LED performance. To achieve the fast turn on and off of the diode by minimizing effects of transient phenomena the self-built amplifier was developed. With it the noises at the fronts of the light pulses were shortened down to one microsecond. Also in order to quickly change the wavelength of the exciting light five separate diodes with cooling and light focusing elements were made. The second part of the work was connecting all the instruments into one system and controlling all of them via the computer GPIB and USB interfaces by the originally developed program. The program was written in Labview programming environment, so that all experiment can be completed quickly and precisely without tedious manual adjustments. Program itself can separately control the generators, changing basic parameters of the light pulse and the voltage sent to sample separately or together. The voltage sent to the sample has a specific waveform, because of that the program builds an arbitrary waveform and supplies it to the Hameg generator via the USB bus. Temperature control is achieved simply by providing the required value and the program sets the temperature controller to needed settings via the GPIB bus. Kinetics of the extraction current through the sample is recorded and saved to file via the oscilloscope control block, which has 2 separate displays for each input channel and other necessary controls.

A program to measure TSC (thermally stimulated current) was also written in the same environment which also helps to accomplish experiments faster and more conveniently. This program changes sample temperature via the Cryo-Con temperature controller and reads current flowing through it via the combined Keithley 2400 digital electrometer-voltage source. Results are updated and displayed as diagram and graph as they are read.

[1] G. Juška, A. J. Mozer, N. S. Sariciftci, L. Lutsen, D. Vanderzande, R. Österbacka, M. Westerling. Charge transport and recombination in bulk heterojunction solar cells studied by the photoinduced charge extraction in linearly increasing voltage technique, Appl. Phys. Lett. 86, 112104 (2005).

PROFILING OF RADIATION INDUCED DEFECTS IN Si STRUCTURES BY MICROWAVE PROBED PHOTOCONDUCTIVITY TRANSIENT TECHNIQUE

Arnoldas Jasiūnas, Aurimas Uleckas, Eugenijus Gaubas

Institute of Applied Research, Vilnius University, Saulėtekio Ave. 9-III, LT-10222 Vilnius, Lithuania
arnoldasj@gmail.com

Silicon based detectors are commonly employed in high energy particle detection due to reliability and highly developed technology. Tracking of high energy particles is based either on direct registration of the Ramo's current transients or by collecting particle generated electron-hole pairs [1]. However, high energy particles cause a detector material damage, which leads to permanent degradation of particle detector operational characteristics [1]. As a result, radiation induced defects affect the detectors functional parameters, such as sensitivity, switching speed, charge collection efficiency, etc. On the other hand, the irradiation technologies are routinely applied in semiconductor device industry to optimize a performance of semiconductor devices by reduction of the minority carrier lifetime. In power switchers design, the injected carriers during forward bias cycle should be rapidly removed to reinstate the blocking mode and, thus, to achieve the faster switching speed. Position of fast recombination centres within diode base region is an essential parameter to achieve trade-off between switching speed of device, leakage current and forward voltage drop. Penetration depth of the protons depends on the energy of the beam. Thereby, irradiation with protons of different energy enables one to manipulate location of enhanced recombination layer, induced by irradiations. It is rather well-known technologies [2] how to introduce desirable deep levels within the band gap by irradiation with penetrative particles, e.g. by 2- 10 MeV electron beam.

The bombardment of silicon structures with high energy particles produces a displacement of the Si crystal lattice in the form of vacancies and interstitial atoms. The dominant defects in Si, those are formed by irradiations, are ascribed to complexes of vacancy with impurity atoms and to divacancy. In high resistivity regions of silicon bipolar devices, the divacancy has been identified to be the dominant recombination site for both p-type and n-type regions [2]. Advantages of usage of the irradiation techniques are the allowance of initial testing of device characteristics before and after the irradiation, cleaner process and possibility of recovery of the device characteristics by annealing, in case the device may have received an overdose during the irradiation [2]. The desirable density of defects and location of the enhanced recombination layer can be reached by controlling of the energy and fluence for a proton beam. Therefore, precise evaluation of a density and in-depth distribution profile of defects produced by different irradiation regimes is very important.

In this work, profiles of defect density within a cross-section of a semiconductor device layered structure were examined by measuring carrier lifetime distribution by employing contact-less microwave probed photo-conductivity (MW-PCD) technique. The spatial resolution of MW-PCD technique has been improved by using near-field microwave needle-tip antennas and a focusing system for excitation laser beam. Float Zone (FZ), Czochralski (Cz) Si wafers and diode structures irradiated by protons with energies ranging from 1.5 MeV to 26 GeV were examined, and distribution of defect density was measured. Profiles of carrier lifetime distribution after irradiation by penetrative and stopped particles have been compared. It has been proved that the employed carrier lifetime profiling arrangement reproduces well profiles of radiation damage simulated by TRIM software platform.

[1] G. Lutz, *Semiconductor Radiation Detectors* (Springer-Verlag Berlin and Heidelberg GmbH and Co. Kg, Berlin, 2007).

[2] B. J. Baliga, *Fundamentals of Power Semiconductor Devices* (Springer Science Business Media, LLC, New York, 2008).

ASYMMETRIC ANTHRACENE DERIVATIVES FOR OPTOELECTRONIC APPLICATIONS

Regimantas Komskis[1], Tomas Serevičius[1], Povilas Adomėnas[2], Ona Adomėnienė[2], Renaldas Rimkus[2], Vygintas Jankauskas[3], Karolis Kazlauskas[1] and Saulius Juršėnas[1]

[1]Institute of Applied Research, Vilnius University, Saulėtekio al. 9-III, LT-10222 Vilnius, Lithuania
[2] UAB „Tikslioji Sintezė“ (Ltd), Kalvarijų g. 201E, LT-03225 Vilnius, Lithuania
[3]Departament of Solid State Electronics, Vilnius University, Saulėtekio al. 9-III, LT-10222 Vilnius, Lithuania
regimantas.komskis@gmail.com

Anthracene is considered as a perspective emissive material for fabricating organic blue light – emitting devices (OLED). It demonstrates good emission efficiency, colour purity and stability. However, unsubstituted anthracene tends to crystallize in thin films and strongly deteriorates colour purity and efficiency of OLED device. Additionally, for inexpensive and efficient production of anthracene – based OLED devices it is necessary to improve solubility of anthracene in common solvents. A key of solution to these problems is synthesys of anthracene derivatives with various groups, attached to 9^{th}, 10^{th} [1] or 2^{nd} [2] positions of athracene.

In this work optical and electrical properties of a set of asymmetric anthracene derivatives was investigated. The size of π-conjugated electron system was enhanced with phenyl ring in the second position of anthracene molecule. The rotation of phenyl ring was fixed (see table 1) with sulphur, oxygen and nitrogen heteroatoms.

ad-1		ad-4		AA-6	
ad-2		ad-5		AA-7	
ad-3					

Table 1. Asymmetric anthracene derivatives

The detailed spectroscopic analysis of asymmetric anthracene derivatives showed typical vibronic structure of absorbtion and fluorescence bands. Fixation of phenyl group with different heteroatoms caused red shift of absorbance and fluorescence bands both in solution and solid state and reduced the strength of electron – vibronic interaction. Phenyl ring fixation enhanced fluorescence quantum yield from 24% up to 46% in dilute solutions. The formation of excimer states and decreased fluorescence quantum yield was observed in thin films due to a close molecular packing. As a result, reduction of fluorescence quantum yield in thin films from 21% to 0,005% was observed.

5,25 ns fluorescence decay time of 2-phenylanthracene (ad – 1) in solution is almost equal to unsubstituted anthracene. Phenyl ring fixation of anthracene derivatives increased fluorescence decay time up to 14 ns and also enhanced radiative (from 21,8 ns up to 39,64 ns) and non – radiative (from 6,91 ns to 25,93 ns) relaxation decay time in solution. The decreased rate of non – radiative relaxation in respect of radiative one enhanced fluorescence quantum yield in solutions. Fluorescence decay transients in the solid state exhibited the non – exponential behavior implying competing exciton radiative relaxation and diffusion processes.

Asymmetric anthracene films showed good hole mobilities, in the order of 10^{-4} cm^2/Vs. Moreover, phenyl ring fixation with different heteroatoms enabled the tuning of ionization potential, and thus HOMO level, in a wide range of energies (4.9-5.7 eV), what is important for design of asymmetric anthracene – based organic light – emitting devices.

[1] Yuin – Hi Kim, Hyun – Cheol Jeong, Sung – Han Kim, Kiull Yang, Soon – Ki Kwon, High – Purity – Blue and high efficiency electroluminescent devices based on anthracene, Adv. Fun. Mater., 15, 1799 – 1805, (2005)
[2] Jinhai Huang, BoXu, Mei-Ki Lamb, Kok-Wai Cheah, Chin H. Chen, Jian-Hua Su, Unsymmetrically amorphous 9,10-disubstituted anthracene derivativesfor high-efficiency blue organic electroluminescence devices., Dyes and Pigments, 89, 155 – 161, (2011)

SIMULATIONS OF THE ANNEAL CAUSED VARIATIONS OF THE DEEP LEVEL TRANSIENT SPECTROSCOPY CHARACTERISTICS IN Si THYRISTOR STRUCTURES

Andrius Krasauskas, Aurimas Uleckas, Eugenijus Gaubas

Institute of Applied Research, Vilnius University, Sauletekio Ave. 9-III, LT-10222 Vilnius, Lithuania
krasauskas.andrius@gmail.com

The power thyristors provide both foward and reverse voltage-blocking capability making it well suited for AC (altering current) power circuit applications. The device can be switched by using a relatively small gate control current [1]. However, due to technological reasons, the impurity defects as usually appear modifying the thyristor operational parameters. An impact of these defects can be reduced by annealing structure. Therefore, it is important to identify these defects in thyristor structures and to measure the main signatures of deep traps associated with impurities.

In this work, analysis of the as-fabricated and annealed silicon p-n-p thyristor structures has been performed by measurements of the deep level transient spectra (DLTS). A commercial DLS-82E spectrometer has been used to measure DLT spectra before and after anneal of the thyristor structures. Samples were annealed within special oven, when temperature values had been precisely controlled by personal computer.

DLTS is method based on measurements of the thermal emission from a carrier trap relaxation characteristics, registered as a capacitance transients. Reverse bias was applied on the sample under test, and it pulsed between low bias and higher bias with selected repetition time. At low reverse voltage traps are filled with carriers. During the higher reverse voltage pulse the trapped carriers are emitted at a rate e_n producing the exponential transients in the capacitance [2]. Each trap has its specific thermal emission rate, which is reciprocal to carrier emission lifetime τ, as $e_n = 1/\tau$. A maximum on DLT output is observed when emission lifetime coincides with filter time constant set on spectrometer. Thus, varying temperature, a peak structure spectrum is recorded. To perform temperature scans, sample has been placed into liquid nitrogen immerse cryostat. Repeated temperature scans varying spectrometer time constants set values of emission rate and peak position within temperature scale. From these spectral parameters Arrhenius graphs, displaying a function $\ln(e_n^{-1}T^2)$ versus T^{-1}, are plotted, and the main trap signatures, as activation energy E_n and carrier capture-cross section σ_n , are extracted.

The rather complicated DLT spectrum structures have been obtained on the examined thyristors. Due to complicated DLT spectra, anneal induced transformations of traps and variations of their density have been analyzed by decomposing the DLT spectra into separate Gaussian-shape peaks. Therefore, the specialized simulation algorithm has been created, to separate transformations of each peak on the background of the overlapping multi-peak spectrum. Thereby it has been found that density of defects, acting as majority carrier traps, were changed after annealing. Simultaneously, density of minority carrier traps increased.

[1] B. J. Baliga, Fundamentals of Power Semiconductor Devices. (Springer Science Business Media, LLC, New York, 2008).
[2] P.Blood and J.W. Orton, The Electrical Characterization of Semiconductors: Majority Carriers and Electron States (Academic Press Inc., San Diego, 1992).

SIMULATION OF TRANSIENTS OF THE NON-EQUILIBRIUM CARRIER DENSITY RELAXATION IN RADIATION DAMAGED SEMICONDUCTORS

Jevgenij Kusakovskij, Eugenijus Gaubas

Institute of Applied Research, Vilnius University, Sauletekio Ave. 9-III, LT-10222 Vilnius, Lithuania
jevgenij.kusakovskij@tmi.vu.lt

Trap assisted carrier generation and recombination in semiconductors can be accurately described by Shockley-Read-Hall (S-R-H) statistics [1] if transitions between deep levels can be neglected. Originally mathematical expressions for this model were derived by considering the transition rates of a small non-equilibrium carrier concentration to and from a single-level deep trap. However, this model was generalized for an arbitrary distribution of non-interacting traps in the later publications [2, 3]. The main assumptions of the S-R-H model are valid in the majority of practical problems, but this may not be the case when dealing with low quality or heavily damaged semiconductor materials. It is reasonable to suppose that the recombination process may become similar to a random walk and therefore may be treated by ad hoc methods [4] when trap densities appear to be sufficiently high at low concentration of carriers

In this work a new charge relaxation model has been proposed for description of relaxation processes, when density of carrier traps of various species significantly exceeds equilibrium density of dopants. Random-walk approach has been involved to simulate the intricate redistribution of carriers among trapping centres during relaxation of small density of excess carriers. Results of the numerical simulations, employed to describe the processes of random and repeated events of trapping and release within excess carrier system, have been verified using comparative approach to equivalent low trap/low carrier density regime which can be analytically described through solutions of the master equation system. This comparison showed good agreement between numerical and analytical solutions for equivalent relaxation regimes and illustrates the compatibility of these methods. Furthermore, more intricate numerical experiments were employed to study the behaviour of a model system in the non-linear regime.

[1] W. Shockley, W.T. Read Jr. et al., Statistics of the recombinations of holes and electrons, Physical Review **87**, 835-842 (1952).

[2] J.G. Simmons, G.W. Taylor et al., Non-equilibrium Steady-State Statistics and Associated Effects for Insulators and Semiconductors Containing an Arbitrary Distribution of Traps, Physical Review B **4**, 502-511 (1971).

[3] J. S. Blakemore, *Semiconductor statistics* (Pergamon press, Oxford, 1962).

[4] S. Havlin and D. Ben-Avraham et al., Diffusion in disordered media, Advances in physics **1**, 187-292 (2002).

MODELING OF ELECTRON CONFINEMENT NEAR DISC-SHAPED GATE OF MOS STRUCTURE

Elena A. Levchuk[1], Olga A. Lavrova[1], Leonid F. Makarenko[1]

[1] Department of Applied Mathematics and Computer Science, Belarusian State University, Independence Ave. 4, 220030 Minsk, Belarus
fpm.levchukEA@bsu.by

Doped silicon is a promising candidate for quantum computing due to its scalability, long spin coherence time, and the amazing progress in Si technology. The precise control of the dopant position is necessary for the experimental realization of such a working qubit. For fundamental physics as well as for applications it is interesting to develop models for a better understanding of the physics of single dopants localized near an interface taking into account the complete electrostatics of the problem, i.e., the image charges and a gate of finite size. For the case of a semiconductor/metal interface the energy spectrum was recently investigated in [1] using the finite element technique and in [2-5] the ground state energy of a donor localized in Si near an interface with an insulating layer (semiconductor/dielectric system) was calculated using a variational approach. In many of those calculations it was suggested a metallic gate is of infinite size. However one needs to use more realistic models to study this problem. This work suggests that the gate has nanoscale dimensions which is expected for future devices.

To calculate the electronic spectrum and electron's wave function $F(\vec{r})$ an eigenvalue problem for the following equation (written in dimensionless form) should be solved:

$$\left\{-\nabla^2 - \frac{2}{r_D} + V_{imp} + V_{simp} - e\varphi_0 g(\vec{r})\right\} F(\vec{r}) = EF(\vec{r}), \quad (1)$$

where V_{simp} describes the interaction between electron and its image, V_{imp} is the interaction between electron and donor image, $\varphi_0 g(\vec{r})$ is the potential landscape in the semiconductor due to the gate, r_D denotes the distance between electron and donor. All distances are scaled to units of gate's diameter (d) and the energy E is given in effective units of $\frac{Ry^*}{\delta^2}$, where $\delta = \frac{d}{a^*}$. V_{simp} and V_{imp} can be represented in an analytical form. The value of potential $\varphi_0 g(\vec{r})$ was calculated using finite element method with approximation by linear finite elements on a triangular mesh. The gate voltage is cylindrically symmetric, so cylindrical coordinates were used. The equation is posed in a bounded domain $\Omega = [0, L_\rho] \times [0, L_z]$ chosen for an approximation of the semi-infinite region $[0, +\infty] \times [0, +\infty]$. These calculation were carried out using MATLAB. The problem (1) itself was solved using finite element method.

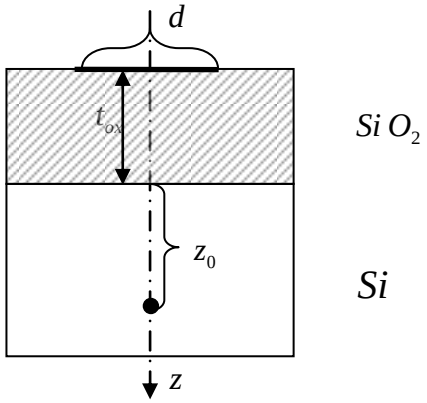

Fig. 1. The layout of the model system.

Using the suggested approach, we have studied the P donor wave function perturbed by an electric field and the Si host geometry, effects of varying several experimental parameters: the gate voltage, donor depth and the gate diameter were examined in order to find conditions of electron shuttling between donor position and surface. The presented results highlight not only the significance of the gate potential in affecting the donor electron wave function, but also the position of the qubits in the device. The proximity of the qubit to the gate is also important in determining the degree to which the electron exchange interaction can be enhanced by the applied voltage.

[1] A. F. Slachmuylders et al., Effect of a metallic gate on the energy levels of a shallow donor, Appl. Phys. Lett. 92, 083104 (2008).
[2] M. J. Calderón, B. Koiller, and S. Das Sarma, External field control of donor electron exchange at the Si/SiO_2 interface, Phys. Rev. B 75,125311 (2007).
[3] Y. L. Hao, A. P. Djotyan, A. A. Avetisyan, and F. M. Peeters, Shallow donor states near a semiconductor-insulator-metal interface, Phys. Rev. B 80, 035329 (2009).
[4] L. M. Kettle et al., Numerical study of hydrogenic effective mass theory for an impurity P donor in Si in the presence of an electric field and interfaces, Phys. Rev. B. 68, 075317 (2003).
[5] G. D. J. Smit et al., Gate-induced ionization of single dopant atoms, Phys. Rev. B. 68, 193302 (2003).

DIELECTRIC PROPERTIES OF $Pb(Fe_{2/3}W_{1/3})+1\%MnO_2$ CARAMICS

Rūta Mackevičiūtė[1], Jūras Banys[1], José Antônio Eiras[2]

[1] Vilnius University, Faculty of physics, Saulėtekio av. 9, III b., LT-10222 Vilnius, Lithuania
[2] Grupo de Cerâmicas Ferroelétricas, Departamento de física, Universidade Federal de São Carlos, Brazil
Rūta.Mackevičiūtė@ff.stud.vu.lt

Recently, there is a great interest in multiferroics – materials which in the certain temperature range are ferroelectrics and ferromagnetics. The most popular multiferroics are lead – iron niobium $Pb(Fe_{2/3}W_{1/3})$ and bismuth ferrite $BiFeO_3$. These multiferroics could be used in microelectronics for example, producing MERAM memories.

PFW ceramics dynamic dielectric properties have not been published anywhere, so the aim is to investigate these properties.

In order to produce high quality samples, a modified B-site precursor method was proposed as an effective method to obtain a pure perovskite phase in lead-based ceramics [1]. $Pb(Fe_{2/3}W_{1/3})$ ceramic was prepared using this method. Dielectric measurements were performed at temperature range (110 – 500) K and in the frequency range (20 – 1000) kHz, (300 MHz – 3GHz) and (24 – 40) GHz. In the low frequency range (20 kHz – 1000 kHz), investigation was performed by measuring samples' capacity and the tangent of loss angle using LCR-meter HP4284A. In the high frequency range (300 MHz – 3GHz) investigation was performed by using network analyzer Agilent 8714ET. Measurements were performed by reducing the temperature of the sample and the temperature variation rate was about 1 K/min.

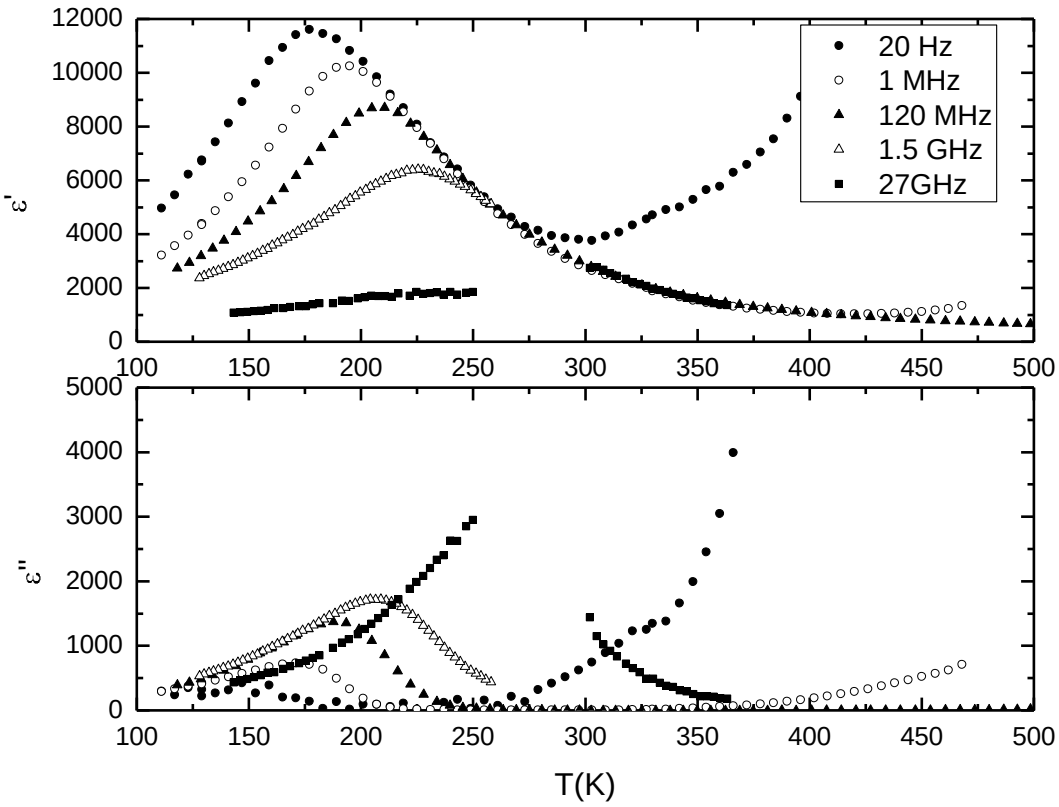

Fig. 1. Temperature dependence of the real and imaginary parts of dielectric permittivity of PFW+1%MnO_2 ceramic.

Figure 1 shows the temperature dependence of the real and imaginary parts of dielectric permittivity of PFW+1%MnO_2 ceramic. This investigation shows that PFW ceramic is ferroelectric relaxor. We observe the anomaly of dielectric permittivity which is typical for the ferroelectric relaxors at the temperature range less than 300 K: increasing frequency the peak point of the curves of dielectric permittivity moves to the higher temperature range.

[1] J. A. Eiras, B. M. Fraygola , D. Garcia, Structural and Dielectrics Properties of (1-x)Pb(Fe2/3W1/3)O3-xPbTiO3 Ceramics, Key Engineering Materials **434-435**, 307-310 (2010).

Peculiarities of galvanomagnetic effects in GaN epilayers and GaN/InGaN quantum wells

Paulius Malinovskis[1,2], Algirdas Mekys[1,2], Vytautas Rumbauskas[1], Edgaras Dvinelis[1], Arūnas Kadys[2], Tadas Malinauskas[2], Tomas Grinys[2], Vitalijus Bikbajevas[2], Rolandas Tomašiūnas[2], Jurgis Storasta[1,2]

[1]*Vilnius University, Physics faculty, Semiconductor Physics department, Sauletekio av. 9 – build III, Vilnius LT-10222 Lithuania*
[2]*Vilnius university, Institute of applied research, Sauletekio av. 9 – build III, Vilnius LT-10222 Lithuania*
paulius.malinovskis@ff.vu.lt

Temperature dependent Hall effect and magnetoresistivity studies have been performed on GaN epilayers and GaN/InGaN multiple quantum wells (MQWs) grown on sapphire films by MOCVD method (Metal Organic Chemical Vapor Deposition). The grown samples were n, p and intrinsic conductivity type GaN thin films and different MQW structures consisted of 5MQWs with 4nm and 6nm thick InGaN wells and 10nm GaN barriers. The growth temperature of the intrinsic GaN base layer was 1090ºC; and 850ºC for quantum structure InGaN and GaN, some samples were annealed at 820 ºC. Time resolved photoconductivity measurements were carried out using 7 ns pulse laser system.

To elucidate the kinetics of carrier recombination [1], we performed photoconductivity (PC) measurements in temperature range from 100 K to 400 K. PC decaying times were about 400 μs and 200 ns for not annealed and annealed quantum well structures respectively, not changing considerably in temperature. Long decay times revealed that the carriers are separated in space by potential barriers and after annealing carrier lifetime drastically changes. Indium is hardly solubable in GaN and may form droplets, which surface act as a recombination centers affecting the carrier lifetime.

In the next stage we measured sample conductivity, photoconductivity, Hall voltage and magnetoresistivity temperature dependencies. From this experimental data we calculated carrier's mobility, concentration and lifetime temperature dependencies, which revealed the scattering mechanisms and forbidden energies gap perturbation effects. We estimated corresponding energy values, which correlate with those given by other authors for nitrogen vacancy (V_N) [2,3]. Some experimental data of our complex researches can be explained by existence of extended defects and forbidden energies gap perturbations attributed to band-tail states.

[1] B.K.Ridley. Kinetics of radiative recombination in quantum wells. Phys.Rev.B(1990),vol.41,no.17.p.12190.
[2] Internet database: http://www.ioffe.ru/SVA/NSM/Semicond/GaN/impurities.htm (looked: 2012-02-13).
[3] A.Žukauskas, M.S.Shur, R.Gaška. Introduction to solid-state lighting. New York: Wiley (2002), 207 p.

FLUENCE AND ANNEAL DEPENDENT VARIATIONS OF CURRENT AND CAPACITANCE CHARACTERISTICS IN Si PAD-DETECTORS AND POWER SWITCHES

Dovilė Meškauskaitė, Tomas Čeponis, Eugenijus Gaubas

Institute of Applied Research, Vilnius University, Saulėtekio Ave. 9-III, LT-10222 Vilnius, Lithuania
dovime@gmail.com

Dependence of the device electrical characteristics on fluence is essential in evaluation of the functionality of high-energy particle detectors under high fluence irradiation conditions. Irradiation by high energy particles is commonly applied to improve a switching speed of the semiconductor power devices. However, this enhancement of the switching speed can be achieved as a trade-off in optimizing the device characteristics when simultaneous degradation of static characteristics appears. In order to suppress the emerged radiation defects created during irradiation, the annealing technologies are routinely employed [1].

In this study, to control an impact of irradiation and anneal procedures, the voltage-current (I-V) characteristics were measured using Keithley 6430 electro-meter combined with internal 0-200V voltage source. Also, voltage-capacitance (C-V) characteristics were examined by using QuadTech 7600 LCR meter. In the latter case, a small ac test signal (U_{ac}≤20mV) regime has been applied, when the test signal is superimposed over a dc bias to measure the barrier capacitance. Capacitance characteristics were measured using *Cp* and *Cs* mode within 1kHz-1MHz frequency range, because C-V characteristics are crucially dependent on test signal frequency after heavy irradiations. In this study, the Si pad-detectors and power switches have been examined.

The CERN standard MCZ (*Magnetic Czochralski*) Si pad-detectors, irradiated by penetrative reactor neutrons with fluences ranging from 10^{12}-10^{16} cm^{-2} and FZ (*float zone*) Si detectors, made at Hamamatsu company and irradiated with penetrative high-energy protons of fluences 10^{13} cm^{-2}, were investigated. Additionally, to compare an impact of homogeneous and local damage by irradiations, the CZ (*Czochralski*) Si industrial power switches made at „Vilniaus Ventos Puslaidininkiai“ company have been examined. The proton irradiations were performed by using a tandem accelerator at Helsinki University. The inhomogeneous δ-shape profile of radiation defects within stopping range of 2.0-2.3 MeV protons was formed in Cz Si using different fluences of $7\cdot10^{12}$-10^{14} cm^{-2}. The triangle profile of density of radiation defects was created by changing gradually an energy of protons in the range of 2-2.7 MeV and by properly varying irradiation fluence. Several irradiated samples were annealed at 120° C and 250° C temperature for 15 hours.

It has been obtained the linear increase of the leakage current with enhancement of fluence in the range of low and moderate irradiations. This increase of leakage current is caused by the radiation induced defects those act as the recombination and generation centres. However, the I-V characteristics become symmetrical, when comparing forward and reverse I-V branches, under irradiation with very large fluences. These observations can be explained by crucial reduction of carrier diffusion length and injection efficiency as well as by increase of leakage current. Analysis of the measured C-V characteristics also showed that high density of carrier traps are formed in FZ and MCZ Si pad-detectors. It was revealed that I-V characteristics of power switches depend on the damage profile and its location within the base region. The C-V characteristics enabled us to establish distribution of the effective charge density in the base region [2]. It has been revealed that heat treatments lead to transformation of radiation defects, however, suppression of radiation induced changes of leakage current and of barrier capacitance was not achieved for the range of applied anneal procedures.

[1] B. J. Baliga, *Fundamentals of Power Semiconductor Devices* (Springer-Science, New York, 2008).

[2] P. Blood, J. W. Orton, *The Electrical Characterization of Semiconductors: Majority Carriers and Electron States* (Academic Press Inc., San Diego, 1992).

Research of Deep Levels and Traps in Hadron Irradiated Silicon

Giedrius Mockevičius , Juozas Vaitkus

Department of Semiconductor Physics, Faculty of Physics, Vilnius University, Saulėtekio Ave. 9-III, LT-10222 Vilnius, Lithuania
giedrius.mockevicius@gmail.com

Large Hadron Collider (LHC), currently used Si detectors is not sufficiently hard for ionizing radiation, which over time may be rendered unsuitable for use. In 2002 European Centre for Nuclear Research (CERN) created RD50 research program that sought to improve existing and new materials and structures suitable for new detectors. One of the most promising material is silicon, the modification is expected to achieve the desired results.

This work goal was to analyse deep levels and traps generated by hadrons in silicon.

Measuring photoconductivity spectra and analysing it using Lucovsky model [1], deep centers activation energy and concentration levels of defects was determined (Fig. 1). Using Gauss approximation was determined samples deep levels bands energies: 0,38eV; 0,66eV; 0,821eV; 0,81eV.

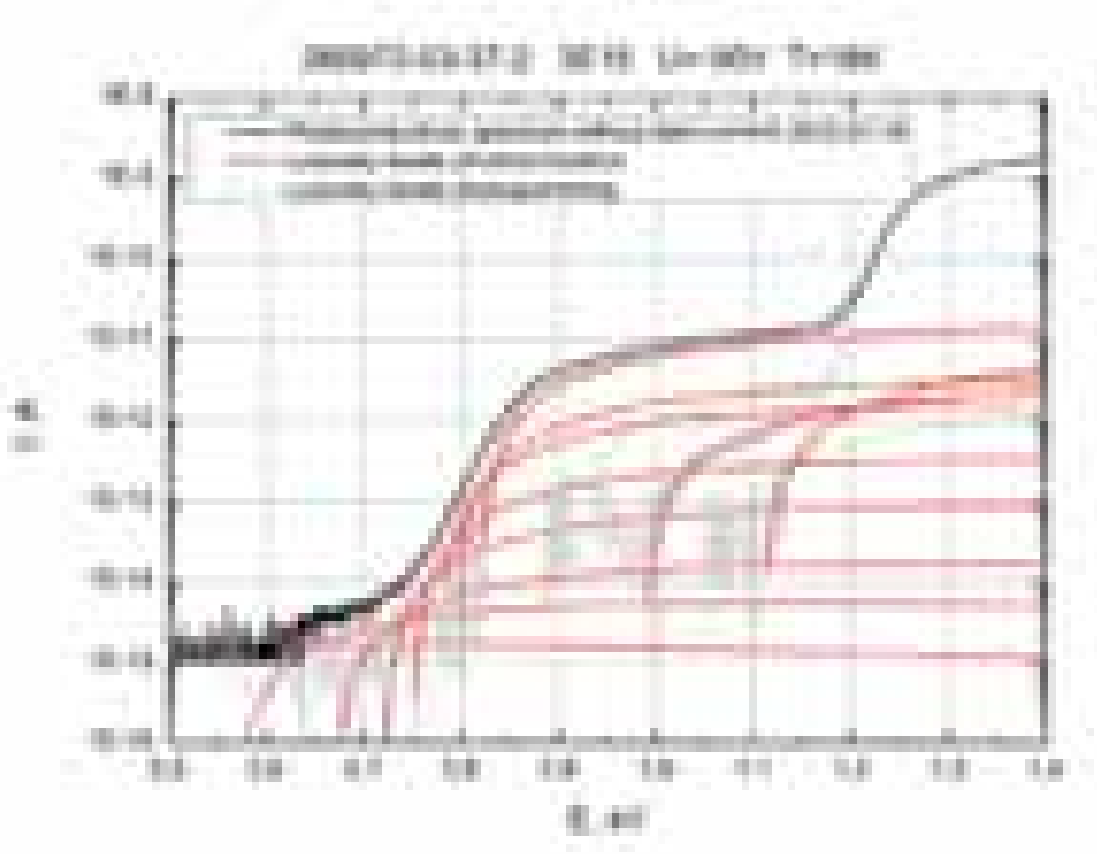

Fig. 1. Photoconductivity spectrum of n type Si and its approximation with Lucovsky model.

Heat stimulated current method was used to determine the adhesion levels, which could not be observed using photoionization spectroscopy, of sample with a thermal activation energy values: 0,456eV; 0,442 eV; 0,413eV; 0,308 eV; 0,243 eV; 0,173 eV; 0,061 eV ir 0,019 eV.

Using additional lighting from second monochromator it was found that localized levels influence the conduction band modulation and ionizing different levels, these barriers can be reduced or increased.

[1] G. Lucovsky, Solid State Communications, 299-302 (1965)

NOISE CHARACTERISTICS OF FOUR DIFFERENT TYPE HIGH POWER AlInGaP RED LIGHT-EMMITING DIODES

Grigorij Muliuk, Jonas Matukas, Sandra Pralgauskaitė

Radiophysics Dep., Vilnius University Saulėtekio 9 (III), 10222 Vilnius, Lithuania
grigorij.muliuk@ff.stud.vu.lt

New technologies of solid-state lighting and material science allowed discovering highly energetically productive AlInGaP red light-emitting diodes (LED's). However, phosphate layers in heterostructure lead to additional defects due to lattice mismatch with substrate [1]. The presence of defects leads to the trapping injected electron-hole pairs and their non-radiative recombination that increases leakage current and lowers efficiency of LED, also accelerates device degradation process.

Improvement in LED performance and reliability needs in-depth understanding the reasons of defect number growth, reasons of migration of defects during device aging, and how these processes affect operation characteristics and degradation of LED. Noise investigation gives valuable information and is useful for evaluating semiconductor device quality and predicting lifetime [2]. The aim of this work is to investigate noise characteristics of different type red light-emitting diodes, to clear up physical processes that take part in different parts of the LED and influence their degradation process during aging.

The experiment contained four LEDs of the same power (1W) and the same emitted wavelenght (643nm). The samples differ by the shape of lens: Phillips side-emmiting (D1), Lambertian (D2), Batwing (D3) and, for comparison, TME Lambertian (D4). Electrical noise spectral dencity of investigated LEDs is presented in Fig. 1. Experiment disclosed, that lens type does not make any effect on the level of noise of the investigated LEDs.

Examined noise characteristics revealed, that Phillips Batwing (D3) has the highest level of electrical noise (Fig. 1 (a)). Furthermore, D1, D2 and D3 electrical noise properties are growing slowly and steadily during the accelerated aging (by 300 mA forward current) experiment (Fig. 1 (b)). Although, TME Batwing (D4) electrical noise characteristics alter completely differently than of other samples'. During the first 500 hours of aging it showed very low level of electrical noise. But after reaching 850 hours of aging, noise spectral density increased very rapidly. Quick jump of the electrical noise spectral density may be determined by crystal lattice defects that might be generated by high current density or high temperature of *p-n* junction, both caused by aging by 300 mA forward current. Defects may create small leakage channels, that can alter current flow, so as non-radiative recombination processes in LED structure, that increases level of the electrical noise. Completing 1100-1300 hours of aging, D4 noise properties have restored because of defects migration in LEDs active layer. As a result, it proves unstable LED material quality and reveales that D4 can degrade much quicker than other samples.

Therefore, noise investigation is a prolific method to explore quality of any semiconductor device and evaluate its production and efficiency.

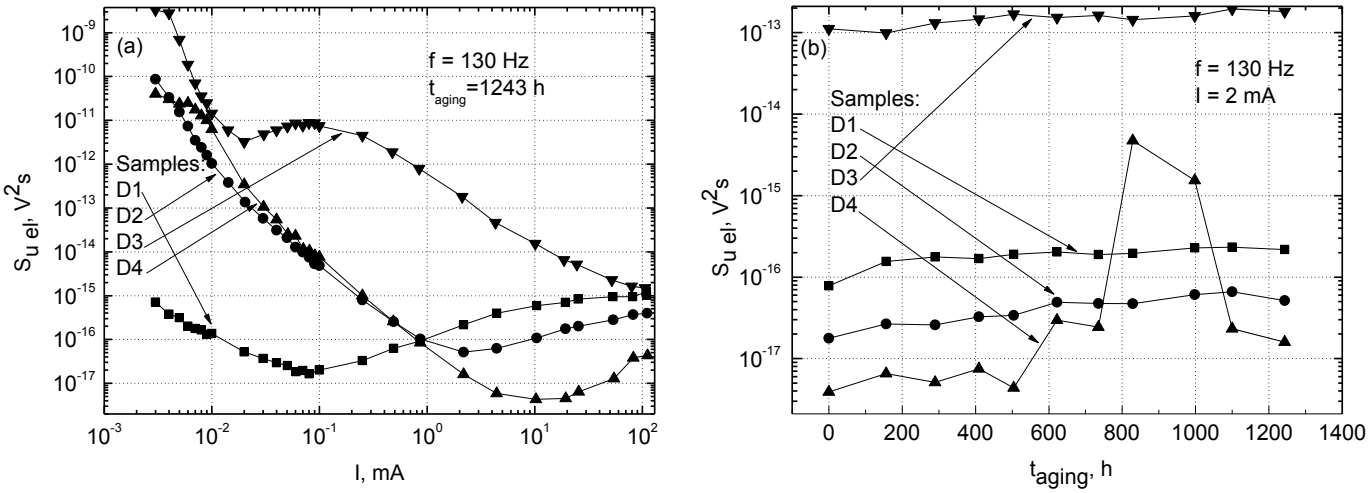

Fig 1. Electrical noise spectral density dependencies on current at fixed 130 Hz frequency (a) and electrical noise spectral density dependencies on aging time at fixed 130 Hz frequency and fixed (2mA) current (b) .

[1] K Y.-J. Lee, H.-C. Kuo, T.-C. Lu, S.-C. Wang, K. W. Ng, K. M. Lau, Z.-P. Yang, A. S.-P. Chang, S.-Y. Lin, *J. Light. Technol*. 26, 1455 (2008).
[2] V. Palenskis, J. Matukas, S. Pralgauskaitė, B. aulys, *Fluct. and Noise Lett*. 9, 179 (2010).

INVESTIGATION OF PHOTOEXCITED CARRIER DYNAMICS THROUGH TIME-RESOLVED PHOTOLUMINESCENCE IN MULTIPLE-QUANTUM-WELLS

Vaiva Nagytė, Mindaugas Karaliūnas

Institute of Applied Research and Department of Semiconductor Physics, Vilnius University, Saulėtekio ave. 9-III, LT-10222 Vilnius, Lithuania
vaiva.nagyte@ff.stud.vu.lt

Recent approaches that introduced nanometer scale multilayer heterostructures made possible artificial semiconductors with outstanding properties. They open new opportunities for applications of semiconductor devices, such as bright light-emitting diodes, laser diodes, tandem solar cells and other. Together with ongoing progress on wide-gap semiconductors, the optical wavelengths accessible by semiconductor devices are steadily expanding towards the short-wavelength ultra-violet, as well as further into the far-infrared and terahertz spectral regions [1]. The multiple-quantum-wells (MQWs) and super-lattices are the main heterostructures for most of contemporary optoelectronic devices. In order to better understand and apply such heterostructures the carrier transition effects need to be studied and well described.

In this work we present the model of photoexcited carrier dynamics. Using this model time-resolved photoluminescence (PL) decay in MQWs is described and compared with experimental data. The model of excess carrier dynamics is conducted using one-dimensional continuity equation [2] assuming that photo-generation of carriers takes place only in quantum wells, they are not captured from the barriers or do not escape to the barriers. Therefore, we assume that carriers prior to the recombination can laterally diffuse in quantum well or be captured in quantum-well/barrier interface states. The model takes into account the reabsorption of emitted light. However, we consider that such effect is not significant and can be neglected. In order to compare results with measured PL dynamics, carrier density was integrated by the quantum well length at different delay time [3].

The experiment of time-resolved PL was carried out two types of MQWs. The InGaN/GaN samples consisted of 5 MQWs and CdZnO/ZnO samples consisted of 3 or 10 MQWs. The samples were grown using molecular beam epitaxy technique in National Taiwan University. The streak camera (*Hamamatsu*, C5860) was used for spatial and temporal PL registration. The samples were excited using frequency doubled laser beam of femtosecond Ti:sapphire laser (*Coherent*, Mira 900) with the repetition rate $f_{rep} = 76$ MHz and pulse duration $\tau_p = 150$ fs. The excitation wavelength was $\lambda_{exc} = 390$ nm resulting the selective excitation of MQWs.

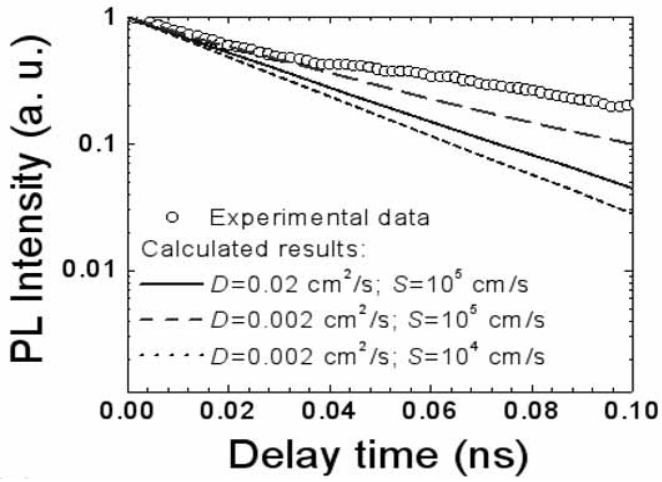

Fig. 1. Dependencies of measured and calculated normalized PL intensity on delay time in CdZnO/ZnO MQWs. D – diffusion coefficient, t – carrier lifetime.

As shown in Fig. 1, the fitting of the calculated results with the experimental data achieved good agreement. Since the measured PL decay was two exponential, the fitting was preformed on the faster PL decay component taking into account the PL intensity range from I_{max} to $I = I_{max}/e$. The PL decay time of CdZnO/ZnO MQWs was measured as 60 ps. The model yields the diffusion coefficient $D = 0.002$ cm^2/s and surface recombination rate $S = 10^5$ cm/s. As a result, the surface recombination plays significant role in PL decay in MQWs due to repetition of quantum-well/barrier interfaces. To sum up, the InGaN/GaN MQWs have better radiative properties due to better quality of the structure.

[1] M. C. Amann, F. Capasso, A. Larsson, M. Pessa. Focus on advanced semiconductor heterostructures for optoelectronics. New Journal of Physics, 11, 125012 (2009).
[2] C. Klingshirn. ZnO: Material, Physics and Applications. ChemPhysChem, 8, 782 – 803 (2007).
[3] E. Kuokstis, G. Tamulaitis, K. Liu, M. S. Shur, J. W. Li, J. W. Yang, M. Asif Khan. Photoluminescence dynamics in highly nonhomogeneously excited GaN. Appl. Phys. Lett., 90, 161920 (2007).

Investigation of (In,Ga)N Quantum Structures by Optical Light-Induced Transient Grating Techniques

Kazimieras Nomeika

Department of Physics, Vilnius University, Lithuania
Kazimieras.Nomeika@ff.stud.vu.lt

Light emitting (LED) and laser diodes are widely used in everyday life in lighting, information storage or telecommunication fields. Although currently quite expensive, LED general lighting is becoming more popular every day for it is far more efficient than ordinary lighting with incandescent light bulbs. Therefore, a lot of effort is put into trying to better understand all the physical processes of such technology and making it cheaper. InGaN is one of the compounds used for various types of LEDs because of suitable optical properties and adjustability. By changing the amount of indium in such a compound one can shift the band gap from 675 nm to 370 nm, which covers near infrared, visible and ultraviolet light.

In this work, four different structures were analyzed using a light-induced transient grating (LITG) technique [1]. In this technique, a sample is excited by an interference field of two coherent beams creating a transient diffraction grating, which is probed by diffraction of the delayed probe beam. In the used experiment setup, the wavelengths of the pump and the probe beams were 355 nm and 532 nm, correspondingly. The samples were GaN, 100 nm thick $In_{0.1}Ga_{0.9}N$ layer and two (In,Ga)N multilayered LED structures.

It has been found that at fixed pump intensity the recombination rate significantly differs from sample to sample; e.g., at 0.375 mJ/cm^{2}the recombination time was τ_R=1.38±0.08 ns in GaN and τ_R=0.32±0.02 ns in $In_{0.1}Ga_{0.9}N$. Furthermore, the recombination rate showed qualitatively different dependence on excitation: in GaN sample it increased with carrier density due to the onset of nonlinear recombination, while with InGaN decay became slower. The latter fact was attributed to the saturation effect of defect-related recombination centers, which were apparently abundant in $In_{0.1}Ga_{0.9}N$ sample [2]. LED structures exhibited non-monotonic recombination rate dependence on excitation. At relatively low intensities, recombination became faster due to nonlinear recombination (most likely band-to-band transitions). But after reaching an intensity of ~0.24mJ/cm^2, recombination rate reached saturation and began to decrease, as shown in Fig. 1. Such dependence can be explained with saturation of electron states in quantum wells ("carrier spillover" effect) and consequent saturation of defect states outside the quantum wells [3]. The samples containing indium showed the decreasing in diffusivity with higher intensity of pumping beam. This might be regarded to the rising number of phonons or electrons, which results in greater scattering.

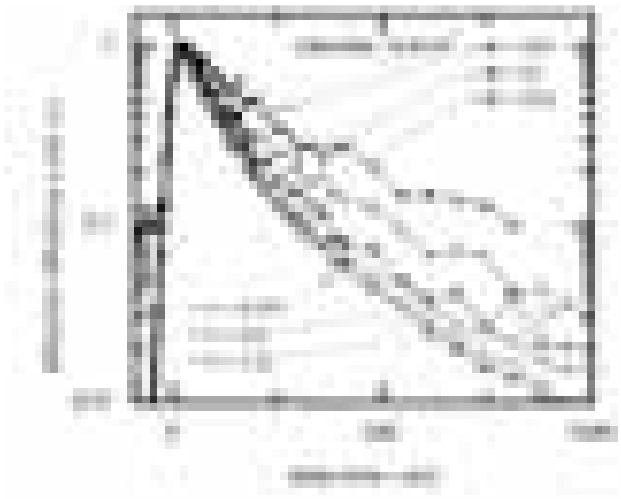

Fig. 1.The dependency of kinetics on pumping beam intensity, with the period of transient grating Λ=22.4 μm. Solid symbols show the increasing, while open symbols show the decreasing of kinetics speed.

Acknowledgement: This work was partly supported by the Lithuanian Science Council Student Research Fellowship Award.

[1] G. Juška, J. Petrulis, Light-Induced Transient Gratings in Semiconductors: A Nondestructive Optical Technique for the Characterization of Materials for Electronics, Physics of Advanced Materials, Winter School (2008).
[2] Z. Liliental-Weber1, K. M. Yu1, M. Hawkridge1, S. Bedair, A.E. Berman, A. Emara, D. R. Khanal1, J. Wu1, J. Domagala, and J. Bak-Misiuk, Structural perfection of InGaN layers and its relation to photoluminescence, Phys. Status Solidi C 6, No. 12, 2626–2631 (2009).
[3] J.-I. Shim, H. Kim, D.-S.Shin, H.-Y.Yoo, An Explanation of Efficiency Droop in InGaN-based Light Emitting Diodes: Saturated Radiative Recombination Rate at Randomly Distributed In-Rich Active Areas, Journal of the Korean Physical Society 58(3), 503-508 (2011).

GaBiAs AS A MATERIAL FOR OPTICAL ABSORBERS STUDIED BY OPTICAL PUMP-PROBE TECHNIQUES

Žydrūnas Podlipskas

Department of Semiconductor Optoelectronics, Institute of Applied Research, Vilnius University, Saulėtekio Avenue 9-3, Vilnius 10222, Lithuania
Zydrunas.Podlipskas@ff.stud.vu.lt

Structural and electronic properties of the $GaBi_xAs_{1-x}$ ternary alloys as well their growth technology became important in recent years because of promising applications in ultrafast electronics for the near infrared region of 1 – 1.5 μm [1,2]. The Bi-induced atomic disorder results in a strong reduction in the band gap E_g for a relatively small alloy concentration (62 meV per 1% of Bi) [1–3] and strongly influences carrier recombination features [4–6]. In this work, I investigated nonequilibrium carrier recombination and transport characteristics of GaBiAs layers grown under different conditions, and studied the suitability of GaBiAs compounds for semiconductor saturable absorber mirrors (SESAM).

These studies were performed using optical pump-probe and transient gratings (TG) experimental techniques. In the studies I used picosecond pump-probe setup designed to measure light-induced refractive index (Δn) and optical transmittance change (ΔT) dynamics over a wide excitation energy and delay range. Nonequilibrium carrier lifetime was determined from the differential transmittance relaxation rate $\Delta T/T$ whereas diffusion coefficient and carrier lifetime values at lower excitation densities were determined from the diffraction signal kinetics. Differential transmittance measurements were also carried out for characterization of saturable absorbers.

In this study, d=1.2 – 1.5 μm thick GaBiAs layers with different molar concentrations of Bi have been grown by molecular beam epitaxy (MBE) on GaAs substrates. Energy band gap E_g of the GaBiAs alloys, determined from the absorption spectra, ranged from 1.04 eV to 1.38 eV and provided the Bi content in the samples. Optical measurements revealed that distribution of bismuth atoms is likely non-homogeneous resulting in diffusive wash-out of absorption edge (within 40 – 150 meV range) and pronounced carrier localization effects, in addition to the valance band shift.

TG measurements showed that at least two types of recombination processes take place in GaBiAs layers. Decay transients of TG signal are nonexponential – in most of the samples I observed rapid initial and slower later components (Fig. 1). The initial component decay time varied from 27 to 1110 ps, while the slow component decay time was as long as 300 – 800 ns. TG measurements with different grating periods also showed that the diffusion coefficient of the carrier associated with slow component was immeasurably small (<0.1 cm^2/s) while the initial component diffusion coefficient was much higher (0.94 cm^2/s). From the later data, it was concluded that the initial component of TG kinetics reflects recombination of free carriers, while the slow part – recombination from the localized carrier states.

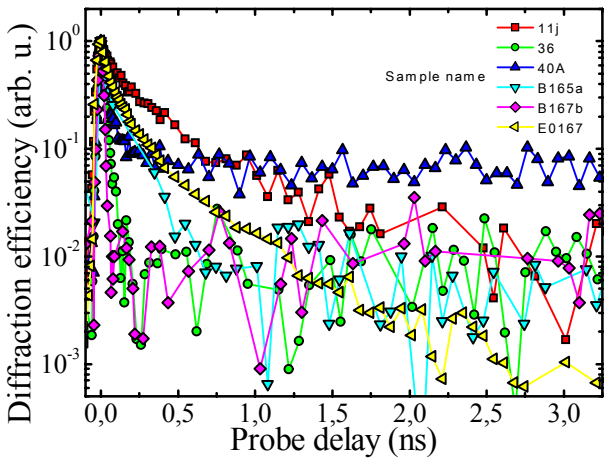

FIG. 1. Diffraction efficiency kinetics for GaBiAs layers with various Bi molar concentrations at excitation energy density of 50 μJ/cm^2 and room temperature. E0167 – reference sample of homoepitaxial GaAs layer.

The samples were characterized as a SESAM active material by measuring the following parameters: response time (<25 ps – 1.2 ns), saturation energy fluence (55 μJ/cm^2 – 1.6 mJ/cm^2) and modulation depth (10% – 200%) at 1064 nm. These parameters are comparable with the parameters of saturable absorbers on the market, so GaBiAs could be used as a full-fledged alternative to other semiconductors, for example InGaAs.

Acknowledgment. This work was partly supported by the Lithuanian Science Council Student Research Fellowship Award (Ž.P.).

[1] V. Pačebutas et al., Growth and characterization of GaBiAs epilayers, Opt. Mater. (Amsterdam, Neth.) **30**, 756 (2008).
[2] V. Pačebutas et al., Characterization of low-temperature molecular-beam-epitaxy grown GaBiAs layers, Semicond. Sci. Technol. **22**, 819 (2007).
[3] K. Alberi et al., Valence band anticrossing in $GaBi_xAs_{1-x}$, Appl. Phys. Lett. **91**, 051909 (2007).
[4] S. Imhof et al., Clustering effects in Ga(AsBi), Appl. Phys. Lett. **96**, 131115 (2010).
[5] S. Francoeur et al., Bi isoelectronic impurities in GaAs, Phys. Rev. B **77**, 085209 (2008).
[6] S. Nargelas et al., Hole diffusivity in GaAsBi alloys measured by a picosecond transient grating technique, Appl. Phys. Lett. **98**, 082115 (2011).

SUBSTITUTION-INDUCED TUNING OF THE OPTICAL PROPERTIES OF PHENANTHROIMIDAZOLE DERIVATIVES

Steponas Raišys[1], Justina Jovaišaitė[1], Karolis Kazlauskas[1], Agnė Ivanauskaitė[2], Ramūnas Lygaitis[2], Juozas Gražulevičius[2] and Saulius Juršėnas[1].

[1]Institute of Applied Research, Vilnius University, Lithuania
[2]Faculty of Chemical Technology, Kaunas University of Technology, Lithuania
steponas.raisys@ff.stud.vu.lt

Phenanthroimidazole derivatives are recognized due to its unique sensing properties, which allow their application in ion sensing [1] or even cancer therapy [2]. Moreover, phenanthroimidazole compounds feature perfect thermal stability, highly efficient blue fluorescence and both electron- and hole-transporting properties, and therefore, are exploited in organic light emitting diodes (OLEDs) [3]. However, owing to their planar structure phenanthroimidazoles tend to crystalize in a solid state facilitating excimers formation and causing aggregation induced fluorescence quenching. For blue emitter application of the compounds prevention of the excimer formation and improvement of the fluorescence quantum yield in the solid state is required.

In this work, fluorescence properties of a series of phenanthroimidazole derivatives possessing various substituents were investigated. Absorption and fluorescence spectroscopy as well as fluorescence quantum efficiency and excited state lifetime measurements were employed to assess the optical properties of the phenanthroimidazole derivatives in diluted solution and condensed phase.

All the studied compounds exhibited deep-blue fluorescence in dilute dimethylformamide solution with high fluorescence quantum yield (up to 81%). Fluorescence quantum yield was found to be dependent on the size of the substituents: smaller substituents exhibited lower quantum yield (49-57%), while bulkier-branched substituents – higher quantum yield (64-81%). It was found that this increase in quantum yield is caused by accelerated radiative decay pathway while non-radiative decay rate remain almost unmodified. As expected in the solid state fluorescence quantum yield were found to be higher (up to 26%) for the derivatives possessing bulkier-branched substituents. Compounds substituted by small substituents in the neat films form excimers which are evident from the broad unstructured fluorescence spectra while bulkier-branched substituents inhibit close molecular packing and reduce fluorescence quenching mostly due to suppression of excitons migration to non-radiative decay sites.

The attachment of the bulkier-branched substituents to the phenanthroimidazole core retains high fluorescence quantum yield in the solid state which enables to use phenanthroimidazole derivatives as a multifunctional material. Multifunctional phenanthroimidazole derivatives are very attractive for the fabrication of triple, double or even single-layered OLEDs [4]. Simple device architecture can reduce the fabrication costs while retaining equally good electrical and optical properties as compared with multi-layered device, thus making it more commercially attractive.

[1] W. Lin, L. Long, L. Yuan et al., A novel ratiometric fluorescent Fe3+ sensor based on a phenanthroimidazole chromophore, Analytica Chimica Acta **634**, 262-266 (2009).
[2] K.-J. Castor, J. Mancini, J. Fakhoury et al., Platinum(II) Phenanthroimidazoles for Targeting Telomeric G-Quadruplexes, Chem. Med. Chem, **7**, 85–94 (2012).
[3] Z. Wang, P. Lu, S. Chen, et al., Phenanthro[9,10-d]imidazole as a new building block for blue light emitting materials, J. Mater. Chem **21**, 5451-5456, (2011).
[4] Y. Zhang, S.-L. Lai, Q.-X. Tong et al., High Efficiency Nondoped Deep-Blue Organic Light Emitting Devices Based on Imidazole-π-triphenylamine Derivatives,Chem. Mater. **24**, 61-70 (2012).

CARIER TRANSPORT IN C60 AND ZnPn SOLAR CELLS

A. Sakavičius

Department of Semiconductor Physics, Faculty of Physics and Institute of Applied Research, Vilnius University, Saulėtekio Ave. 9 – III, LT-10222 Vilnius, Lithuania
Andrius.Sakavicius@ff.stud.vu.lt

We analyzed the solar cells with active ZnPc and C60 layers forming a pn junction. The samples shown in Fig. 1 were produced at Institute of Applied Photophysics in Dresden, Germany. They were fabricated in a high vacuum (<5*10-6 Pa) by deposition of a films on a glass substrate coated with ITO (indium-tin oxide). The upper electrode is formed by deposition of a silver layer. A thin gold layer is used to protect organic layers from oxidation. p-ZnPc – doped by acceptors zinc-phthalocyanine layer.

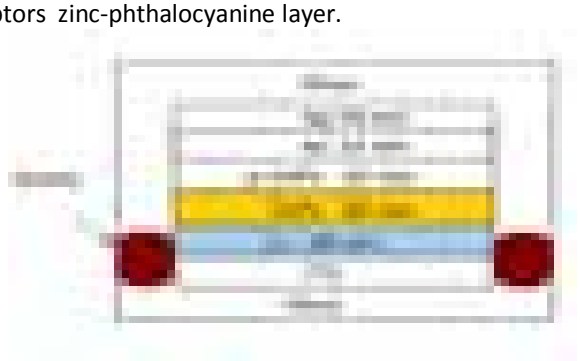

Fig. 1. Structure of the solar cell

Carrier mobility measurements were performed by the CELIV (Charge Extraction by Linearly Increasing Voltage) [1] method. The voltage which is proportional to the current flowing through the sample was measured on the load resistor by oscilloscope. Another channel of the oscilloscope was used to measure the output signal of the generator. Carrier mobility was calculated from current kinetics according to the following expression:

The Gaussian disorder model was used to evaluate the parameters of carrier mobility dependencies on applied electric field:

- Mechanisms and models have been analyzed in order to describe charge transfer in organic disordered materials.
- Properties of ZnPc: C60 structures have been measured at various temperatures, depending on the electric field.
- Experimental dependence was approximated by the Gaussian disorder model to evaluate spatial disorder parameters Σ and distribution parameter of energy σ.

[1] G. Juška, K. Arlauskas, and M. Viliūnas, Extraction Current Transients: New Method of Study of Charge Transport in Microcrystalline Silicon, Phys. Rev. Lett. 84, 4946–4949 (2000).

OPTICAL PROPERTIES OF CdZnO/ZnO MULTIPLE QUANTUM WELLS FOR LIGHT EMITTING DIODES APPLICATION

Marius Stasiūnas[1], Mindaugas Karaliūnas[2]

[1] Semiconductor Physics Department, Vilnius University, Saulėtekio Ave. 9-III, LT-10222 Vilnius, Lithuania
[2] Institute of Applied Physics, Vilnius University, Saulėtekio Ave. 9-III, LT-10222 Vilnius, Lithuania
marstas@gmail.com

Light-emitting diodes (LEDs) with the ZnO-based active region have attracted considerable attention due to the great structural and physical properties and relatively low production costs of ZnO, compared to GaN [1]. The band gap tunability from ultra-violet to yellow spectral range can be achieved. By alloying ZnO with Be or Mg the band gap is increasing, while by alloying it with Cd, the band gap is decreasing [2]. Band gap engineering is an important step for the development of multiple quantum wells (MQWs) structures, which improve LEDs performance by enhancing radiative recombination rate of excitons.

Optical properties of 6 LED samples were investigated in this experiment. In each sample, the Ga-doped ~30 nm thick n-ZnO cap layer and three periods of CdZnO/ZnO QWs (~5 nm thick CdZnO wells separated by ~20 nm thick ZnO barriers) were grown on a p-GaN (~1 μm), which was deposited on a u-GaN template of ~2 μm in thickness on c-plane sapphire substrate. The p-GaN and u-GaN layers were grown using metalorganic chemical vapour deposition (MOCVD), whereas MBE method was used for MQWs and the cap layer growth. Cd effusion cell and substrate temperatures were varied for different samples when growing well (barrier) layers. The samples were fabricated in the Institute of Photonics and Optoelectronics of National Taiwan University.

The temperature dependent photoluminescence (PL) spectra of the samples were measured using laser diode (λ_{exc} = 403 nm) as an excitation source, suitable for selective excitation of CdZnO MQWs. The laser spot diameter was estimated to be around 200 μm on the surface of the sample. PL signal was dispersed using a monochromator (*Jobin Yvon* HRD-1) with holographic diffraction gratings, having 1200 grooves/mm, and registered using a photomultiplier tube (*Hamamatsu* R1463P). Cooling of the samples was performed using a closed-circuit He cryostat, which allows temperature of the sample to be changed in the interval from 8 K to 300 K. Samples' temperature was stabilized with the help of a proportional-integral-derivative controller. During the measurement temperature fluctuations did not exceed 1% deviation.

PL spectra of CdZnO/ZnO MQWs was further investigated by analyzing the temperature dependencies of PL peak position, PL intensity and full width at half maximum (FWHM). Varshni (1) and Bose-Einstein (2) equations were used to fit the PL peak position dependencies on temperature, considering the investigated PL peak being mostly influenced by near-band-edge emission from CdZnO MQWs.

$$E_g(T) = E_g(0) - \frac{\alpha T^2}{T + \beta} \tag{1}$$

$$E_g(T) = E_g(0) - \frac{k}{\exp(\theta/T) - 1} \tag{2}$$

Two models were used to fit PL intensity (I) temperature dependencies. Better fitting results with lower errors were obtained using the equation (3) with the hopping term added [3], if compared with the one without it (4).

$$I(T) = \frac{I_0}{1 + A\exp(-E_a/k_B T + T/T_B)} \tag{3}$$

$$I(T) = \frac{I_0}{1 + A\exp(-E_a/k_B T)} \tag{4}$$

In case of FWHM (Γ) dependency on temperature, Hellman-O'Neill equation (5) was exploited. In this model, the greatest contribution to the behavior of FWHM on temperature is made by carrier interaction with phonons (both acoustic and optical).

$$\Gamma(T) = \Gamma_0 + \gamma_{ph} T + \frac{\Gamma_{LO}}{\exp(\hbar\omega_{LO}/k_B T) - 1} \tag{5}$$

Furthermore, values of internal quantum efficiency (IQE) at 300 K were calculated, after the condition that IQE at 8 K is equal to 100 %. IQE defined in this way can represent the optical quality of MQWs. Evaluated IQE values varied from 11 % to 36 % for different samples.

[1] C. Klingshirn. Fundamental properties of ZnO nanostructures. ChemPhysChem, 8, 782-803 (2007).
[2] Yong-Seok Choi, Jang-Won Kang, Dae-Kue Hwang, Seong-Ju Park. Recent Advances in ZnO-Based Light-Emitting Diodes. IEEE Transactions on Electron Devices, 27 (2010).
[3] Z. Yang, L. Li, Z. Zuo, J. L. Liu. Journal of Crystal Growth 312, 71 (2009).

DYNAMICS OF PHASE TRANSITION IN $0.4Na_{0.5}Bi_{0.5}TiO_3$-$(0.6-x)SrTiO_3$-$xPbTiO_3$ SOLID SOLUTIONS

Šarūnas Svirskas[1], Maksim Ivanov[1], Šarūnas Bagdzevičius[1], Jūras Banys[1], Marija Dunce[2], Maija Antonova[2], Eriks Birks[2], Andris Sternberg[2]

[1] Vilnius University, Faculty of physics, Saulėtekio av. 9, III b., LT-10222 Vilnius, Lithuania
[2] Institute of Solid State Physics, University of Latvia, Kengaraga street 8, LV-1063 Riga, Latvia
sarunas.svirskas@ff.stud.vu.lt

$Na_{1/2}Bi_{1/2}TiO_3$ (NBT) is one of the most studied ferroelectric system. Unique features and peculiarities of phase transitions attracted much attention by the scientists. NBT and its solid solutions were widely studied since it was synthesized in 1960. $SrTiO_3$ (ST) and $PbTiO_3$ (PT) were used as a secondary materials with NBT. It is well known that ST and PT act differently upon the NBT [1]. Strontium titanate enhances relaxor properties while lead titanate increases characteristics of 1st order phase transition.

Dielectric measurements were made for x = 0 - 0.25 in 35-500K temperature range and 0.01 Hz – 40 GHz frequency range on cooling with 1 K/min rate, except near phase transitions where it was lowered to 0.4 K/min. Silver paste was used for contacts. Investigations from 20 Hz to 1 MHz were made by measuring capacity and loss tangent with LCR meter HP-4284A. Measurements in 1 MHz – 3 GHz range were made with vector network analyzer Agilent 8714ET in a coaxial line terminated by a capacitor. In 8 - 40 GHz frequency range measurements have been performed by scalar network analyzers R2400 produced by "Elmika" company in a waveguide setup. Complex dielectric permittivity was calculated from absolute values of reflection and transmission coefficients.

Fig. 1 shows phase diagram of 0.4NBT-(0.6-x)ST-xPT system. Variation of x in the solid solution radically changes physical properties of these ceramics. This indicates that lead titanate plays important role in such solid solutions. Different radii of A-site ions change long range order. Increase of lead expands chemically ordered regions and from certain value of $PbTiO_3$ normal ferroelectric phase occurs which spontaneously transforms to relaxor ferroelectric phase when temperature increases.

The purpose of the report is to discuss dynamic dielectric properties of this system. Also distribution of relaxation times will be presented.

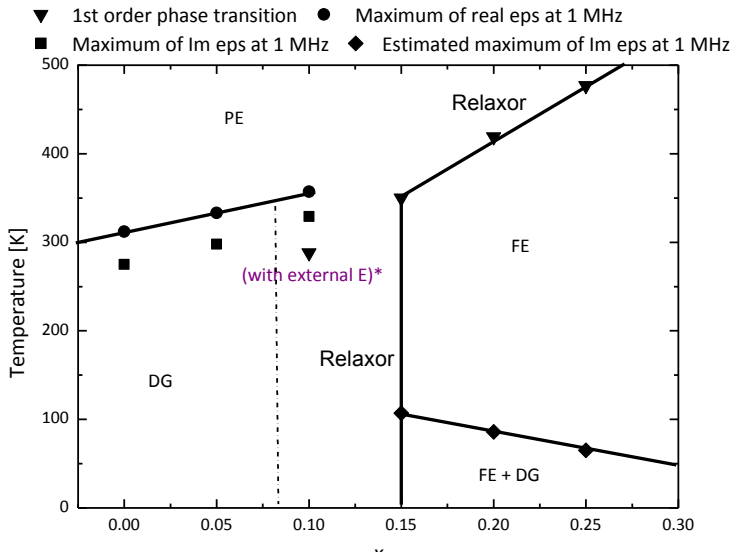

Fig. 1 Phase diagram of $0.4Na_{0.5}Bi_{0.5}TiO_3$-$(0.6-x)SrTiO_3$-$xPbTiO_3$. * indicates results taken from [2]

[1] Lee, J.-K.; Hong, K. S.; Kim, C. K.; Park, S.-E.; Phase transitions and dielectric properties in A-site ion substituted $(Na_{1/2}Bi_{1/2})TiO_3$ ceramics (A=Pb and Sr), *J. Appl. Phys.* 91 (7) (2002)
[2] Birks, E., Dunce, M., Antonova, M. and Sternberg, A., Phase transitions in modified $Na_{1/2}Bi_{1/2}TiO_3$-$SrTiO_3$ solid solutions, *Physica Status Solidi C*, 6 (12) (2009)

STUDY OF PHOTOLUMINESCENCE INHOMOGENEITY IN InGaN QUANTUM WELLS WITH CAPPING LAYERS OF DIFFERENT THICKNESS

Ieva Šimonytė[1]

[1] Semiconductor Physics Department, Vilnius University, Saulėtekio 9-III, LT-10222 Vilnius, Lithuania
ieva.simonyte@ff.stud.vu.lt

Group-III nitrides have attracted a considerable attention for their various use in optoelectronics. The ternary InGaN alloy is the primary compound in commercial production of blue and green light-emitting diodes (LEDs) and laser diodes. A white LED that is currently produced by combining a blue LED with yellow phosphor offers a replacement for conventional sources in general lighting. Though InGaN-based devices have been developed and used on a large scale, photoluminescence inhomogeneity in InGaN quantum wells is still not clearly understood.

Inhomogeneous indium distribution in active layers generates spatial band gap fluctuations. Carrier localization in indium rich areas is beneficial for higher emission intensity. However, InGaN with high indium content exhibits a low quantum efficiency. This is the reason why III-nitride compounds are still not used in production of long-wavelengths LEDs [1].

In this work, spatial inhomogeneity of photoluminescence in InGaN quantum wells with different capping layers were studied. Six samples under study were grown by a MOCVD method and contained identical active layers consisting of five InGaN quantum wells. After growing the quantum wells, a 20 nm thick capping layer of *n*-type AlGaN was deposited on five samples. An additional capping layer of *n*-type GaN layers of 30, 60, 120, and 180 nm in thickness were deposited on four samples. Photoluminescence was studied with spatial and spectral resolution using confocal microscope coupled with a spectrometer. CW emission of He-Cd laser was used for excitation. In each sample, two randomly selected 30 x 30 μm^2 areas have been scanned. Obtained PL intensity and peak wavelengths mappings were used in the further analysis of PL parameters.

Correlations between PL intensity, peak position, and full width at half maximum (FWHM) were calculated for each sample. Small correlation between peak intensity and FWHM was observed in the samples, where the averaged PL intensity is higher. The correlation is the stronger the higher is the averaged PL intensity. Correlation between PL intensity and FWHM is stronger. Strong anticorrelation was observed in the samples with the highest intensity. The anticorrelation becomes smaller in the samples, where the intensity is smaller. The anticorrelation shows that the PL band in bright areas have a larger band width.

The values of Spearman‘s and Pearson‘s correlation coefficients are small and do not reveal any statistically reliable correlation between the peak position and PL intensity in samples with 60, 120, and 180 nm thick GaN capping layers. Small correlation was observed in samples with 30 nm thick GaN layer, without the GaN layer, and with no capping layer at all. In samples where correlation was small, integrated PL spectra from bright areas was slightly (~3 nm) redshifted in respect of the integrated PL spectra from dark areas.

The analysis of the averaged spatially integrated PL intensity from each sample revealed that the integrated PL intensity is a nonmonotonous function of GaN capping layer thickness. The highest PL intensity was observed in the sample with the GaN capping layer of ~100 nm in thickness.

[1] K. Okamoto, A. Kaneta, Y. Kawakami, S. Fujita, J. Choi, M. Terazima, T. Mukai, Confocal microphotoluminescence of InGaN-based light-emitting diodes. Journal of Applied Physics 98**,** 064503 (2005)

STRUCTURAL AND OPTICAL PROPERTIES OF MgZnO EPITAXIAL LAYERS

Vilmantas Šukauskas, Mindaugas Karaliūnas

Semiconductor Physics Department, Vilnius University, Lithuania
vil.sukauskas@gmail.com

Recently, wide band-gap semiconductor ZnO attracts a lot of attention because of its potency to be used for the production of cheap and efficient optoelectronic devices. The incorporation of MgO into ZnO gives a possibility for band-gap engineering in range from 3.4 eV (band-gap of ZnO) to 7.8 eV (band-gap of MgO). For the meantime, the growth of MgZnO layers is difficult because of low thermodynamic solubility of MgO in ZnO. However, recent works show a high improvement in growing techniques for MgZnO layers. Despite the difficulties to grow good quality layer it was reported that MgZnO shows better photoluminescence (PL) efficiency compared to pure ZnO [1] and it was explained [1,2,3] by assuming that the exciton localization processes take a place in MgZnO because of inhomogeneous spatial distribution of Mg concentration. Finally, according to the recent research, MgZnO shows high potential to become extensively used material for production of the optoelectronic devices where wide band-gap semiconductor is required.

In this work, a series of $Mg_xZn_{1-x}O$ epitaxial layers with different Mg mole fraction (x = 0.025; 0.166; 0.303; 0.318) grown by MBE has been investigated. Time-resolved photoluminescence (TRPL) measurements and scanning near field optical microscopy (SNOM) technique have been implemented in order to obtain PL spectra and decays as well as spatial distribution of the PL intensity and peak wavelength. Atomic force microscopy (AFM) technique has been chosen to evaluate structural properties. Images of epitaxial layer surface profile (fig. 1), obtained by AFM technique, have revealed distinct characteristics for all samples and a strong surface roughness dependence on Mg concentration.

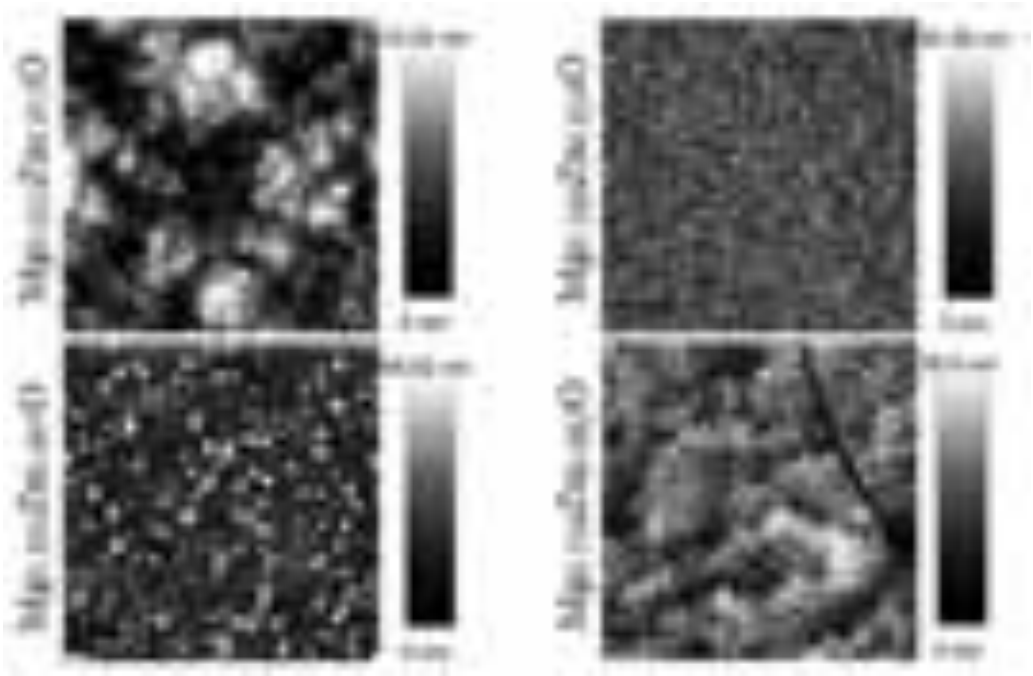

Fig. 1. AFM topographies of $Mg_xZn_{1-x}O$ layers.

Time-resolved PL decays have revealed a biexponential shape for all four samples at low temperatures. Three samples with the highest Mg mole fraction show an increase of the PL decay time at low temperature. Arrhenius plots for the PL intensity dependence on temperature have been drawn and parameters have been extracted. Samples with higher Mg mole fraction show higher value of activation energy. The PL mappings, obtained by SNOM technique, have revealed considerable spatial variation of PL intensity, peak wavelength and FWHM. However, the correlation between PL intensity and peak wavelength are negative and it contradicts to the usual exciton localization model providing positive correlation between those parameters. The possible reasons of this phenomenon are discussed.

[1] H. Shibata, H. Tampo, K. Matsubara, A. Yamada, K. Sakurai, S. Ishizuka, S. Niki, and M. Sakai, Appl. Phys. Lett. 90, 124104 (2007).
[2] Z. L. Liu, Z. X. Mei, R. Wang, J. M. Zhao, H. L. Liang, Y. Guo, A. Yu Kuznetsov, and X. L. Du, J. Phys. D: Appl. Phys. 43 (2010) 285402.
[3] H. Zhu, C. X. Shan, B. H. Li, Z. Z. Zhang, J. Y. Zhang, B. Yao, D. Z. Shen, and X. W. Fan, J. Appl. Phys. 105, 103508 (2009).

BARRIER CAPACITANCE CHARGING CURRENT TRANSIENTS DEPENDENT ON BIAS ILLUMINATION IN Si pin DIODE STRUCTURES

Adomas Tumas, Tomas Čeponis, Eugenijus Gaubas

Institute of Applied Research, Vilnius University, Sauletekio Ave. 9-III, LT-10222 Vilnius, Lithuania
adomas.tumas@ff.stud.vu.lt

Barrier capacitance charging current transients provide comprehensive information on junction doping, carrier generation current and fast traps inside diode base region [1]. The barrier evaluation by linearly increasing voltage (BELIV) technique [2-4] proved to be an efficient tool to examine switching rate, carrier emission time scale and to evaluate barrier capacitance. In this work, the BELIV technique was applied to examine the fluence dependent variations of barrier capacitance charging currents in reactor neutrons and accelerated protons irradiated pin diodes. To highlight the impact of radiation defects, the BELIV technique is combined with bias illuminations.

A set of Si pin diodes of CERN standard particle detectors and of industrial power switchers has been investigated. The doping density of base region was 10^{12} cm^{-3} in particle detectors and 7×10^{14} cm^{-3} in power switchers, respectively.

Room temperature BELIV transients were examined varying linearly increasing voltage (LIV) pulse durations and amplitudes. Simultaneously, intensity of broad spectrum bias steady-state illumination was varied.

BELIV transients showed a decrease of barrier capacitance with enhancement of irradiation fluence. This reduction of barrier capacitance is explained by a reduction of effective doping due to radiation induced carrier traps. Bias illumination appeared to be efficient to suppress traps and to recover partially barrier capacitance. The rise to peak times as a function of bias illumination intensity also was analyzed. These characteristics enabled us to evaluate changes of the serial resistance within diode base region under radiation damage and traps charging.

The parameters of carrier generation lifetime and of effective doping have been extracted. Variations of these parameters dependent on irradiation fluence and on defect distribution profile will be presented and discussed.

[1] E. Gaubas, T. Ceponis, and J. Kusakovskij, REVIEW OF SCIENTIFIC INSTRUMENTS **82** (2011) 083304
[2] E.Gaubas, T.Čeponis, S.Sakalauskas**,** A.Uleckas, and A. Velička, **LJP** (Lithuanian Journal Physics), **51** (2011) 227–233.
[3] E. Gaubas, T. Ceponis, A. Uleckas and R. Grigonis. **JINST** (Journal of INSTrumentation), **7** (2012) P01003.
[4] E.Gaubas, T.Čeponis, V.Kalendra, J.Kusakovskij, and A.Uleckas, ISRN Materials Science, vol. 2012, article ID543790, 17 pages doi:10.5402/2011/543790

DLTS SPECTROSCDOPY ON Si SOLAR CELLS

Vaidvilė Ulbikaitė, Eugenijus Gaubas, Aurimas Uleckas

Institute of Applied Research, Vilnius University, Saulėtekio av. 9-III, LT-10222 Vilnius, Lithuania
vaidvile.ulbikaite@ff.stud.vu.lt

To optimize the conversion efficiency of photovoltaic cells within design and manufacturing of junction structures, spectrum and density of deep traps, introduced during technological procedures of Si material growth and junction formation, are very important characteristics. One of the ways to reach the highest conversion efficiency of solar cells is to minimize or suppress the recombination processes in the *p-n* junction of solar cell [1]. Commonly these traps are examined and identified using deep level transient spectroscopy technique [2].

In this work, Deep Level Transient Spectroscopy (DLTS) has been employed to identify specific defects and to evaluate density of these deep centres within base region of Si solar cells fabricated at enterprise „PRECIZIKA MTC“. Two peaks have been clearly resolved within deep level spectra measured on two sets of samples, made by slightly different technology. It has been revealed that metal Cu and Ni ascribed traps dominate within these deep level spectra. Density of Ni ascribed traps observed at 260 K within temperature scan DLTS spectra was found to be of the order of magnitude 10^{14} cm^{-3}. In different set of the investigated junction Si solar cell structures, density of Cu associated traps (observed at 150 K within temperature scan DLTS spectra) was evaluated to be (1-3)× 10^{14} cm^{-3}, i.e. of the same order as Ni impurities. Introduction of metal traps is associated with imperfection of metallization technological processes.

[1] A.Luque and S.Hedegus, Handbook of photovoltaic science and engineering. John Wiley & Sons, England, 2003.
[2] P.Blood and J.W. Orton, The Electrical Characterization of Semiconductors: Majority Carriers and Electron States (Academic Press Inc., San Diego, 1992).

ELECTRO-OPTICAL CHARACTERIZATION OF SEMICONDUCTOR NANOWIRE DEVICES

Neimantas Vainorius[1], Simon Zihlmann[2]

[1] Institute of Applied Research, Vilnius University, Lithuania
[2] Department of Physics, University of Basel, Switzerland
neimantasv@gmail.com

III-V semiconductor compounds offer a large amount of advantages, especially in optical applications. Many of them are direct band gap materials, and therefore emission and absorption of photons are favored compared to indirect bang gap semiconductors. Properties like band gap or carrier mobility can easily be changed by varying the proportions of the materials used in binary, ternary or quaternary compounds. This makes it possible to develop complex heterostructure solar cells, light emitting diodes and other useful devices.

Some combinations of III-V materials cannot be grown in planar structures, as the lattice constants differ too much and defect would be formed at the interface. Due to this properties of the fabricated device are degraded. Growing the structures in a nanowire form avoids this problem in releasing strain by radial relaxation. This results in defect free semiconductor heterostructures and even better, allows growing them on top of silicon with intention of easy integration with already existing silicon technology.

Indium phosphide (InP) nanowires were one of the investigated objects. Usually, undoped InP nanowires show an equal share of zincblende (ZB) and wurtzite (WZ) crystal structure [1]. The amount of WZ can be increased by *n*-doping with sulfur during the growth process. As the WZ crystal structure of InP does not exist in bulk material, it is not fully investigated, but some interesting properties are already known, for example, the existence of a second conduction band 0.24 eV above the first one [2]. The mixture of ZB and WZ InP forms a type 2 alignment. Figure 1 indicates the spatial separation between the electrons and holes in it. The ZB segments act as traps for electrons and therefore the conductivity is determined by the longest ZB segment [3].

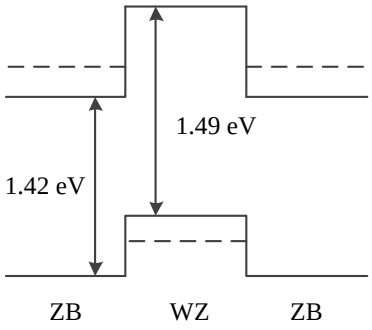

Fig.1. Type 2 alignment of ZB and WZ InP.

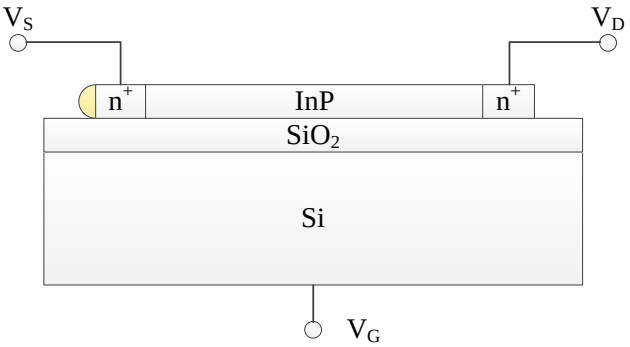

Fig. 2. InP nanowire sample schematic drawing.

We used a Fourier transform spectrometer to investigate single InP nanowires with different doping levels (fig. 2). Spectral photocurrent measurements did not show a blue shift for highly n-doped nanowires which would correspond to state filling in the conduction band. Furthermore, electro-optical properties of GaSb/InAsSb/InAs nanowire based infrared photodetectors were investigated.

Acknowledgements: This work was performed in the Nanometer Structure Consortium ant the University of Lund. The sample preparation and help from Dan Hessman, Johannes Svensson, Mats-Erik Pistol and Jesper Wallentin is greatly acknowledged.

[1] Jansu J.-M, et. Al. Type II Heterostructure Formed by Zinc-blende Inclusions in InP and GaAs Wurtzite Nanowires. *Applied Physics Letters*, 97, (2010).
[2] Wallentin J., et al. Probing the Wurtzite Conduction Band Structure Using State Filing in Highly Doped InP Nanowires. *Nano Letters*, 11, 2286-2290 (2011).
[3] Wallentin J., et al. Electron Trapping in InP Nanowire FETs with Stacking Faults. *Nano Letters*, Article ASAP, (2011).

SPATIAL DISTRIBUTION OF LUMINESCENCE IN InGaN EPITAXIAL LAYERS WITH DIFFERENT INDIUM CONTENT

Augustas Vaitkevičius

Semiconductor Physics Department, Vilnius University, Saulėtekio Ave. 9-III, LT-10222 Vilnius, Lithuania.
Augustas.Vaitkevicius@ff.stud.vu.lt

Indium gallium nitride (InGaN) is already commercially used in white and blue light emitting diodes (LEDs), has prospectives for use in electronics and photovoltaics. However, carrier dynamics in InGaN epilayers and heterostructures is still under intense study. One of the key issues under study is spatial inhomogeneity of InGaN compounds. Here, we report on spatial distribution of photoluminescence in InGaN epilayers.

Two sets of InGaN epitaxial layers on sapphire substrate with a GaN buffer layer were analyzed. The samples in the first set were grown under different temperatures, while the growth time vas a variable parameter in the second set of samples.. Both sets of samples were grown by metalorganic chemical vapour deposition at the German based company AIXTRON SE and sent to Vilnius University for characterization. Photoluminescence spatial distribution was measured using confocal technique with 200nm spatial resolution. WITec alpha300 system coupled with a spectrometer was used. Laser diode ALPHALAS emitting at 405nm was exploited for excitation. Photoluminescence measurements were compared to the results on surface morphology obtained using the WITec alpha300 system in atomic force microscopy mode.

In the samples grown at different temperatures, photoluminescence intensity increased with growth temperature up to the highest temperatures used. The highest grow temperatures correspond to the lowest indium content (17 %). Spatially averaged spectra shifted to the blue side as the growth temperature increased and In amount decreased, as expected due to a broader band gap of InGaN as the indium content decreases. At higher growth temperatures, photoluminescence was more homogenous leading to a smaller full width at half maximum (FWHM) of the spatially averaged spectra. Correlation between integrated intensity and band peak wavelength changed from anticorrelation to zero correlation as sample growth temperature was increased. Atomic force microscope (AFM) scans revealed that as the temperature growth results in decreasing roughness of the sample surface, indicating a smaller defect density.

The photoluminescence spectrum in the samples grown for different durations consists of two overlapping bands, likely caused by inhomogeneous distribution of In. In the sample with the lowest indium amount the two lines were clearly distinct. Correlation between integrated photoluminescence intensity and peak photoluminescence wavelength changed from positive to negative to near zero as growth time was increased. No difference in photoluminescence homogeneity between samples grown for different durations was observed. Comparison of photoluminescence study and AFM scans revealed that sample roughness and photoluminescence intensity correlate.

DESIGN AND INSTALLATION OF THE DOSIMETER VUTEG-5-AIDA AND CALIBRATION OF FLUENCE DEPENDENT VARIATION OF DEFECTS DENSITY

Arūnas Velička, Aurimas Uleckas, Tomas Čeponis, and Eugenijus Gaubas

Institute of Applied Research, Vilnius University, Sauletekio Ave. 9-III, LT-10222 Vilnius, Lithuania
Arunas.Velicka@ff.stud.vu.lt

Operation of CERN Large Hadron Collider (LHC) results in production of the background radiation due to high energy proton or ion interaction with surrounding matter (magnets, collimators, pipes, etc). These events produce secondary particles that may be energetic enough to cause further interactions in form of particle showers. Such radiative environment is dangerous for the LHC machine controlling electronic devices that undergo two categories of damage effects: gradual and Single Event Effects (SEE) [1, 2]. Gradual effects in electronics are caused by creating or activating individual microscopic defects by deposition of Total Ionizing Dose (TID) and Non-ionizing Energy Loss (NIEL) induced displacement damage. Each individual defect does not significantly change characteristics of the device, nevertheless, accumulation of these defects leads to device degradation. SEEs are caused by single energetic particles by direct ionization or induction of nuclear reaction. The consequence of these may be corruption of data (eg. Single Event Latch-Up - SEL) or permanent damage of the device (eg. Single Event Upset - SEU). Furthermore, radiation is extremely dangerous for working personnel. Therefore, measurements of radiation levels are necessary for performing correct and human-safe experiments in the LHC machine.

The radiation detectors must fulfil challenging conditions that include prolonged operation time (10 years), different operating temperatures and variable intensity of particles with diverse range of energies [3]. These conditions are met by RadFET (Radiation-sensitive Field Effect Transistor) transistors and p-i-n diodes that are currently used as detectors in radiation dosimeters in the LHC machine [4].

The aim of this work is to propose non-invasive microwave-probed photoconductivity (MW-PCD) transient technique based VUTEG-5-AIDA dosimeter as an alternative approach for radiation measurements. The development of such dosimeter is a part of CERN FP7 AIDA project.

In this research analysis of excess carrier lifetime, dependent on fluence of reactor neutrons, accelerated protons and on dose of gamma rays, has been performed on MCZ Si n- and p-type material wafers and n-Si base p-i-n diodes. Calibrational measurement of fluence dependent excess carrier lifetime variations were carried out on different material and device structures by comparing non-capsulated and polyethylene bag capsulated samples.

[1] G. G. Daquino, G. Corti, G. Folger, Background Radiation Studies at LHCb Using Geant4, IEEE Transactions on Nuclear Science, vol. 53, no. 5 (2006).

[2] F. Faccio, COTS for the LHC radiation environment: the rules of the game, Proc. 6th Workshop on Electronics for LHC Experiments, 2000, ISBN92-9083-17203, p.p. 50-65.

[3] F. Ravotti, M. Glaser, M. Moll, *Sensor catalogue* (2005).

[4] F. Ravotti, M. Glaser, A. B. Rosenfeld et al., Radiation Monitoring in Mixed Environments at CERN: From the IRRAD6 Facility to the LHC Experiments, IEEE Transactions on Nuclear Science, vol. 54, no. 4 (2007).

PROFILING OF SPREADING RESISTANCE AND BARRIER CAPACITANCE PARAMETERS WITHIN LAYERED THYRISTOR AND PIN DIODE STRUCTURES

Martynas Velička, Tomas Čeponis, Eugenijus Gaubas

Institute of Applied Reasearch, Vilnius University, Saulėtekio Ave. 9-III, LT-10222 Vilnius, Lithuania
velicka.m@gmail.com

The operational characteristics of semiconductor power devices strongly depend on junction, formed by technological procedures, profiles and depths. Junctions are commonly formed by thermal diffusion procedures when dopant atoms are introduced. However, together with the dopants, undesirable impurities can be introduced as well, which affect the device functional parameters. On the other hand, certain impurity atoms (gold, platinum) can be intentionally introduced or ions can be expediently implanted to create the enhanced recombination layers of various profiles within power device structures and to handle the switching rates of power devices. Thus, these modifications of material should be precisely controlled to predict the operational characteristics of devices.

Various techniques are employed in profiling of the chemical structure of materials, such as scanning spreading resistance microscopy (SSRM), scanning capacitance microscopy (SCM) [1]. However, these techniques do not provide information about undesirable impurities or defects introduced during implantation.

In this work a technique for barrier evaluation by linearly increasing voltage (BELIV) is presented based on measurements of current transients at reverse and forward pulsed bias [2]. This barrier control technique is combined with a step-positioning of the needle-tip probe, located on the cross-sectional boundary of a parallel-plate layered structure [3]. The spreading current pulsed measurements are performed by scanning a boundary of the structure using the needle-tip electrode. The other contact is connected to the parallel plate electrode at sample surface. When a needle probe is positioned at the same layer as the plate electrode, the measured transient then repeats the linearly increasing voltage pulse shape and its amplitude depends on the layer resistance. The barrier charging and charge extraction currents are measured when the probe is positioned at the other layer of the junction. Spreading resistance, barrier capacitance and parameters of deep traps can be evaluated when analyzing the shape, the amplitude and duration of measured current transient. Profiles of the current amplitudes and transients duration, which correspond to the profile of dopants density, measured in pin diode structure are presented in Fig. 1.

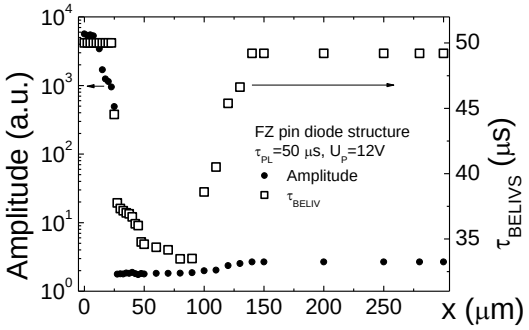

Fig. 1. Profiles of the current amplitudes and transient durations measured in pin diode structures by BELIV technique.

Variations of barrier capacitance and spreading resistance parameters measured in power pin diode and thyristor structures by employing the BELIV technique will be discussed in this presentation.

[1] D.K.Schroder, Semiconductor material and device characterization 3rd Ed. (John Wiley and Sons, New Jersey 2006).

[2] E. Gaubas, T. Čeponis, J. Kusakovskij, and A. Uleckas. Barrier evaluation by linearly increasing voltage technique applied to Si solar cells and irradiated pin diodes. ISRN Materials Science **2012**, Article ID 543790 (2012).

[3] E. Gaubas, T. Čeponis, and J. Kusakovskij. Profiling of barrier capacitance and spreading resistance by transient linearly increasing voltage technique. Review of scientific instruments **82**, 083304 (2011).

INVESTIGATION OF PHOSPHORS FOR FAR-RED CONVERSION LIGHT-EMITTING DIODES

Akvilė Zabiliūtė[1], Skirmantė Butkutė[2]

[1]Semiconductor Physics Department and Institute of Applied Research, Vilnius University, Saulėtekio al. 9, LT-10222 Vilnius, Lithuania
[2]Department of General and Inorganic Chemistry, Vilnius University, Naugarduko g. 24 LT-03225 Vilnius, Lithuania
akvile.zabiliute@ff.stud.vu.lt

Due to the limited amount of fossil fuels and an increasing interest in sustainable energy light emitting diodes (LEDs) are getting more popular in lighting applications [1]. In order to design a white light LED two different methods are used. One is to combine red, green and blue LEDs and other is to use a phosphor converted LED (pcLED) [2]. The latter method requires a blue or a UV LED which is covered by a thin layer of phosphorous material. A phosphor is excited by blue light and emits yellow light, this process is called photoluminescence [1]. The excess of blue light penetrates the phosphor and mixes with yellow thus creating white light [2]. In case of a UV LED it is covered by two different phosphor materials that convert UV light to blue and yellow. Different phosphors enable to design LEDs in a broad range of wavelengths thus they can be used for various applications. One of them is to use LEDs in greenhouses for illumination of plants. It is known that in order to grow and develop plants need three ranges of wavelengths - 400-500, 620-680 and 700-760 nm. These wavelengths are responsible for the processes of photomorphogenesis, phototrophy and photosynthesis [2]. While LEDs with quite good characteristics in ranges around 460 and 600 nm were designed, there is still no good LED in a far-red region which is important for the process of photomorphogenesis. The GaAs LED that emits around 730 nm is made of toxic materials and is very sensitive for temperature differences and humidity thus it is not applicable for greenhouses [3].

The aim of this reasearch was to design a pcLED based on a blue 445 nm GaN LED and a $Gd_3Ga_5O_{12}$:Cr phosphor and which could satisfy the photomorphogenetic needs of plants in greenhouses. During the experiment phosphors with different dopant concentrations converting blue light to far-red light were sintered in the faculty of Chemistry of Vilnius University by a sol-gel method. Their optical properties such like excitation, luminescence and quantum efficiency were measured in the faculty of Physics of Vilnius University. The most efficient material was found to be $Gd_3Ga_5O_{12}$:Cr 5 mol%. It was used to design a pcLED which emits light in the ranges of 400-500 and 700-760 nm that satisfy the photomorphogenetic needs of plants. The spectrum of a designed pcLED is given in the figure bellow.

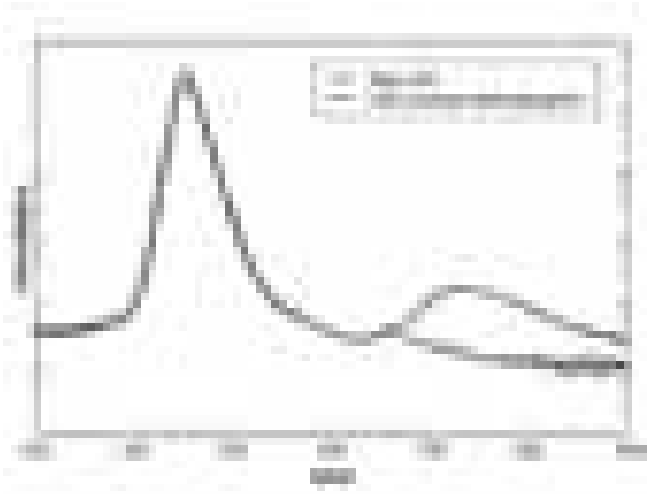

1 Fig.. The comparison of a blue 445 nm LED with the same LED covered by a thin layer of $Gd_3Ga_5O_{12}$:Cr phosphor and silicone mix.

[1] S. Ye, F. Xiao, Y.X. Pan, Y.Y. Ma, Q.Y. Zhang, "Phosphors in phosphor-converted white light-emitting diodes: Recent advances in materials, techniques and properties", *Mat. Science and Engineering*, **71**, 1-34 (2010).
[2] A. Žukauskas, "Puslaidininkiniai šviestukai", Vilniaus universitetas, Vilnius, (2008).
[3] A. Žukauskas, P. Duchovskis, UAB "Hortiled", "Konversijos fosfore šviesos diodas, skirtas augalų fotomorfogeneziniams poreikiams tenkinti", LT patentas A 2008 084, (2008).

POSTER SESSION II

Tidal tail structure of star clusters in dwarf galaxies

Karolis Manfreds Lyvens[1,2], Algimantas Kostas Sabulis[1,2], Donatas Narbutis[1,2], Jorge Peñarrubia[3], Tadas Mineikis[1,2], Philippe de Meulenaer[1,2], Justas Tamašauskas[2]

[1] Center for Physical Sciences and Technology, Lithuania
[2] Vilnius University, Lithuania
[3] Instituto de Astrofisica de Andalucia, Spain
karolis.lyvens@ff.stud.vu.lt

Tidal tails are thin, elongated and transient stellar structures, resulting from interaction of star cluster with its host galaxy. They tell us about dynamical history of their progenitor cluster – we can reconstruct its past orbit from alignment and shape of the tails [1]. Substructures, like density variations in the tidal tail, that can be observed while the cluster is losing stars, can be linked to the galactic potential along its orbit.

To understand how stellar populations in dwarf galaxies were built up, it is important to know how clusters are disrupted depending on initial conditions (like mass and orbit) and how long the resulting tidal structures last. We explore evolution of tidal tail structures as a function of cluster's density ($10^{-2} \div 1$ $M_\odot/pc^3$), mass ($10^3 \div 10^5$ $M_\odot$), and orbital parameters.

For N-body simulations we employ Superbox mesh code [2]. Star cluster models are placed on various orbits in spherically symmetrical dark matter halo potential [3], by assuming that dwarf galaxy is dominated by dark matter. We generate [4] star distribution in the cluster according to the Plummer model [5]. We analyse evolution of tidal tail structures in 6D (position and velocity) parameter space. The main limitation is that we perform simulations using a spherical dark matter halo, while realistic potential is more complex and should be replaced by triaxial halo potential in future simulations.

---

[1] Küpper, A. H. W., Lane, R. R., & Heggie, D. C. 2012, MNRAS, 2272
[2] Fellhauer, M., Kroupa, P., Baumgardt, H., et al. 2000, AN, 5, 305
[3] Navarro, J. F., Frenk, C. S., & White, S. D. M. 1997, ApJ, 490, 493
[4] Aarseth, S. J., Henon, M., & Wielen, R. 1974, A&A, 37, 183
[5] Plummer, H. C. 1911, MNRAS, 71, 460

Disruption of star clusters in dwarf galaxies

Algimantas Kostas Sabulis[1,2], Karolis Manfreds Lyvens[1,2], Donatas Narbutis[1,2], Jorge Peñarrubia[3], Tadas Mineikis[1,2], Philippe de Meulenaer[1,2], Justas Tamašauskas[2]

[1] Center for Physical Sciences and Technology, Lithuania
[2] Vilnius University, Lithuania
[3] Instituto de Astrofisica de Andalucia, Spain
algimantas.sabulis@ff.stud.vu.lt

Dynamical evolution of star clusters is a slow process compared to human timescale, therefore we are forced to employ gravitational *N*-body simulations to explore the pathways of buildup of stellar structures in galaxies. Dwarf galaxies are especially interesting for such studies. They have low stellar mass, enabling to setup a population of star clusters and trace its disruption in dark matter halo – a gravitationally dominating component of the system. Such simulations allow us to explore how the lifetimes of star clusters depend on their initial parameters (e.g. mass and density) in a given galactic potential.

For this study, we employ *N*-body mesh code Superbox [1] and randomly place star cluster models of Plummer profile [2] in a spherically symmetrical dark matter halo [3]. We analyze the disruption of star clusters as a function of their mass ($10^3 \div 10^5$ $M_\odot$), density ($10^{-2} \div 1$ $M_\odot/pc^3$), and orbit parameters by tracing a movement of gravitationally bound stellar core. Model contains two limitations: 1) close interactions between stars are not accounted for, and 2) all stars have the same mass. However, Superbox allows fast simulations, therefore a large population of clusters can be explored in various orbits.

We find that for a fixed initial mass, a disruption of dense star clusters is slower than disruption of the lower density ones, which do not survive to be observed in present day galaxies. In the future we will simulate star clusters in a more realistic triaxial dark matter halo of dwarf galaxy.

---

[1] Fellhauer, M., Kroupa, P., Baumgardt, H., et al. 2000, AN, 5, 305
[2] Aarseth, S. J., Henon, M., & Wielen, R. 1974, A&A, 37, 183
[3] Navarro, J. F., Frenk, C. S., & White, S. D. M. 1997, ApJ, 490, 493

Evolution of mass-segregated and non-segregated star clusters

Justas Tamašauskas[1], Donatas Narbutis[1,2], Mark Gieles[3], Algimantas Kostas Sabulis[1,2], Karolis Manfreds Lyvens[1,2], Tadas Mineikis[1,2], Philippe de Meulenaer[1,2]

[1] Vilnius University, Lithuania
[2] Center for Physical Sciences and Technology, Lithuania
[3] Institute of Astronomy, University of Cambridge, UK
justas.tamasauskas@ff.stud.vu.lt

Structure of star cluster – distribution of positions and velocities of its stars – depends primarily on properties of progenitor molecular cloud and various processes that are affecting it during evolution. They can be divided into internal, e.g., random close interactions of stars and their ejection from cluster, and external, e.g., tidal forces of the host galaxy, which depend on cluster's orbital motion.

One of unsolved problems in star formation is initial conditions: do star clusters form mass-segregated – massive stars are initially located in the center of cluster, or non-segregated – massive stars are initially at random positions in the cluster and gradually migrate to its center? We investigate if these differences lead to distinct scenarios of dynamical evolution and can they be distinguished observationally.

We perform *N*-body simulations, using direct integration NBODY6 code [1], of star clusters with a standard stellar initial mass function [2], simulating objects having 8000, 16000, and 32000 stars and being initially: 1) mass-segregated [3], and 2) non-segregated. Plummer's model [4] was used to setup initial positions and velocities of stars. Several runs of each model were performed without external potential, allowing only for cluster's self-gravity to drive its evolution in isolation. We analyze change of cluster's radius and mean mass of stars in spherical shells and find that on a short timescale the dynamical evolution of mass-segregated and non-segregated clusters becomes similar.

---

[1] Sverre J. Aarseth, Gravitational N-body Simulations, 2003, Cambridge University Press
[2] P. Kroupa 2001, MNRAS, 322, 231
[3] H. Baumgardt, G. D. Marchi, P. Kroupa 2004, The Astrophysical Journal, 685, 247
[4] S. J. Aarseth, M. Henon, R. Wielen 1974, Astronomy and Astrophysics, 37, 183

AN IMPACT OF DIFFERENT SAMPLE PREPARATION METHODS FOR FLUORESCENCE SPECTRA OF SALINE USED IN SALINE INFUSION HYDROSONOGRAPHY OF UTERUS

Vilmantas Gėgžna [1,2], Aurelija Vaitkuvienė[2], Povilas Sladkevičius[3]

[1] Faculty of Natural Sciences, Vilnius University, Vilnius, Lithuania
[2] Institute of Applied Research, Vilnius University, Vilnius, Lithuania
[3] Department of Obstetrics and Gynaecology, Skanes University Hospital, Lund University, Malmo, Sweden
Vilmantas.Gegzna@gf.stud.vu.lt

Fluorescence spectroscopy methods have never been used to diagnose uterine pathologies.

The purpose of this work is to estimate an impact of several sample preparation methods to fluorescence spectra of the saline that was used for saline infusion hydrosonography of uterus endometrium in proliferative and secretory phases.

As a conventional procedure, saline was injected to uterine cavity during assessment of endometrium by transvaginal ultrasound examination. After examination the saline was collected back to syringe. Microlaser STA-01-TH (355nm) was used to excite fluorescence. Spectra of liquid saline, saline dried in room temperature as well as saline dried using air flow were registered. 3 spectra per sample were registered. Spectra were normalized using the peak between 485-515nm. The examples of spectra are illustrated in fig.1. Different regions of spectra were extracted using spectra filtration method [1] and statistically compared using receiver operating characteristic (ROC) method. The groups (proliferative and secretory phases) were determined by anamnesis and the results of ultrasound examinations.

The results of statistical evaluation will be presented.

Fig. 1. The examples of normalized fluorescence spectra.

[1] V. Gegzna, D. Varanius, A. Vaitkuviene, R. Kurtinaitiene, J Vaitkus. Method of cervical smears material autoflorescence spectra filtration for cervical pre-cancer diagnostics, 54th scientific conference for young students of physics and natural sciences Open Readings 2011, ISSN 2029-4425, Vilnius University, 117-118 (2011).

PLATELET-TUMOUR CELL HETEROAGGREGATES FORMATION IN PRESENCE OF ASCORBIC ACID

Elena Golubeva, Anna Mukhortova, Ekaterina Shamova

Department of Physics, Belarusian State University, Republic of Belarus
golubeva.ln.87@gmail.com

Enhancement of reactive oxygen species (ROS) production plays a crucial role in disease development. Excessive intracellular ROS levels are observed in different pathological conditions, including inflammation, atherosclerosis and cancer. Cancer cells have been shown to possess an ability to produce more ROS when compared to normal cells [1]. Excessive ROS production may promote cancer cell survival and proliferation, thus contributing to cancer development. Moreover high levels of ROS may potentiate metastatic processes mediating cell invasiveness and cell migration. Platelets may contribute to propagation of cancer cells. During cancer metastasis, formation of platelet-tumor cell heteroaggregates, facilitating immune evasion and microvascular arrest of cancer cells at distant sites, is observed [2]. Therefore development of new therapeutic strategies aimed at prevention of platelet-tumor cell heteroaggregates formation and targeted to persistent pro-oxidative state characterizing cancer cells is considered to be of significance.

In the present study processes of platelet and breast adenocarcinoma cells MCF-7 heteroaggregates formation in presence of ascorbic acid was investigated. Cancer cells (2×10^5 cell/ml) were added to platelet suspension and incubated under continuous stirring at 37 ^{o}C. Pletelet-tumor heteroaggregates formation was shown to have three phases of aggregation: lag-phase with duration of about 10-14 min and two aggregation waves (Fig. 1, curve 1, lag-phase and first aggregation wave are shown). Preliminary incubation of platelets with ascorbic acid (antioxidant, have being shown to induce death of cancer cells with no cytotoxic effect on normal cells) at different concentrations led to a dose-dependent increase in duration of lag-phase (Fig. 1, curves 2 and 3). In presence of physiological ascorbic acid concentrations (200 μM) increase in lag-phase time was 36%, while at pharmacological ascorbic acid concentrations (5 mM) increase in lag-phase time was about 200%.

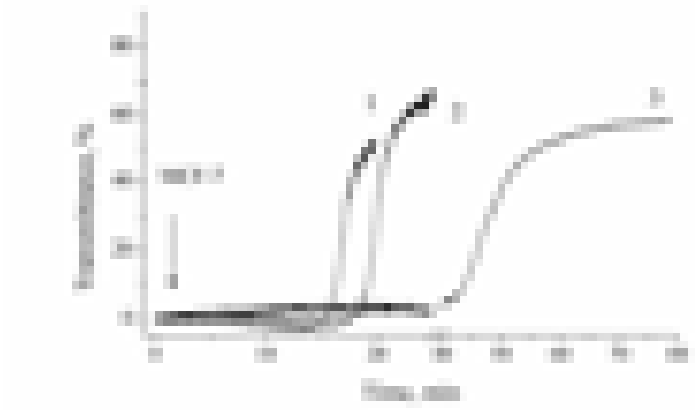

Fig. 1. Platelets aggregation induced by MCF-7 cells. 1 – control, without ascorbic acid in suspension; 2 – 200 μM of ascorbic acid in suspension; 3 – 5 mM of ascorbic acid in suspension.

Data obtained are in agreement with [3], where ascorbate depletion in mice unable to synthesize ascorbic acid has been shown to increase growth and metastasis of melanoma cells.

Tumor-induced platelet activation may cause the release of various cytokines, including CD40 ligand (CD40L – a transmembrane protein structurally related to tumor necrosis factor-α). Activation of the CD40/CD40L pathway has been suggested to enhance the procoagulant activity of tumor cells [4]. Recently ascorbic acid has been ascertained to inhibit platelet CD40/CD40L pathway [5] permitting to assume that inhibitory effect of ascorbic acid on platelet-tumor heteroaggregates formation, obtained in our present work, is likely associated with influence of ascorbic acid on CD40/CD40L pathway.

[1] L. Gibellini, M. Pinti et al., Interfering with ROS metabolism in cancer cells: the potential role of quercetin, Cancers **2**, 1288-1311 (2010).

[2] L. Borsig, The role of platelet actication in tumor metastasis, Expert Reviews Anticancer Therapies **8**, 1247-1255 (2008).

[3] J. Cha, M.W. Roomi et al., Ascorbate depletion increases growth and metastasis of melanoma cells in vitamin C deficient mice, Experimental Oncology **33**, 226-230 (2011).

[4] M. Roselli, T.C. Mineo et al., Soluble CD40 ligand plasma levels in lung cancer, Clinical Cancer Research **10**, 610-614 (2004).

[5] P. Pignatelli, V. Sanguigni et al., Vitamin C inhibits platelet expression of CD40 ligand, Free Radical Biology and Medicine **38**, 1662-1666 (2005)

EXPLORATION OF OPTICAL TWEEZING EFFICIENCY IN GELATIN SCAFFOLD – CELL SYSTEM

Marina Juralevičiūtė[1,2], Janez Štrancar[2], Rok Podlipec[2]

[1]Faculty of Physics, Vilnius University, Sauletekio ave. 9-III, LT-10222, Vilnius, Lithuania
[2]Jožef Stefan Institute, Jamova cesta 39, 1000 Ljubljana, Slovenia
marina.juraleviciute@ff.stud.vu.lt

Degeneration is a process occurring due to mechanical loading such as walking, running, bicycling or any other form of intense movement. Treatment of degenerative diseases and injuries is quite challenging. New methods are being developed constantly, for example, gelatin scaffolds are now applied for tissue engineering purposes, more accurately to foster *in vivo* regeneration of cartilage tissue. The basic aim of the research was to characterize cell-gelatin scaffold interactions using optical tweezing method.

Basic materials that were used for the research: cells and gelatin scaffolds. Experiments were held using mouse fibroblast cell line L-929. They are widely used in many experiment aspects as the fibroblasts are the most common cells of connective tissue in animals and they play an important role in wound healing. Gelatin scaffolds were made after crosslinking procedure of B type gelatins. Type B gelatins are derived from collagen of beef hides and are produced by partial hydrolysis and denaturation of collagen, during which the regular triple helix structure is broken down to form random gelatin coils [1].

Research has showed, that proliferation of cells in the gelatin scaffolds is very good - cells are growing profusely. Cells were labeled with amphiphilic fluorescent dye with the high value of membrane/water partitioning coefficient. The efficiency of trapping is in general dependent on the differences in refractive indexes of a dielectric object and surrounding media, the laser beam itself (beam characteristics, wavelengths) and the objective properties (numerical aperture, immersion objectives, etc.)[2]. Very promising is that, despite a little higher refractive index of cells (n=1.35-1.37) [3], [4] compared to refractive index of surrounding water (n=1.33), cells still can be trapped and slightly manipulated, considering of moving, stretching, etc. as it is showed in the picture (Fig. 1).

Fig. 1. Trapped cell in gelatin scaffold

Force acting on the cell trapped in optical field when moving the cell away from the surface is the force of binding proteins, which bind extracellular matrix and scaffold matrix. If the force of binding proteins exceeds estimated trapping force, then the cell disappears from the trap (Fig. 2).

The total force on an object due to refraction of light is:

$$\mathbf{F} = \left(\frac{\mathrm{n}}{\mathrm{c}}\right)\int\int\left(\mathbf{S}_{in} - \mathbf{S}_{out}\right)\mathrm{dA} \tag{1}$$

where n – refractive index of surrounding media, c – speed of light, $\mathbf{S}_{in}$- Poynting vector, which describes the momentum flux of photons entering the object, respectively $\mathbf{S}_{out}$ - momentum flux of photons leaving the object, dA – an element of area normal to $\mathbf{S}$ [5]. The integral represents the total power of the light. In real case the maximum efficiency is hardly achieved so the force equation is multiplied with the quality factor Q which depends on the direction in which force is measured. The highest factor is in perpendicular direction according to propagation of laser beam. Eq. 1 becomes then:

$$\mathbf{F} = \left(\frac{\mathrm{n}}{\mathrm{c}}\right)\cdot \mathrm{W}\cdot \mathrm{Q} \tag{2}$$

SEAFLOOR VIDEO MOSAIC ALGORITHM DEVELOPMENT AND ANALYSIS

Šarūnas Knabikas, Radvilė Budrytė, Benas Bakevičius, Olegas Ramašauskas

[1] Department of Informatic, Faculty of natural science and mathematcs, University of Klaipėda,
H. Manto st. 84, LT-92291 Klaipėda, Lithuania
sarunas.knabikas@gmail.com

After recording seafloor with remotely operating vehicle (ROV) [1] which has high-resolution video imagery we get high quality video material. Since in this field still is a lack of methods for the automatic analysis of these materials. Manual analysis of video material is complex, time-consuming as well as human resources. This problem requires the seafloor video mosaicing algorithm and exists as a main operating part of the image analysis.

Filming of seafloor can be done in different trajectories: straight, spiral and etc, as shown in [2], [3]. With such a variety of materials require different methods of mosaicing. Differences not only scatered of capture trajectory, but also has differences of video material quality, such as the distance from the bottom, water transparency and the result of different shots of lighting and color contrasts differences mismatches [4], [5]. While recording underwater video images appear on the distortions of volatility against the bottom of the ROV positioning. All of this creates problems in order to arrange the frames of the mosaic of the seafloor.

Our goal is to create an algorithm that helps to lay out mosaics of various the seafloor video material, and allow assembly tasks from manual to automated work.

Feature detection and matching:

- A pair of overlapping image of the same scene can be related by a motion model. (Fig.1)
- Matching the same object on different pictures.
- Matching two pictures on the same opacity.
- Matching two pictures making one of them more transparency.
- Maching pictures making one of them (A or B) cut α angle. (Fig. 2)

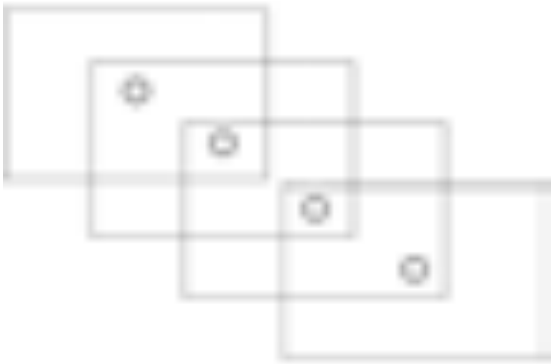

Fig. 1. Temporal sequence

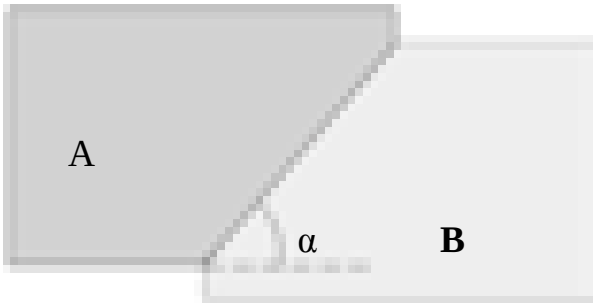

Fig. 2. Maching

The first stage of the algorithm is expected to create a mosaic from the conclusion of a straight trajectory filmed video material. In the second stage of the algorithm to continuously improve the conclusion of a mosaic of different trajectories filmed video material. The final phase is planned to create program prototype with a different shot trajectories of seafloor video material.

The goal of presented research is to create the seafloor mosaic processing algorithms, dedicated to reduce the required time and cost of human resources and increase video frames quality.

[1] M. Lukas, O. Ramašauskas (2011). Methods of color correction and object indentification in seafloor video mosaic // Open Readings 2011; 54th Science Conference for Young Students of Physics and Natural Sciences. Vilnius, VU, 2011-03-17/19, 80 □81 p.

[2] V. L.Ferrini, H. Singh, M. E. Clarke, W. Wakefield and K. York, Computer-Assisted Analysis of Near-Bottom Photos for Benthic Habitat Studies, Oceans 2006, 1-4 (2006)

[3] Pizarro, O., Singh, H. "Towards Large Area Mosaicing for Underwater Scientific Applications", IEEE J Oceanic Eng., Special Issue on Underwater Image and Video Processing, pp. 651-672, vol. 28, no. 4, 2003.

[4] J. Jaffe, "Computer modeling and the design of optimal underwater imaging systems," *IEEE J. Oceanic Eng.*, vol. 15, pp. 101□111, Apr. 1990.

[5] H. Sawhney ang R. Kumar, "True multi-image alignment and its application to mosaicing and lens disortion correction," *IEEE Trans. Pattern Anal. Mechine Intell.*, vol. 21, pp. 235 □243, 1999.

CONJUGATION OF QUANTUM DOTS WITH PDGF-BB FOR CANCER CELLS BIOIMAGING

Mantvydas Lopeta[1], Vitalijus Karabanovas[2], Zigmantas Zitkus[3], Ricardas Rotomskis[2], Mindaugas Valius[3]

[1] Faculty of Natural Sciences, Vilnius University, Lithuania
[2] Biomedical Physics Laboratory, Oncology Institute Vilnius University, Lithuania
[3] Proteomics centre, Biochemistry Institute Vilnius University, Lithuania
mantvydas.lopeta@gmail.com

Quantum dots (QD) are fluorescent semiconductor nanoparticles with unique physicochemical properties which make them attractive for early cancer cells diagnostics and therapy . In contrast with organic dyes QD are stable, bright fluorophores with high photoluminescence (PL) quantum yields, narrow PL bands, high absorbance and high resistance to photobleaching and degradation in vivo. PL wavelength of these fluorophores is dependent on their size which is adjustable. However use of QD for cancer cell visualization is complicated because they are not selective probes by themselves.

The goal of our study was to prepare selective QD conjugates that could recognize cancer cells. For that purpose platelet derived growth factor (PDGF-BB) was selected. This protein is homodimeric growth factor which binds to platelet derived growth factor receptor (PDGFR) and initiates its dimerization, autophosporylation and activation. This leads to cascade of signaling events in the cells that regulate cell growth, proliferation, differentiation, migration and other processes. To date, PDGF expression has been demonstrated in a number of different solid tumors, from glioblastomas to prostate carcinomas [1]. Characterization of photophysical properties of PDGF targeted QD conjugates (PDGF-QD) was performed by using steady-state spectroscopy. Absorbance and photoluminescence (PL) spectra of none coupled QD and PDGF-QD is presented in Fig. 1A. Both non-coupled and PDGF-QD absorb light in wide spectral region and have PL band peak at 628nm. This shows that surface modification of QD does not change their colloidal stability; however, coupling of PDGF-BB to QD surface slightly increases PL intensity. To evaluate how surface modification of QD with PDGF-BB affects biological properties we investigated their effect on DNA synthesis induction in embryonic mouse fibroblast NIH3T3 cells. Cells were treated with none targeted QD, PDGF-QD and PDGF alone and their proliferation was estimated by confocal microscopy using Click-iT EdU Imaging Kit. Treatment of cells with PDGF or PDGF-QD, but not with none coupled QD, induced DNA synthesis to the similar level (Fig. 1B). Fig 1B shows, that PDGF-QD are capable to elicit potent mitogenic response.

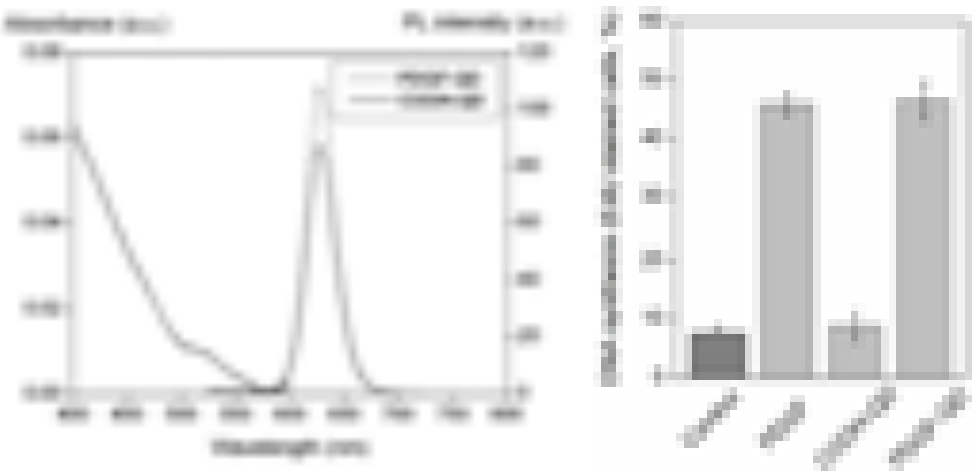

Fig. 1 A. Absorption and photoluminescence spectra of none coupled QD and PDGF-QD. B. DNA synthesis induction in non-treated or PDGF, none coupled QD or PDGF-QD treated cells.

For cancer cells detection it would be necessary that ligand do not cause proliferation of cells. For that purpose PDGF protein was monomerized and coupled to QD. Its validity as biosensor was evaluated by imunoprecipitation and fluorescence methods.

Mantvydas Lopeta acknowledges Student Research Fellowship Award from the Lithuanian Science Council.

[1] George D., Targeting PDGF receptors in cancer-rationales and proof of concept clinical trials, Advances in experimental medicine and biology **532**, 141-151 (2003).

PROTON RADIATION INFLUENCE ON SURVIVAL OF MIA PACA-2 CANCER CELLS

Mindaugas Malcius

Center for Physical Sciences and Technology, Lithuania
mmalcius@gmail.com

The most convienient way to investigate radiation effects is to use protons or ions beams produced by accelerators. It is because of simplicity to control dose and high probability of double strand breaks (DSBs) in the DNA because of direct ionizing. Free electrons are the key particles to cause lesions of the DNA [1]. But the enegy of these electrons is low and there is no experimental data for that spectrum. Though it exist GEANT 4 – DNA extension where it is possible to simulate protons of energy from 100 eV to 100 MeV and electrons of energy from 8 eV to 1 MeV [2].

It was calculated that in experimental conditions (100 μm diameter slit [3] for protons exit and 1.6 MeV initial energy) beam radius at intensity FWHM expands to 410 μm(Fig. 1). It was also investigated that enegy of protons at the surface of cells should be 1.075 MeV which means that range of a proton in water is ~30 μm and it is three times more than a cell. To determine dose it was important to know how many energy one proton leaves in a cell. So LET curve was calculated(Fig. 2). Calculations were done with GEANT4 [4, 5] and MCNPX [6].

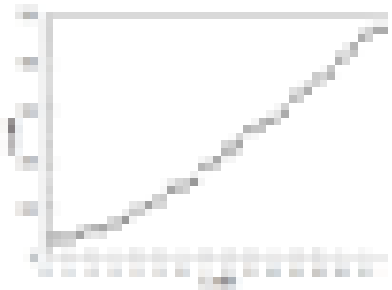

Fig. 1. Beam radius dependence on distance in air(at intensity FWHM)

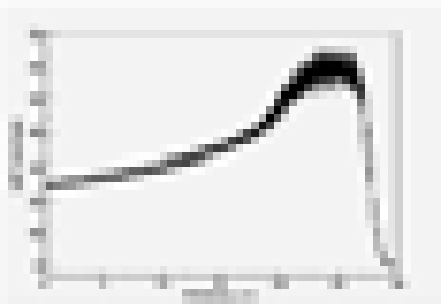

Fig. 2. LET curve

The main thing doing radiobiological experiments is to deterimine absorbed dose. Faraday cup was used in this particular investigation. Evaluated dose was 200±40 mGy which is near declared hormesis threshold. That is possibly why survival of irradiated cells were 7% better than non – irradiated cells (82±1% VS 75±1%). Cell line MIA PaCa-2 was used in this investigation [7]. Viability was checked with cell counter ADAM.

[1] O. I. Obolensky et al., Ion beam cancer therapy: Fundamental aspects of the problem, Nuclear Instruments and Methods in Physics Research **266**, 1623-1628 (2008).
[2] C. Villagrasa et al., Physical models implemented in the GEANT4-DNA extension of the GEANT4 toolkit for calculating initial radiation damage at the molecular level, Radiation Protection Dosimetry **143**, 214-218 (2010).
[3] M. Gasparīūnas et al., Proton and ion microbeam collimation for irradiation of biological samples in air, Lithuanian Journal of Physics **50**, 363-368 (2010) .
[4] J. Allison et al., Geant4 Developments and Applications, IEEE Transactions on Nuclear Science **53**, 270-278 (2006).
[5] S. Agostinelli et al., Geant4 - A Simulation Toolkit, Nuclear Instruments and Methods **506**, 250-303 (2003).
[6] MCNPX 2.6.0 Manual (2008).
[7] http://cellbank.nibio.go.jp/celldata/jcrb0070.htm (Checked: 2012-01-16)

INFRARED SPECTROSCOPICAL STUDIES OF SYNOVIAL FLUID OF PATIENTS WITH ACTIVE RHEUMATOID ARTHRITIS

Pavel Ryncevič, Sandra Tamošaitytė, Valdas Šablinskas

[1] Department of General Physics and Spectroscopy, Faculty of Physics, Vilnius University, Lithuania
pavelryncevic@gmail.com

Rheumatoid arthritis (RA) is a chronic, inflammatory disease that primarily attacks flexible (synovial) joints. About 1% of the world's population is afflicted by the disease, with women being three times more likely to have it than men. The most common age of onset is between 40 and 50, however it can develop for people of any age. The disease is usually followed by pain and finally it can lead to a loss of mobility and everyday functioning without proper treatment [1]. About 60% of synovial fluid samples collected from patients with arthritis contain calcium pyrophosphate dihydrate (CPPD) or basic calcium phosphate (BCP) crystals [2]. The presence of CPPD or BCP crystals can cause severe joint damage and rapid progression of RA. The relationship between CPPD and BCP and RA is still an unsolved puzzle [3]. Infrared (IR) microspectroscopy method for the investigation of synovial fluid has the potential to provide early diagnosis of the RA and also to grade the severity of the illness in arthritis patients by analyzing the chemical structure of crystals found in the affected joints[2, 4].

The sample of synovial fluid was collected from a patient suffering from active rheumatoid arthritis. 50 µl of synovial fluid was left to dry on a CaF_2 optical window. Then the spectra from different regions of dried synovial fluid film were collected: for areas dense with small crystals and for areas where no crystals were deposited. The measurements have been done over the 890-4000 cm^{-1} spectral region using a Bruker Vertex 70 spectrometer with an integrated IR microscope Hyperion 3000.

The summarized findings can be seen in Fig. 1. Most obvious IR absorption spectral band at 1044 cm^{-1} appears in the spectra of synovial fluid area which is dense with small crystals. Those are most likely to be CPPD crystals having absorption bands in the region shown in Fig. 1(b). The same absorption bands do not appear in the spectra of areas which are not affected by crystals accumulation.

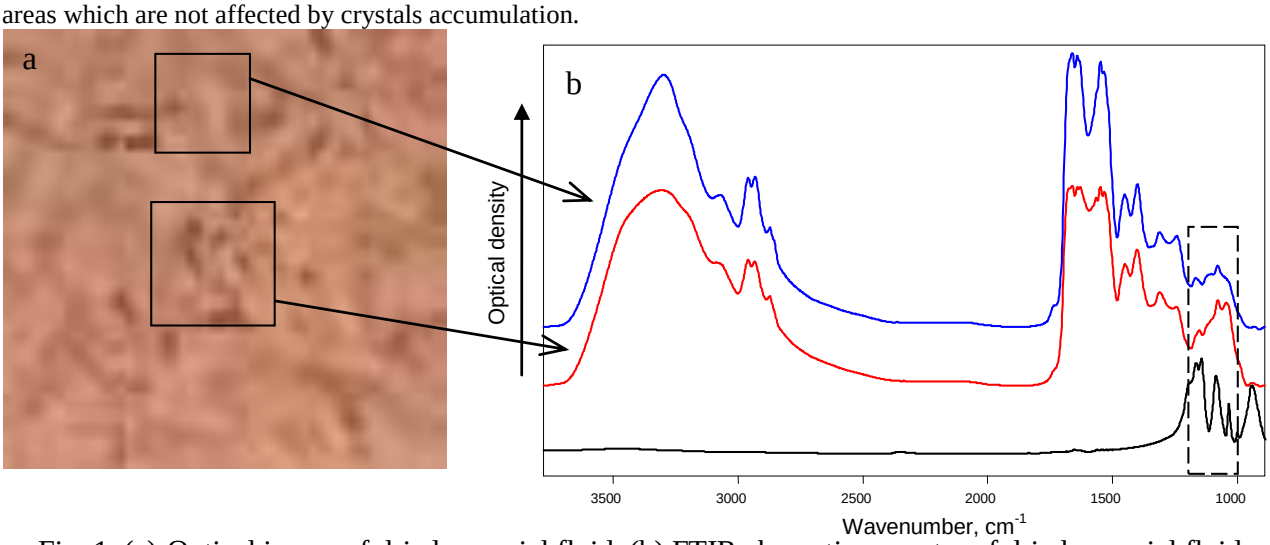

Fig. 1. (a)-Optical image of dried synovial fluid. (b) FTIR absorption spectra of dried synovial fluid from selected regions (top, middle) and Calcium pyrophosphate (bottom).

Our results show that infrared spectroscopy is able to supply information about chemical constitution of crystals of synovial fluid. This method is superior to optical imaging – conventional method used in contemporary medicine. Information about chemical structure of the crystals is essential to help the patient's physicians ascribe the appropriate treatment. Infrared spectral microscopy could be a possible technique to diagnose arthritis – it can be applied to investigate the crystals responsible for degeneration of joint tissue.

[1] P. Fishman, S. Bar-Yehuda, Rheumatoid Arthritis: History, Molecular Mechanisms and Therapeutic Applications Adenosine Receptors from Cell Biology to Pharmacology and Therapeutics **6**, 291-298 (2010).

[2] A. K. Rosenthal, et al., Characterization of articular calcium-containing crystals by synchrotron FTIR, Osteoarthritis Cartilage **16(11)**, 1395-1402 (2008).

[3] H. S. Cheung, I. V. Kurup, et al., Inhibition of Calcium Pyrophosphate Dihydrate Crystal Formation in Articular Cartilage Vesicles and Cartilage by Phosphocitrate, The Journal of Biological Chemistry **271(46)**, 28082–28085, (1996).

[4] R. A. Shaw, S. A. Kotowich et al., Arthritis diagnosis based upon the near-infrared spectrum of synovial fluid**,** Rheumatology International **15(4)**, 159-165 (1995).

SOLUBILIZATION OF QUANTUM DOTS BY PHOSPHOLIPIDS: STABILITY AND COMPLEX FORMATION WITH CHLORIN E_6

Artiom Skripka[1], JurgaValančiūnaitė[2], Ričardas Rotomskis[2]

[1] Institute of Oncology Vilnius University, Baublio 3b., LT-08406, Vilnius, Lithuania
[2] Faculty of Physics, Vilnius University, Saulėtekio ave. 9, bldg. 3, LT-10222 Vilnius, Lithuania
awefbeu@gmail.com

Luminescent semiconductor quantum dots (QDs) are intensively studied as promising nanoparticles for diagnostics and therapy in various fieldsof medicine. Due to the broad absorption, size-dependent photoluminescence (PL), high quantum yield, flexible surface modification, great photo- and chemical stability QDs are potential energy donors for conventional photosensitizers (PS) used in photodynamic therapy of cancer (PDT) [1]. QDs used along with PS could ensure more precise delivery to cancerous tissue and improve excitation of PS via energy transfer subsequently leading to enhanced efficiency of PDT. In our previous studies, we have demonstrated the formation of stable non-covalent complex between QDs and PS chlorin e_6 (Ce_6) with the ability of efficient energy transfer [2]. We have showed that QD-Ce_6 complex forms due to the hydrophobic interaction between non-polar moiety of Ce_6 and lipid part of QD coating.Therefore, the formation and stability of QD-Ce_6 complex is highly dependent on the type of lipids encapsulating QDs.

Here, we investigated the stability and spectral properties of CdSe/ZnS QDs (625nm) coated by different phospholipids in aqueous solution (PB pH 7). The spectral properties of QD-Ce_6 complex using commercially available QDs and those encapsulated in phospholipids were compared as well.

The surface of hydrophobic QDs was modified using different phospholipids containing saturated and unsaturated fatty acids: 16:0 PEG2000 PE 1,2-dipalmitoyl-*sn*-glycero-3-phosphoethanolamine-N-[methoxy(polyethylene glycol)-2000] (ammonium salt) (PEG-DPPE); 18:1 PEG2000 PE1,2-dioleoyl-*sn*-glycero-3-phosphoethanolamine-N-[methoxy(polyethylene glycol)-2000] (ammonium salt) (PEG-DOPE); 18:1 (Δ9-Cis) PC (DOPC)1,2-dioleoyl-*sn*-glycero-3-phosphocholine (DOPC).

QDs were successfully solubilized by saturated PEG-DPPE and unsaturated PEG-DOPE. However, an attempt to solubilize QDs using PEG free unsaturated phospholipids (DOPC) was ineffective. Further, mixing DOPC with either PEG-DPPE or PEG-DOPE resulted in a solubilization of QDs in aqueous solution. On the other hand, while QDs encapsulated into DOPC/PEG-DOPE micelles with molar ratios of 1:1 and 2:1 showed long term stability in aqueous solution, the colloidal solution of QDs modified by DOPC/PEG-DPPE (molar ratio 2:1) was unstable.

The modification of QDs surface with different phospholipids had no effect on the absorption spectra of QDs compared to the absorption spectrum of QDs in toluene. However, the PL spectra of QDs after modification by phospholipids significantly decreased. PL intensity of QDs encapsulated in PEG-DPPE micelles decreased more than three times, compared to the PL intensity of QDs in toluene. The third of PL intensity was lost upon encapsulation of QDs into PEG-DOPE micelles. Only negligible decrease in the PL intensity was observed for QDs modified by DOPC/PEG-DOPE at molar ratio 1:1 and the third of the PL intensity was lost when molar ratio of DOPC/PEG-DOPE was 2:1.

The formation of QD-Ce_6 complex was observed by adding a small amount of concentrated Ce_6 solution to 50 nM QDs solution to obtain QD:Ce_6 molar ratio 1:5. Addition of Ce_6 to PEG-DPPE encapsulated QDs had no effect on the spectral properties of QDs or Ce_6. Addition of Ce_6 to QDs encapsulated into micelles of unsaturated phospholipids PEG-DOPE and DOPC/PEG-DOPE resulted in significant spectral changes of the PL of QDs and Ce_6. PL intensity of QDs decreased while simultaneous increase in the fluorescence of Ce_6 was observed along with a spectral shift of the fluorescence band of Ce_6 from 660nm to 670nm. The same spectral changes were obtained upon QD-Ce_6 complex formation with commercially available QDs [2]. Formation of complex between Ce_6 and QDs modified by unsaturated phospholipids as well commercial QDs allowed the energy transfer from QDs to bound Ce_6 molecules to occur.

Based on the experimental results we conclude that highly stable QDs in aqueous solution can be made by encapsulation in phospholipid micelles. QDs-Ce_6 complex forms with QDs encapsulated in micelles comprised from unsaturated phospholipids. The efficient energy transfer from QDs to Ce_6 molecules can occur in such QD-Ce_6 complex which is crucial for its further application in PDT.

This work was supported by a grant (No. MIP-095/2011) from the Research Council of Lithuania.

[1] A.C.S. Samia, X.B. Chen, C. Burda, "Semiconductor quantum dots for photodynamic therapy" Journal of the American Chemical Society **125**(51), 15736-15737, 2003.

[2] J.Valanciunaite, A. Skripka, G. Streckyte, R. Rotomskis "Complex of water-soluble CdSe/ZnS quantum dots and chlorin e6: interaction and FRET" SPIE Proc. (2010)

Quantum dots as tools for phallotoxin delivery into living cells

Karolis Stašys[1], Vitalijus Karabanovas[1], Ričardas Rotomskis[1,2]

[1] Laboratory of Biomedical Physics of Vilnius University institute of Oncology, Lithuania
[2] Department of Physics, Vilnius University, Lithuania
Karolis.Stasys@ff.stud.vu.lt

Semiconductor nanoparticles known as quantum dots (QD) are very promising in biomedical apllications due to their unique photophysical properties such as wide absorption and narrow emission bands. In order to use QD for cellular visualization and cancer treatment including drug delivery systems, it is vital to understand the fundamental mechanisms of their entrance and trafficking within cells. Before this could be done, QD surface has to be modified using specific ligands in order to make them hydrophilic and able to pass through cell membrane. After modification of QD surface with different thiols we observed that mercaptorpopionic acid (MPA) is most suitable for QD surface modification. In previous works [1] it is shown that the best QD surface ligand is QD-MPA retains high colloidal stability and good optical properties. We also showed that QD-MPA enter cells by endocytotic pathway but does not affect cells viability. However if we want to use quantum dots as nanoplatform for drug delivery additional information is needed.

The goal of our study was to investigate how QD and their phallotoxin conjugates accumulate in mouse embryo fibroblast cells (NIH3T3) by using fluorescence confocal microscopy. Phalloidin was selected as phallotoxin which is isolated from the deadly Amanita phalloides mushroom and is commonly used in imaging applications to selectively label F-actin in fixed cells, permeabilized cells, and cell-free experiments. Therefore, this dye does not work on living, nonfixed cells and do not pass the cell membrane. In this work, we used QD-MPA with 625 nm emission band and Alexa Fluor 488 Phalloidin conjugate with 488 nm emission band. QD-MPA and phalloidin was mixed together to create one conjugate in order to investigate if QD can be used as drug carriers.

As shown in Fig. 1A,B QD-MPA and QD-MPA-phalloidin conjugates successfully accumulate in NIH3T3 cells after 24h of incubation. However, QD-MPA accumulate only in late endosomes while QD-MPA-phalloidin conjugates pass into cell and separately Alexa Fluor 488 Phalloidin conjugate labels actin filaments and QD pass to cell nucleus.

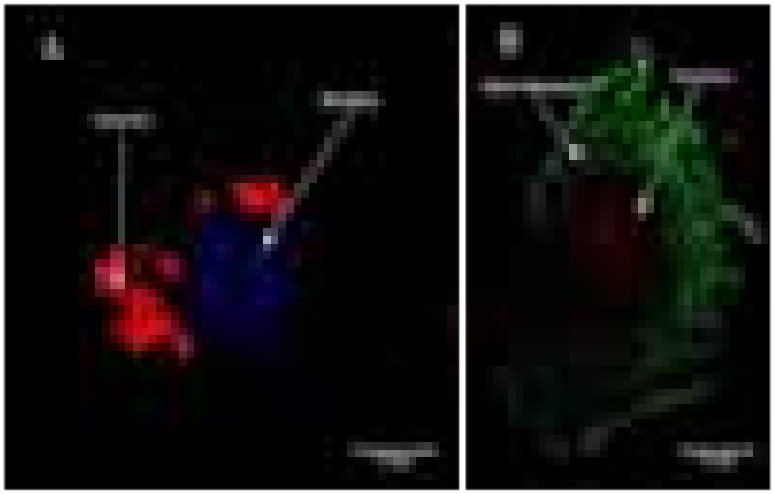

Fig. 1. NIH3T3 cell after 24 h incubation with QD-MPA (red) and cell nucleus is marked with DAPI (blue) (A). NIH3T3 cell with QD-MPA (red) and Alexa Fluor 488 Phalloidin (green) conjugate after 24 h incubation (B).

These results show that QD-MPA can be used as phalotoxin delivery system. Although, QD-MPA accumulation in cell nucleus suggests that phalotoxins affect cell viability and inner processes which results in the change of nucleus membrane permeability. All in all, this phallotoxin delivery system is a great breakthrough in creating an universal QD based drug delivery systems which will change the modern medicine as we know it and greatly improves cancer treatment.

[1] Stašys K, Karabanovas V, Rotomskis R, Valius M. Surface modification of (CdSe) ZnS quantum dots using thiols – characterization, photophysical and biological studies. Medical Physics in the Baltic States: proceedings of the 8th international conference on medical physics. Kaunas, Lithuania. 2010, 2:77–81.

CHEMISTRY OF HUMAN HAIR AS STUDIED BY MEANS OF INFRARED MICROSPECTROMETRY

Mindaugas Sutkatis, Milda Pučetaitė, Valdas Šablinskas

Department of General Physics and Spectroscopy, Faculty of Physics, Vilnius University, Saulėtekio Ave.9-III, LT-10222 Vilnius, Lithuania
Mindaugas.Sutkaitis@ff.stud.vu.lt

Keratin - fibrous structural protein, is the main component of human hair. Analysis of its distribution along the hair fiber allows determining its distance from the root, a degree of pigmentation and human origin. Testing of human hair fibers is an essential study in forensic science and its results may be the clear evidence presented in the court [1].

Fourier transform infrared spectroscopy (FTIR) is an excellent tool for morphological analysis of human hair. Microscope Hyperion 3000 combined with the spectrometer Vertex 70 from "Bruker" was used in this experiment. Untreated, blond and dark (homogenous) hair strands were collected from European origin 15 and 13 year-old females. The samples were flattened by applying a pressure of 10 tons on them, placed on CaF_2 (calcium fluoride) optical window and absorbance spectra were recorded. Firstly, the spectrum of blond hair at the centre of the fiber was obtained. The spectrum of amino acid - cysteine consists from strong amide I band at 1650 cm^{-1}, amide II band at 1540 cm^{-1}, NH stretch bands at 3290 cm^{-1} and 3060 cm^{-1}, medium intensity CH stretch bands at 2963 cm^{-1}, 2931 cm^{-1} and 2875 cm^{-1}. Nucleic acid (amide III) band was also observed at 1238 cm^{-1}. After washing the hair with liquid soap, no major spectral differences were detected. Secondly, dark hair strand's root, centre and tip were analyzed.

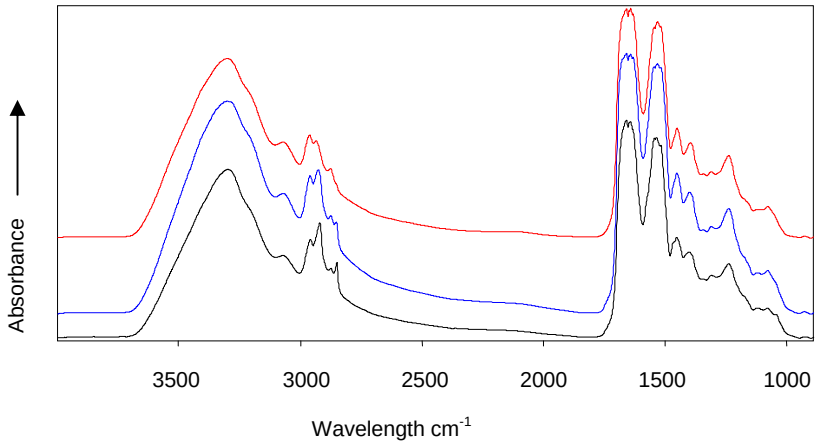

Fig. 1. Infrared absorption spectrum of dark hair strand at the tip (top), at the centre (middle) and at the root (bottom).

As shown in the figure 1, the hair composition along the hair strand slightly changes. An intense CH_2 stretch band is observed at 2920 cm^{-1} and 2850 cm^{-1} in the spectrum of the hair tip. These bands are observed in the spectrum of the medulla – inner part of the hair fiber [2]. This implies that hair strand decreases in diameter due to degradation of the cuticle – the outermost part of the hair fiber, and is the thinnest at the tip. Less intense 2920 cm^{-1} and 2850 cm^{-1} spectral bands are also observed in the spectrum of the hair strand's centre. This suggests gradient decrease in diameter.

Another important spectral band which emerges in hair tip's spectrum is seen at 1040 cm^{-1}, which indicates about increase of cysteic acid concentration. Cysteic acid is a product of oxidation process which occurs as a result of UV radiation. As the tip of the fiber has been affected by this process for a longer time the concentration of cysteic acid is higher in it. However, there were no major differences between dark and blond hair spectrum detected.

In conclusion, the results of infrared microscpectroscopical analysis show that the chemistry of the hair fiber changes from root to tip. These changes are caused by oxidation as well as cuticle degradation. A grey hair will also be morphologically analyzed, thus we will compare it with the investigated ones. The difference in degree of pigmentation is expected. We will also analyze a hair sample of drug addict, particularly cannabis user. Thus more detailed information will be presented.

[1] S. Brandes, Near Infrared studies of human scalp hair in a forensic context, Thesis, Queensland University of technology, (2009).
[2] P. Dumas, L. Miller, The use of synchrotron infrared microspectroscopy in biological and biomedical investigations, Vibrational Spectroscopy 32, 3-21, (2003).

.

SPECTROSCOPIC STUDY OF CdSe/ZnS QUANTUM DOTS-CHLORIN e_6 COMPLEX PHOTOSTABILITY AND SINGLET OXYGEN GENERATION

Gediminas Špogis[1,2], Jurga Valančiūnaitė[2], Ričardas Rotomskis[1,2].

[1]Faculty of Physics, Vilnius University, Saulėtekio Ave. 9-III, LT-10222 Vilnius, Lithuania
[2]Institute of Oncology, Vilnius University, Baublio 3b, LT-08406 Vilnius, Lithuania
Gediminas.Spogis@gmail.com

Semiconductor nanocrystals, called quantum dots (QDs), are inorganic particles with unique size-dependent optical and electrical properties due to quantum confinement. The combination of the size-tunable narrow photoluminescence (PL) spectra, high quantum yield, broad absorption spectra with large extinction coefficients and extreme photostability has already verified QDs as effective labels for biological imaging [1]. Presently, QDs are widely studied as potential energy donors to photosensitizers (PSs) with the intent of applying such QD-PS conjugates in the photodynamic therapy of cancer (PDT) [2]. There are certain requirements for optimal PDT photodrug, including the most important requirement to generate singlet oxygen ($^1O_2$), which is a main reactive intermediate in photosensitized cancer cell killing.

In this work, we present a steady-state spectroscopic study on the photostability and $^1O_2$ generation of water-soluble CdSe/ZnS QDs and photosensitizer chlorin e_6 (Ce_6) complex. The formation of $^1O_2$ was measured with the fluorescent dye singlet oxygen sensor green (SOSG). The irradiation of samples was performed using continuous 460 nm light source (106,4 mW/cm^2) .Since the absorption of Ce_6 at 460 nm is minimal, this allows estimating $^1O_2$ amount produced by QD-Ce_6 complex via energy transfer from QDs to bound Ce_6 molecules only.

The emission intensity changes under 460 nm irradiation of 20 nM QD, 0.2μM Ce_6, and QD-Ce_6 (c_{QD}=20 nM, QD:Ce_6 molar ratio 1:10) aqueous solutions (PB pH 7) at respective maxima are shown in Fig. 1A. After 134 J/cm^2 irradiation dose, the fluorescence intensity of pure Ce_6 solution decreased by 5%, while the PL intensity of pure QD solution did not change significantly. The irradiation of QD-Ce_6 solution produced a large decrease in the fluorescence of bound Ce_6 at 670 nm, while QD emission at 630 nm was increasing simultaneously. After 128 J/cm^2 irradiation dose, the fluorescence intensity of bound Ce_6 decreased by 77%, while QD PL intensity increased 3.6 times. The recovery of QD PL intensity is associated with the photobleaching of bound Ce_6 molecules as energy acceptors.

The emission intensity changes of SOSG fluorescence at 528 nm under 460nm irradiation of pure QD, Ce_6 and mixed QD-Ce_6solutions are presented in Fig. 1B. Any significant changes in SOSG fluorescence intensity in neither QD, nor Ce_6 pure solutions were observed. However, irradiation of QD-Ce_6 solution produced a significant increase in intensity of SOSG fluorescence confirming that QD-Ce_6 complex is able to generate $^1O_2$.

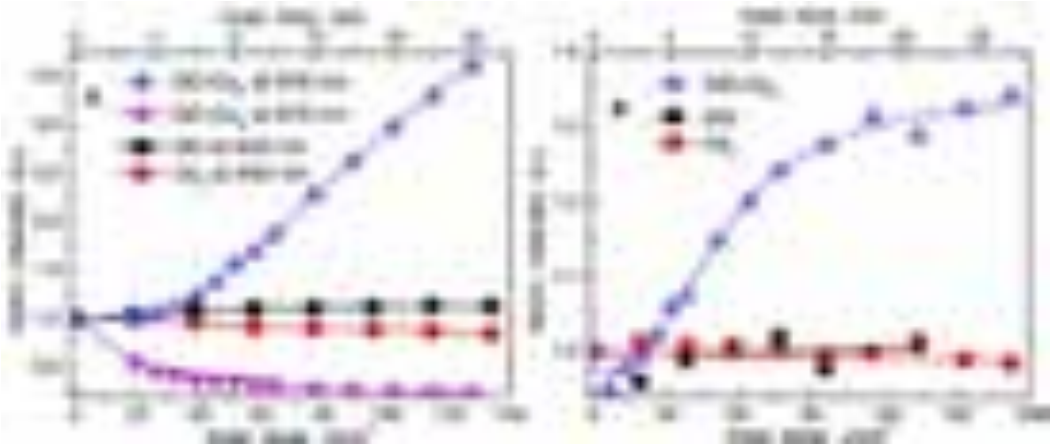

1 Fig. A – Emission intensity changes of QD and Ce_6 at respective maxima in pure QD, Ce_6 and mixed QD-Ce_6 solutions after different irradiation doses. B – Fluorescence intensity changes of SOSG at 528 nm in pure QD, Ce_6 and mixed QD-Ce_6 solutions at respective irradiation doses.

We conclude that QD-Ce_6 complex activated by light is able to produce $^1O_2$ more effectively than QD or Ce_6 alone. The generation of $^1O_2$ within QD-Ce_6 complex occurs via energy transfer from QD to bound Ce_6 molecules. $^1O_2$ generated by bound Ce_6 molecules reacts with Ce_6 itself causing its photobleaching.

Acknowledgments. This work was supported by Lithuanian Science Council Student Research Fellowship Award (G.Š).

[1] Bruchez, M.J., Moronne, M., Gin, P., Weiss, S., Alivisatos, A.P. Semiconductor nanocrystals as fluorescent biological labels. Science 281, 2013-2016 (1998).
[2] Samia, A.C.S., Chen, X., Burda, C. Semiconductor Quantum Dots for Photodynamic Therapy. Journal of The American Chemical Society 125(51), 15736-15737 (2003).

APPLICATION OF INFRARED SPECTRAL MICROSCOPY FOR CHEMICAL COMPOSITION STUDIES OF URINARY SEDIMENTS

Sandra Tamošaitytė, Valdas Šablinskas

Department of General Physics and Spectroscopy, Faculty of Physics, Vilnius University, Lithuania
sandra.tamosaityte@ff.stud.vu.lt

Kidney stone disease is a common disease with prevalence for about 10 % of human population [1]. Most kidney stones formers have disorders either in metabolism and excretion of stone forming materials or in promoters and inhibitors of their crystallization [2, 3]. As crystalline components coalesce in clusters they start to form solid kidney stones. The early identification of kidney stone forming crystals in human urine is essential for taking early preventive actions for kidney stone disease [4]. Usually optical microscopy is employed for the identification of the chemical composition of such crystals or crystal clusters, and such identification is based on their morphological structure. However, the examination of optical view is based on laboratory personnel skills and has significant probability of misinterpreting the chemical composition of urinary crystals. Infrared spectroscopic microscopy (mFTIR) could be used as a more reliable method to correctly identify chemical composition of urinary crystalline components.

Urine samples were taken just before kidney stone removal surgery, centrifuged and filtered on ashless filters for 24 hours to separate urea and water from bigger urinary crystals. The latter were transferred on IR transparent CaF_2 (3800 – 890 cm^{-1} spectral region) or ZnSe (3800 – 600 cm^{-1} spectral region) window and examined by Bruker Hyperion 3000 IR microscope.

We examined 72 kidney stones patients' of Vilnius Santariskes clinics and 5 healthy persons' urinary sediment. In order to evaluate the correlation between urinary crystals and kidney stone chemical composition of the same patient, both were investigated. In 52 % cases, patients with kidney stone disease had the same chemical composition of crystals in their urine as their kidney stone chemical composition. It was found no kidney stones forming sediment in the urine of healthy people.

There were found both regular shape crystals and some undefined shape crystals or crystal clusters. Optical images of some typical examples of urinary crystals and their infrared spectra are presented in Fig. 1. Whatever morphological shapes of the crystals, we were able to discover main kidney stones forming materials: calcium oxalate, uric acid, hydroxyapatite, brushite, struvite – as monocrystals or in crystal clusters. Drug metabolites and proteins were also found as sediments.

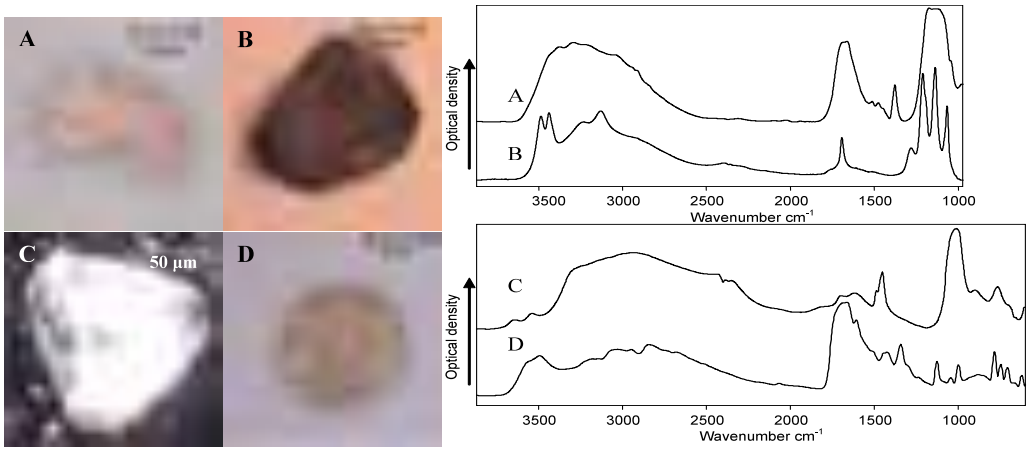

Fig. 1. Optical images of urinary crystals (left) and corresponding IR absorbance spectra (right): A - Calcium Oxalate and Uric Acid cluster, B – Brushite, C – Struvite, D – Uric Acid Dihydrate.

Our experiments revealed that mFTIR method is informative enough, reliable and easy to implement in order to define the chemical composition of urinary crystals no matter their morphological structure. Also, the correlation between chemical composition of both, kidney stones and urinary sediments of the same patients suggests, that examination of urinary sediments by mFTIR spectroscopy can be considered as a relevant technique for early identification of kidney stones and determination of appropriate actions to prevent their formation.

[1] A. Hesse, R. Siener, Current aspects of epidemiology and nutrition in urinary stone disease, World J Urol **15**, 165-171 (1997).
[2] S. Jawalekar, V. T. Survey, A. K. Bhutey, Inhibition efficiency of urine towards stone forming minerals, IJPSR **1**, 23-27 (2010).
[3] D. R. Basavaraj, Ch. S. Biyani, A. J. Browning, J. J. Cartledge, The Role of Urinary Kidney Stone Inhibitors and Promoters inthe Pathogenesis of Calcium Containing Renal Stones, EAU-EBU Update Series **5**, 126–136 (2007).
[4] E. Gnessin, J. E. Lingeman, A. P. Evan, Pathogenesis of renal calculi, Turkish J Urol **36(2)**, 190-199 (2010).

INVESTIGATION OF BLOOD MICROCIRCULATION IN INTEGUMENTS BY NON-INVASIVE SPECKLE-OPTICAL METHOD UNDER THE PHOTODYNAMIC ACTION

Aliaksandr Tserakh[1], Sergey Dick[1], Ivan Khludeyev[2]

[1] Belarusian State University of Informatics and Radioelectronics

[2] Belarusian State University

Shura_tereh@rambler.ru

The experimental research was carried out on laboratory rats with the weight of 200–250 gr. The surface of symmetrically located areas of right and left animals' thighs was depilated before hand. Only the right thigh area skin was exposed to light treatment. The received results were compared with the check indices registered in the symmetric zone on the lower left extremity. Photosensitizers (PS) aqueous solution was injected into the caudal vein.

During experiment animals were held in light-protected cages. Measurements were carried out in a darkened room with faint lighting of inactive green light as the maximum of absorption chlorine e6 makes 668 nm. Sites of tissues of an experimental animal, used as the reference sample, were additionally protected by a lightproof material to avoid any casual light exposure.

The measurements were carried out with the help of laser diagnostic device [1].

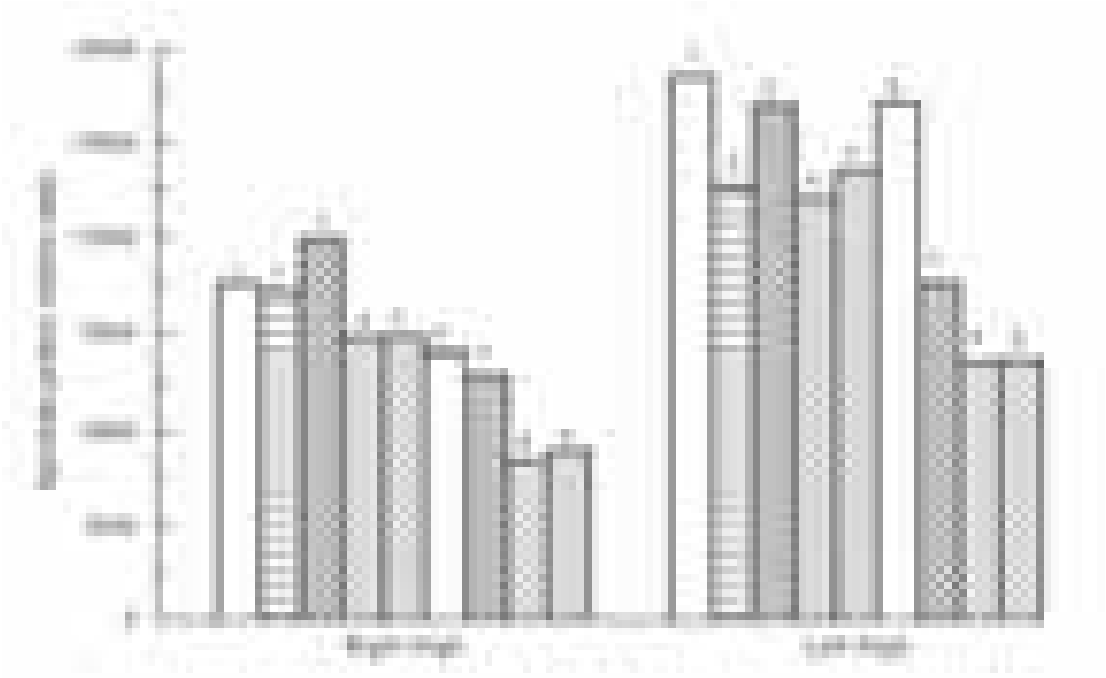

Fig.1. The state of superficial microhemocirculation of the rat's skin under Chl e6 sensitized photodynamic action. 1 – initial, 2 – Chl e6 injection, 3 – 30 min of light treatment, 4 – 30 min after light treatment, 5 – 60 min after light treatment, 6 – 23 hours afte rthe injection of Chl e6, 7 – repeated 30 min light treatment, 8 – 30 min after repeated light treatment, 9 – 60 min after repeated light treatment.

[1] Dick S.K., Marhvida I.V., Rachkovskiy L.I., et al. The Way of measurement of muscles biomechanical parameters and the device for its realization. Patent № 1620037, The USSR, 1990.

TRANSMURAL OXYGEN TRANSFER

Nadzeya Tserakh[1], Lyudmila Parkhach[2], Ernst Titovets[2]

[1] Belarussian State University of Informatics and Radioelectronics

[2] Republican Scientific Research Center of Neurology and Neurosurgery

tereshenka@yahoo.com

The classical scheme of tissue oxygenation is based on the fact that oxygen delivery is taken in through by the capillary network [1]. In accordance with modern experimental measurements of the longitudinal and radial oxygen gradients in blood vessels, it was shown that oxygenation in tissues is being provided, first and foremost, with arterioles and secondarily with capillary. The velocity of transmural oxygenation for these tissues is so high, that couldn't be explained by the diffusive concept, because oxygen permeability of the arteriole wall in vivo was much more higher than in vitro. In accordance with convective mechanism of tissue oxygenation concept the vectorial water and oxygen mass transfer between vessels and water compartments in tissues is taken in through by aquaporins [2].

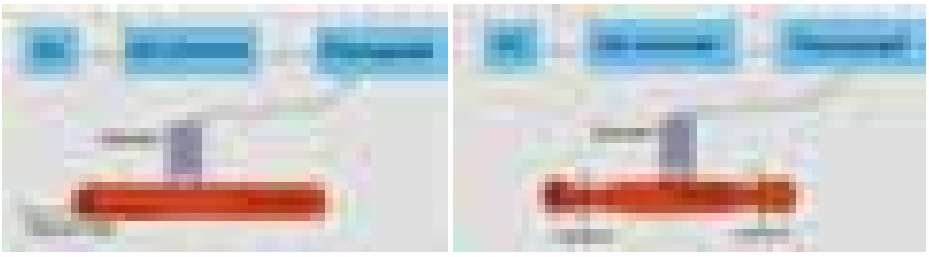

Fig . 1. Scheme of the device for oxygen mass transfer measurement before ligaturing and after ligaturing.

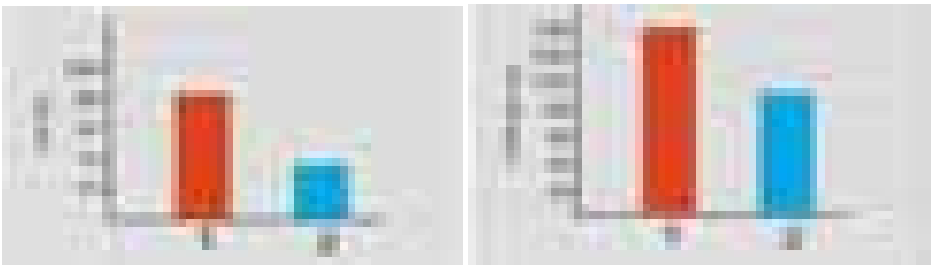

Fig.2. Fractional oxygen pressure (pO_2) on the external carotid's surface 1) before ligaturing 2) after ligaturing.

Fig.3. Mass transferring 1) from inside to outside the carotid; 2) from outside to inside the carotid.

We have installed a sensor on the rabbit's carotid in vivo and we measured pO_2 level on it (before and after ligaturing) (fig 1). We have estimated oxygen permeability of the part of rabbit's ligatured carotid in internal and external directions. The carotid was cut, unfolded and placed on the muscle, at first, with an internal surface on the top, secondary, with an external one. We had measured oxygen mass transfer trough the vessel's wall to the muscle, oxygen consumption velocities of the muscle and of internal and external surfaces of the carotid's wall. The carotid'swall permeability is a difference between oxygen transfer and carotid's wall cells oxygen consumption.

On the external surface of artery it was detected physiologically high levels of pO_2 (81 mm Hg). Ligaturing leads to the pressure decreasing (fig.2). It is obvious that transmural oxygen mass transfer is taking place. It determines high levels of pO_2 on external surface of carotid's wall and could take part in nearest tissues oxygenation. It was developed that oxygen mass transferring from inside to outside the vessel is higher than backwards (fig. 3).

[1] Krogh A. Anatomy and physiology of capillaries.- New Haven.- 1936.

[2]. Tsai A.G., Cabales P., Hangai-Hoger N., Intaglietta M. Oxygen distribution and respiration by the microcirculation //Antioxidants & Redocs Signaling. –2004. –V.6. – № 6. - P.1011-1018.

RAMAN MICROSCOPY METHOD USE OF INTERVERTEBRAL HERNIA TISSUE RESEARCH *IN VITRO* CHARACTERISTICS

Jonas Jovaišas[1], Valdemaras Aleksa[1], Darius Varanius[2,3], Aurelija Vaitkuvienė[2], Paulius Naujalis[1], Gunaras Terbetas[4]

[1] Faculty of Physics, Vilnius University, Saulėtekio al. 9-III, LT-10222 Vilnius, Lithuania
[2] Institute of Applied Research, Vilnius University, Saulėtekio al. 9-III, LT-10222 Vilnius, Lithuania
[3] Faculty of Natural Sciences, Vilnius University, M.K.Čiurlionio g. 21/27, LT-03101 Vilnius, Lithuania
[4] Clinics of Neurology and Neurosurgery, Vilnius University Hospital, Šiltnamių g. 29, LT-04130 Vilnius, Lithuania

darius.varanius@tmi.vu.lt

Creating new intervertebral disc hernia diagnostics means is necessary. Not only because sciatica (lower limbs and low back pain) induces pain and makes people suffer from it, but also because it causes economical damage as well [1]. According to studies, 70 to 85% of people population will suffer from sciatica in their lifetime [2].

Pairing contemporary intervertebral disc hernia diagnostics methods (Magnetic Resonance Imaging and Computed Tomography) with vibrational spectroscopy (and maybe luminescence) may help developing new tools to diagnose and to spot intervertebral disc herniation sooner than ever before.

Fourier transform Raman spectroscopy (FT-Raman) is a powerful technique to examine all kinds of material's properties. In this experiment we used modern FT-Raman microspectrometer "MultiRAM" (Bruker Optik GmbH, Rudolf-Plank-Str. 27, D-76275 Ettlingen, Germany. Software version: OPUS 6.5) to register scattering spectra of intervertebral disc hernia tissue *in vitro*.

Samples were excited by Nd:YAG Senza HP - 1064nm laser (KLASTECH - Karpushko Laser Technologies GmbH. Konrad-Adenauer-Allee 11, D-44263 Dortmund, Germany). Gathered data was processed with OPUS 6.5 and OriginPro 8.5 software. Results helped to find and to assign certain vibrational bands to this material's specific molecular vibrations.

Spine, vertebral, intervertebral disc anatomy, diagnostic methods like MRI and CT were reviewed. Raman scattering mechanism was also explained in a theoretical investigation. Intervertebral disc hernia tissue Raman spectra were registered for the first time. The parameters for the best sample spectra were defined.

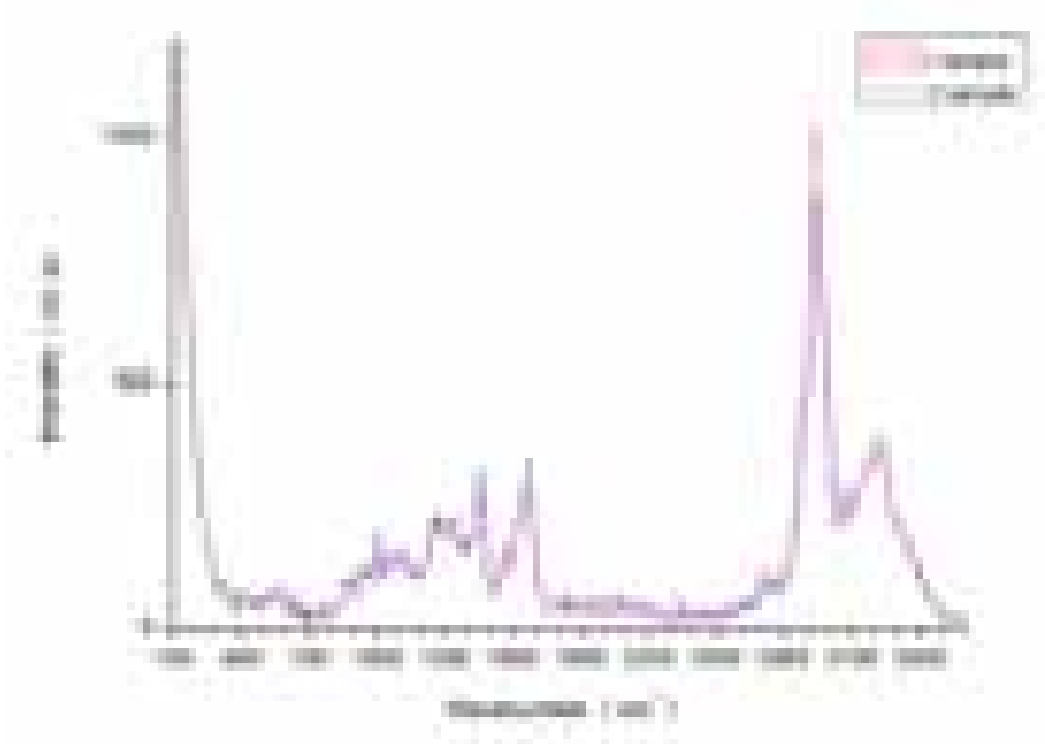

Fig. 1. Intervertebral disc hernia tissue FT-Raman spectra (2 samples).

[1] Abenhaim L, Suissa S., Importance and economic burden of occupational back pain: a study of 2,500 cases representative of Quebec, *J Occup Med*., 29(8), 670-4 (1987).

[2] G. Andersson. Epidemiological features of chronic low-back pain. Lancet, 354, 581-585 (1999).

THE INTERNAL ROTATION BARRIERS AND TORSIONAL STATES OF METHANOL MOLECULE.

A.Bedulin[1], G.Pitsevich[1]

[1]Belarusian State University, Minsk, Belarus
xa4a4a@gmail.com

The potential functions of internal rotation, the torsional state energies for a free methanol molecule have been computed. The potential energy of internal rotation with respect to C–O bond was computed at the fixed values of the dihedron H–C–O–H by steps of 20º, the geometry being optimized for all other internal parameters. In the process of internal rotation the inertial parameters of the frame and top are invariable. A torsional equation has the form:

$$\frac{I_{bb}I_{cc}-I_{bc}^2}{2I_\alpha d}p'^2\Psi+V(\alpha)\Psi=E\Psi, \tag{1}$$

where

$$p'=-i\hbar\frac{\partial}{\partial\alpha}. \tag{2}$$

The effective internal-rotation constant may be transformed to:

$$F=\frac{I_{bb}I_{cc}-I_{bc}^2}{2I_\alpha d}=\frac{I_{bb}I_{cc}-I_{bc}^2}{2I_\alpha(I_{bb}I_{cc}-I_{bb}I_\alpha-I_{bc}^2)}=\frac{1}{2rI_\alpha}, \tag{3}$$

A value of r is easily computed in a system of the principle axes of inertia (*x*, *y*, *z*) whose positions, according to the data of GAMESS computations. Principal moments of inertia, and effective internal-rotation constant *F* were computed based on the data of quantum-mechanical computations for the optimized molecular geometry: γ_{cx} = 0.9985, I_x =3.9276 $amu\cdot$Å^2, I_y =20.4214 $amu\cdot$Å^2, I_z =21.1549 $amu\cdot$Å^2, *F* =27.2642 cm^{-1}. The potential energy function computed with GAMESS may be approximated by the expression of the form:

$$V(\alpha)=\frac{1}{2}\sum_{m=0}^{3}V_m(e^{i3m\alpha}+e^{-i3m\alpha}), \tag{4}$$

where V_0 = 185.504, V_1 = 185.886, V_2 = 0.472, and V_3 = 0.090 cm^{-1}. The computed value for the potential barrier height turns to be *V*(0) = 371.952 cm^{-1}. This value is in a perfect agreement with the value 372.22 $\pm$ 0.21 cm^{-1} obtained in [1] using the frequencies of the torsional-rotational spectrum for a methanol molecule. With due regard for symmetry of the potential energy $V(\alpha)=V(\alpha+\frac{2\pi}{3}k)$, where *k* = 0; ±1; ±2;…, solutions for equation (1) should be sought in the basis of the eigenfunctions for a free rotator as follows [2]:

$$\Psi_\sigma=\sum_{k=-\infty}^{\infty}A_{3k}e^{i\sigma}e^{i3k\alpha}, \tag{5}$$

where σ = 0; ±1. Each torsional energy level, labeled with the quantum number τ (τ = 1, 2, …), is split into three sublevels characterized by the quantum number σ. The case when σ = 0 is associated with nondegenerate energy levels of the *A*-type interpreted as vibrational motions within a potential well. The case when σ = ±1 is associated with the doubly degenerate energy levels of the *E*-type caused by tunneling through the barrier. Substituting (5), (4), and (3) into equation (1), we derive a system of linear equations with respect to the Fourier series-expansion (5). In the simplest case of a potential of the form $V(\alpha)=V_0(1+\cos 3\alpha)$ for nondegenerate states (σ = 0) such a system may be generated by the following equation:

$$(E'-9k^2-2V_0')A_{3k}+V_0'A_{3(k-1)}+V_0'A_{3(k+1)}=0, \tag{6}$$

where $E'=\frac{E}{F}$ and $2V_0'=\frac{V_0}{F}$. Then eigenvalues of the energy $E_{\tau\sigma}$ and eigenfunctions expansion coefficients A_{3k} are found by diagonalization of the energy matrix.

[1] Y.Y. Kwan, D.M. Dennison. Analysis of the torsion-rotation spectra of the isotopic methanol molecules. J. Mol. Spectrosc., 43 (1972), 291-319.

[2] H. Jeffreys, B. Swirles. Methods of Mathematical Physics. Third edition. Cambridge, Cambridge University press (1966), v.3, 23-30.

THE NATURE OF PARAMAGNETIC CENTERS IN MoO_3 AND TiO_2-MoO_3 SYSTEM, OBTAINED BY SOL-GEL ROUTE

Natalia Boboriko

Department of Chemistry, Belarusian State University, Minsk, Belarus
natchem@tut.by

TiO_2-MoO_3 systems are widely used catalysts in the processes of dehydration, alcohols oxidation [1], ammoxidation [2] et al. These systems are also used for the formation of gas sensing layers in chemical gas sensors [3]. Our earlier investigations [4] showed the availability of using TiO_2-MoO_3 multioxide systems with different oxide molar ratio as gas sensing material for hydrogen detection. Doping of titanium dioxide with molybdena leads to the increase of sensor response towards hydrogen. However the ascertainment of the mechanism of the influence of doping agents on gas sensing properties needs further investigation. The aim of this work was to establish correlations between gas sensing characteristics of sensors on the basis of molybdena doped titanium dioxide and the nature of the paramagnetic centers of these multioxide systems.

Primary elements for chemical gas sensors on the basis of doped titanium dioxide were formed by sol-gel technique. The procedure of primary elements formation and gas sensing properties measurements is described in [4]. Gas sensing coating was formed from multihydroxide sols. The initial sol of hydrated titanium dioxide was obtained by precipitation by ammonium hydrate from the aqueous solution of titanium chloride in hydrochloric acid, dispersed by ultrasonic and stabilized by concentrated nitric acid. MoO_3 sol was prepared by precipitation from ammonium paramolybdate water solution by nitric acid. Sols for TiO_2-MoO_3 multioxide systems formation were obtained by adding of the calculated amount of ammonium paramolybdate hydrate to the initial sol of titanium dioxide with subsequent ultrasonic treatment. Heat treatment of synthesized sols results in hydroxides decomposition and oxides formation. The content of molybdenum trioxide in the multioxide system was varied from 0.5 to 10 mol.%.

Molybdenum trioxide is a perspective material for gas sensing devices. The peculiarities of its crystalline structure, which consists of two-dimensional networks connected by Van der Waals forces, permits forming superposed structures with oxygen removal. All this makes lattice oxygen along with chemisorbed surface oxygen species active in the processes of thermocatalytic oxidation of burning gases on the surface. The mechanism of gas sensing properties enhancement with molybdena doping can implicate modification of acid-base and redox properties of the surface of multioxide system, which affect adsorption and catalytic activity of the material. Valence- and coordinative-unsaturated metal atoms play the main role in the processes of burning gas detection. Sol-gel method of multioxide system synthesis and the features of molybdenum trioxide chemical nature allow obtaining materials with Mo^{5+} and Ti^{3+} centers, which can play the role of adsorption sites for gas molecules. ESR spectroscopy allows detecting paramagnetic centers in gas sensing materials. ESR spectroscopy was carried out for multioxide samples, obtained by sols heat treatment at 600 ºC for 2 hours.

The ESR spectrum of molybdenum trioxide, synthesized by sol-gel route, consists of 5 main signals. Paramagnetic center with g_1=2,07, g_2=2,00, g_3=1,97 is fixed and it is attributed to $(Mo\text{-}O)^{5+}$ hole center. In addition line with g=1,97 can be attributed to 6-fold coordinate Mo^{5+} species with one O^{2-} in its octahedral environment substituted to OH^- group or H atom: $[Mo^{5+}(O^{2-})_5OH]$ or $[Mo^{5+}(O^{2-})_5H^+]$. Signals with $g_\perp$=1,94 and $g_\parallel$=1,89 characterize 6-fold coordinated Mo^{5+} in crystallographic shear structures. Most of all hole centers O^- (g=2,04) and adsorbed anion radicals O_2^- (g=2,02) are fixed. Investigation of TiO_2-MoO_3 multioxide systems with different oxide molar ratio by ESR spectroscopy at the room temperature does not give any concrete information on the nature of paramagnetic centers, which exist in the material, as spectrum of these systems consist of one broad line undistinguished from zero line. This broadening does not allow separating signals from certain paramagnetic centers and can be due to strong dipole-dipole interaction between Ti^{3+} paramagnetic centers from one hand and the consequence of the surface coating with adsorbed oxygen from the other hand. Bearing in mind low concentration of molybdena in TiO_2-MoO_3 system (up to 10 mol.%) lines from Mo^{5+} paramagnetic centers in different oxygen environment become undistinguished because of broadening from Ti^{3+} centers and because of adsorbed oxygen. Partially chemical nature of paramagnetic centers in TiO_2-MoO_3 systems can be deciphered by the data of paramagnetic centers in MoO_3, as crystalline phase of α-MoO_3 can be registered in the multioxide systems by XRD-analysis. But for complete understanding further researches are to be done.

The research conducted shows that enhancement of gas sensing properties of titanium dioxide with its doping with molybdenum trioxide can be due to the modification of redox and adsorption properties of the sensing material surface. Valence-unsaturated Mo^{5+} species are registered in MoO_3 by ESR spectroscopy, which can couple with Mo^{6+} and effectively take part in the processes of burning gases molecules oxidation. In addition fixed in the materials hole centers $(Mo\text{-}O)^{5+}$ and O^- can play the role of additional adsorption sites for gas molecules.

[1] Komandur V.R. Chary et al., Characterization and reactivity of molybdenum oxide catalysts supported on anatase and rutile polymorphs of titania, Appl. Catal., A. **208**, 291-305 (2001).
[2] Hideaki Yoshitake, Yuko Aoki, Shinnosuke Hemmi, Mesoporous titania supported-molybdenum catalysts: The formation of a new mesophase and use in ethanol–oxygen catalytic reactions, Microporous Mesoporous Mater. **93**, 294-303 (2006).
[3] Y.X. Li et al., Microstructural characterization of MoO_3-TiO_2 nanocomposite thin films for gas sensing, Sens. Actuators, B **77**, 27-34 (2001).
[4] N.E. Boboriko, Structural peculiarities of titanium dioxide – molybdenum oxide system and its use in chemical gas sensors, International forum for students "Pervyj shag v nauku-2011", ISBN 978-985-08-1281-0, Minsk, Belaruskaya navuka, 664-667 (2010).

FORMATION OF NON-EMPIRIC FORCE FIELDS IN REDUNDANT COORDINATES OF CYCLIC MOLECULES USING FORCE FIELDS IN INDEPENDENT COORDINATES

A.Bogush , G.Pitsevich

Belarusian State University, Minsk, Belarus
andynew.by@mail.ru

Optimization of the geometry and computations of a force field for a benzene molecule have been performed using the quantum-chemical package GAMESS (VERSION = 1 OCT 2010 (R3)) [1] in the approximation B3LYP/cc-pVTZ based on D_{6H} symmetry. A set of independent coordinates $\|q\|$ included all valence coordinates, with the addition of deformation and torsional coordinates up to 3*N*–6. The 54 redundant natural coordinates $\|Q\|$ included complete sets of equivalent natural coordinates ($\|Q\| = A\|q\|$). To find the matrix *A*, it is necessary to define a system of linear equations relating the redundant coordinates. As known [2], an addition of redundant coordinates leads to the appearance in the matrix of the kinematic coefficients *G* for new rows and columns forming linear combinations of the earlier ones. In the process the eigenvectors associated with zero eigenvalues of the matrix *G* constructed for the redundant coordinate set involve the same coefficients for the coordinates as should be in their linear combinations which are equal to zero. The matrix *G* for a molecule of C_6H_6 has been computed using the geometry in Cartesian coordinates optimized with the help of [1] and the redundant set of 54 vibrational coordinates. Values for the elements of *G* matrix have been found with the use of the computational package for normal molecular vibrations [3]. Further automatization of the computations was realized using special software with *Mathematica* package [4]. The initial data are represented by the elements of *G* matrix computed for a redundant set of the coordinates, by the matrix elements of the force constants *k* computed with the help of [4] for the redundant coordinate set and converted to cm^{-2}, and by lists of the coordinates in two sets. In this way the matrix *G* was diagonalized and the eigenvectors associated with its zero eigenvalues were found. Then a system of linear equations was derived to relate the redundant coordinates. As a result of solving this system, a redundant set of coordinates was expressed in terms of independent coordinates. On this basis the matrix *A* was generated and a form of the pseudoinverse matrix A^{-1} was found. Finally, with the use of relation $K = \tilde{A}^{-1}kA^{-1}$, the matrix of force constants *K* was generated, whose elements were averaged in subsets of the equivalent sets. Keeping the geometry invariable, this force field was used as initial data in the package [3], and its adequacy was tested by comparison of the computed frequencies [3] for normal vibrations with the data given in [1]. Thus, the force field of a benzene molecule computed by the non-empiric quantum-mechanical methods using a set of independent vibrational coordinates has been transformed to a set of redundant coordinates offering the possibility to recover a symmetry of the force field up to D_{6H}. Invariability of the frequencies for normal molecular vibrations when using the transformed force fields provides support for the approach, especially because the forms of normal vibrations become more adequate and clear. Based on agreement between the non-empiric force constants for sets of redundant coordinates and the corresponding empiric force constants computed using the frequencies of the molecules under study and of their isotopic substituted derivatives, r.m.s. vibrational amplitudes, Coriolis constants, both approaches are adequate enough and efficient in computations of molecular force fields. The force constants, both scaled and non-scaled, transformed to a set of redundant coordinates may be easily extended to the related molecular fragments in large molecules with the help of the well-developed techniques for automated separation of force constants in standard program facilities used to compute normal vibrations [3].

[1] http://www.msg.ameslab.gov/GAMESS/GAMESS.html
[2] M.V. Vol'kenshtein, L.A. Gribov, M.A. El'yashevich, and B.I. Stepanov. Molecular Vibrations [in Russian], Nauka, Moscow (1972), p. 291.
[3] V.V. Sivchik and K.M. Grushetskii. J. Appl. Spectrosc. **19**, Is. 2, (1973), 317.
[4] http://www.wolfram.com/mathematica/

THE POSSIBILITY OF TRANSFERRING AB INITIO FORCE FIELDS BY CONVERTING THEM TO DEPENDENT COORDINATES SET

Dmitriy Borisevich, Georgiy Pitsevich

Belarusian State University, Minsk, Belarus
fiz.boriseviDV@bsu.by

For the case of a planar molecular fragment with three valence angles having a common vertex and involving a single dependent coordinate the problem of reconstructing the force field in the dependent set of coordinates has been solved successfully [1]. However, as the tetrahedral fragment is most usual in polyatomic molecules, elucidation of the possibility for similar transformations in this case will contribute considerably to the applicability of the method.

We denote the dependent set of normal coordinates as and the independent set – as . Both sets are related to each other by the matrix A :

(1)

For the regular tetrahedral fragment the matrix A well known and pseudoinverse matrix A^{-1} can be found. Denoting the matrix of force constants for the dependent set of natural coordinates by and the corresponding matrix of the independent set – by , we can state that for the known one can always find the matrix unambiguously as soon as the matrix , expressing the dependent set of natural coordinates in terms of the independent one, is defined [2]. Proceeding from the general considerations, the matrix must be of the form

(2)

Using the transformation

(3)

we can derive the general form of the matrix of force constants for deformation coordinates in the dependent set as follows:

(4)

With the use of the inverse transformation

(5)

we can see that the form of the matrix remains similar to (2). The acceptability of such transformations was checked with a molecule of methane. Based on the quantum-chemical program packages [3], for this molecule in the approximation B3LYP/cc-PVTZ a force field has been calculated in the independent set of vibrational coordinates together with a spectrum for normal vibrations. With the help of relation (5), the force field was reconstructed in the dependent set of coordinates. Then the original molecular geometry and the matrix of force constants K have been used as the starting data for the computation of normal vibrations with the package [4]. Coincidence in the frequencies calculated with the help of the packages [3] and [4] supports the applicability of the developed method to the regular tetrahedral fragment.

[1] Pitsevich G.A., Kostopravova A.V., Pitsevich G.G. Works of International Conference “Fundamental problems of optics - 2010” , St. Petersburg, (2010), 218-221.
[2] Pitsevich G.A., Zjat’kov I.P. , Journal of Applied Spectroscopy 58, № 1-2 (1993) 70—76.
[3] http://www.msg.ameslab.gov/GAMESS/GAMESS.html
[4] Sivchik V. V., Grushetskii K. M., Journal of Applied Spectroscopy, 19 (1975), 1062-1064.

BIOGENIC TRANSFORMATION OF REDOX-SENSITIVE PLUTONIUM

Šarūnas Buivydas[1], Bena Lukšienė[1], Rūta Druteikienė[1], Dalia Pečiulytė[2], Dalis Baltrūnas[1], Rasa Gvozdaitė[1]

[1]Center for Physical Sciences and Technology, Savanorių ave 231, LT–02300 Vilnius, Lithuania
[2]Nature Research Centre, Akademijos str. 2, LT–08412 Vilnius, Lithuania
sarunas.buivydas@chf.stud.vu.lt

Long-lived radionuclides (actinides, ^{99}Tc, ^{137}Cs and others) in the environmental ecosystems mainly occur as a consequence of nuclear weapon testing and accidental releases from Nuclear Power Plants or fuel reprocessing plants. Besides, development of nuclear energetic is related to the utilization of radioactive waste of different activity level, therefore radioactive waste treatment and storage are related with risk to the environmental pollution as well as to the human health.

The chemical state of radionuclides released to the environment, combined with the complexity and diversity of their environmental behavior, creates difficulties in modeling their behavior over the life time of their radioactivity [1]. The radionuclide behaviour in the soil is often considered only from a physico-chemical point of view, although the biogenic factor, microbial activity, can affect either directly or indirectly their speciation and change mobility. Microorganisms because of their interaction with radionuclides affect geochemical processes, in particular radionuclide migration [2, 3]. Interaction of microorganisms with redox–sensitive radionuclides (Pu isotopes) is very often linked to a change in their oxidation states. In order to investigate a capability of aerobic bacteria and fungi to change plutonium oxidation state, a suspensions of each microorganism (Bacteria *Bacillus mycoides*, *Rhodococcus luteus*, Gram and fungi *Paecillomyces lilacinus*, *Absidia* sp.), isolated from the low-level waste repository of the Ignalina NPP, were treated with ^{239}Pu(IV) at pH 2.7-2.9 for a 24 hours. Radiochemical analysis applying modified anion exchange method allowed us to identify Pu of oxidation state (III), formed by microbial activity. Percentage distribution of Pu(III) calculated according to the results of alpha spectrometric measurement following radiochemical analysis is presented in Table 1. Results obtained in our investigations indicate that Pu(IV) is more sensitive to bacteria activity compared to that of fungi (Table 1). We determined that tested bacteria after 24-hour interaction converted from (0.7±0.15) % to (15.0.±2.4) % of Pu(IV) to Pu(III) in brine and from (0.3±0.06) % to (1.1±0.22) % in biomass. Tested fungi *Paecillomyces lilacinus and Absidia* sp. had insignificant influence on Pu (IV) oxidation state change under studied aerobic conditions.

Table 1. Percentage amount of reductively solubilized plutonium in tested medium of Na brine at low pH after 24-hour interaction under aerobic conditions

Tested microorganism	^{239}Pu(IV) added	Pu (III), % Brine/biomass	Brine/biomass, S.d., ±
Bacterium *Bacillus mycoides*	$9.2\ 10^{-12}$ M	14.4/1.1	2.6/0.22
Bacterium *Rhodococcus luteus*	$9.2\ 10^{-12}$ M	0.7/0.5	0.15/0.12
Bacterium Gram$^-$	$9.2\ 10^{-12}$ M	15.0/0.3	2.4/0.06
F. *Paecillomyces lilacinus*	$9.2\ 10^{-12}$ M	0.6/1.0	0.14/0.23
F. *Absidia* sp.	$9.2\ 10^{-12}$ M	0.2/0.3	0.05/0.06

Generalizing results of our investigations we can state the following approaches. Application of radiochemical method that included co-precipitation and modified anion exchange chromatography was very useful in the Pu oxidation state study. The capability of microorganisms to convert at some extent Pu(IV) into Pu(III) under aerobic conditions indicates that presence of such microorganisms under reducing conditions, i.e. in geochemical systems of nuclear waste repositories, is potential tool of Pu being changed into more mobile state.

Acknowledgments. The research leading to these results has received funding from the European Atomic Energy Community Seventh Framework Programme [FP7/2007-2013] under grant agreement n 212287, Collaborative Project Recosy and from the Lithuanian Agency for Science, Innovation and Technology (Grant No 31V-6).

[1] G.R.Choppin, Actinide Science: Fundamental and Environmental Aspects, J. Nucl. Radioch. Sci. 6 (1), 1-5 (2005).
[2] K. Pedersen, Microorganisms and their influence on radionuclide migration in igneous rock environments, J Nucl. Radioch. Sci. 6 (1), 11-15 (2005).
[3] L. Levinskaitė, A. Smirnov, B. Lukšienė, R. Druteikienė, V. Remeikis, D. Baltrūnas, Pu(IV) and Fe(III) accumulation ability of heavy metal-tolerant soil fungi, Nukleonika 54, 4, 285-290 (2009).

TESTING OF BASIS SETS AND DFT APPROXIMATIONS ON INTERNAL ROTATION BARRIERS CALCULATIONS IN METANOL MOLECULE.

H.Khrol[1], G.Pitsevich[1]

[1]Belarusian State University, Minsk, Belarus
Khroll@mail.ru

The barriers to internal rotation of the free methanol molecule in the B3LYP/cc-pVTZ, B3LYP/acc-pVTZ, wB97X-D/cc-pVTZ, wB97X-D/acc-pVTZ approximations. Then we calculated the energy of torsional states.

As seen from calculations the results obtained in the wB97X-D/acc-pVTZ approximation are close to those in B3LYP/ acc-pVTZ. The same can be said of the wB97X-D/cc-pVTZ and B3LYP/acc-pVTZ approxi-mations. The results of the calculations are more sensitive to basis and cc-pVTZ significantly more preferable than acc-pVTZ. Comparing the calculations in B3LYP/cc-pVTZ and wB97X-D/cc-pVTZ should be noted that in the first case the results are somewhat close to the experimental. Complete information not only about the width but also the shape of the potential curve as a whole, can be obtained expanding the potential energy function in a Fourier series. In accordance with the results of [1], obtained using microwave and rotational spectra data of CH_3OH, CD_3OH, CH_3OD and CD_3OD, the potential curve can be represented as follows: $f(t) = V_0+V_3 \cos(3t)+V_6 \cos(6t)+V_9 \cos(9t)$, where $V_0= V_3=186.13$; $V_6=-0.035$; $V_9=0.0$ cm^{-1}. As noted in [1] "Thus the value of $V_6 = -0.035\pm0.105$ cm^{-1} should measure the true deviation from a sinusoidal barrier potential. Our result indicates that the deviation is indeed very small for methanol." Let us now compare the Fourier series of potential functions, calculated in different approximations:

1.B3LYP/cc-pVTZ: $V_0= V_3=185.698$; $V_6 =0.471$; $V_9=0.0898$.
2. wB97X-D/cc-pVTZ: $V_0= V_3=183.641$; $V_6 =3.186$; $V_9=1.7081$.
3. B3LYP/acc-pVTZ: $V_0= V_3=170.774$; $V_6 =1.569$; $V_9=-1.3609$.
4. wB97X-D/acc-pVTZ: $V_0= V_3=169.727$; $V_6 =-1.722$; $V_9=2.0041$.

Considering as a deviation from experimental potential curver the expression: $\Delta = \sum_i (V_i^{\exp} - V_i^{calc})^2$ one can obtain:

1. B3LYP/cc-pVTZ: $\Delta = 0.6373$
2. wB97X-D/cc-pVTZ: $\Delta = 25.6826$
3. B3LYP/acc-pVTZ: $\Delta = 476.5911$
4. wB97X-D/acc-pVTZ: $\Delta = 544.9792$

Thus, despite the fact that the energy values calculated at any point in the approximations 2-4 lower, than in approximation 1, the relative positions of points on the potential curve is reproduced better by using the approximation 1. In addition, the deviation from sinusoidal is minimal for potential curve, calculated in approximation 1, too. The choice in favor of B3LYP/cc-pVTZ approximation in particular based on the fact that it has established itself well in our calculations of force fields and vibrational spectra of some organic molecules [2,3].

[1] Y.Y. Kwan, D.M. Dennison. Analysis of the torsion-rotation spectra of the isotopic methanol molecules. J. Mol. Spectrosc., 43 (1972), 291-319.
[2] G.A. Pitsevich, Maksim Shundalau, M. A. Ksenofontov, D. S. Umreiko Vibrational analysis of 4, 4-methylene diphenyl diisocyanate Global Journal of Analytical Chemistry, Volume 2, Issue 3, (2011), p.114-124.
[3] G.A. Pitsevich, I.Yu. Doroshenko, V.Ye. Pogorelov, D.S. Umrejko. Quantum chemical simulation and low-temperature FTIR investigations of the structure and spectral characteristics of methanol monomer and dimer in an argon matrix. J. Spectrosc. Dyn. (2011), 1: 9.

RESEARCH OF ORGANIC-INORGANIC LAYERS

R. Dobužinskas

Department of Solid State Electronics, Faculty of Physics, Vilnius University, Saulėtekio Ave. 9-III, LT-10222 Vilnius, Lithuania
ramblerlt@gmail.com

Hybrid organic-inorganic layers of V-606, P-TPD, S-100 with ZnCdS were formed on ITO glasses by spray and spin coating methods and their absorption spectra and photoelectric properties were investigated.

a b c

Fig 1: Various layers microscopic photographs (a & c) and scanning probe 3D microscopic image (b)

Sprayed liquid tended to create spherical cap shape rather than forming thin wet layer. Full crystallization of hybrid layer with 150 mg/cm³ concentration of solution occur in 10 min. Less concentration of solution makes the process of crystallization longer. Wet layer solution was formed with thicker layer (10 μm) but during the process of drying the layer formed into porous surface which makes similar electrical properties to cap shape surface.

Spin-coated layers are even-surfaced (10%), stable and effective electrically and mechanically. Crystallization is local which ordinary starts from crystallization centre.

Both of the methods for formation of single layer demand similar duration of work. Spray coating layer formation is more effective with more samples and large-squared layers and spin-coating makes small but even and electrically better layers.

Measured optical absorption spectra of hole transport materials with different concentration and ZnCdS saline granules. The volt-ampere characteristics of different compound layers were measured. In the hole drift mobility, carrier lifetime and other interesting parameters was estimated.

[1] S. Juršėnas. Organinės optoelektronikos prietaisai, Vilniaus universitetas, Vilnius, 2008, 136.

[2] National Renewable Energy Laboratory. Best Research-Cell Efficiencies, Rev. 09-2010.

[3] C. Brabec, V. Dyakonov, J. Parisi, N.S. Sariciftci. Organic Photovoltaics Concepts and Realization, Springer-Verlag, Berlin 2003, 299.

RADAR SIGNALS SIMULATOR FOR TESTING THE DYNAMIC FREQUENCY SELECTION OF WIRELESS RADIO COMMUNICATIONS SYSTEMS OPERATING IN 5 GHz FREQUENCY BAND

Mantas Juškauskas[1], Vaidas Stadalius[2]

[1] VU-Omnitel-Huawei Telecommunications Research Center, Vilnius University, Saulėtekio 9 III, LT-10222, Lithuania
[2] UAB Wilibox, Saulėtekio 15-610, Vilnius, LT-10224, Lithuania
Mantas.Juskauskas@ff.vu.lt

The lack of available radio frequency (RF) bands leads to a solution for allowance of spectrum sharing between different communications systems. Such an example is radio local area network systems (RLAN) that operate at 5 GHz frequency band which is also used by many radar systems. The problem that occurs is that the interference between these systems becomes probable and may seriously damage the output data of radar systems. For this reason European Telecommunications Standards Institute (ETSI) has released a standard, known as ETSI EN 301 893 [1], which says that manufacturers of RLAN devices must employ the dynamic frequency selection (DFS) mechanism in order to protect radar systems. RLAN designers have to ensure the employed DFS is working properly, and a way to do that is to test RLAN devices by nearby generating radar test signal which properties are defined by ETSI standard. The task of our work was to investigate the parameters of radar test signals defined by ETSI and to create a radar signals generator as a testing device.

The DFS mechanism is necessary when RLAN devices operate at frequencies between 5250 and 5350 MHz or 5470 and 5725 MHz. In these ranges RLAN devices must detect the radar signal, stop the operation and switch to another frequency band and start the data transfer if the band is clear. According to the standard there are six types of radar signals which RLAN device must detect: 1-3rd type is a constant pulse repetition frequency signal, 4th type is a constant pulse repetition frequency signal with variable frequency modulation, 5-6th type is a staggered pulse repetition frequency signal [2]. All these types of signals differ in their pulse widths, lengths, structures, etc.

To create, realize and generate the radar test signal we chose to use the software defined radio (SDR) platform. The software part we used was the GNU Radio packet loaded on Ubuntu operational system. The hardware part was the low-cost universal software radio peripheral 2 (USRP2). Emulated signals were analyzed with Rohde & Schwarz FSH8 spectrum analyzer. The program code was written by adding the necessary syntax into the one particular GNU Radio software block. This block was useful cause of its capabilities to quickly and comfortably connect to the USRP2 device and generate a specific signal which parameters were defined in one command line.

During the time of our task we have analyzed ETSI standards and successfully prepared a program which was able to generate the 1-3rd and 5-6th type radar signals using USRP2. Fig. 1 shows the generated form of 5th type radar signal. Emulated signals were studied using spectrum analyzer and their correspondence to the standards was proven. The 4th type signal with variable frequency modulation was not implemented in our main software, but its mathematical model was made using MATLAB.

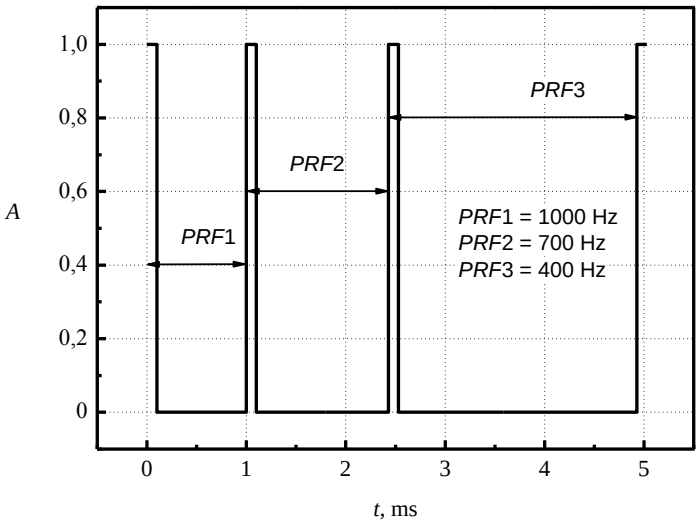

Fig. 1. The form of 5th type radar signal with three different pulse repetition frequencies (PRF)

[1] ETSI EN 301 893 V1.5.1, Harmonized European Standard (Telecommunications series). *Broadband Radio Access Networks (BRAN); 5 GHz high performance RLAN; Harmonized EN covering the essential requirements of article 3.2 of the R&TTE Directive* (2008).

[2] ETSI TR 102 651 V1.1.1, Technical Report: *Broadband Radio Access Networks (BRAN); 5 GHz high performance RLAN; Guide to the implementation of Dynamic Frequency Selection (DFS)* (2009).

ORGANIC BASED MATERIALS WITH QUANTUM DOTS FOR SILICON PHOTOVOLTAIC MODULES APLICATION

Daiva Juškevičiūtė

[1]Department of Physics, Faculty of Fundamental Sciences, Vilnius Gediminas Technical University, Saulėtekio Ave 11, LT-10223 Vilnius, Lithuania
[2]JSC „Modern E-Technologies“, Saulėtekio Ave 15, LT-10224 Vilnius, Lithuania
daiva.juskeviciute@gmail.com

Nowadays photovoltaic systems are really reliable and moderately effective but further innovations in this field are required to ensure sustainable industry growth and to increase competitive of photovoltaic technology. All standard photovoltaic modules incorporates antireflection layer usually it is tempered glass. Usage of tempered glass has its own downsides such as increased weight of PV module. Tempered glass weight limits areas where PV modules could be used. Organic based materials may be solution that can help reduce module weight.

Lighter PV modules could be made from organic based materials but all organic based materials properties decrease under UV radiation. Organic based coatings can be protected from UV by incorporating quantum dots which will absorb higher energy photons (2,5 -3,5 eV) and re-emits two or more lower energy photons (1 - 2,5 ev).

Down converting layer on silica PV element has capability to generate more than one low energy photon form a high energy photon. Down shifting process is based on luminescence effect but in this type of application the high frequency quantum that is being absorbed is converted into one long-wave quantum.

To create down converting layer Lumidot^{TM} quantum dots were being used together with Leucophor OBO organic material to form down shifting layer which absorbs light at 340-370 nm and emits in a blue range of spectrum 420-470 nm.

PV samples were coated using centrifugal coating device KW-4A. Analysis of spectral transmittance of top coating layer that incorporates CdSe-ZnS quantum dots was tested with UV-VIS spectrophotometer. The results are shown in Fig.1 .

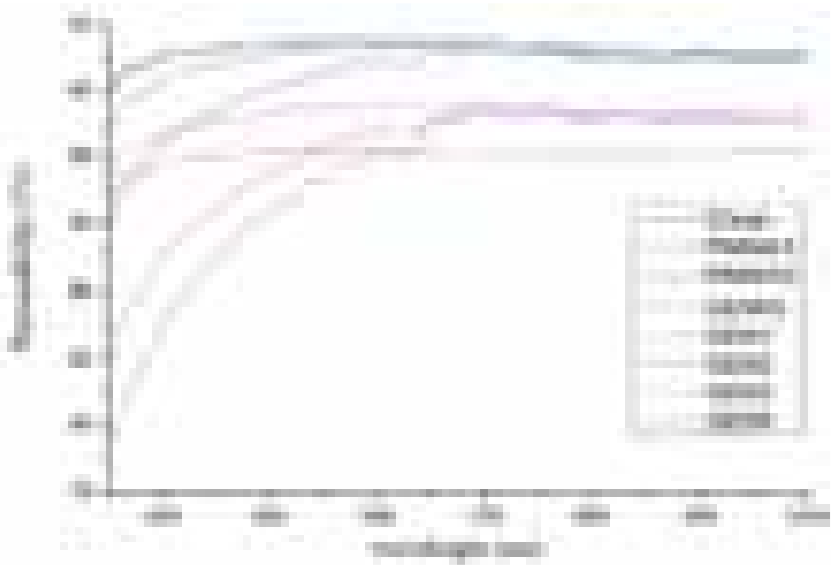

Fig. 1. Sample base and Lumidot ™ 640 solution coated specimens spectral bandwidth dependence of wavelength

Electromagnetic wave absorption can be seen in a wide (350-650 nm) wave length range. Few maximums can be seen in results chart which amplitude depends on organic solution concentration.

Results confirmed that it is possible to widen PV absorption spectrum using quantum dots in organic based materials. This method increased PV efficiency by 1 percent.

[1] M. Mohanty, A. Acharya, B. Panda et al., Characterization of ZnS Quantum dot (q-dot) by Ultraviolet Visible (UV-VIS) Absorption Spectrum Studies & Comparison with CuO Nanocrystal. Journal of American Science, 2011;7(1):348-351.
[2] S. Pillai, K. R. Catchpole, T. Trupke et al., Surface plasmon enhanced silicon solar cells. Journal of applied physics 101, 093105 (2007).

DIELECTRIC STUDIES OF BISMUTH DOPED STRONTIUM TITANATE

I. Kranauskaitė[1], Š. Bagdzevičius[1], R. Grigalaitis[1], J. Banys[1], A. Sternberg[2], K. Bormanis[2]

[1] Department of Radiophysics, Faculty of Physics, Vilnius University, Saulėtekio Ave. 9-III, LT-10222 Vilnius, Lithuania
[2] Institute of Solid State Physic, University of Latvia, Kengaraga str. 8, 1063 Riga, Latvia
Ieva.Kranauskaite@ff.stud.vu.lt

Lead containing piezoelectric ceramics and single crystals have been widely used as actuator, transducer, and sensor materials. However, the toxicity of lead oxide has led to a demand for alternative materials that are more environment friendly. $(Sr_{1-1.5x}Bi_x)TiO_3$ - strontium bismuth titanate (SBT) is one of such compounds.

It is well known that in pure incipient ferroelectrics, like $KTaO_3$ or $SrTiO_3$ polar phonons, mainly soft modes, are responsible for the dielectric permittivity and no pronounced dielectric dispersion is observed below the soft-mode frequency [1]. The ferroelectricity in such materials can be induced by application of sufficiently strong electric field, uniaxial stress or substitution of A-site ions by isovalent or heterovalent ions. Scanavi [2] discovered that $(Sr_{1-1.5x}Bi_x)TiO_3$ ceramic with small to moderate Bi content exhibits dispersion similar to relaxor ferroelectrics. Further dielectric studies on SBT ceramic (up to $x \leq 0.17$) [3, 4] showed that Bi doping induces formation of local antiferrodistortive and polar regions. This causes complex relaxational dynamics below the phonon frequency range. The aim of this work was to extend the investigations of dielectric dispersion in SBT for concentrations x=0.1 and x=0.15 to GHz range, since no broadband dielectric studies (on our knowledge) have been carried out for SBT with bigger bismuth content.

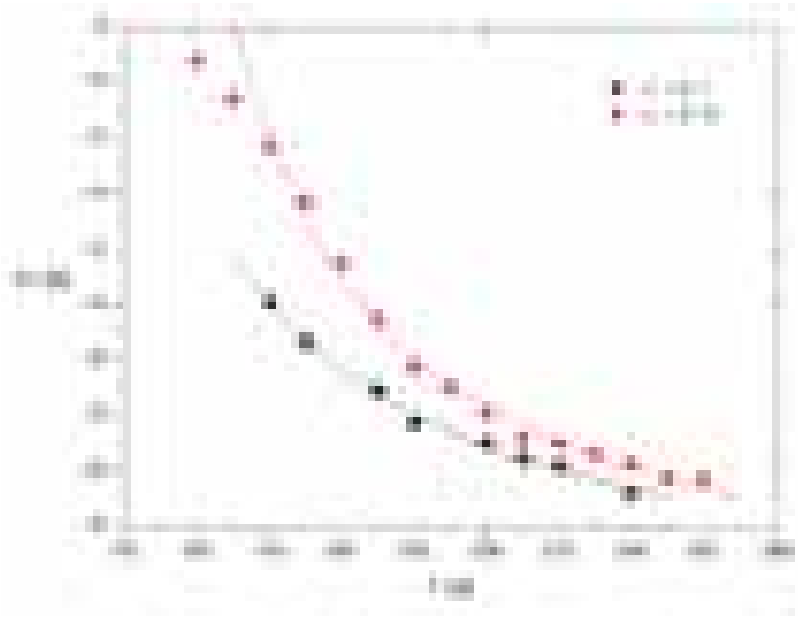

Fig 1. Mean relaxation times calculated from Havriliak-Negami formula fits. The solid lines are fits of Vogel-Fulcher relationship.

Experimental data have been analysed in terms of Havriliak-Negami formula. The obtained mean relaxation times fulfills the Vogel-Fulcher relationship with following parameters for SBT with x=0,1 and x=0,15 respectively: dipole freezing temperature T_0=60,94 K and T_0=87,93 K, dipole activation energy U=950,67 K and U=952,72 K, dipole relaxation at very high temperatures $\tau_0 = 9{,}7 \cdot 10^{-14}$ s and $\tau_0 = 7{,}69 \cdot 10^{-14}$ s.

[1] K.A. Muller and H. Burkard, SrTiO3: An intrinsic quantum paraelectric below 4 K, Phys. Rev. B. **19**, 3593-3602 (1979).

[2] G.I. Scanavi, I.J. Ksendzov, V.A. Trigubenko, and V.G. Prokhvatilov, Zh. Eksp. Teor. Fiz. **33**, 320 (1957).

[3] V. Porokhonskyy, A. Pashkin, V. Bovtun, J. Petzelt, M. Savinov, P. Samoukhina, T. Ostapchuk, J. Pokorny, M. Avdeev, A. Kholkin and P. Vilarinho, Broad-band dielectric spectroscopy of SrTiO3:Bi ceramics. Phys. Rev.B. **69**, 144104 (2004).

[4] Che Ang, Zhi Yu, P.Lunkenheimer, J. Hemberger, and A. Loidl, Dielectric relaxation modes in bismuth-doped $SrTiO_3$: The relaxor behavior, Phys. Rev B **59**, 6665-6669 (1999).

FORMATION OF FLUORESCENT ORGANIC NANOPARTICLES BASED ON 1,4-DIVINYLBENZENE DERIVATIVES

Gediminas Kreiza[1], Karolis Kazlauskas[1], Arūnas Miasojedovas[1], Eglė Arbačiauskienė[2], Vytautas Getautis[2], Algirdas Šačkus[2], Saulius Juršėnas[1]

[1]Institute of Applied Research, Vilnius University, Saulėtekio 9-III, LT-10222 Vilnius, Lithuania
[2]Department of Organic Chemistry, Kaunas University of Technology, Radvilėnų 19, LT-50254 Kaunas, Lithuania
gediminas.kreiza@ff.vu.lt

Fluorescent organic nanoparticles (FONs) with dimensions ranging from tens to few hundreds of nanometers have attracted much interest because of their potential technological application in optoelectronic systems, such as organic light emitting diodes or fluorescence sensors [1]. These nanoparticles are usually formed from non-planar molecules that are non-emissive in the solution, but demonstrate high fluorescence intensity when aggregated. The so called aggregation-induced emission (AIE) phenomenon occurs only in certain-structure-containing molecules, which leads to specific molecular packing and restriction of intramolecular torsions in the aggregated state [2].

In this work, fluorescent organic nanoparticles based on novel divinylbenzene derivatives with cyano groups were formed by a simple reprecipitation method in the aqueous phase. Different volume fractions of distilled water were injected into chromophore/THF solution under vigorous stirring. In all samples concentration of chromophore was kept constant. Consisting of different end-groups, divinylbenzene derivatives were studied and compared in regard to nanoparticle formation morphology and fluorescence turn-on ratio.

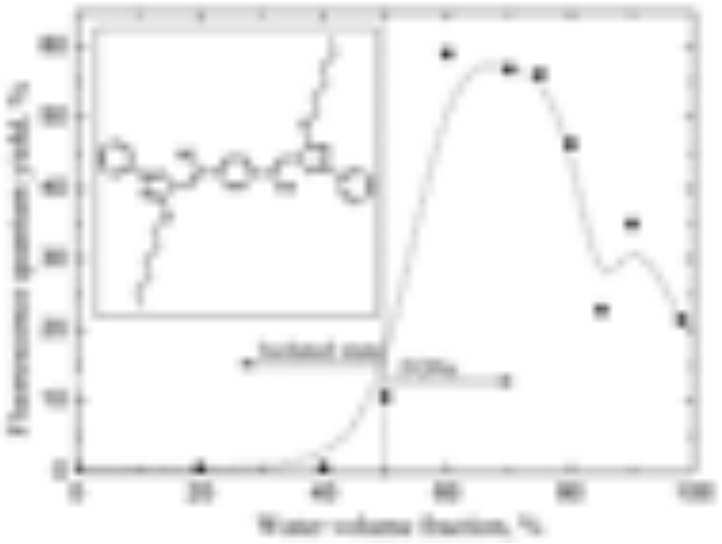

Fig. 1. Fluorescence quantum yield of the divinylbenzene derivative with cyano and pyrazole groups in THF/water mixture as a function of water volume fraction. Inset shows chemical structure of the divinylbenzene derivative. Line serves as the guide for the eye.

Formation of FONs was examined by performing optical spectroscopy and electron microscopy measurements. Isolated molecules in a dilute solution exhibited very low fluorescence quantum efficiency (0.6%). Divinylbenzene derivatives became highly emissive upon aggregation into nanoparticles due to the restriction of intramolecular torsions and due to the specific molecule arrangement in the nanoparticles. The possibility to control the fluorescence turn-on ratio by exploiting various end-groups of cyano-substituted divinylbenzene derivatives was demonstrated. Maximum increase of the fluorescence quantum yield by a factor of 100 upon formation of FONs in water/THF mixture was observed (Fig. 1.). The latter result is promising for possible technological application of divinylbenzene based FONs in sensing of water/organic vapor via fluorescence “on/off” switching.

[1] B.K. An, S.K. Kwon, S.D. Jung and S.Y. Park, Enhanced emission and its switching in fluorescent organic nanoparticles, J. Am. Chem. Soc. 124, 14410–14415 (2002).
[2] Yuning Hong, Jacky W. Y. Lamab and Ben Zhong Tang, Aggregation-induced emission, Soc. Rev. 40, 5361–5388 (2011).

OPTICAL SPECTROSCOPY OF MEROCYANINE DERIVATIVES. SIMULATION OF OPTICAL SPECTRA BY MEANS OF QUANTUM CHEMISTRY METHODS

Augė Zaveckaitė

Department of General Physics and spectroscopy, Faculty of Physics, Vilnius university,
Saulėtekio 9, korp. 3, Vilnius, Lithuania
Email: augute.z@gmail.com

Quantum chemistry calculations have been provided for ground state optimization of compound MD376 (neutral, see Fig. 1, also cationic, anionic) using *ab-initio* Hartree-Fock (HF) methods (*Gaussian03* package). Optical absorption spectrum distribution (in the near UV and visible area) of MD376 solution was explained according to the results of the optimized geometry, taking into account the fact that the MD376 compound represents an behavior of neutral, cationic and anionic forms[1-2]. Estimated molecular charge redistribution during the optical excitation was related to the recombination of structural fragments as conformational exchanges (CC bridge and diciano group).

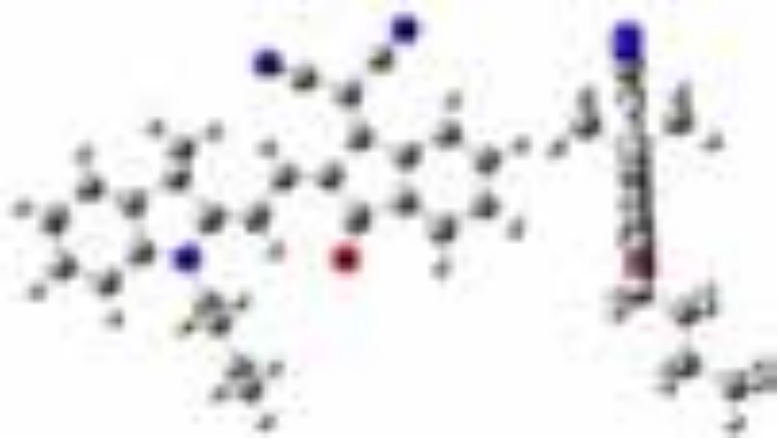

Fig. 1. Merocyanine MD376. Two projections.

Simulation of several MD376 dimeric forms (when two molecules overlaps by indan-(1-diciano) dione fragments) allows us to claim that dimer derivatives create the environmental conditions for two-sided perturbation only. Electronic absorption states of individual molecules and dimer molecules are almost identical (according to Ref. [3]).

[1] Amaresh Mishra, Rajani K. Behera, Pradipta K. Behera, Bijaya K. Mishra, and Gopa B. Behera. Cyanines during the 1990s: A Review // *Chem. Rev*. 2000, 100, 1973-2011.

[2] N. M. Kronenberg, V. Steinmann, H. Bürckstümmer, J. Hwang, D. Hertel, F. Würthner, K. Meerholz, Direct comparison of highly efficient solution- and vacuum-processed organic solar cells based on merocyanine dyes // *Adv. Mater*. 22, pp. 4193-4197, 2010.

[3] N. M. Kronenberg, M. Deppisch, F. Würthner, H. W. Lademann, K. Deing, K. Meerholz. Bulk heterojunction organic solar cells based on merocyanine colorants, *Chem. Commun.* 48, pp. 6489-6491, 2008.

Orientation of branched polymer structures by all-optical poling

Audronė Žemaitytė

Department of Advanced Technologies, Institute of Applied Research, Vilnius University, Lithuania
audrone.zemaityte@gmail.com

Optical storage is an important area for information technologies. Already lots of materials have been investigated, however, the effectiveness and rewritable qualities remain serious issues for the development. The breakthrough of organic optoelectronics gives a good chance for polymers to be developed applied as storage material. Still people from organic synthesis have ideas for creating new interesting materials, in particular, also for optical storage applications.

All-optical poling is a good experiment to investigate optical storage features of the material. The task is to create noncentrosymmetry in optically isotropic material and as a result to observe second order nonlinear optical effect. This work presents all-optical poling and relaxation processes of azophenylcarbazole chromophore doped into polycarbonate matrix forming guest-host system. The beam source was nanosecond Nd:YAG laser operating at the wavelength of 1064 nm. Noncentrosymmetry is created mixing first (ω) and second (2ω) harmonic beams of laser in the material.

New in our work is the temperature dependence of all-optical poling. The poling efficiency decreased when decreasing the temperature of the sample (temperature was changed from 150 K to 300 K). However, main result expected was a decrease of relaxation speed, when decreasing the temperature (Figs. 1 and 2). This very important result for optical storage applications will be presented and discussed.

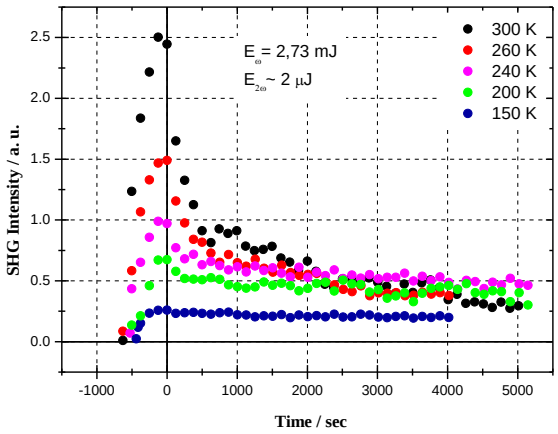

Fig.1. Second harmonic radiation measured from optical poled azophenylcarbazole in polycarbonate at different temperatures.

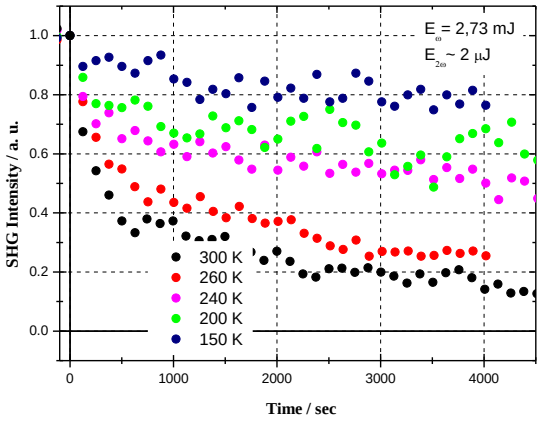

Fig.2. Decay of second harmonic radiation generated by optically poled azophenylcarbazole for different temperatures (normalized).

DEVELOPMENT OF SMART SUPPLY UNIT DESIGNED FOR TESTING QUALITY OF ELECTRICAL POWER

Rima Birškytė , Gediminas Gricius, Antanas Andrius Bielskis

Department of Informatics, Faculty of natural science and mathematics, University of Klaipėda, H.Manto st. 84,

LT-92291 Klaipėda, Lithuania

rima.birskyte@gmail.com

In the modern rapidly changing world new more and more environmentally friendly ways of producing electricity are gradually emerging, people are beginning to economise electricity. For this reason smart supply unit was designed in order to reduce consumption of electricity. It consists of a power regulator and a meter for measuring amount of energy consumed.

Model of Smart supply unit and a power regulator was designed as circuit diagram.

In the first block alternating current (~220V) falls into current transformer where during flowing along the winding of transformer induces current in the secondary winding (it consists of 1000 turns). Current of secondary winding will be used for equipment which is connected to smart unit supply designed to measure amount of energy consumed.

In the second block voltage transformer of one primal and two secondary windings is used for supplying control circuits of smart supply unit and for measuring voltage.

In the third and fourth parts of smart supply unit power regulator is shown. Opto-isolator (OK2) which is situated in the third part is used for discovering the point ‘0‘ of crossing. The forth part is used for controling level of average voltage of equipment connected to smart supply unit (with aid of Triac (T2)). Such circuits are appropriate to use when control is performed digitally. Control is performed by the programme of modulation of wave length which is situated in Atmega32 microcontroller and connected to the circuit SV2 with link.

Values of current and voltage are measured using analogical digital converter of microcontroller. After processing the values of current and voltage the values of instantaneous voltage and current are obtained, values of RMS (root-mean-square) are calculated real, apparent and reactive powers and power factor as well.

In order to control transmitted power the controling element semiconductor of alternate current is chosen, Triac (T2).This element is being opened after transfering an impulse to the controling terminal in certain time when a sinusoid is crossing the point ‘0‘. When Triac (T2) opens it transmits the current until the sinusoid of value again crosses the point ‘0‘.

Below the formula Eq.(1) is given where output voltage of power regulator is calculated:

$$V_{out} = \frac{T_{DC}}{T_{total}} \cdot V_{in} \qquad (1)$$

where $T_{total} = \frac{1}{50}$ s, V_{in} - input voltage, T_{DC} – duty cycle

The graph Fig.1 given below shows that average voltage while outgoing fluctuates proportionally the delay of opening Triac (T2)

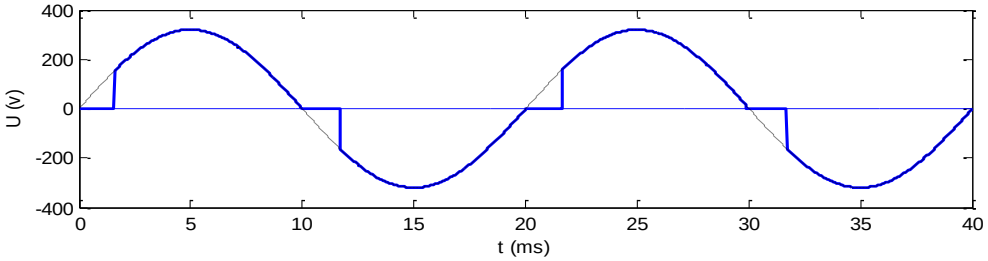

Fig.1 The phase pulse modelling.

So such method of control is characterised by spreading large amount of harmonics into network, also by the factor of little power. For this reason decent filtration is necessary.

[1] Antanas Andrius Bielskis, Antanas Kazakauskas, Aušra Jurgilait, Alina Lenkauskait, Valmantas Palikša, Edgaras Pocius, Vaida Skarulskyt, Tomas Stonys, Laimonas Žutautas. 2011. AFEKTO BUSENOS ATPAŽINIMU PAGRISTU MIKROKLIMATO KOKYBĖS RODIKLIU MATAVIMO SISTEMOS KURIMAS. // Virtualūs instrumentai biomedicinoje, Klaipėda

REPLICATION OF MICROSTRUCTURED POLYMER SCAFFOLDS AND THEIR BIOCOMPATIBILITY TESTS FOR TISSUE ENGINEERING

Evaldas Balčiūnas[1, 2, 3], Linas Jonušauskas[1], Daiva Baltriukienė[2], Mangirdas Malinauskas[1]

[1] Laser Research Centre, Vilnius University, Lithuania
[2] Institute of Biochemistry, Vilnius University, Lithuania
[3] Department of Chemistry and Bioengineering, Vilnius Gediminas Technical University, Lithuania
evaldas89@gmail.com

In the field of tissue engineering, there is a demand for many equal scaffolds made of different polymer substances. Traditional fabrication techniques such as direct laser writing (DLW) [1] are limited in their speed and have a relatively high price per scaffold. PDMS (polydimethylsiloxane) soft lithography overcomes these limitations and allows for the use of new materials that would not be processable by DLW [2]. PDMS soft lithography is a replication technique, so it requires a primary structure to be fabricated by other methods.

We have fabricated primary structures using DLW and replicated them using PDMS soft lithography in PDMS and PEG-DA-258 polymers. Scaffolds with different porosities were made to evaluate the optimal pore size suited for rabbit myogenic stem cell growth.

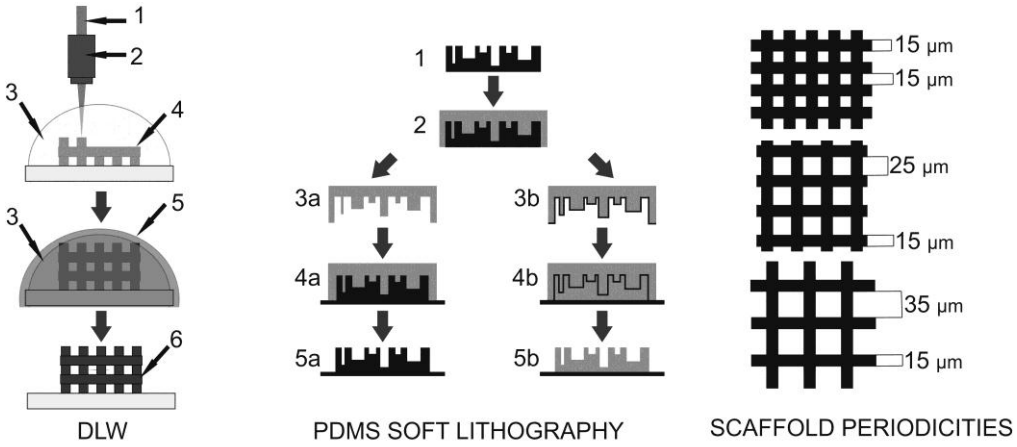

Fig. 1. DLW: 1 – laser beam; 2 – objective; 3 – monomer solution; 4 – three-dimensional structure is written by changing the spatial orientation of the laser focal point to the monomer solution; 5 – developer is used to wash out unexposed monomers; 6 – a primary structure. PDMS SOFT LITHOGRAPHY: 1 – primary structure; 2 – a PDMS stamp is acquired by pouring PDMS prepolymer over the primary structure and thermal curing; 3a – a PDMS stamp of the primary structure; 4a – the stamp is used for replication in another substance by UV curing; 5a – a replica of the primary structure. 3b – the PDMS stamp, acquired in step 2 is covered by a thin layer of gold; 4b – the stamp covered in Au is used to replicate in PDMS by thermal curing. 5b - a replica of the primary structure in PDMS. SCAFFOLD PERIODICITIES: 15|15, 15|25 and 15|35.

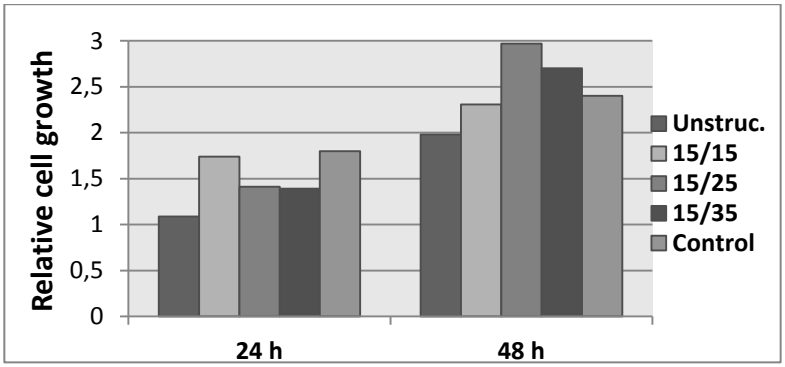

Fig. 2. Relative cell growth after 24 and 48 hours on PEG-DA-258 surface. Unstruct. – unstructured (flat) polymer surface, 15|15, 15|25 and 15|35 – scaffolds with different porosities (as in Fig. 1), Control – polystirene surface.

[1] Y. Xia, G. M. Whitesides, Soft Lithography, Annu. Rev. Mater.Sci. **28**, 153-184 (1998).

[2] A. Ovsianikov, S. Schlie, A. Ngezahayo, A. Haverich, B. Chichkov, Two-photon polymerization technique for microfabrication of cad-designed 3D scaffolds from commercially available photosensitive materials, J. Tissue Engin.Regen. Med. **1**, 443-449 (2008).

EFFECTIVE INACTIVATION OF RESISTANT *SALMONELLA ENTERICA* : COMBINED PHOTOSENSITIZATION AND PULSED UV LIGHT TREATMENT

Rita Kokstaite, Kristina Kairyte, Irina Buchovec, Zivile Luksiene

Institute of Applied reserch, Vilnius University, Sauletekio 10, 10223, Lithuania
r.kokstaite@gmail.com

Salmonellosis is one of the most common food-borne diseases in the world. Foods commonly involved in transmission of *Salmonella* spp. include eggs, meat and meat products, unpasteurized milk, raw poultry, fresh vegetables and fruits. The major existing technologies for food preservation have various shortages, for example, thermal effects, which usually induce different physical and chemical changes in the food. In this context, modern light technologies, including high power pulsed light and photosensitization might serve as promising antibacterial tools. Therefore, the aim of this study was to evaluate the susceptibility of resistant Gram (-) food-borne pathogen *S. enterica* to photosensitization and pulsed UV light.

Photosensitization is based on interaction of three indispensable components: photosensitizer, light and oxygen. There are two mechanisms by which photosensitizer can react with biomolecules, and eventually induce unrepairable injuries and cell death: Type I radical-based reactions and type II – oxidation-based reactions [1].

Pulsed UV light (200–1,000 nm, maximal emission at 260 nm, pulse duration t = 112 μs, frequency 5 Hz, power of each pulse ranges from 0.07 to 0.9 MW) is FDA approved technology for decontamination of food or food-related surfaces. The main target for this UV-light based treatment is bacterial DNA [2]. Formation of unrepairable pyrimidine dimers influences transcription and replication processes and is lethal injury for bacteria.

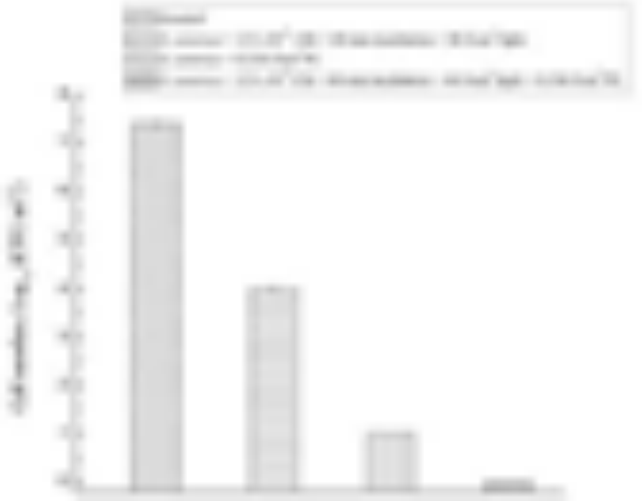

Fig. 1 Inactivation of *Salmonella enterica* by the combined treatment of Chl–based photosensitization and pulsed UV light

According to our data, *Salmonella enterica* due to complicated structure of cell wall is resistant to photosensitization treatment, but might be effectively inactivated by pulsed light. Combined treatment of pulsed UV light and photosensitization diminishes bacterial counts to undetectable level and enables to reduce the exposures of both treatments what is very important developing hurdle technologies. Moreover, no regrowth of bacterial culture was observed even at 12 h after combined treatment of photosensitization and pulsed UV light. Thus, our results confirmed that combining photosensitization with pulsed UV light might be effective tool to combat Gram (-) bacteria *S. enterica* in environmentally friendly way.

[1] D. P. Häder, G. Jori, *Photodynamic therapy*, chapter 1, 3-4, (2003).
[2] V. M. Gomez – Lopez, P. Ragaert, J. Debevere and F. Devlieghere, *Trends in Food Science & Technology*, 18, 464 – 473, (2007).

VARIOUS WAYS OF INTRODUCING HERDING BEHAVIOR INTO THE AGENT BASED MODELS OF COMPLEX SYSTEMS

Petras Purlys[1,2], Aleksejus Kononovicius[2], Vygintas Gontis[2]

[1]Faculty of Physics, Vilnius University
[2]Institute of Theoretical Physics and Astronomy, Vilnius University
petras.purlys@gmail.com

Most of the complex systems can not be understood using traditional physicists approach. Complex systems exhibit behavior essence of which lies in the interaction of the different parts inside the system. As complex systems include not only physical, but also social and economical systems, it is convenient to introduce agents - very general concept describing varying parts of the systems (ex. atoms, humans, animals). One of the signature features of human society as a complex system is that it creates orderly structures - political ideologies, religions, fan clubs, brand-name phenomena and etc. While speaking very generally these observations can be blamed on the human herding instinct. Thus a successful agent based model should pay attention of how effective is its description of agents' herding.

Evidently there are two distinct simple ways (actually there is a third more complex - network modeling - way) to treat herding behavior - agents might be allowed to interact with single colleague per time step (ex. a friend recommends to watch the movie) [1] or might be in some way coupled to the source of information expressing opinion of each agent in the system (ex. mass media, social networks) [2]. Unidirectional version of Kirman's model and the GLM model were shown to have the same asymptotic behavior as renowned Bass diffusion model, which describes diffusion of successful products in the market [3, 4]. From our point of view it is rather interesting to see how well these distinct definitions of herding behavior work in case of bidirectional transitions. Note that while Kirman's model was originally defined as bidirectional birth-death process [1], the GLM model was defined only as unidirectional process [2]. Thus introducing the bidirectionality into the GLM model is the main novelty presented in this work.

Following the mathematical formalism of the GLM model and applying ideas of bidirectional transitions by Kirman, let each agent occupying state s_1, here X is their number, to move to state s_2 with probability:

$$p(s_1 \to s_2) = 1 - (1-\Sigma_1)(1-H)^{N-X}, \tag{1}$$

consequently $N-X$ agents occupying state s_2 can move to s_1 with probability:

$$p(s_2 \to s_1) = 1 - (1-\Sigma_2)(1-H)^{X}. \tag{2}$$

In the above probabilities H is present in the herding terms (thus it has a meaning of probability to be recruited by the herd during the time step), while Σ_i represents individual transitions (also during the time step). Both H and Σ_i can be assumed to be linearly dependent on the time step ($\Sigma_i = \sigma_i \Delta t$, $H = h\Delta t$) [2].

By expanding the bidirectional transitions probabilities of the GLM model in the short time step limit, $\Delta t \to 0$, one can obtain per-agent transition probabilities identical to the Kirman's model:

$$p(s_1 \to s_2) \approx [\sigma_1 + h(N-X)]\Delta t = \frac{p(X \to X-1)}{X}, \quad p(s_2 \to s_1) \approx [\sigma_2 + hX]\Delta t = \frac{p(X \to X+1)}{N-X}, \tag{3}$$

where $p(X \to X \pm 1)$ is a Kirman model one-step transition probabilities. This result serves as analytical proof that in the aforementioned limit of short time steps we can use the results obtained for Kirman model and its financial market treatment [5] towards the GLM model.

In this contribution we have shown that the GLM model and Kirman model describe asymptotically identical behavior. These models agree well in the limit of small time steps, though note that the selection of the time step should inversely depend on the square of the size of the system, $\Delta t \sim N^{-2}$.

To reach the main conclusion one needs to recall that the GLM model describes agent-to-community interaction during the time step, while Kirman's model is concerned with agent-to-agent interaction during the time step. The asymptotic agreement of the models might be interpreted via Monte Carlo method formalism - completely random polling is statistically the same as polling whole population.

---

[1] A. P. Kirman, Ants, rationality and recruitment, Quarterly Journal of Economics **108**, 137-156 (1993).
[2] J. Goldenberg, B. Libai, E. Muller, Using Complex Systems Analysis to Advance Marketing Theory Development, Academy of Marketing Science Review **01** (9), 2001.
[3] V. Daniunas, V. Gontis, A. Kononovicius, Agent-based versus macroscopic modeling of competition and business processes in economics, ICCGI 2011, The Sixth International Multi-Conference on Computing in the Global Information Technology, 84-88 (2011).
[4] G. Fibich, R. Gibori, E. Muller, *A Comparison of Stochastic Cellular Automata Diffusion with the Bass Diffusion Model* (NYU Stern School of Business, 2010).
[5] A. Kononovicius, V. Gontis, Agent based reasoning for the non-linear stochastic models of long-range memory, Physica A **391**, 1309-1314 (2012).

EVALUATION OF OPTICAL PROPERTIES EMPLOYING CUSTOM AUTOMATED MEASUREMENT SETUP

Ieva Gražulevičiūtė[1], Tomas Tamulevičius[2]

[1] Department of Physics, Kaunas University of Technology, Lithuania
[2] Institute of Materials Science, Kaunas University of Technology, Lithuania
ieva.grazuleviciute@stud.ktu.lt

The precise control of optical properties such as refractive index or absorption coefficient is essential in optical technologies. There exist several optical metrology techniques that enable determination of optical constants and critical dimensions, i.e. refractometry, spectroscopic ellipsometry, scatterometry, evanescent wave sensors [1], etc. As it was demonstrated previously [1] spectral analysis of polarized light reflected from the diffraction grating enables determination of the dielectric function of the material in vicinity of the grating surface. In order to achieve better accuracy and repeatability of the measurements a motorized goniometric stage with automated spectra acquisition was designed and fabricated. The setup can be employed in angular reflectance or transmittance measurement configurations covering polarized visible wavelength range light. In this work possible application of the measurement setup for determination of the Brewster angle is presented.

Measurement setup consisted of a white light source (incandescent light bulb), collimating optics (three fused silica lenses), a Glan-Taylor polarizing prism on motorized rotational stage and motorized sample/detector goniometric stage (full step resolution 0.6 arcmin, Standa). The reflected light was coupled to the optical fiber via a quartz lens and the spectra were measured with AvaSpec-2048 spectrometer (spectral range: 360-860 nm, resolution 1.2 nm, Avantes). The angular polarized light reflection spectra measurements from fused silica and indium tin oxide (ITO, Sigma Aldrich) were performed (see Fig. 1 a, b). Experimental results were compared with theoretical calculations obtained employing equations (1) and (2) [2, 3]:

$$R_P = \left| \frac{-n^2 \cos\theta + \sqrt{n^2 - \sin^2\theta}}{n^2 \cos\theta + \sqrt{n^2 - \sin^2\theta}} \right|^2 \quad (1)$$

$$R_S = \left| \frac{\cos\theta - \sqrt{n^2 - \sin^2\theta}}{\cos\theta + \sqrt{n^2 - \sin^2\theta}} \right|^2 \quad (2)$$

where R_P and R_S are reflection coefficients for s and p polarizations respectively, n – refractive index of the specimen, θ – angle of incidence.

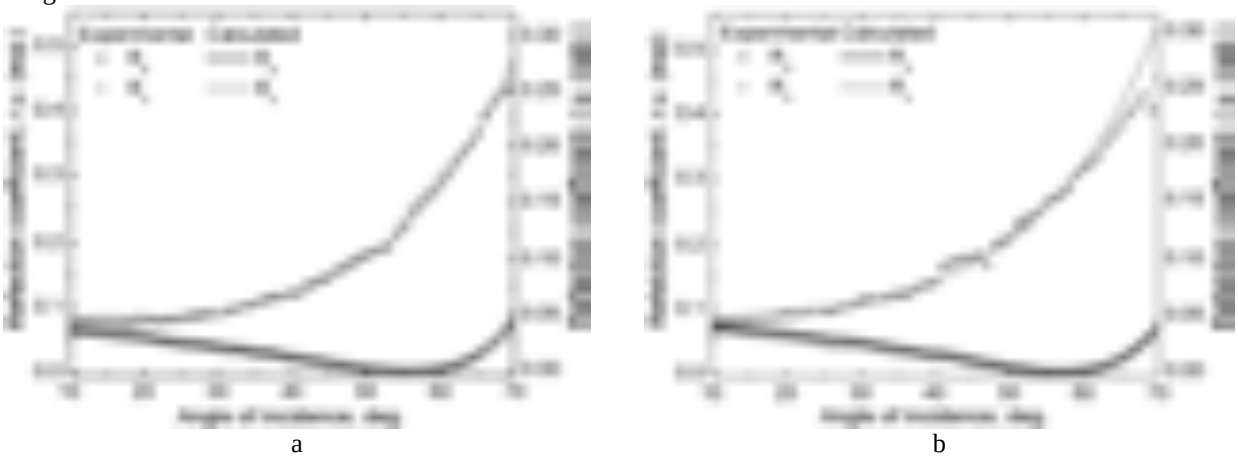

a b

Fig. 1. Experimental and calculated (eq. (1-2)) reflection coefficient values obtained for different types of polarization vs. angle of incidence for two different materials: a – fused silica; b – ITO. Analysis was performed at 589.29 nm wavelength and 10-70° angle range with increment of 1°.

We have demonstrated that the experimental setup is suitable for angular reflectance measurements covering polarized visible wavelength range light. From the experimental results we have estimated the Brewster's angle for fused silica - 55.92° and ITO - 57.13° that are in good agreement with theoretical (calculated) results - 55.55° and 56.57° respectively.

[1] T. Tamulevičius et al., Total internal reflection based sub-wavelength grating sensor for the determination of refractive index of liquids, Photonics Nanostruct. Fundam. Appl 9, 140–148 (2011).

[2] M. Born, E. Wolf, Principles of Optics, sixth ed. Pergamon Press, Oxford, 1980.

[3] http://www.cvimellesgriot.com/products/Documents/Catalog/Dispersion_Equations.pdf

RAMAN STRUCTURAL STUDIES OF LOW CONCENTRATION IONIC LIQUID AQUEOUS SOLUTIONS

Tautvydas Junkna, Jonas Kausteklis, Martynas Pareigis,Valdemaras Aleksa

[1]Department of General Physic and Spectroscopy, Faculty of Physics, Vilnius University, Lithuania

juknat@gmail.com

jonas.kausteklis@gmail.com

Ionic liquids possess interesting properties, for more than twenty years they have been the subject of a lot of experimental and theoretical investigations. Many interesting phenomena are observed in ionic liquids aqueous solutions [1,2]. Many applications of ionic liquids forced us to investigate ionic liquid and water solutions at low concentration of water.

Raman spectra of 1-decyl-3-methyl imidazolium bromide/water and 1-decyl-3-methyl imidazolium chloride/water solutions at different concentrations of water were recorded. Critical micelle concentration and anion influence on it in ionic liquids aqueous solutions were explained. Two-dimensional correlation analysis let us look deeper in imidazolium ring stretching modes frequency shift (Fig.1).

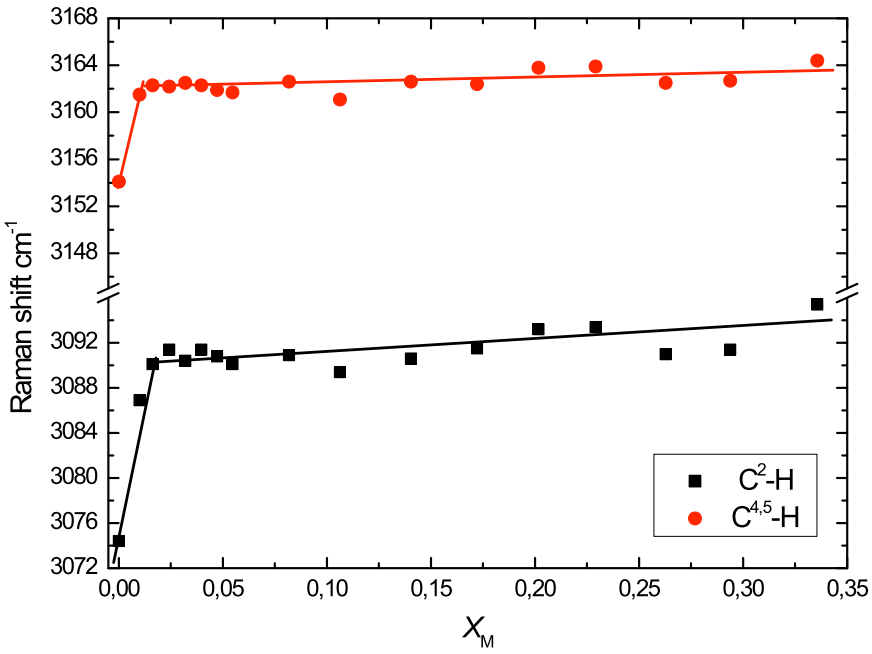

Fig. 1. 1-decyl-3-methyl-imidazolium chloride and water mixtures Raman spectral bands

$\nu_{C^2\text{-}H}$ and $\nu_{C^{4,5}\text{-}H}$ shift in OH stretching region.

[1] V. Aleksa, J. Kausteklis, V. Klimavicius, Z. Gdaniec, V. Balevicius. Raman and NMR spectroscopy study of liquid crystalline ionogel phase in ionic liquid/H2O mixtures: The states of water. J. Mol. Struct. 2011, 933, 91–96.

[2] V.Balevičius, Z.Gdaniec, L.Džiaugys, F. Kuliešius and A. Maršalka. 1H, 13C NMR and DFT Study of Hydrogen Bonding in Imidazolium-based Ionic Liquids. Acta Chim. Slov. 2011, 58, 458–464.

EFFECTS OF PROTEIN AND LIGHT ON STABILITY OF CdSe/Zn-TGA QUANTUM DOTS IN AQUEOUS MEDIA: SPECTROSCOPIC STUDY

Agnė Kalnaitytė[1*], Saulius Bagdonas[1] and Ričardas Rotomskis[2]

[1] Quantum Electronics Department, Faculty of Physics, Vilnius University, Saulėtekio ave. 9, c. 3, LT-10222, Vilnius, Lithuania
[2] Vilnius University Institute of Oncology, Baublio 3b, LT-08406, Vilnius, Lithuania
agne.kalnaityte@ff.stud.vu.lt

Quantum dots (QDs) - semiconductor nanometer-size particles are promising fluorescent markers. Compared with organic dyes, QDs have a narrow and tunable emission band, broad absorption and sharp emission spectra, high brightness, enhanced photostability, resistance to chemical degradation and photobleaching [1]. The research on QDs is important in order to provide safe and effective biosensing materials for medicine [2].

In this study, absorption and steady state spectroscopy measurements were performed on CdSe/ZnS quantum dots coated with thioglycolic acid (TGA) in biological model system. Stability, photostability and spectral properties of quantum dots were investigated in aqueous media to reveal the effects of QDs interaction with bovine serum albumin (BSA) (Albumin, V fraction, M=69000 g/mol, Carl Roth GmbH, Germany).

It was found that protein increases photoluminescence (PL) intensity of QDs straight after its addition (Fig. 1a). Interaction of quantum dots with BSA caused a blue shift of photoluminescence band from 548 nm to 545 nm. PL intensity of CdSe/Zn-TGA quantum dots solution with protein was the most intensive on the second day. However, the PL intensity of QDs without BSA was decreased (Fig. 1b). It seems that protein interaction with quantum dots increases a photoluminescence quantum yield and makes them more stable. This effect could be resulted by formation of a new layer of quantum dot coating [3].

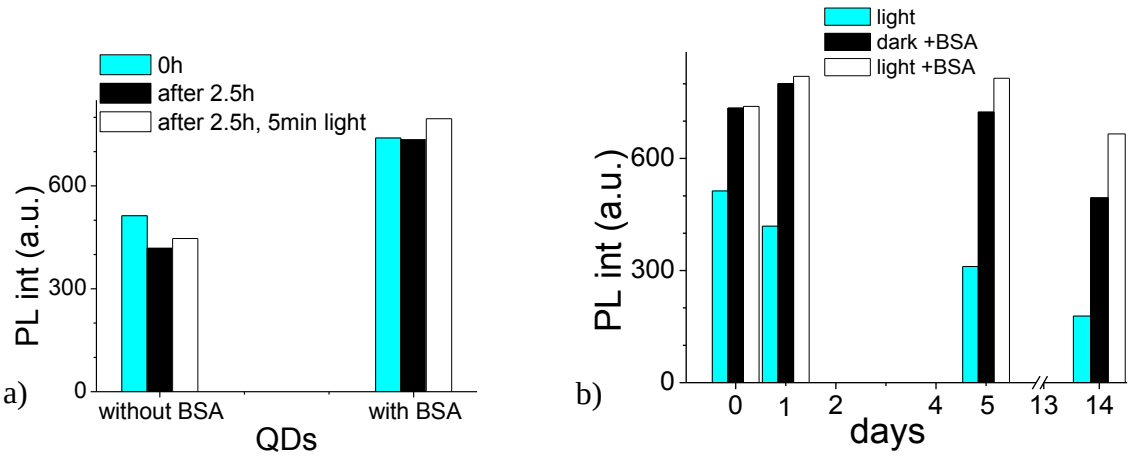

Fig. 1. a) Quantum dots solutions with and without protein 0 hour, after 2.5 hours (before exposition of laser light) and after 5 minute exposition. b) The photoluminescence intensity of quantum dots solution during days, when it was lightened with laser, and samples of QDs with BSA (one sample was exposed to laser light or another was not exposed).

Samples in quartz cuvette were exposed to laser light (532 nm, 35 mW/cm^2) to measure photostability. A uniform decrease in PL intensity occurred during 2.5 h in QDs solution, but for QDs with BSA this decrease was not observed (Fig. 1a). Laser light immediately increased PL intensity of QDs and also made samples more stable. As figure 1b shows, the PL intensity of the samples, which were exposed to light, decreases less when all samples are kept in the dark. Also, photoluminescence intensity of QDs decreased less in exposed solution with BSA during 14 days. The CdSe/Zn-TGA quantum dots in aqueous media were the most stable with bovine serum albumin and exposed to laser light. It seems that both light expose and protein can be used to enhance QDs the photoluminescence intensity.

[1] Liang Li, Huifeng Qian, Nenghu Fang, Jicun Ren., Significant enhancement of the quantum yield of CdTe nanocrystals synthesized in aqueous phase by controlling the pH and concentrations of precursor solutions, Journal of Luminescence **116** (2006) 59-66.

[2] J. Drbohlavova, V. Adam, R. Kizek and J. Hubalek., Quantum Dots Characterization, Preparation and Usage in Biological Systems, Int J. Mol. Sci 2009, **10**, 656-673.

[3] M. Matulionytė, D. Motiekūnas, V. Poderys, R. Rotomskis. CdTe quantum dots stabilization by protein in agueous solution. Laser Applications in life Sciences, edited by Matti Kinnunen, Risto Myllyla, Proc. of SPIE Vol. 7376, 737603, (2010).

TERAHERTZ RESPONSIVITY AND LOW-FREQUENCY NOISE STUDY OF BIASED SILICON CMOS DETECTORS

Vladimir Kornijčuk[1], Jonas Matukas[1], Sandra Pralgauskaitė[1], Vilnius Palenskis[1], Alvydas Lisauskas[2]

[1] Radiophysics Dep. of Vilnius University, Saulėtekio 9 (III), 10222 Vilnius, Lithuania
[2] Physikalishes Institut, Goethe-Universitat, Max-von-Laue-Str. 1, D-60438 Frankfurt am Main, Germany
Vladimir.Kornijcuk@ff.stud.vu.lt

There is an increased interest in terahertz technologies for imaging and spectral analysis in security, medical and inspection applications. That is why research of new terahertz detector types for almost a decade has been one of the „hottest" trends in solid state physics [1]. By means of new opportunities given by modern physics and technologies, several detector types were proposed. Unfortunately their operation is often bond to low temperatures. Alternative way of detecting THz frequencies is based on plasma wave excitation in ballistic field effect transistors (FETs) and for the first time was proposed by M. Dyakonov and M. Shur [2, 3]. It appears that such detectors can operate at room temperatures. Theory additionally suggested few important conclusions: 1) plasma wave frequency can be tuned by the gate voltage, 2) depending on external factors, detectors can work as resonant or non-resonant, 3) detector operation has no temperature restrictions [1].

Detector theory also predicts possible improvement of signal detection by current biasing transistor channel. However, experimental studies present, that in these conditions, device noise increases drastically, what can lead to the lower signal to noise ratios than in not biased devices. In order to clarify this matter, we present low frequency noise and detection characteristics study of silicon based CMOS detectors in both biased and not biased regimes.

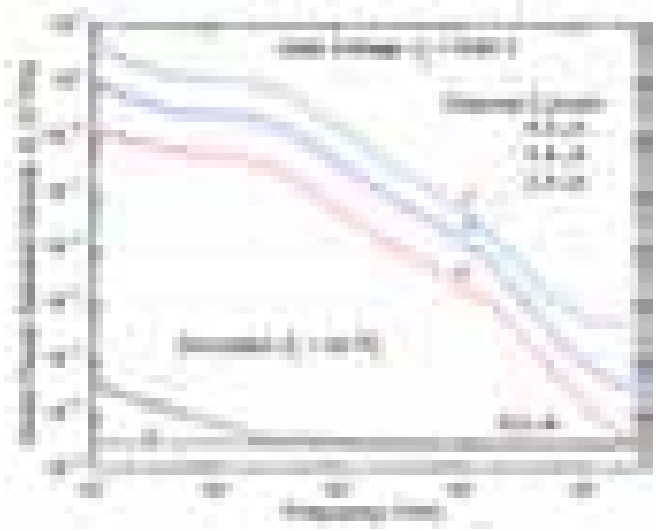

Fig. 1. Detector noise power spectral density dependences on frequency at different operation conditions.

Fig 1. represents noise power spectral density dependence on frequency while transistors gate voltage is set to 0,64 V and it operates at different bias conditions. One can notice, that at zero bias the only noise source at middle and high frequencies is channel thermal noise (it perfectly matches its theoretical value given by $4kTR$, where R is channel differential resistance) but at currents higher than 0 μA, it is strongly exceeded by $1/f$ and generation-recombination (GR) type fluctuations. The reason of such strong excessive noise is random carrier generation-recombination processes through impurities and GR centers dislocated in both transistors channel and oxide layer. Moreover, by driving detectors close to the saturation currents, differential resistance increasement (what leads to channel thermal noise increasement) should be taken into account as well.

All in all, although silicon CMOS technology based detectors can experience significant signal increase with applied current, this enhancement is strongly threatened by excessive $1/f$ and GR type fluctuations and thermal channel noise increasement with applied source to drain voltage.

[1] D.Seliuta, E. Širmulis, Z. Martūnas, V. Tamošinas, J. Devensos, A. Juozapavičius, G. Valušis, Rezonansinės ir nerezonansinės terahercinės spinduliuotės detekcija nanometriniais lauko tranzistoriais, Puslaidininkių fizikos instituto XVII mokslinės konferencijos darbai, Vilnius, 57 (2006).

[2] M. Dyakonov, M. Shur, Shalow water analogy for a ballistic field effect transistor: new mechanism of plasma wave generation by dc current, Phys. Rev. Lett. 71, 2465-2468 (1993).

[3] M. Dyakonov, M. Shur, Detection, Mixing, and Pnr equency Multiplication of Terahertz Radiation by Two-Dimensional Electronic Fluid, IEEE Transactions on electron devices Vol. 41, No. 3 (1996).

MECHANOSYNTHESIS AND CHARACTERIZATION OF IRON NANOCOMPOSITES BY MOSSBAUER SPECTROSCOPY

Aurimas Krauleidis, Jonas Reklaitis

Center for Physical Sciences and Technology, Savanoriu ave. 231, LT-02300, Vilnius, Lithuania
Aurimas.Krauleidis@ff.stud.vu.lt

The synthesis of the iron oxide particles have been a field intense study due to the novel properties and potentiality on the practical applications to ferrofluids [1], high density magnetic recording and microwave devices [2]. Various preparation techniques, such as sol-gel method, chemical precipitation [3] and mechanical alloying [4] are used to produce ferrite nanoparticles.

In this study iron oxide nanocomposites were synthesized by high energy ball milling of iron(II) sulfate, iron(III) hidroxide – sulfate and sodium hidroxide. The synthesis equation was:

$$FeSO_4 + 2Fe(OH)SO_4 + 6NaOH \rightarrow Fe_3O_4 + 3Na_2SO_4 + 4H_2O \quad (1)$$

The physical parameters governing the milling process have been strictly controlled so as to achieve the results. Samples were taken after different synthesis time. It was determined, that black precipitates formed faster than 15 minutes of milling (Fig. 1,2.). According to Mossbauer sprectroscopy measurements in 13 K temperature, the synthesized iron oxide nanoparticles were similar to magnetite (Fe_3O_4), which have feromagnetic properties. From XRD measurements it was found that the magnetite formed during mechanical milling. In room temperature Mossbauer spectra shows paramagnetic characteristics, which can be related to very small (<10 nm) magnetite particles. Particles size were studied by X-ray diffraction, which shows that after 8 h of milling formed about 5 nm particles. It was also determined, that planetary mill wears out, because the fraction of iron was detected in samples. Mossbauer results also showed, that the chemical composition of samples does not depend on milling time.

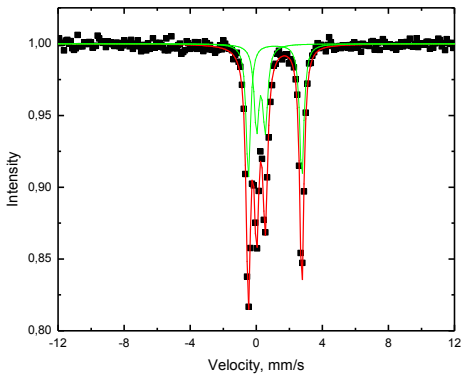

Fig. 1. Mossbauer spectra of precursor.

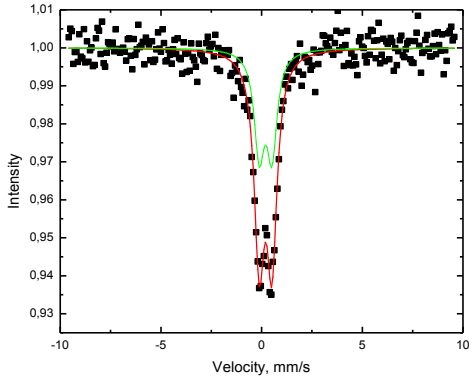

Fig. 2. Mossbauer spectra after mechanical milling at 360 rpm for 15 min.

[1] B.M. Berkovsky, V.F. Medvedev, M.S. Krakov, Magnetic Fluids: Engineering Applications, Oxford University Press, Oxford, 1993.
[2] A.K. Giri, E.M. Kirkpatrick, P. Moong khaml lang, S.A. Majetich, J. Appl. Phys. Lett. 80
[3] W. Roos, J. Am. Ceram. Soc. 63 (1980) 601.
[4] Y. Shi, J. Ding, X. Liu, J.Wang, J. Magn. Magn. Mater. 205 (1999) 249.

STUDY OF SOLVATATION IN 1-DECYL-3-METHYLIMIDAZOLIUM BASED IONIC LIQUID SOLUTIONS BY RAMAN SPECTROSCOPY

Jonas Kuliešius, Arnas Drazdauskas, Martynas Pareigis, Valdemaras Aleksa, Vytautas Balevičius

Faculty of Physics, Vilnius University, Lithuania
jonas.kuliesius@ff.stud.vu.lt

Stretching frequency of C2-H bond in 1-decyl-3-methylimidazolium ionic liquids with different anions in organic solutions depends on the strength of H-bond between H atom and the anion [1]. Therefore spectral band position of C2-H stretching vibration could provide information about the effects of solvatation [2].

In this work Raman spectra of different 1-decyl-3-methylimidazolium chloride solutions (with different dipole moment solvents) were registered (Fig. 1) using Fourier transform Raman scattering spectrometer.

Fig. 1. Raman spectra of different solutions containing 1-decyl-3-methylimidazolium chloride in the region of C2-H stretching vibrations

The spectral band in question of 1-decyl-3-methylimidazolium chloride was registered at 3142 cm^{-1}. Spectral bands of solutions are blueshifted by about 20 cm^{-1} compared to the corresponding spectral lines of pure IL's.

As shown in Figure 2, the different shift of C2-H band is obvious when using different dipole moment solvents and IL containing bromide anion. This correlates with the results obtained using FTIR-ATR spectrometry. However when using IL with chloride anion, the C2-H band displays no such behavior.

This can be explained when taking into consideration the IL's ability to form complex structures in aqueous solutions.

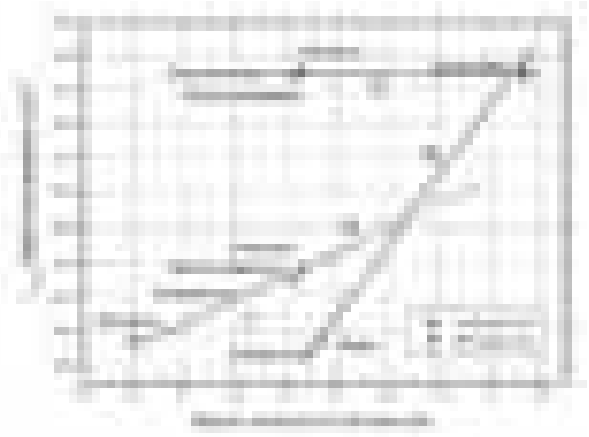

Fig. 2. $\nu_{C2\text{-}H}$ band dependancy on dipole moment of solvents

[1] Yan Gao, Liqun Zhang, Yong Wang, and Haoran Li, Probing Electron Density of H-Bonding between Cation-Anion of Imidazolium-Based Ionic Liquids with Different Anions by Vibrational Spectroscopy, J. Phys. Chem. **B 114**, 2828–2833 (2010).

[2] Yoonnam Jeon, Jaeho Sung, Doseok Kim, Chungwon Seo, Hyeonsik Cheong, Yukio Ouchi, Ryosuke Ozawa, and Hiro-o Hamaguchi, Structural Change of 1-Butyl-3-methylimidazolium Tetrafluoroborate + Water Mixtures Studied by Infrared Vibrational Spectroscopy, J. Phys. Chem. **B 112**, 923-928 (2008).

FT-RAMAN SPECTROSCOPY OF VARIOUS CARBON STRUCTURES

Ieva Puodžiūtė, Inga Rumskaitė, Justinas Čeponkus and Valdas Šablinskas

Faculty of Physics, Vilnius University, Saulėtekio Ave. 9-III, LT-10222 Vilnius, Lithuania
iewute.puodzius@gmail.com; inga.rumskaite@ff.stud.vu.lt

Carbon structures are very perspective and important materials in the field of physics, chemistry, medicine and material sciences. Nowadays science still faces a problem identifying various carbon structures in mixture samples. Therefore the goal of this project is to investigate main carbon structures: diamond, graphite, fullerene, multi-walled carbon nanotubes (MWCNT), single-walled carbon nanotubes (SWCNT), and functionalized carbon nanotubes with hydroxyl group by the means of FT-Raman spectroscopy in order to find a suitable experimental technique to identify various carbon structures in their mixtures. Conventional Raman spectroscopy is difficult to apply to study carbon structures due to the fact that in many cases the Raman spectra are disturbed by strong fluorescence background. FT-Raman spectroscopy with NIR excitation is easy, fast, cheap and precise method to study such complicated structures [1]. In FT-Raman spectrometers Nd:YAG laser (1064 nm) is usually used for the Raman excitation, the photon energy is too low to excite fluorescence. High sensitivity, high speed and possibility to average high number of spectral scans allow to observe even very weak spectral bands in the FT-Raman spectra.

The samples were prepared using "*pallet*" technique (except diamond crystal). Carbon materials were mixed with potassium-bromide (KBr) powder in proportion of 1:5000 and mechanical pressure of 10 ton per cm^2 was applied. Measurements were performed using a FT-Raman spectrometer MultiRAM from "Bruker". The spectra were measured in range of 3600 to 50 cm^{-1}. Raman spectra of various carbon structures are presented in figure 1.

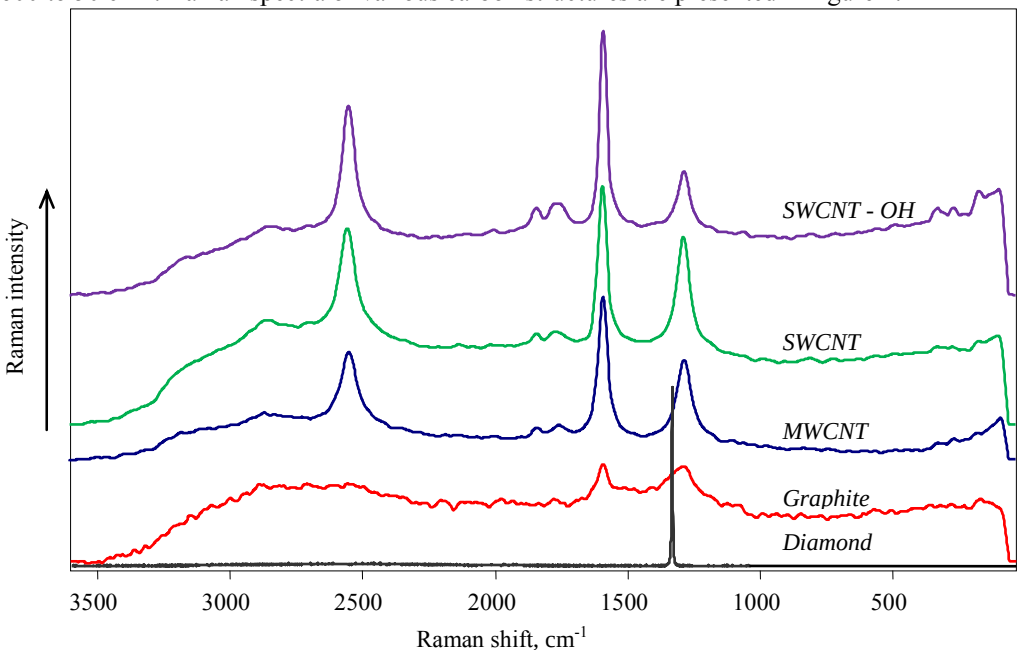

Fig. 1. FT-Raman spectra of various carbon structures (diamond, graphite, MWCNT, SWCNT, SWCNT-OH)

As can be seen in the figure, pure diamond has a very intense narrow band at 1332 cm^{-1}, because of its highly ordered structure. Graphite has two weak bands at 1285 cm^{-1} and 1589 cm^{-1} [2]. The same bands are observed in the spectra of nanotubes, but being much stronger than in graphite. The band at 1589 cm^{-1} seems to be the most important one for characterization of carbon nanotubes. The band localized at 2551 cm^{-1} also is characteristic for carbon nanotubes and is attributed to the first overtone of 1589 cm^{-1} band. A low-frequency weak band at 171 cm^{-1} is attributed to the breathing mode (RBM – radial breathing mode) of nanotubes [1]. This spectral band is often used to determine the length to radius ratio in nanotubes under study.

Our results show that FT-Raman with NIR excitation spectroscopy can be efficiently used for qualitative and quantitative analysis of various carbon compounds.

[1] T. Belin, F. Epron. Characterization methods of carbon nanotubes: a review, Materials Science and Engineering B, 119 (2005) 105–118).

[2] C. Stephan, T.P. Nguyen, M. Lamy de la Chapelle, S. Lefrant, C. Journet, P. Bernier. Characterization of singlewalled carbon nanotubes-PMMA composites, Synthetic Metals, 108 (2000)139–149.

ON THE ORIGIN OF STRUCTURE OF ACETONITRILE C≡N STRECHING RAMAN BAND

Linas Tamašauskas, Valdemaras Aleksa, Vytautas Balevičius, Martynas Pareigis

Vilnius University, Faculty of Physics, Department of General Physic and Spectroscopy,
Saulėtekio al. 9 – 3, LT – 10222 Vilnius, Lithuania
linas.tamasauskas@ff.stud.vu.lt

The study of the vibrational and orientational dynamics of acetonitrile molecules is attracting the attention of researchers for a long time. Acetonitrile contains a highly environment sensitive C≡N stretch mode at 2252cm^{-1}. There are believed that asymmetric shoulder of ν_2 band shows intermolecular effects – AN in the liquid state may be in monomer (M) and aggregated (dimer (D)) states [1,2], whereas in others works it is attributed to the hot band [3,4].

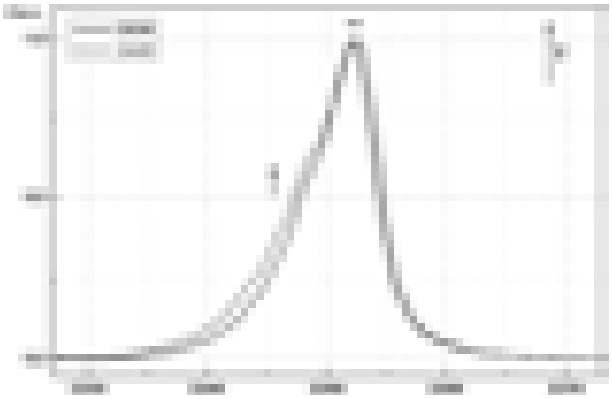

Fig. 1. Raman scattering spectra of acetonitrile in C≡N stretching region in 295, 344 K temperatures.

Raman scattering spectra of pure acetonitrile in the C≡N stretching region were recorded in altering the temperature within 296 – 361 K and 248 – 295 K. Experimental spectra of acetonitrile mode (C≡N) were processed using two dimensional (2D) correlation method. The structure of C≡N stretching band which consist of several peaks is considered. Analysis of the different overlapping Lorentzians has shown growth of the logarithm of low frequency component of ν_2 band intensity (ν_{2248}) with increasing temperature. However, in case dimeric C≡N vibrations, this component intensity should decrease with increasing temperature. The Increase of intensity of ν_{2248} component with increasing temperature shows possibility of hot band.

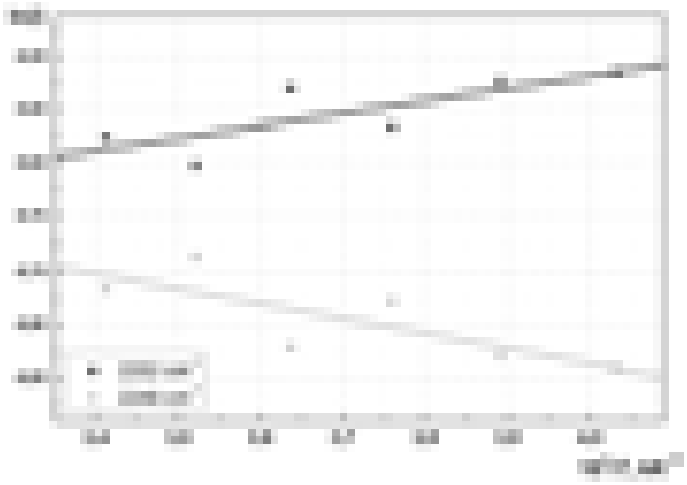

Fig. 2. Integrated logarithmic intensities dependence on inverse temperature from Raman scattering spectra of acetonitrile in C≡N stretching region.

The origin of the C≡N band structure of acetonitrile is discussed in the light of the recent research.

[1] F.H.Tukhvatullin, A.Jumabaev, G.Muradov, H.A.Hushvaktov and A.A.Absanov. Raman spectra of C≡N vibrations of acetonitrile in aqueous and other solutions. Experimental results and abinitio calculations. // J. Raman Spectrosc. 36, 932-937 (2005).

[2] M. Stoev, A. Makarow, J.M. Robledo. Raman and IR spectroscopy of a mixed CH3CN – H2O solvent in the CN streching region. // Spectrosc. Letters. 28(8), 1251 – 1258 (1995).

[3] U.M. Biermann, W. Mikosch, T. Dorfmüller, and W. Eimer, Comparison of solvent and probe reorientation in polycrylamide gels. // J. Phys. Chem. 100, 1705, 1710 (1996)

[4] V. Aleksa, V. Barkauskas, V. Pogorelov, H. Fuess, V. Balevičius, Raman spectroscopy of vibrational and rotational relaxation of acetonitrile molecules dissolved in ionic liquids. Lithuanian Journal of Physics 47, 435-441 (2007).

SURFACE-ENHANCED RAMAN SPECTROSCOPY OF BACTERIA

Evelin Witkowska[1,3], Anna Kelm[2,3], Agnieszka Michota-Kaminska[3], Robert Holyst[3]

[1]Faculty of Chemisty, University of Warsaw
[2]College of Inter-Faculty Individual Studies in Mathematics and Natural Sciences, University of Warsaw
[3]Department of Soft Condensed Matter, Institute of Physical Chemistry, Polish Academy of Sciences
ewitkowska@ichf.edu.pl, akelm@ichf.edu.pl

Surface-enhanced Raman scattering (SERS) is a spectroscopic technique dating back to 1970s [1] that utilizes metal (Ag, Au, Cu) nanoparticles and roughened metal surfaces to enhance Raman signal from adsorbed molecules. Primary effect responsible for SERS enhancement by 5 to 6 orders of magnitude comes from local surface plasmons excited by incident laser radiation [2]. Secondary effect (providing ~10^2 enhancement) involves resonant charge-transfer (CT) transitions between adsorbate and metal [3]. Currently, applications of SERS range from surface chemistry [4] to biological chemistry [5] and biomedical analysis [6]. Investigations on employing SERS in bacteria characterization and analysis made a huge progress during last 10 years. Thanks to this method, microorganism detection and identification in food, clinical, and environmental samples could be much easier than other time-consuming, complicated, traditional procedures like PCR-based methods (reporter labeling, cell lysis, DNA extraction) [7] or new immunoassay methods [8]. The microfluidic chip with a roughened metal surface for on-chip SERS detection of bacteria has already been demonstrated to be a good method to distinguish gram positive and gram negative Prokaryota [9]. Further development of this technique would enable determination of bacteria species.

[1] M. Fleischmann, P.J. Hendra, A.J. McQuillan, *Raman spectra of pyridine adsorbed at a silver electrode*, Chemical Physics Letters, 26(2):163 – 166, 1974.

[2] Harald Kneipp, Katrin Kneipp, Martin Moskovits, editor, S*urface-Enhanced Raman Scattering. Physics and Applications*, chapter: S*urface-Enhanced Raman Spectroscopy: a Brief Perspective,* Springer-Verlag, Berlin Heidelberg, 2006.

[3] R. Aroca, *Surface enhanced vibrational spectroscopy*, chapter 4. *Chemical Effects and the SERS Spectrum,* Wiley, 2006.

[4] W. B. Caldwell, K. Chen, B. R. Herr, C. A. Mirkin, J. C. Hulteen, R. P. Van Duyne, *Self-assembled Monolayers of Ferrocenylazobenzenes on Au(111)/mica Films: Surface-Enhanced Raman Scattering (SERS) Response vs. Surface Morphology*, Langmuir 1994, 10, 4109-4115.

J. Weaver, *Electrochemical Interfaces: Some Structural Perspectives*, Journal of Physical Chemistry 1996, 100, 13079-13089.

[5] N. Weissenbacher, B. Lendl, J. Frank, H. D. Wanzenböck, B. Mizaikoff, R. Kellner, *Continuous surface enhanced Raman spectroscopy for the detection of trace organic pollutants in aqueous systems*, Journal of Molecular Structure 1997, 410-411, 539-542.

X. Zhang, M. A. Young, O. Lyandres, R. P. Van Duyne, *Rapid Detection of an Anthrax Biomarker by Surface-Enhanced Raman Spectroscopy*, Journal of the American Chemical Society 2005, 127, 4484-4489.

[6] T. Vo-Dinh, D. L. Stokes, G. D. Griffin, M. Volkan, U. J. Kim, M. I. Simon, *Surface-enhanced Raman Scattering (SERS) method and instrumentation for genomics and biomedical analysis*, Journal of Raman Spectroscopy 1999, 30, 785-793.

[7] C.C. Chen, L.J. Teng, S.K. Tsao, T.C. Chang, *Identification of Clinically Relevant Viridans Streptococci by an Oligonucleotide Array*, Journal of Clinical Microbiology, 43(4): 1515- 1521, 2005.

[8] A. Gupta, D. Akin, R. Bashir, Detection of bacterial cells and antibodies using surface micromachined thin silicon cantilever resonators, Journal of Vacuum Science and Technology B, 22: 2785- 2792, 2004.

[9] I.F. Cheng, C.C. Lin, D.Y. Lin, H.C. Chang, A dielectrophoretic chip with a roughened metal surface for on-chip surface-enhanced Raman scattering analysis of bacteria, Biomicrofluidics, 4(3): 034104, DOI: 10.1063/1.3474638, 2010.

DETERMINATION OF THE DEGREE OF DISSOCIATION OF HYDROGEN IN HIGH – FREQUENCY LOW – TEMPERATURE PLASMA

Madara Zinge

Institute of Atomic Physics and Spectroscopy, University of Latvia, Latvia
madara.zinge@gmail.com

The goal of the present work is the determination of the degree of dissociation of hydrogen in high-frequency electrodeless lamp (HFEDL). HFEDLs are widely used in analytical devices, such as absorption spectrometers, and they are used in studies of plasma-surface interactions (due to lack of electrodes) [1]. Hydrogen containing discharges are used in different technological processes, for instance in surface treatment and in thin-film deposition [2]. It is of great importance to understand the processes in these plasmas. The dissociation degree of hydrogen is considered one of the most important parameters of hydrogen and hydrogen-containing low-temperature plasmas, and it has been investigated for different kind of plasmas, for example, for microwave, DC and RF (excited at 200 kHz frequency) plasmas [3,4], but for hydrogen containing HFEDLs it has not been done before.

The degree of dissociation is defined as the ratio of the number densities of dissociated molecules and molecules in all states:

$$D = \frac{[H]}{[H]+2[H_2]} = \frac{\frac{[H]}{[H_2]}}{\frac{[H]}{[H_2]}+2}, \quad (1)$$

where [H] is the number density of atomic hydrogen in the ground state $1^2S_{\frac{1}{2}}$ and $[H_2]$ is the number density of hydrogen molecules in the electronic ground state $X^1\Sigma_g^+$, summarized over all vibrational and rotational levels.

Method used in this experiment is based on spectroscopic measurements of the relative intensities of two atomic lines of the Balmer series, H_α and H_β, and one molecular line of the Fulcher-α system, line (2-2) Q1. This method is described in detail elsewhere [3,4]. Briefly, in this method the ratios of measured line intensities are used, which are connected with number densities of atomic hydrogen and molecular hydrogen. It means that apart from experimental measurements, it is necessary to solve equation system, which describes the processes leading to the emission of Balmer lines and hydrogen molecular lines.

For the description of the emission of atomic hydrogen lines, two processes where considered, which dominate in populating excited levels (with subsequent emission of Balmer lines), namely, (1) the direct electron excitation of atom from the ground state, and (2) dissociative electron impact excitation [3]. To describe intensity of single molecular line, in this case (2-2) Q1 line of Fulcher-α band system, a simple excitation-deactivation model was used, which includes electron impact excitation and spontaneous emission [3].

Intensity ratio of the atomic and molecular lines strongly depends on the gas temperature, to take into account this influence it was necessary to determine plasma temperature. In the case of hydrogen containing plasmas, one of the commonly used techniques for the determination of gas temperature is based on the measurements of the intensity distribution in the rotational bands of hydrogen molecule [5]. The H_2 temperature was obtained from measurements of relative intensities of Fulcher-α (2-2) Q-branch lines.

HFEDL under study was filled with helium and hydrogen mixture ($p_{He} \approx 0.9$ Torr, $p_{H2} \approx 0.1$ Torr). The cylindrical lamp (diameter of 2 cm and length of 4 cm) was placed into induction coil and an inductive coupled discharge was excited by means of high-frequency field of about 100 MHz.

The emission spectra of the discharge was registered by means of JobinYvon SPEX 1000M high resolution spectrometer (grating 1200 $l \cdot mm^{-1}$) and charge coupled device matrix detector (2048×512 Thermoelectric Front Illuminated UV Sensitive CCD Detector, Simphony).

The results, which were obtained using the measured intensity ratios of Balmer and Q1 molecular lines and by solving equation system, will be shown for the helium-hydrogen HFEDL.

Acknowledgments: The work was partly supported by European Social Fund project Nr. 2009/0210/1DP/1.1.1.2.0/09/APIA/VIAA/100.

[1] A. Skudra, Z. Gavare, N. Zorina, M. Zinge, E. Gavars, R. Poplausks, A. Svagere, Plasma Temperature and Surface Studies of Argon-Hydrogen Containing Low-Temperature Dumbbell form Light Sources, Journal of Materials Science and Engineering **B 1**, 439-444 (2011)

[2] A. Rousseau, A. Granier, G. Gousset, P. Leprince, Microwave discharge in H_2: influence of H-atom density on the power balance, J. Phys. D: Appl. Phys. **27**, 1412 (doi:10.1088/0022-3727/27/7/012) (1994)

[3] B. P. Lavrov, A.V. Pipa, J. Röpcke, On determination of the degree of dissociation of hydrogen in non-equilibrium plasmas by means of emission spectroscopy: I. The collision-radiative model and numerical experiments, Plasma sources Sci. Technol. **15,** 135-146 (2006)

[4] B. P. Lavrov, A.V. Pipa, J. Röpcke, On determination of the degree of dissociation of hydrogen in non-equilibrium plasmas by means of emission spectroscopy: II. Experimental verification, Plasma sources Sci. Technol. **15,** 147-155 (2006)

[5] Z. Gavare, G. Revalde, and A. Skudra, Plasma temperature determination of hydrogen containing high-frequency electrodeless lamps by intensity distribution measurements of hydrogen molecular band, International Journal of Spectroscopy: Special Issue on Spectral Line Shapes in Plasmas and Gases, vol. 2010, Article ID: 804506, 8 pages (doi:10.1155/2010/804506) (2010)

MEASUREMENT CAPABILITIES OF ^{14}C USING THE TRIPLE-TO-DOUBLE COINCIDENCE RATIO METHOD

Paulius Butkus[1], Arūnas Gudelis[2]

[1] Faculty of Physics, Vilnius University, Saulėtekio Ave. 9-III, LT-10222 Vilnius, Lithuania
[2] Center for Physical Sciences and Technology, Institute of Physics, Ionizing Radiation Metrology Laboratory, Savanorių Ave. 231, LT-02300, Vilnius, Lithuania
p.s.butkus@gmail.com

The triple-to-double coincidence ratio (TDCR) method is a primary standardization method in liquid scintillation counting with three-photomultiplier tubes (PMT) developed for the absolute activity measurement of pure beta minus and electron capture emitters in solution. It is a direct method, although the decay scheme data for a given radionuclide are necessary for the detection efficiency calculation. The method itself is based on a physical and statistical model of the distribution of scintillation photons and their detection probability in a three-photomultiplier counter. The non-linearity of the scintillator response due to the ionization-quenching phenomenon is also taken into account.[1] The software TDCRB-02 available from the ICRM LSC working group web site was used for the specific activity determination.

In previous work low-level samples containing known amounts of ^{36}Cl, ^{63}Ni and ^{90}Sr were prepared and measured with the TDCR device. The specific activities were determined with the help of the software TDCRB-02 and compared with known values. It was found that the divergence from the expected value for ^{36}Cl, ^{63}Ni and ^{90}Sr was 0.9 %, 2.7 % and 1.7 %, respectively, within the specified uncertainty limits. Results suggested the suitability of the TDCR techniques for low-level counting. As an application for measurement of low energy beta-radiation, further investigations on the assessment of the measurement capabilities of the TDCR instrument for pure beta-emitters ^{3}H and ^{14}C at varying activity levels were planned. [2]

The aim of this study was to apply the TDCR method for the activity measurement of unquenched samples with pure beta-emitter ^{14}C and determine the best conditions in which the discrepancy from the "true value" is the lowest. For this purpose different samples of beta-emitter ^{14}C in different conditions were measured with the TDCR instrument.

The first sample with ^{14}C was prepared in a polyethylene counting vial from the working solution by mixing 0.15 mL of it with 16 mL of the Ultima Gold LLT scintillator. The blank sample containing 16 mL of the same type of a scintillator was used for the background correction. Five repeat measurements of 600 s each were carried out for all samples at three fixed high voltage values set to the PMTs for varying the detection efficiency of the LS-detector. It was found that the divergence from the expected value was 2.59 %. To reduce the divergence a new approach of measurement was investigated. This time, six repeat measurements of 60 s each were carried out for all samples at six fixed high voltage values set to the PMTs. The final absolute activity was taken as a mean value of all measurements activities at this condition. It was found that the divergence from the expected value was 7.46 %. In this case the discrepancy was unacceptable and it was decided to prosecute an inquiry. A new sample with ^{14}C was prepared in a 16 mL glass vial and measured at the same conditions as previously. It was found that for ^{14}C the discrepancy was 1.59 %, within the specified uncertainty limits. Results of the standardization of ^{14}C with the TDCR device and the use of the TDCRB-02 software are summarized in Table 1.

Table 1. Results of standardization of ^{14}C with the TDCR device

Specific activity (kBq g^{-1})		Relative discrepancy (%)
Calculated from the certificate	Determined from experiment	
40.01 ± 0.60	41.048 ± 1.207	+2.59
39.81 ± 0.60	42.997 ± 1.620	+2.7
39.93 ± 0.60	39.305 ± 0.074	-1.59

All results show that the TDCR primary standardization method gives a potential to measure activity of ^{14}C with high accuracy. However, divergence from the expected values is still unacceptable and further investigations must be taken to improve the accuracy.

[1] R. Broda, A review of the triple-to-double coincidence ratio (TDCR) method for standardizing radionuclides, Applied Radiation and Isotopes 58 (2003) 585–594
[2] A. Gudelis, A. Vinčiūnas, P. Butkus, M. Pranaitis, Measurements of some radionuclides using a new TDCR system and an ultra low-level conventional LSC counter in CPST, Lithuania, Applied Radiation and Isotopes, DOI: 10.1016/j.apradiso.2012.02.091

SUPERSYMMETRIC PARTICLE DECAY CHAINS

Andrius Balčiūnas, Thomas Gajdosik

Faculty of Physics, Vilnius University, Saulėtekio Ave. 9-III, LT-10222 Vilnius, Lithuania
Andrius.Balciunas@ff.stud.vu.lt

Supersymmetry is a fermion – boson symmtery. It relates elementary particles of one spin to other particles that differ by half a unit of spin and are known as superpartners. Each fermion should have a massive partner boson, the fermion's superpartner and each boson should have a massive partner fermion, the boson's superpartner.

Supersymmetric particles decay quickly into the lightest supersymmetric particle and some standard model particles. Every supersymmetric interaction must involve two supersymmetric particles. In other words, all supersymmetric particles are produced in pairs, and if a SUSY particle decays, it must decay into another SUSY particle (plus any number of normal particles). This means that the lightest supersymmetric particle cannot decay, since there aren't any supersymmetric particles that it can decay into. That mechanism is called R-parity [1].

The standard model particles, such as leptons, quarks, and the vector bosons all have positive R-parity, while the supersymmetric partners, such as sleptons, squarks, neutralinos and charginos have negative R-parity. This means that, in order to conserve the R-parity, only the following two-body decay transitions are allowed:

$$\begin{array}{ll} N \to NN & \\ N \to SS & \ldots \quad \text{this is the production process} \\ S \to NS & \end{array} \tag{1}$$

I labeled standard fundamental particles N and supersymmetric fundamental particles S. This means, for example, that a top quark could not decay into a charm quark and a neutralino, but a top quark could decay into a charm squark and a neutralino [2]. Similarly, a squark cannot decay into another squark and a neutralino, but can decay into a quark and a neutralino [2]. In all this, the standard decays which are well known in experimental physics remain allowed, such as quark transitions involving weak bosons. But it should be pointed out that a supersymmetric particle cannot decay into two new supersymmetric particles. All of these rules are a direct result of R-parity [1]. For example:

$$\begin{array}{l} \tilde{q} \to q\tilde{\chi}^0 \\ \tilde{g} \to q\bar{q} \to q\bar{q}\tilde{\chi}^0 \end{array} \tag{2}$$

Decay chains were calculated from basic parameters of supersymmetric Lagrangian. Then the relations between the masses of supersymmetric particles and various coupling constants were determined.

---

[1] S. P. Martin, *A Supersymmetry Primer* (Department of Physics, Northern Illinois University and Fermi National Accelerator Laboratory, 2011).

[2] H. Baer, X. Tata, *WEAK SCALE SUPERSYMMETRY:From Superfields to Scattering Events* (Cambridge University Press, 2006).

QUANTUM CHEMICAL MODELING OF THE DNA SEQUENCE RECOGNITION MECHANISM IN RESTRICTION ENDONUCLEASE

Gytis Bašinskas[1], dr. Mindaugas Mačernis[1],doc. Juozas Šulskus[1], prof. habil. dr. Leonas Valkūnas[1]

[1] Department of Theoretical Physics, Faculty of Physics, Vilnius University, Saulėtekio ave. 9-III, LT-10222 Vilnius, Lithuania
drakagytis5@gmail.com

Restriction endonuclease is an enzyme that recognizes a specific DNA sequence and cuts it without damaging the critical structures of the DNA. This effect is known as restriction. If the restriction mechanism could be understood biotechnologists could achieve unprecedented DNA manipulation by creating restriction endonucleases which are not found in nature.

BncI restriction endonuclease has a unique recognition site which allows recognition of two different DNA sequences. In addition, mutation of this recognition site changes not only the restriction speed but allows for two new DNA sequences recognition. Experimental analysis of BcnI restriction endonuclease and its mutants were done by Biotechnology Institute at Vilnius University[1]. Theoretical interaction mechanism was suggested. However, why restriction reaction speeds of different sequences are so different were unknown. Therefore, this restriction endonuclease was chosen to be further analyzed.

BcnI and its mutants H77A and H219Q effects on 5' -CC↓CGG -3' (↓ the cleavage position), 5' -CC↓GGG- 3', 5' -CC↓AGG -3' and 5' -CC↓TGG- 3' DNA sequences were analyzed (one of the structures is shown in Fig. 1). Experimental crystallographic structures [2] were used for analysis. These experiments are not accurate enough to see hydrogens. Therefore, positions of hydrogens was uncovered after topological analysis. The eligibility of these positions was analyzed using *AMBER* classical molecular dynamics package. Semi-empirical quantum mechanical PM3 method was used to optimized restriction endonuclease, DNA sequence and surrounding water systems to reach their minimal energy structures. The analysis of these structures suggested that a small part of the recognition site and this site's mutations interactions with DNA are responsible for the whole recognition mechanism [3]. The simplified recognition site and DNA sequence were modeled using quantum chemical *GAUSSIAN* package with B3LYP/6-11G(d,p) basis functions. The public access supercomputer from the High Performance Computing Center (HPCC) of the Lithuanian National Center of Physical and Technology Sciences (NCPTS) at Vilnius University was used. Various structures imitating BcnI restriction endonuclease and its mutant's interactions with DNA sequence were tested. The interaction energy and orientation of these structures were analyzed.

The results show that orientation of recognition site and DNA sequence is very important. If the plane of the recognition site is not the same as the plane of nucleotides in the DNA sequence the binding to the DNA does not occur. If the restriction occurs interaction energy can be used to predict how fast the binding will be. The next aim of the work will be to further analyze the problem of hydrogen positions.

Fig. 1. BcnI restriction endonuclease and 5' -CC↓CGG -3' sequence structure.

1. Georgij Kostiuk, Giedrius Sasnauskas, Giedre Tanulaitiene and Virginijus Siksnys, *Degenerate sequence recognition by the monomeric restriction enzyme: single mutation converts BcnI into a strand-specific nicking endonuclease*, Nucleic Acids Research 2011, 1-1 doi:10.1093/nar/gkql1351
2. Structure can be found at *PROTEIN DATA BANK* (http://www.rcsb.org) codes *2ODI* and *3IMB*.
3. Gytis Bašinskas, *The Modeling of the DNA Sequence Recognition Mechanism in Restriction Endonuclease*, Bachelor work (2011)

1/f NOISE GENERATED BY SUPERPOSITION OF RELAXATION PROCESSES GENERATED BY IDENTICAL WHITE NOISE

Rytis Kazakevičius[1], Bronislovas Kaulakys[1],

[1] Institute of Theoretical Physics and Astronomy, Vilnius University, Lithuania
rytis.kazakevicius@tfai.vu.lt

The power-law of spectra of signals, including 1/f noise (also known as $1/f$ fluctuations, flicker noise or pink noise) is common in both physics and other fields (computer networks, financial markets). This subject has been a hot research topic for many decades [1]. $1/f$ noise received a growing interest in biology, psychology, and movement sciences during the last decade. For example, $1/f$ fluctuations are generally evidenced in young and healthy systems, performing in a stable, unperturbed environment, and facing easy or over learned tasks. In contrast, $1/f$ fluctuations seems to disappear with aging or disease. So, there is a close relationship between health and $1/f$ noise [2].

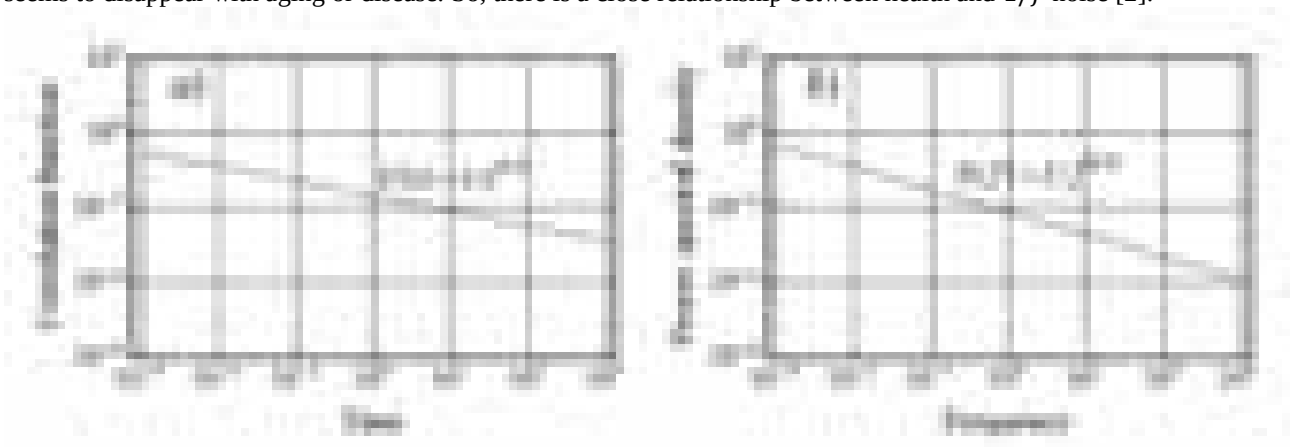

Fig. 1. Signal $I(t)$ a) correlation function and b) power spectral density. Parameters: $\eta = 0.3$, : $\gamma_2 = 100$.

We analyzed a model based on signal $I(t)$ that is a superposition of stochastic processes

$$I(t) = \sum_{l=1}^{N} I_l\,(\mathrm{t}), \tag{1}$$

where N is a number of processes and $I_l\,(t)$ is stochastic process described by the Langevin equation

$$\dot{I}_l = -\gamma_l I_l + \sigma\xi(t)\,. \tag{2}$$

Here γ_l is relaxation rate of process $I_l\,(t)$, $\xi(t)$ is a white noise and σ is standard deviation of white noise.

We assume that relaxation rates γ_l value is restricted in interval $[\gamma_1,\gamma_2]$ and γ_l are distributed according to power-law, $P(\gamma_l)\sim\gamma_l^{-\eta}$. Where γ_1 and γ_2 are minimal and maximal values of the relaxation rates.

The correlation function of signal $I(t)$ is

$$C(s) = \left(\frac{1-\eta}{\gamma_2^2}\right)^2 \frac{1}{\sin(\pi\eta)}\frac{1}{s^{1-2\eta}},\ 0<\eta<0.5,\ \gamma_2^{-1} << s << \gamma_1^{-1}. \tag{3}$$

The power spectral density of signal $I(t)$ is

$$S(f) = \frac{1}{(2\pi)^{2\eta}}\left(\frac{1-\eta}{\gamma_2^2}\frac{\pi\sqrt{2}}{\sin(\pi\eta/2)}\right)^2 \frac{1}{f^{2\eta}},\ 0<\eta<0.5,\ \gamma_1 << f << \gamma_2. \tag{4}$$

If the stochastic process exhibit spectral density proportional $1/f^{\alpha}$ and exponent α varies between 0 and 1, then it is called long-memory process [3].

Model generated power spectral density as function of frequency is presented in figure 1. We proved that the model in specific frequency range $\gamma_1 \ll f \ll \gamma_2$ generate spectral density proportional $1/f^{\alpha}$. It means that superposition of earlier mentioned processes exhibits $1/f$ fluctuations with long-memory.

[1] W. Li, (2012), http://www.nslij-genetics.org/wli/1fnoise
[2] A. L. Goldberger, L. A. N. Amaral, J. M. Hausdorff, P. Ch. Ivanov, C.-K. Peng, H. E. Stanley, Fractal dynamics in physiology: Alterations with disease and aging, PNAS **99**, 2466–2472 (2002).
[3] A. Diniz, M. L. Wijnants, K. Torre, J. Barreiros, N. Crato, A. M.T. Bosman, F. Hasselman, R. F.A. Cox, G. C. Van Orden, D. Delignières, Contemporary theories of 1/*f* noise in motor control, Human Movement Science **30,** 889-905 (2011).

MODELING THE ELECTROCHEMICAL BEHAVIOR OF POLYETHERS ON COPPER AND TIN ELECTRODES BY QUANTUM CHEMISTRY METHODS

Julija Litvaitytė[1], Mindaugas Mačernis[1], Arvydas Survila[2], Leonas Valkūnas[1], Juozas Šulskus[1]

[1] Department of Theoretical Physics, Faculty of Physics, Vilnius University, Lithuania
[2] Institute of Chemistry, Center for Physical Sciences and Technology, Lithuania
julija.litvaityte@stud.ff.vu.lt

Electrochemical deposition of metals is widely used in producing high quality films of different metals and their alloys. Bronzing – forming of a bronze layer – is the codeposition of copper and tin. Because of properties like resistance to corrosion and high strength bronze layers found their industrial application [1]. The composition and properties of an alloy coating can be modified by changing the conditions of electroplating or using different solutions. Usually optimal conditions for the codeposition of two metals are achieved by using surface active substances (SAS) that make a selective influence on partial electrode processes. However, the exact mechanism by which SAS are added to improve the quality of electrodeposits is not known.

A version of bronze electroplating process was developed in the Institute of Chemistry, Center for Physical Sciences and Technology (Vilnius, Lithuania). In addition to the main components, the solution contains polyethers – ethylene glycol oligomers. Ethylene glycol molecules act as inhibitors and the length of hydrocarbon chain is considered to be the major factor responsible for its inhibition activity on copper and tin substrates. Oligomers of ethylene glycol, $HO–(CH_2–CH_2–O)_m–H$ demonstrate surfactant properties only when $m \geq 4$ **[2].** In order to understand the codeposition of copper and tin, electrodepostion processes of both metals were investigated separately. In the presence of ethylene glycol oligomers different behavior can be observed in copper and tin systems. While these additives demonstrate weak surface activity on copper substrate, their effect is overwhelmingly higher in tin system [2]. The surface activity of ethylene glycol oligomers on copper substrate is considerably enhanced by halide additives, whereas their adsorption in solutions protected from halides is quite weak [3].

The complex mechanism of the electrodeposition of copper and tin was simplified during the modeling and the main structures of metal ions and ethylene glycol oligomers were analyzed further. From the experimental data it is known that the shortest chain that show strong inhibition on tin substrate is tetraethylene glycol (TEG). Thus metal ion and diethylene glycol (DEG) (that does not exhibit inhibitive behavior) structures and also metal ion and TEG structures have been chosen to be examined by performing geometry optimizations at different levels. Geometry optimizations were done using density functional method (DFT) with B3LYP functional employing various basis sets. Final energies have been calculated at DGDZVP level with the optimized geometries.

During the calculations different DEG and TEG conformers were found, that also gives a variety of conformations of ethylene glycol oligomer – metal ion complexes. Structural parameters were found and vibrational frequencies were calculated for the most stable conformers.

[1] D. Padhi, S. Gandikota, H. B. Nguyen, C. McGuirk, S. Ramanathan, J. Yahalom, G. Dixit, Electrodeposition of copper – tin alloy thin films for microelectronic applications, Electrochimica Acta **48**, 935-943 (2003)
[2] A. Survila, Z. Mockus, S. Kanapeckaitė, V. Jasulaitienė, R. Juškėnas, Codeposition of copper and tin from acid sulphate solutions containing polyether sintanol DS-10 and benzaldehyde, J Appl Electrochem **39**, 2021-2026 (2009)
[3] A. Survila, Z. Mockus, S. Kanapeckaitė, M. Samulevičienė, Halide-suppressed adsorption of polyether laprol 240 C on tin electrode, Chemija T. 14, Nr. 1, ISSN 0235-7216, Vilnius (2003).

FOCUSING ELEMENTS FOR TERAHERTZ FREQUENCY DETECTORS

Karolis Madeikis[1, 2], Linas Minkevičius[2]

[1] Vilnius University faculty of physics, Saulėtekio al. 9, bldg. III, LT-10222 Vilnius, Lithuania
[2] Semiconductor Physics Institute of Center for Physical Sciences and Technology,
A. Goštauto str. 11, LT-01108, Vilnius, Lithuania
karolismadeikis@gmail.com

Application of terahertz (THz) waves for security, medical diagnostic and imaging needs [1] remains the main stimulus to develop compact and sensitive THz detectors which will work at room temperature. The improved designs of antenna and various focusing elements like integrated Silicon lenses are used to increase the detectors sensitivity.

In this work zone plates feature of focusing different frequency waves to different focal distances (f) was analyzed. Zone plate capability of concentrating THz electromagnetic field in desired focus with different values of wavelength (λ), distance to the focus (f), permittivity (ε) and modeling area (x, y, z) were simulated using finite-difference time-domain (FDTD) [2] method. It is based on Kane Yee idea [2, 3] to separate modeling space in to cells that each E-field vector component is located midway between a pair of H-field vector components, and conversely. In that cells grid the laws of Ampere and Faraday is applied. That solution helps to deal with Maxwell equations and to calculate electromagnetic field components. In simulations zone plate model was made by using zones radius equation:

$$r_n = \sqrt{n\lambda f + \frac{n^2\lambda^2}{4}}. \quad (1)$$

Here r_n-distance to the n zone, λ- wave length, f- distance to the focus, n- number of zone. Simulation area is shown in Fig. 1. Because zone plate is symmetrical, symmetric boundary conditions were applied and just a quarter of area was simulated. This let us to get same result as calculating all area and it requires less computer recourses and time. In simulation was considered that zones were made of molybdenum on polyimide plane with permittivity ε=2.89. Lighter gray circles (Fig. 1) shows where molybdenum layer was removed. Red plane on the left shows where wave is input and grey plane on the right shows where detector should be. Result of focused electromagnetic field amplitude at focal length of 5 mm is shown in Fig. 2. Peak is located in corner due to quarter of full zone plate simulation. As we can see from fig.2, zone plate with 5 zones can concentrate electric field about 8 times.

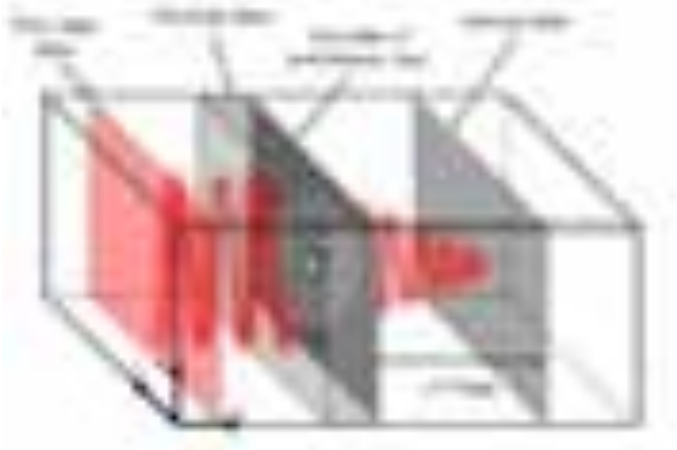

Fig. 1. Simulation area

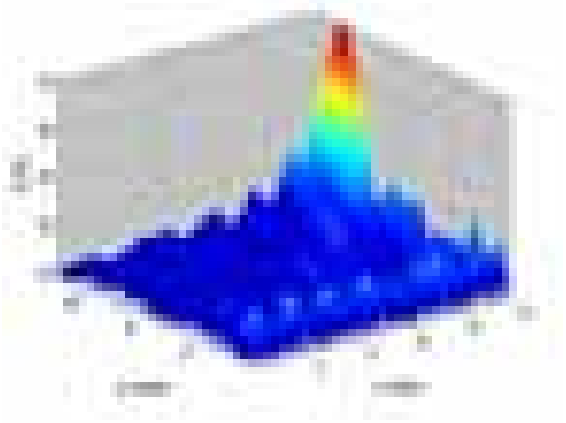

Fig. 2. Distribution of electromagnetic field E_z/E_0 in simulation area.

In conclusion, zone plates could be used to concentrate THz electromagnetic field in order to increase detector sensitivity and also to filter required frequency by changing zone plate focal length.

This work was partly supported by the Lithuanian Science Council Student Research Fellowship Award (K. M).

[1] John F Federici, Brian Schulkin, Feng Huang, Dale Gary, Robert Barat, Filipe Oliveira and David Zimdars, THz imaging and sensing for security applications—explosives, weapons and drugs, Semicond. Sci. Technol. 20 (7), 266-280 (2005).

[2] A. Taflove, in: *Computational electrodynamics: the finite-difference time domain method*, second edition,(Norwood: Artech House, 2000).pp. 866.

[3] Kancleris, G. Šlekas, V. Tamošiūnas, R. Simniškis, P. Ragulis, and M. Tamošiūnienė, SEMICONDUCTOR PLATE INTERACTING WITH TE_{01} MODE IN CIRCULAR WAVEGUIDE, Lithuanian Journal of Physics, Vol. 49, No. 1, pp. 35 □ 43 (2009).

SELF ASSEMBLY OF ANTHRAQUINONE MOLECULES ON Cu(111) BY MONTE CARLO MODELING

Mantas Šimėnas[1], Evaldas Tornau[2]

[1] Faculty of Physics, Vilnius University, Lithuania
[2] Semiconductor Physics Institute, Center for Physical Sciences and Technology, Lithuania
mantas.simenas@ff.stud.vu.lt

Recently, a lot of self-assembled ordered molecular networks formed by organic molecules coupled by highly directional H-bonds have been found [1]. Porous molecular network of anthraquinone (AQ) [2] is one of the most beautiful examples of such orderings (fig 1.). The network originates from a delicate balance between substrate-mediated repulsion and intermolecular attraction involving H-bond coupling of neighboring molecules. Hexagon sides consist of three parallel anthraquinone molecules, while hexagon vertices are formed of three molecules in pin-wheel arrangement. As a result, honeycomb network with huge molecular pores (~50Å) occurs.

We propose the statistical model for anthraquinone ordering into such porous network. This model considers short-range (caused by H-bonds) and long-range (caused by dipole-dipole forces) interactions between molecules. It also accounts for the elongated form of the molecule for short range interactions. There are two short-range interactions which differ by their chemical bonding: interaction of two nearest neighbor (NN) molecules which are arranged in parallel ("side-by-side") corresponding to double H-bonding of two AQ molecules, and NN "side-by-head" interaction corresponding to one H-bonding. Our model takes into account these attractive pair interactions together with short-range pin-wheel triangular trio interaction (three molecules interconnected by "side-by-head"-type H-bonds). In addition, the model considers some long-range surface-mediated interactions: repulsive dipole-dipole and Friedel-type oscillatory [3] interactions. To mimic the oscillatory behavior of these interactions, long-range attractions at the distances corresponding to the honeycomb pore diameter were considered and were shown to be crucial to obtain porous honeycomb structure.

During MC simulations the experimentally observed porous structure was obtained (fig. 1), and the set of interaction parameters required to obtain this phase was determined. In addition, the ordered systems with analogous pin-wheels, but different hexagon side length were observed at different set of interactions.

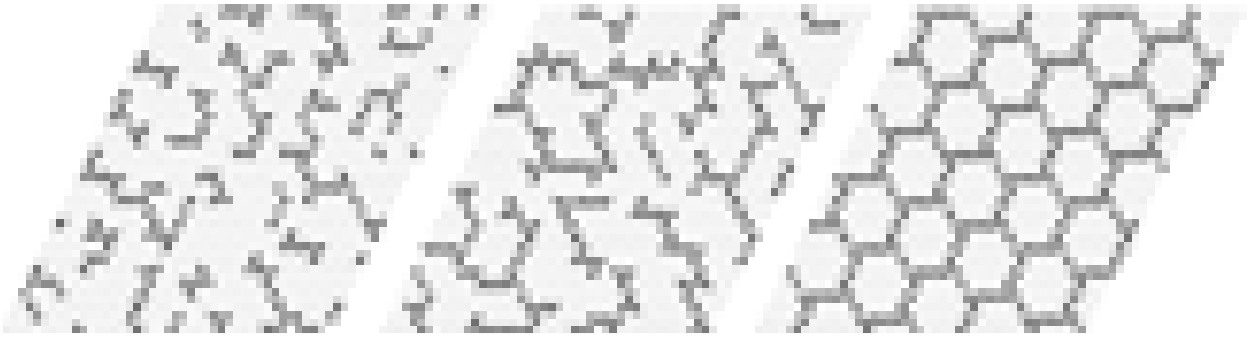

a) $k_BT/\varepsilon_1 = 0.12$ b) $k_BT/\varepsilon_1 = 0.08$ c) $k_BT/\varepsilon_1 = 0.06$

Fig. 1. Molecular assembly of AQ molecules (shown by elongated ellipses) obtained by Monte Carlo simulations at different temperatures

[1] Kind, M; Woell, C. *Progress in Surface Science* **84**, 230 (2009).
[2] G. Pawin, K.-L. Wong, K.-Y. Kwon, L. Bartels, *Science* **313**, 961 (2006).
[3] Kim, K.; Einstein, T. L. *Phys. Rev. B* **83**, 245414 (2011).

NIOBIUM AND SILICON DIOXIDE THIN FILMS PROCESSING USING REACTIVE MAGNETRON SPUTTERING

Rimantas Žičkus[1] and Kęstutis Juškevičius[2]

[1] Faculty of Physics, Vilnius University, Sauletekio Ave 9, build. 3, LT-10222 Vilnius, Lithuania
[2] Institute of Physics, Center for Physical Sciences and Technology, Savanoriu ave. 231, LT-02300 Vilnius, Lithuania
ri.zickus@gmail.com

Up to the mid-1970s the evaporation dominated over the sputtering of solid materials in the physical vapor deposition (PVD) of thin films technologies but the breakthrough arrived in 1974 when the planar magnetron was discovered. From this moment, a very intense development started. The main principle of magnetron sputtering method is controlling magnetron discharges, plasma and high-energy charged particles by magnetic fields and keeping them in appropriate vicinity of the sputtered target and the substrate. These physical conditions and other properties (target materials, substrate-to-target distance, gas total or partial pressure and flow, magnetron vertical axis angle, discharge voltage U_d and etc.) are accountable for growing films process and its characterization (duration and sputter deposition rate v, particle energy, ionization, layer density and thickness). The aim of magnetron sputtering method development is applying it in the fabrication of thin films.

In our experiments and observations we attempt to figure out operating modes of magnetron sputtering method, features and issues of condition combinations, characterize main advantages and disadvantages.

Firstly, it was checked how cooling system works in order to ensure stable and fail-safe performance. No lacks and target over-heating were established using niobium (Fig. 1), the dependences of target voltage vs power after 30 min were compared with previous experiments and no big difference observed, which is important for continuous sputtering processes. The next monitoring related reactive gas (RG) flow and sputtering speed. Obtained result is shown in Fig. 2. and it is called hysteresis loop.

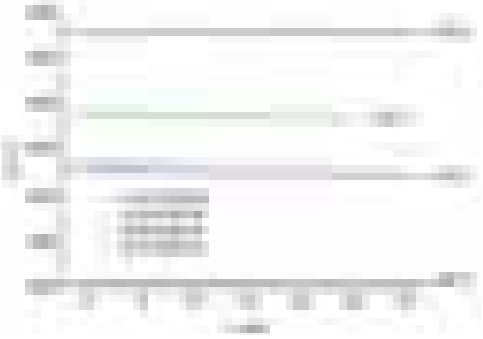

Fig. 1. Dependence of target voltage vs time at different power level.

Fig. 2. Hysteresis of reactive Nb sputtering at different powers.

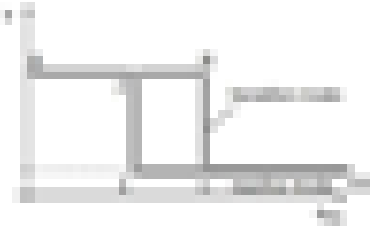

Fig. 3. Schematic illustration of hysteresis effect.

The hysteresis effect arises in consequence of two competitive processes: the sputtering of the target surface and the covering of its surface by reaction products. At low values of RG flow rate ϕ_{RG} (Fig. 3, interval A–B) all RG is gettered by the sputtered material. In the point B, every small increase in ϕ_{RG} results in a jump of the film deposition rate v. A further increase of ϕ_{RG} (interval C–D) results almost constant value of v, which is typical for reactive mode of sputtering. The decrease of ϕ_{RG} from D to E is accompanied by the decrease of p_{RG}, but a return to the interval E–C is delayed. This is because p_{RG} remains high until the compound layer on the surface of sputtered target is fully removed and material is again exposed to be sputtered. As a result, the consumption of RG increases and p_{RG} decreases to a background level. This way a closed hysteresis loop is formed.

The next step is defining optimal conditions for Si and Nb sputtering, measuring uniformity, roughness, thickness, microstructure and other properties of films on substrates (optical coatings). Further, solving other disadvantages (for example, removing insulating layers formed on the uneroded areas of sputtered target and avoiding arcing in process), improving control of the energy of condensing and bombarding ions over a wide range of sputtering gas pressure, increasing of the ionization of atoms and optimize magnetron reactive sputtering systems and etc.

Acknowledgements. Rimantas Žičkus acknowledges Student Research Fellowship Award from the Lithuanian Science Council.

[1] Y. Pauleau (Ed.), Magnetron Discharges for Thin Films Plasma Processing (Chapter 3), Materials Surface Processing by Directed Energy Techniques, Elsevier (2006), p. 67.

ZERO PHOTOVALTAIC EFFECT IN LED MATERIALS

Vytautas Jakštas, Donatas Meškauskas

Instititute of Applied Reasherch, University of Vilnius
Vytautas.Jakstas@stud.ff.vu.lt

Recent technological progress in light emitting diodes (LEDs) opened the way for using them in various applications where various emission wavelengths and/or emitter's high-brightness are of vital importance. Photovoltaic (PV) devices are in turn increasingly used in energy generation. Although these devices are widely investigated separately both devices are based on pn junction physics. Due to this fact, improvements of both devices are expected by investigation only one of them.

Here we report on the technique for the investigation PV effect versus heating. By taking into account these competing effects, we demonstrate an easy method for the LED characterisation and the evaluation of thermal constants. A commercial high-power (1 W) red AlGaInP LED (Philips Lumileds Lighting model MD1D) was investigated. The LED was driven by a source meter (Keithley 2430) in dc range of 10 nA to 1 A. During the measurements LED was attached to a heatsink and was illuminated by the second commercial high-power (1 W) red-orange AlGainP LED (Philips Lumileds Lighting model MH1D), that was driven by a sinusoidally modulated current with the bias somewhat below than the nominal current $I_0 = 300$ mA and modulation depth $m_I = 20\%$. Modulated current was provided by a custom made operational current amplifier, which was driven by a function generator (Tektronix AFG-3252). A digital lock-in amplifier (Signal Recovery model 7265) was used for detecting the respond signal on the first LED and measuring the amplitude and phase of the forward voltage variation. The zero photovoltaic effect was investigated at various frequencies, where the major of them were 0.25 Hz and 50 kHz. This range of frequencies spans from below to above the thermal cutoff (a frequency when junction temperature oscillation vanishes, 4.3 kHz for the model MD1D) of the LED. Figure 1 depicts the experimental data of the first measurement.

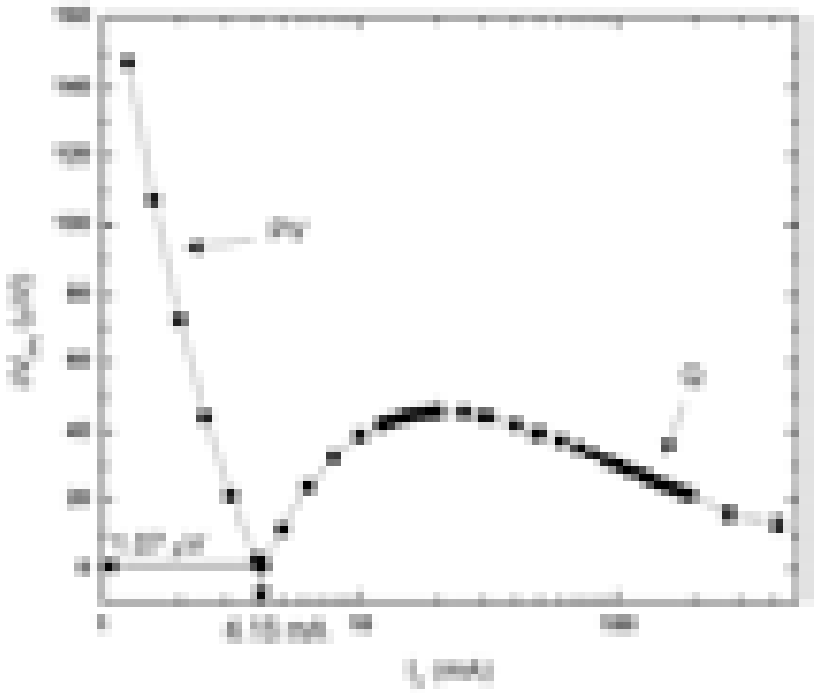

Fig. 1. Measured voltage variation δV_{PV} from the reference over forward current I_F.

Authors index

K

L

M

N

O

P

R

S

T

U

V

W

Z

Ž

PHAROS

High-power Industrial Femtosecond Lasers

- 200 fs-10 ps pulse duration adjustable
- Up to 1.5 mJ pulse energy
- Single pulse to 1 MHz
- Up to 15 W average power
- Industrial, sealed design
- Compact, modular setup
- Yb based with SSLD pumping
- Complete range of harmonic converters and OPA's available

LIGHT CONVERSION

For more information, contact
Light Conversion
Sauletekio al. 10,
LT-10223 Vilnius,
LITHUANIA
Tel: +370 5 2491830
E-mail: company@lightcon.com
www.lightcon.com

ALTECHNA

Altechna Co. Ltd. is a laser technology company operating in the fields of photonics and laser research since 1996.

Altechna is a reliable supplier of laser products: laser optics, crystals, lasers and optomechanics.

Our products:

- Lasers and their equipment
- Spectroscopes
- CCD cameras
- Positioning systems
- Laser crystals and optics
- Other laboratory equipment

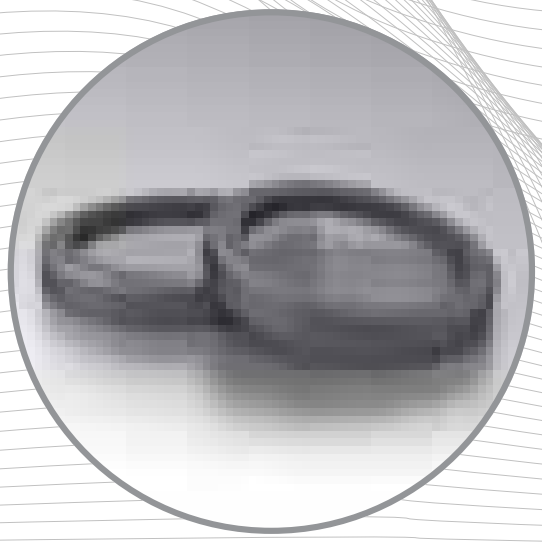

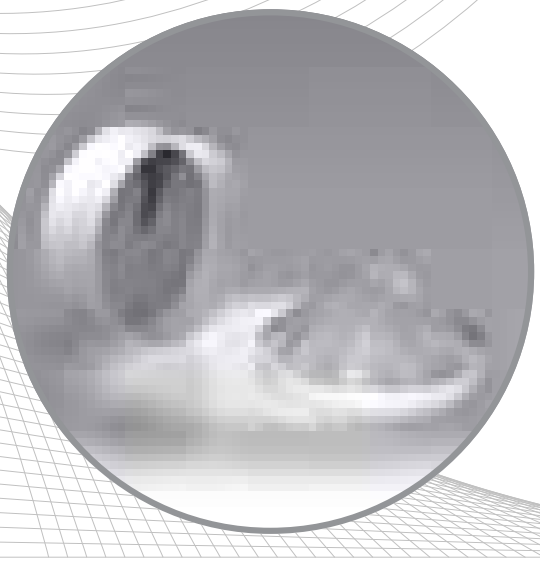

Altechna represents:

Altechna Co. Ltd. • Konstitucijos ave. 23C, LT-08105 Vilnius, Lithuania
Tel. +370 5 2725738 • Fax +370 5 2723704 • E-mail: info@altechna.com
www.altechna.com

Ruptela is young company, which seeks to help people and organizations to manage their property effectively, while using the latest communication technologies. Our main objective is to provide high quality services. By doing this we ensure the peace of mind of our clients.

Ruptela has a professional team with strong background of communications technologies (GSM, 3G, GPS), electronics and software systems. About company

Our vision – Business and society, effectively managing current resources.

Our mission – To give an opportunity to companies and people to monitor their most valuable asset in real time.

Our values:

- Inovative services and products of high quality
- Responsible attitude towards customer and employee.
- Long-term and reliable partnership.

Strategic objectives and directions of activity:

- To continously improve quality management system;
- To foresee and set the demand of clients;
- Systemically improve the qualification of employees;
- To affirm responsibility of each employee according to duties and competence.

Our geography:

EKSPLA

ADVANCED LASER TECHNOLOGIES

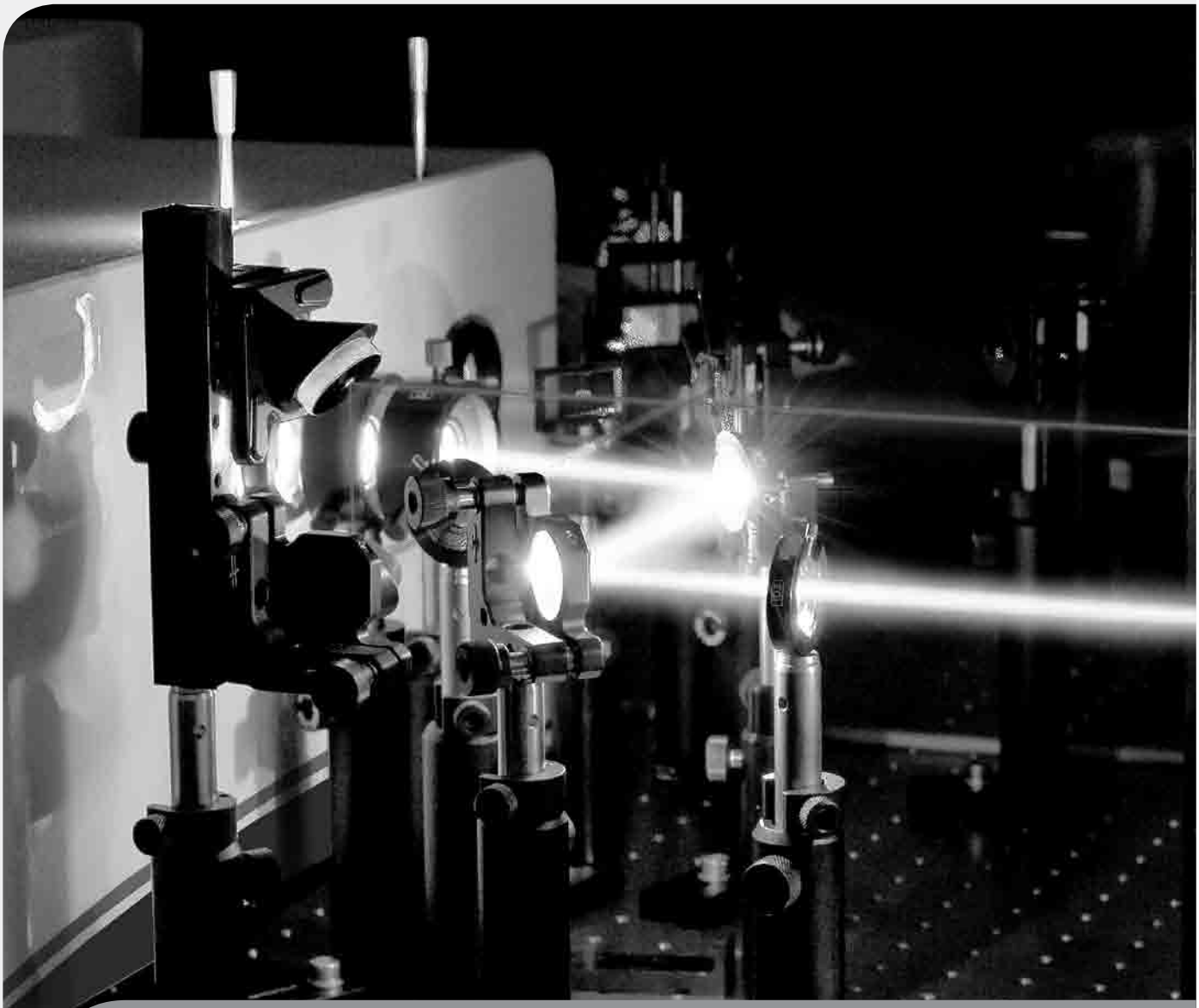

Lasers | Laser systems | Optoelectronics

www.ekspla.com